BİLGE INTERNATIONAL JOURNAL OF SCIENCE AND TECHNOLOGY RESEARCH

Yıl 2019 Year | Cilt 3 Volume | Özel Sayı Special Issue | p-ISSN: 2651-401X e-ISSN: 2651-4028

ICONST'19

www.iconst.org

BİLGE INTERNATIONAL JOURNAL OF SCIENCE AND TECHNOLOGY RESEARCH

VOL: 3 ISSUE: Special Issue 2019 ISSN: 2651-401X e-ISSN: 2651-4028

Press:
Kutbilge Association of Academicians
Distribution, Sales, Publisher;
Certificate No: 42086
32040, Isparta, TURKEY

Contact:
Kutbilge Association of Academicians,
32040, Isparta, TURKEY

Web : dergipark.gov.tr/bilgesci
E-mail : kutbilgescience@gmail.com

BILGE INTERNATIONAL JOURNAL OF SCIENCE AND TECHNOLOGY RESEARCH

CİLT: 3 SAYI: Özel Sayı 2019 ISSN: 2651-401X e-ISSN :2651-4028

Baskı:
Kutbilge Akademisyenler Derneği,
Dağıtım, Satış, Yayınevi
Sertifika No: 42086
32040, Isparta, TÜRKİYE

İletişim:
Kutbilge Akademisyenler Derneği,
32040, Isparta, TÜRKİYE

Web : dergipark.gov.tr/bilgesci
E-mail : kutbilgescience@gmail.com

BİLGE INTERNATIONAL JOURNAL OF SCIENCE AND TECHNOLOGY RESEARCH

ISSN: 2651-401X
e-ISSN: 2651-4028

A peer reviewed journal, published biannually by
Kutbilge Association of Academicians.

Yılda iki sayı olarak yayınlanan hakemli bir dergidir.
Kutbilge Akademisyenler Derneği tarafından
yayınlanmaktadır.

Year/Yıl: 2019, Volume/Cilt: 3, Issue/Sayı: Special Issue/Özel Sayı

The journal is indexed in Researchbib, AcademicKey, International Institute of Organized Research (I2OR), Cosmos Index, Google Scholar, Journal Factor, Index Copernicus, JIFACTOR, Science Library Index, Sindexs, Rootindexing, Eurasian Scientific Journal Index (ESJI), Directory of Research Journals Indexing (DRJI), ROAD, Araştırmax and BASE.

Dergimiz Researchbib, AcademicKey, International Institute of Organized Research (I2OR), Cosmos Index, Google Scholar, Journal Factor, Index Copernicus, JIFACTOR, Science Library Index, Sindex, Rootindexing, Eurasian Scientific Journal Index (ESJI), Directory of Research Journals Indexing (DRJI) ROAD, Araştırmax ve BASE'de taranmaktadır.

Bilge International Journal of Science and Technology Research

Year / Yıl: 2019, Volume / Cilt: 3, Special Issue / Özel Sayı

Editorial to the Special Issue on Selected Papers from International Conferences on Science and Technology, ICONST 2019

This special issue of the Bilge International Journal of Science and Technology Research contains selected papers from ICONST 2019 which was held on August 26-30, 2019 in Prizren, Kosovo with international attendance.

The 2st International International Conferences on Science and Technology (ICONST 2019) organised by Kutbilge Association of Academicians is held on the August 26-30, 2019 in Prizren, Kosovo. The aim objective of "ICONST 2019" is to bring together leading academicians, researchers, scholars and administrators from all over the world to exchange and share their experiences and research results about all aspects of Life Sciences, Natural Sciences, Engineering Sciences and Technology and discuss the practical challenges encountered and the solutions adopted.

ICONST-2019 offered three different thematic symposiums in 2019 These are:

International Conference on Natural Sciences and Technology (NST): The aim of the conference is to prepare a qualified discussion environment in the frame of sustainability perspective by bringing together the scientists involved in natural science research. Because science is critical to overcome complexities such as climate change, loss of biodiversity, pollution and poverty reduction. Science is the basis for new approaches and solutions to these issues.

International Conference on Life Sciences and Technology (LST): The aim of the conference is to bring together the scientists working in the field of life sciences and to develop new knowledge in the life sciences by combining the most cutting edge areas of research in academic disciplines such as medicine and biology with new, advanced methods of analysis from disciplines such as mathematics, chemistry, pharmacology, physics and computer science.

International Conference on Engineering Sciences and Technology (EST): The aim of the conference is to contribute to scientific development by discussing the studies of scientists who are involved in the design of engineering products with sustainable design skills and creating a lasting impact on future generations. Creating knowledge and understanding through science makes us equipped to find solutions to today's economic, social and environmental challenges, to reach sustainable development and more green societies.

223 papers have been submitted for presentation at ICONST 2019 (NST, LST and EST). Based on review reports by experts in the Scientific Committee, 203 papers (191 orals and 12 posters) have been accepted for presentation at the conference.

We would like to thank the contributing authors for accepting our invitation, and also to the anonymous reviewers who helped us ensure the high technical quality of the accepted papers.

The Organizing Committee

Bilge International Journal of Science and Technology Research

Year/Yıl: 2019, Volume/Cilt: 3, Issue/Sayı: Special Issue/Özel Sayı

CONTENTS/İÇİNDEKİLER

- A Data Classification Method in Machine Learning Based on Normalised Hamming Pseudo-Similarity of Fuzzy Parameterized Fuzzy Soft Matrices
  Samet Memiş, Serdar Enginoğlu, Uğur Erkan 1-8

- An Empirical Comparison of Machine Learning Algorithms for Predicting Breast Cancer
  Hamit Taner Ünal, Fatih Basciftci 9-20

- Classification of The Monolithic Columns Produced in Troad and Mysia Region Ancient Granite Quarries in Northwestern Anatolia via Soft Decision-Making
  Serdar Enginoğlu, Murat Ay, Naim Çağman, Veysel Tolun 21-34

- Controlling structural and electronic properties of ZnO NPs: Density-functional tight-binding method
  Mustafa Kurban, Hasan Kurban, Mehmet Dalkılıç 35-39

- The effects of a single atom substitution and temperature on electronic and photophysical properties F8T2 organic material
  Mustafa Kurban 40-44

- Numerical Simulation of Annular Flow boiling in Millimeter-scale Channels and Investigation of Design Parameters Using Taguchi Method
  Aliihsan Koca, Mansour Nasiri Khalaji 45-57

- Review of traditionally consumed antidiabetic fruits in the diet
  Pınar Ünsal, Ebru Aydın, Gülcan Özkan 58-76

- Topografik Özellikleri Kullanarak Arazi Morfolojisi Analizi: Uşak Ulubey Kanyonu Örneği/ Landform Analysis using Topographic Characteristics: An Example of Usak Ulubey Canyon
  Ahmet Çilek, Süha Berberoğlu, Müge Ünal Çilek, Cenk Dönmez 77-88

- Adana Katı Atık Toplama Tesisinin Mevcut Yer Seçim Uygunluğunun Konumsal Bilgi Teknolojileri ile Değerlendirilmesi/
  Evaluation of the Location Selection Suitability of Adana Municipality Solid Waste Facility with Spatial Information Technologies
  Müge Ünal Çilek, Ahmet Çilek, Esra Deniz Güner 89-105

- Effects of Using JP8-Diesel Fuel Mixtures in a Pump Injector Engine on Engine Performance
  Hasan Aydogan, Emin Cagatay Altinok 106-111

- Development of Reinforced Composites Containing Tea Tree Oil and Propolis for the Treatment of Horse Hoof Cracks
  Kamila Sobkowiak, Tomasz Gozdek, Mustafa Karaboyacı 112-116

Bilge International Journal of Science and Technology Research

Web : http://dergipark.gov.tr/bilgesci - **E-mail:** kutbilgescience@gmail.com

Received: 06.11..2019
Accepted: 25.12.2019
DOI: 10.30516/bilgesci.643821

ISSN: 2651-401X
e-ISSN: 2651-4028
3 (Special Issue), 1-8, 2019

A Data Classification Method in Machine Learning Based on Normalised Hamming Pseudo-Similarity of Fuzzy Parameterized Fuzzy Soft Matrices

Samet Memiş[1]*, Serdar Enginoğlu[1], Uğur Erkan[2]

Abstract: In this study, we propose a classification method based on normalised Hamming pseudo-similarity of fuzzy parameterized fuzzy soft matrices (*fpfs*-matrices). We then compare the proposed method with Fuzzy Soft Set Classifier (FSSC), FussCyier, Fuzzy Soft Set Classification Using Hamming Distance (HDFSSC), and Fuzzy k-Nearest Neighbor (Fuzzy kNN) in terms of the performance criterions (accuracy, precision, recall, and F-measure) and running time by using four medical data sets in the UCI machine learning repository. The results show that the proposed method performs better than FSSC, FussCyier, HDFSSC, and Fuzzy kNN for "Breast Cancer Wisconsin (Diagnostic)", "Immunotherapy", "Pima Indian Diabetes", and "Statlog Heart".

Keywords: Fuzzy sets, soft sets, *fpfs*-matrices, similarity measure, data classification.

1. Introduction

Soft sets (Molodtsov, 1999), a standard and practical mathematical tool, are often used for modelling uncertainties, and a great variety of studies have been conducted on this concept (Çağman and Deli, 2012a, b; Deli and Çağman, 2015; Enginoğlu et al., 2015; Şenel, 2016; Zorlutuna and Atmaca, 2016; Atmaca, 2017; Çıtak and Çağman, 2017; Riaz and Hashmi, 2017; Atmaca, 2019; Çıtak, 2018; Riaz and Hashmi, 2018; Riaz et al., 2018; Şenel 2018a, b; Jana et al., 2019; Karaaslan, 2019a, b; Sezgin et al., 2019a, b). Fuzzy soft sets (Maji et al., 2001; Çağman et al., 2011b), fuzzy parameterized soft sets (Çağman et al., 2011a), and fuzzy parameterized fuzzy soft sets (*fpfs*-sets) (Çağman et al., 2010) are among known general forms of soft sets. Also, studies on the matrix representations of these sets have been increasingly continued such as soft matrices (Çağman and Enginoğlu, 2010), fuzzy soft matrices (Çağman and Enginoğlu, 2012), and fuzzy parameterized fuzzy soft matrices (*fpfs*-matrices) (Enginoğlu, 2012; Enginoğlu and Çağman, In Press). Even if parameters and objects have uncertainties, *fpfs*-matrices can successfully model such problems.

The rest of the paper is organised as follows: In Section 2, we present definitions of *fpfs*-sets (Çağman et al., 2010; Enginoğlu, 2012), *fpfs*-matrices (Enginoğlu, 2012; Enginoğlu and Çağman, In Press), and normalised Hamming pseudo-similarity of *fpfs*-matrices. In Section 3, we propose Fuzzy Parameterized Fuzzy Soft Normalized Hamming Classifier (FPFSNHC) using normalised Hamming pseudo-similarity of *fpfs*-matrices. In Section 4, we compare FPFSNHC with Fuzzy Soft Set Classifier (FSSC) (Handaga et al., 2012), FussCyier (Lashari et al., 2017), Fuzzy Soft Set Classification Using Hamming Distance (HDFSSC) (Yanto et al., 2018), and Fuzzy k-

[1]Department of Mathematics, Faculty of Arts and Sciences, Çanakkale Onsekiz Mart University, Çanakkale, Turkey
[2]Department of Computer Engineering, Faculty of Engineering, Karamanoğlu Mehmetbey University, Karaman, Turkey
*Corresponding author: samettmemis@gmail.com

Citation (Atıf): Memiş S., Enginoğlu, S., Erkan U., (2019). A Data Classification Method in Machine Learning Based on Normalised Hamming Pseudo-Similarity of Fuzzy Parameterized Fuzzy Soft Matrices. Bilge International Journal of Science and Technology Research, 3 (Special Issue): 1-8.

Nearest Neighbor (Fuzzy kNN) (Keller et al., 1985) in terms of the performance criterions (accuracy, precision, recall, and F-measure) and running time by using four medical data sets in the UCI machine learning repository (Dua and Graff, 2019). The results show that proposed method performs better than FSSC, FussCyier, HDFSSC, and Fuzzy kNN for "Breast Cancer Wisconsin (Diagnostic)", "Immunotherapy", "Pima Indian Diabetes", and "Statlog Heart". Finally, we discuss the need for further research. This study is a part of the first author's PhD dissertation.

2. Preliminaries

In this section, firstly, we present the concept of *fpfs*-matrices (Enginoğlu, 2012; Enginoğlu and Çağman, In Press). Throughout this paper, let E be a parameter set, $F(E)$ be the set of all fuzzy sets over E, and $\mu \in F(E)$. Here, a fuzzy set is denoted by $\left\{{}^{\mu(x)}x : x \in E\right\}$ instead of $\{(x, \mu(x)) : x \in E\}$.

Definition 2.1. (Çağman et al., 2010; Enginoğlu, 2012) *Let U be a universal set, $\mu \in F(E)$, and α be a function from μ to $F(U)$. Then, the set $\{({}^{\mu(x)}x, \alpha({}^{\mu(x)}x)) : x \in E\}$ being the graphic of α is called a fuzzy parameterized fuzzy soft set (fpfs-set) parameterized via E over U (or briefly over U).*

In the present paper, the set of all *fpfs*-sets over U is denoted by $FPFS_E(U)$. In $FPFS_E(U)$, since the $graph(\alpha)$ and α generated each other uniquely, the notations are interchangeable. Therefore, as long as it does not cause any confusion, we denote an *fpfs*-set $graph(\alpha)$ by α.

Example 2.1. *Let* $E = \{x_1, x_2, x_3, x_4\}$ *and* $U = \{u_1, u_2, u_3, u_4, u_5\}$. *Then,*

$\alpha = \{({}^{0.5}x_1, \{{}^{0.7}u_1, {}^{0.3}u_4\}), ({}^{0}x_2, \{{}^{0.1}u_1, {}^{0.8}u_3, {}^{1}u_5\}), ({}^{0.9}x_3, \{{}^{0.4}u_1, {}^{0.2}u_2, {}^{0.7}u_4\}), ({}^{1}x_4, \{{}^{0.6}u_1, {}^{0.9}u_5\})\}$

is an fpfs-set over U.

Definition 2.2. (Enginoğlu, 2012; Enginoğlu and Çağman, In Press) *Let $\alpha \in FPFS_E(U)$. Then, $[a_{ij}]$ is called the matrix representation of α (or briefly fpfs-matrix of α) and is defined by*

$$[a_{ij}] \coloneqq \begin{bmatrix} a_{01} & a_{02} & a_{03} & \dots & a_{0n} & \dots \\ a_{11} & a_{12} & a_{13} & \dots & a_{1n} & \dots \\ \vdots & \vdots & \vdots & \ddots & \vdots & \vdots \\ a_{m1} & a_{m2} & a_{m3} & \dots & a_{mn} & \dots \\ \vdots & \vdots & \vdots & \ddots & \vdots & \ddots \end{bmatrix}$$

such that for $i \in \{0,1,2,\cdots\}$ and $j \in \{1,2,\cdots\}$,

$$a_{ij} \coloneqq \begin{cases} \mu(x_j), & i = 0 \\ \alpha({}^{\mu(x_j)}x_j)(u_i), & i \neq 0 \end{cases}$$

Here, if $|U| = m - 1$ and $|E| = n$, then $[a_{ij}]$ has order $m \times n$.

Throughout this paper, the set of all *fpfs*-matrices parameterized via E over U is denoted by $FPFS_E[U]$.

Example 2.2. *The fpfs-matrix of the fpfs-set α provided in Example 2.1 is as follows:*

$$[a_{ij}] = \begin{bmatrix} 0.5 & 0 & 0.9 & 1 \\ 0.7 & 0.1 & 0.4 & 0.6 \\ 0 & 0 & 0.2 & 0 \\ 0 & 0.8 & 0 & 0 \\ 0.3 & 0 & 0.7 & 0 \\ 0 & 1 & 0 & 0.9 \end{bmatrix}$$

Secondly, we present the normalised Hamming pseudo-similarity of *fpfs*-matrices.

Definition 2.3. *Let $[a_{ij}], [b_{ij}] \in FPFS_E[U]$. The normalised Hamming pseudo-similarity of $[a_{ij}]$ and $[b_{ij}]$ is defined by*

$$s([a_{ij}], [b_{ij}]) \coloneqq 1 - \frac{\sum_{i=1}^{m-1}\sum_{j=1}^{n}|a_{0j}a_{ij} - b_{0j}b_{ij}|}{(m-1)n}$$

3. Fuzzy Parameterized Fuzzy Soft Normalized Hamming Classifier (FPFSNHC)

In this section, firstly, we give some necessary notations. Let $u, v \in \mathbb{R}^n$. Then, the Pearson correlation coefficient between u and v is defined by

$$P(u,v) \coloneqq \frac{n\sum_{i=1}^{n}u_iv_i - (\sum_{i=1}^{n}u_i)(\sum_{i=1}^{n}v_i)}{\sqrt{[n\sum_{i=1}^{n}u_i^2 - (\sum_{i=1}^{n}u_i)^2][n\sum_{i=1}^{n}v_i^2 - (\sum_{i=1}^{n}v_i)^2]}}$$

Throughout this paper, let $[dm]$ be a data matrix having order $m \times n$, $[\widetilde{dm}]$ be the feature fuzzification of $[dm]$, the last column of $[\widetilde{dm}]$ be the class column, $[tm]$ be a training matrix which is a submatrix of $[dm]$, $[tm^r]$ be a submatrix of $[tm]$ whose values of the last column are equal to r, and $[tm]^j$ be j^{th} column of $[tm]$.

Secondly, we propose FPFSNHC classification algorithm. FPFSNHC's steps are as follows:

FPFSNHC's Algorithm Steps

Step 1. Read a nonempty $[dm]$

Step 2. Calculate the feature weight vector $[fw_{1j}]$ based on the Pearson correlation coefficient between feature vectors and class vector defined by

$$fw_{1j} \coloneqq P([dm]^j, [dm]^n), for\ j \in \{1,2,\dots,n-1\}$$

Step 3. Obtain $[\widetilde{dm}]$ such that for $i \in \{1,2,\dots,m\}$ and $j \in \{1,2,\dots,n\}$,

$$\widetilde{dm}_{ij} \coloneqq \begin{cases} \dfrac{dm_{ij}}{\max\limits_{k} dm_{kj}}, j \neq n \\ dm_{ij}, \quad j = n \end{cases}$$

Step 4. Obtain $[tm]$ from the $[\widetilde{dm}]$

Step 5. Obtain $[tm^r]$ for all r

Step 6. Calculate the cluster centre matrix $[e_{rj}]$ such that for $i \in \{1,2,\dots,k_r\}$ and $j \in \{1,2,\dots,n-1\}$,

$$e_{rj} \coloneqq \frac{1}{k_r}\sum_{i=1}^{k_r} tm_{ij}^r$$

Here, k_r is row number of $[tm^r]$.

Step 7. Obtain the train *fpfs*-matrices $[a_{ij}^r]$ such that for all r, $a_{0j}^r = fw_{1j}$ and $a_{1j}^r = e_{rj}$

Step 8. Obtain the unknown class data $[u_{1j}]$ from the test data

Step 9. Obtain the test *fpfs*-matrix $[b_{ij}]$ such that $b_{0j} = fw_{1j}$ and $b_{1j} = u_{1j}$

Step 10. Compute S_r for all r defined by

$$S_r \coloneqq s([a_{ij}^r],[b_{ij}]) = 1 - \frac{\sum_{i=1}^{m-1}\sum_{j=1}^{n}|a_{0j}^r a_{ij}^r - b_{0j}b_{ij}|}{(m-1)n}$$

Step 11. Obtain c such that $c = \arg\max\limits_{r} S_r$

Step 12. Assign the data $[u_{1j}]$ without class to class c

Step 13. Repeat Step 9-12 for all data $[u_{1j}]$ without class in test data

4. Simulation Results

In this section, we first simulate the algorithms using "Breast Cancer Wisconsin (Diagnostic)", "Immunotherapy", "Pima Indian Diabetes", and "Statlog Heart" datasets provided in UCI Machine Learning Repository (Dua and Graff, 2019) and detailed in Table 1. We then compare the performance of the algorithms by using four performance criterions: accuracy, precision, recall, and F-measure, defined by

$$Accuracy \coloneqq \frac{TP+TN}{TP+TN+FP+FN}$$

$$Recall \coloneqq \frac{TP}{TP+FN}$$

$$Precision \coloneqq \frac{TP}{TP+FP}$$

$$F-Measure \coloneqq \frac{2(Precision \times Recall)}{Precision + Recall} = \frac{2TP}{2TP+FP+FN}$$

where TP: True positive, FP: False positive, TN: True negative, and FN: False negative.

Here, the accuracy of a classifier is calculated by dividing the total correctly classified positives and negatives by the total number of samples, the precision of a classifier is calculated by dividing correctly classified positives by the total positive count, the recall of a classifier is calculated by dividing correctly classified positives by total true positive class, and the F-measure of a classifier is harmonic mean of precision and recall values.

Table 1. Description of The UCI data sets.

No.	Name	Instances	Attributes	Class
1	Breast Cancer	569	30	2
2	Immunotherapy	90	7	2
3	Pima Diabetes	768	8	2
4	Statlog Heart	270	13	2

Secondly, we present the performance results of the algorithms in Table 2 for "Breast Cancer Wisconsin (Diagnostic)", in Table 3 "Immunotherapy" data sets, in Table 4 for "Pima Indian Diabetes", and in Table 5 "Statlog Heart" data sets. In Figures 1-4, we give the figures of Table 2-5. In Table 6 and Figure 5, we give the running times of algorithms for all of four medical data sets. We use MATLAB R2019a and a workstation with I(R) Xeon(R) CPU E5-1620 v4@3.5 GHz and 64 GB RAM for simulation. All simulation results are obtained at random 100 independent runs. A split of data 80 per cent is a training set, and 20 per cent is a testing set. The performance results are obtained by averaging the performance values of each class.

Table 2. The average accuracy, precision, recall, and F-measure results (%) of algorithms for "Breast Cancer Wisconsin (Diagnostic)" data set.

	Breast Cancer Wisconsin (Diagnostic)			
Classifier	**Accuracy**	**Precision**	**Recall**	**F-Measure**
FSSC	93.54	93.16	**92.98**	93.00
FussCyier	93.77	94.40	92.27	93.11
HDFSSC	92.90	92.90	91.79	92.23
Fuzzy kNN	91.35	91.05	90.30	90.56
FPFSNHC	**94.10**	**94.64**	92.70	**93.48**

Table 3. The average accuracy, precision, recall, and F-measure results (%) of algorithms for "Immunotherapy" data set.

	Immunotherapy			
Classifier	**Accuracy**	**Precision**	**Recall**	**F-Measure**
FSSC	62.28	61.15	65.84	56.69
FussCyier	68.00	63.48	68.12	60.99
HDFSSC	67.89	62.98	68.09	60.78
Fuzzy kNN	61.33	45.04	45.60	43.18
FPFSNHC	**70.67**	**66.68**	**73.16**	**64.63**

Table 4. The average accuracy, precision, recall, and F-measure results (%) of algorithms for "Pima Indian Diabetes" data set.

	Pima Indian Diabetes			
Classifier	**Accuracy**	**Precision**	**Recall**	**F-Measure**
FSSC	70.69	69.97	71.70	69.62
FussCyier	73.01	70.62	70.91	70.58
HDFSSC	73.24	71.23	**72.28**	71.41
Fuzzy kNN	67.27	64.25	64.22	64.03
FPFSNHC	**73.94**	**71.51**	71.61	**71.43**

Table 5. The average accuracy, precision, recall, and F-measure results (%) of algorithms for "Statlog Heart" data set.

	Statlog Heart			
Classifier	**Accuracy**	**Precision**	**Recal**	**F-Measure**
FSSC	80.78	81.30	81.61	80.49
FussCyier	82.46	82.54	81.69	81.73
HDFSSC	79.81	79.50	79.36	79.18
Fuzzy kNN	58.22	57.84	57.70	57.01
FPFSNHC	**83.39**	**83.79**	**82.50**	**82.62**

Table 6. The mean running times of the algorithms for the data sets (In Seconds).

Classifier	**Breast Cancer**	**Immunotherapy**	**Pima Indian Diabetes**	**Statlog Heart**
FSSC	0.00113	0.00039	0.00125	0.00063
FussCyier	0.00077	0.00041	0.00074	0.00050
HDFSSC	0.00085	0.00036	0.00089	0.00050
Fuzzy kNN	0.00681	0.00041	0.00557	0.00114
FPFSNHC	0.00157	0.00053	0.00157	0.00084

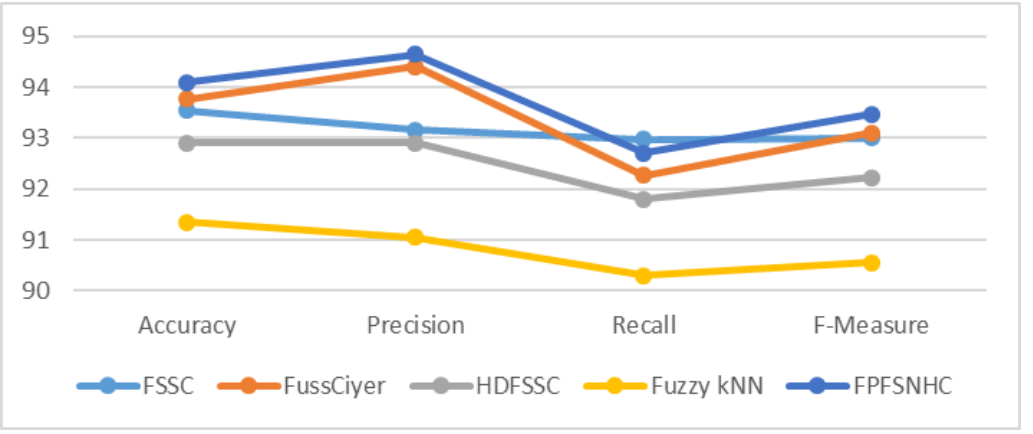

Figure 1. The Figure of the average accuracy, precision, recall, and F-measure results (%) of algorithms for "Breast Cancer Wisconsin (Diagnostic)" dataset in Table 2

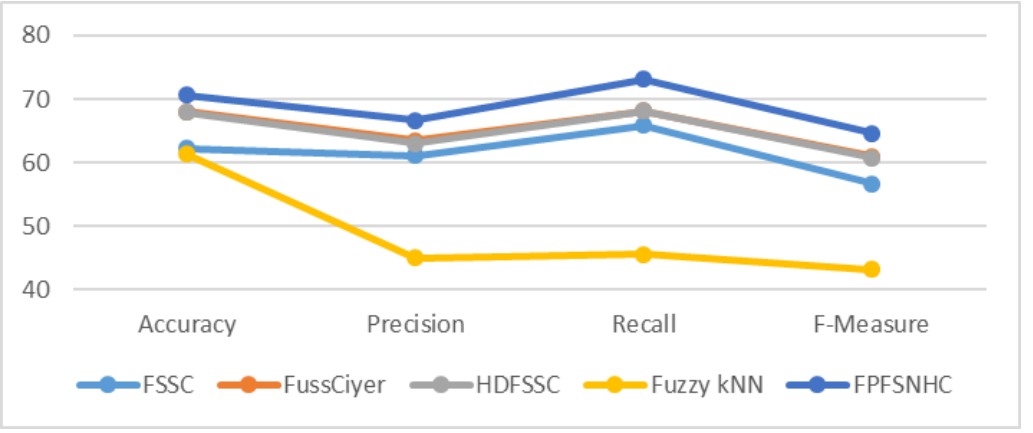

Figure 2. The Figure of the average accuracy, precision, recall, and F-measure results (%) of algorithms for "Immunotherapy" dataset in Table 3

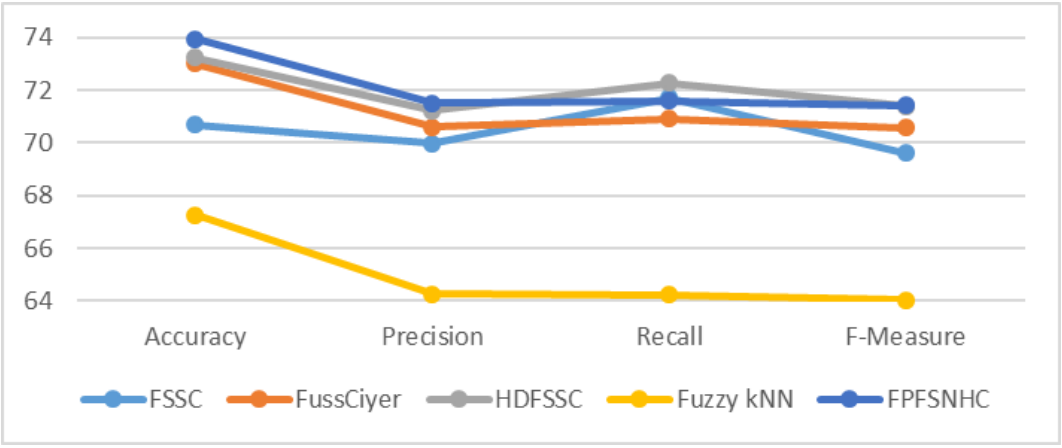

Figure 3. The Figure of the average accuracy, precision, recall, and F-measure results (%) of algorithms for "Pima Indian Diabetes" dataset in Table 4

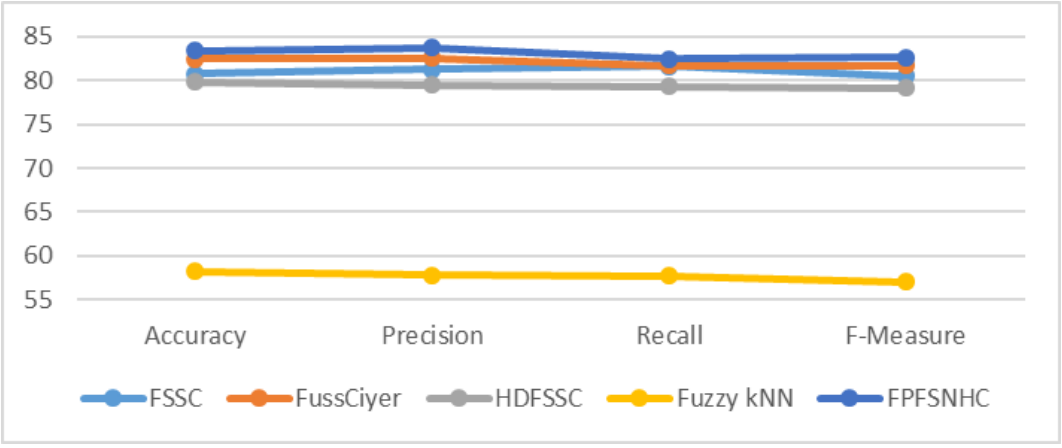

Figure 4. The Figure of the average accuracy, precision, recall, and F-measure results (%) of algorithms for "Statlog Heart" dataset in Table 5

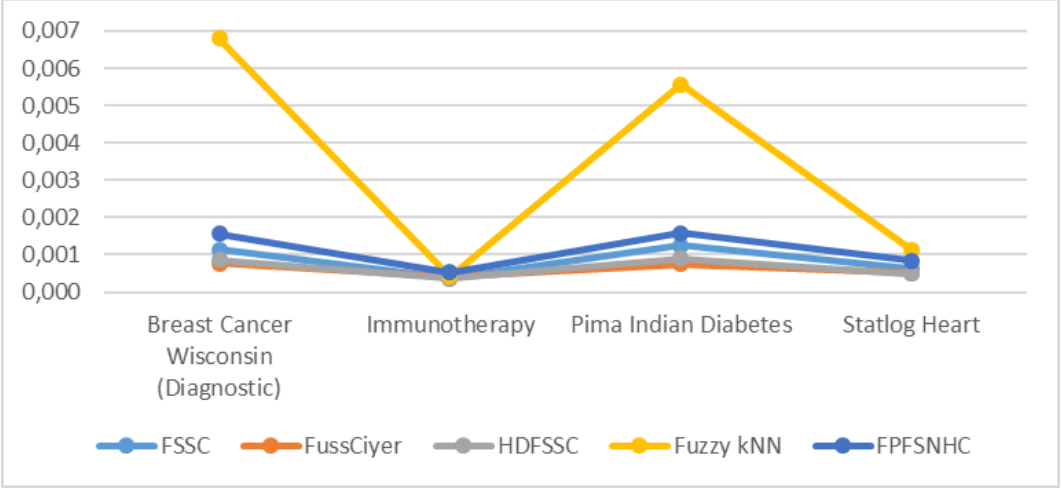

Figure 5. The Figure of the mean running times of the algorithms for the data sets in Table 6

5. Conclusion

In this paper, we have proposed the classification method FPFSNHC based on normalised Hamming pseudo-similarity of *fpfs*-matrices. We then compare proposed method with FSSC (Handaga et al. 2012), FussCyier (Lashari et al. 2017), HDFSSC (Yanto et al., 2018), and Fuzzy kNN (Keller et al. 1985) in terms of the performance criterions (accuracy, precision, recall, and F-measure) and running times by using four medical data sets in the UCI machine learning repository (Dua and Graff, 2019). In Immunotherapy data set, FPFSNHC (70.67, 66.68, 73.16, 64.63) has advantage over FSSC (62.28, 61.15, 65.84, 56.69), FussCyier (68.00, 63.48, 68.12, 60.99), HDFSSC (67.89, 62.98, 68.09, 60.78), and Fuzzy kNN (61.33, 45.04, 45.60, 43.18) and in Statlog Heart data set, FPFSNHC (83.39, 83.79, 82.50, 82.62) has advantage over FSSC (80.78, 81.30, 81.61, 80.49), FussCyier (82.46, 82.54, 81.69, 81.73), HDFSSC (79.81, 79.50, 79.36, 79.18), and Fuzzy kNN (58.22, 57.84, 57.70, 57.01), concerning accuracy, precision, recall, and F-measure results, respectively. The results show that the proposed method performs better than FSSC, FussCyier, HDFSSC, and Fuzzy kNN for the data sets. Moreover, *fpfs*-matrices can model classification problems containing uncertainty about which parameters being more effective to classify data. Therefore, it is worthwhile to study developing different classification algorithms by using different similarity measures of *fpfs*-matrices because success can be increased by using different data sets and membership functions.

Moreover, different classification algorithms also can be developed by using soft decision-making methods via *fpfs*-matrices such as (Enginoğlu and Memiş, 2018a, b, c, d; Enginoğlu et al., 2018a, b, c, d; Enginoğlu and Çağman, In Press). Additionally, this study also gives an inspiration about how to construct *fpfs*-matrices for real-life problems such as data classification.

References

Atmaca, S. (2017). Relationship between fuzzy soft topological spaces and (X, τ_e) parameter spaces. Cumhuriyet Science Journal, 38(4-Supplement), 77-85.

Atmaca, S. (2019). Fuzzy soft separation axioms with sense of Ganguly and Saha. Afrika Matematika, 30, 777-785

Çağman, N., Çıtak, F., Enginoğlu, S. (2010). Fuzzy parameterized fuzzy soft set theory and its applications. Turkish Journal of Fuzzy Systems, 1(1), 21-35.

Çağman, N., Çıtak, F., Enginoğlu, S. (2011a). FP-soft set theory and its applications. Annals of Fuzzy Mathematics and Informatics, 2(2), 219-226.

Çağman, N., Deli, İ. (2012a). Means of FP-soft sets and their applications. Hacettepe Journal of Mathematics and Statistics, 41(5), 615-625.

Çağman, N., Deli, İ. (2012b). Products of FP-soft sets and their applications. Hacettepe Journal of Mathematics and Statistics, 41(3), 365-374.

Çağman, N., Enginoğlu, S. (2010). Soft matrix theory and its decision making. Computers and Mathematics with Applications, 59, 3308-3314.

Çağman, N., Enginoğlu, S. (2012). Fuzzy soft matrix theory and its application in decision making. Iranian Journal of Fuzzy Systems, 9(1), 109-119.

Çağman, N., Enginoğlu, S., Çıtak, F. (2011b). Fuzzy soft set theory and its applications. Iranian Journal of Fuzzy Systems, 8(3), 137-147.

Çıtak, F. (2018). Soft k-uni ideals of semirings and its algebraic applications. Journal of The Institute of Science and Technology, 8(4), 281-294.

Çıtak, F., Çağman, N. (2017). Soft k-int-ideals of semirings and its algebraic structures. Annals of Fuzzy Mathematics and Informatics, 13(4), 531-538.

Deli, İ., Çağman, N. (2015). Relations on FP-soft sets applied to decision making problems. Journal of New Theory, 3, 98-107.

Dua, D., Graff, C. (2019). UCI Machine Learning Repository. University of California, Irvine, School of Information and Computer Sciences. http://archive.ics.uci.edu/ml (Date Accessed: 10.06.2019).

Enginoğlu, S. (2012). Soft matrices, PhD Dissertation. Tokat Gaziosmanpaşa University, Tokat, Turkey.

Enginoğlu, S., Çağman, N. Fuzzy parameterized fuzzy soft matrices and their application in decision-making. TWMS Journal of Applied and Engineering Mathematics, (In Press).

Enginoğlu, S., Çağman, N., Karataş, S., Aydın, T. (2015). On soft topology. El-Cezerî Journal of Science and Engineering, 2(3), 23-38.

Enginoğlu, S., Memiş, S. (2018a). Comment on fuzzy soft sets [The Journal of Fuzzy Mathematics 9(3), 2001, 589–602]. International Journal of Latest Engineering Research and Applications, 3(9), 1-9.

Enginoğlu, S., Memiş, S. (2018b). A configuration of some soft decision-making algorithms via *fpfs*-matrices. Cumhuriyet Science Journal, 39(4), 871-881.

Enginoğlu, S., Memiş, S. (2018c). A review on an application of fuzzy soft set in multicriteria decision making problem [P. K. Das, R. Borgohain, International Journal of Computer Applications 38 (2012) 33–37]. M. Akgül, İ. Yılmaz, A. İpek (Eds.) International conference on mathematical studies and applications 2018 (pp. 173-178). Karaman, Turkey.

Enginoğlu, S., Memiş, S. (2018d). A review on some soft decision-making methods. M. Akgül, İ. Yılmaz, A. İpek (Eds.) International conference on mathematical studies and applications 2018 (pp. 437-442). Karaman, Turkey.

Enginoğlu, S., Memiş, S., Arslan, B. (2018a). Comment (2) on soft set theory and uni-int decision-making [European Journal of Operational Research, (2010) 207, 848–855]. Journal of New Theory, 25, 84-102.

Enginoğlu, S., Memiş, S., Arslan, B. (2018b). A fast and simple soft decision-making algorithm: EMA18an. M. Akgül, İ. Yılmaz, A. İpek (Eds.) International conference on mathematical studies and applications 2018 (pp. 428-436). Karaman, Turkey.

Enginoğlu, S., Memiş, S., Öngel, T. (2018c). Comment on soft set theory and uni-int decision-making [European Journal of Operational Research, (2010) 207, 848–855]. Journal of New Results in Science, 7(3), 28-43.

Enginoğlu, S., Memiş, S., Öngel, T. (2018d). A fast and simple soft decision-making algorithm: EMO18o. M. Akgül, İ. Yılmaz, A. İpek (Eds.) International conference on mathematical studies and applications 2018 (pp. 179–186). Karaman, Turkey.

Handaga, B., Onn, H., Herawan, T. (2012). FSSC: An algorithm for classifying numerical data using fuzzy soft set theory. International Journal of Fuzzy System Applications, 3(4), 29-46.

Jana, C., Pal, M., Karaaslan, F., Sezgin, A. (2019). (α,β)-soft intersectional rings and ideals with their applications. New Mathematics and Natural Computation, 15(2), 333-350.

Karaaslan, F. (2019a). Some properties of AG*-groupoids and AG-bands under SI-product operation. Journal of Intelligent & Fuzzy Systems, 36(1), 231-239.

Karaaslan, F. (2019b). Hesitant fuzzy graphs and their applications in decision making. Journal of Intelligent & Fuzzy Systems, 36(3), 2729-2741.

Keller, J. M., Gray, M. R., Given, J. A. (1985). A fuzzy k-nearest neighbor algorithm. IEEE Transactions on Systems, Man, and Cybernetics, 15(4), 580-585.

Lashari, S. A., Ibrahim, R., Senan, N. (2017). Medical data classification using similarity measure of fuzzy soft set based distance measure. Journal of Telecommunication, Electronic and Computer Engineering, 9(2–9), 95-99.

Maji, P. K., Biswas, R., Roy, A. R. (2001). Fuzzy soft sets. The Journal of Fuzzy Mathematics, 9(3), 589-602.

Molodtsov, D. (1999). Soft set theory-first results. Computers and Mathematics with Applications, 37(4-5), 19-31.

Riaz, M., Hashmi, R. (2017). Fuzzy parameterized fuzzy soft topology with applications. Annals of Fuzzy Mathematics and Informatics, 13(5), 593-613.

Riaz, M., Hashmi, R. (2018). Fuzzy parameterized fuzzy soft compact spaces with decision-

making. Punjab University Journal of Mathematics, 50(2), 131-145.

Riaz, M., Hashmi, R., Farooq, A. (2018). Fuzzy parameterized fuzzy soft metric spaces. Journal of Mathematical Analysis, 9(2), 25-36.

Sezgin, A., Ahmad, S., Mehmood, A. (2019a). A New Operation on Soft Sets: Extended Difference of Soft Sets. Journal of New Theory, 27, 33-42.

Sezgin, A., Çağman, N., Çıtak, F. (2019b). α-inclusions applied to group theory via soft set and logic. Communications Faculty of Sciences University of Ankara Series A1 Mathematics and Statistics, 68(1), 334-352.

Şenel, G. (2016). A new approach to Hausdorff space theory via the soft sets. Mathematical Problems in Engineering, 2016, Article ID 2196743, 6 pages.

Şenel, G. (2018a). Analyzing the locus of soft spheres: Illustrative cases and drawings. European Journal of Pure and Applied Mathematics, 11(4), 946-957.

Şenel, G. (2018b). The relation between soft topological space and soft ditopological space. Communications Faculty of Sciences University of Ankara Series A1 Mathematics and Statistics, 67(2), 209-219.

Yanto, I. T. R., Seadudin, R. R., Lashari, S. A., Haviluddin. (2018). A numerical classification technique based on fuzzy soft set using hamming distance. In: R. Ghazali, M. M. Deris, N. M. Nawi, J. H. Abawajy (Eds.) Third international conference on soft computing and data mining (pp. 252-260). Johor, Malaysia.

Zorlutuna, İ., Atmaca, S. (2016). Fuzzy parametrized fuzzy soft topology. New Trends in Mathematical Sciences, 4(1), 142-152.

Bilge International Journal of Science and Technology Research

Web : http://dergipark.gov.tr/bilgesci - **E-mail:** kutbilgescience@gmail.com

Received: 11.11.2019
Accepted: 26.12.2019
DOI: 10.30516/bilgesci.645067

ISSN: 2651-401X
e-ISSN: 2651-4028
3 (Special Issue), 9-20, 2019

An Empirical Comparison of Machine Learning Algorithms for Predicting Breast Cancer

Hamit Taner Ünal[1], Fatih Başçiftçi[2]*

Abstract: According to recent statistics, breast cancer is one of the most prevalent cancers among women in the world. It represents the majority of new cancer cases and cancer-related deaths. Early diagnosis is very important, as it becomes fatal unless detected and treated in early stages. With the latest advances in artificial intelligence and machine learning (ML), there is a great potential to diagnose breast cancer by using structured data. In this paper, we conduct an empirical comparison of 10 popular machine learning models for the prediction of breast cancer. We used well known Wisconsin Breast Cancer Dataset (WBCD) to train the models and employed advanced accuracy metrics for comparison. Experimental results show that all models demonstrate superior accuracy, while Support Vector Machines (SVM) had slightly better performance than other methods. Logistic Regression, K-Nearest Neighbors and Neural Networks also proved to be strong classifiers for predicting breast cancer.

Keywords: Breast Cancer, Artificial Intelligence, Machine Learning, Medical Decision Support Systems

1. Introduction

Breast cancer is the second largest cause of cancer deaths among women (American Cancer Society, 2018). According to studies (Siegel & Jemal, 2015), there is an increase in the occurrence rate recently. Fortunately, breast cancer is also among the most curable cancer types if it is diagnosed in early stages (Akay, 2009). Early diagnosis followed by appropriate cancer treatment helps eliminate the deadly risk significantly. Furthermore, accurate classification of benign tumors can prevent patients undergoing unnecessary treatments.

Diagnosis of breast cancer and classification of patients into malignant or benign groups is the subject of recent research. Artificial Intelligence and Machine learning plays a vital role in a wide range of critical applications, such as image recognition, natural language processing, time series forecasting, regression and prediction. The use of an accurate machine learning algorithm for early detection could definitely save precious lives. Because of its unique advantages in critical features detection from complex breast cancer datasets, machine learning (ML) is widely recognized as the methodology of choice in breast cancer pattern classification and forecast modeling (Yue, Wang, Chen, Payne, & Liu, 2018). Previous studies had significant results for the classification of breast cancer by employing various Machine learning models (Agarap, 2018).

In this paper, we compare popular and trending machine learning methods effectively used in real-world classification problems. We utilized breast Cancer data available from the Wisconsin dataset from University of California at Irvine (UCI) machine learning repository with the aim of developing an accurate comparison.

The remainder of this paper is organized as follows. Firstly, a brief literature review has been conducted in Section 2. Then, basic information about ML models is documented in Section 3.

1 Selçuk University, Institute of Natural and Applied Sciences, Department of Information Technologies Engineering (PhD Student), Konya, Turkey
2 Selçuk University, Faculty of Technology, Department of Computer Engineering, Konya, Turkey
*Corresponding author (İletişim yazarı): basciftci@selcuk.edu.tr

Citation (Atıf): Ünal, H. T., Başçiftçi, F. (2019). An Empirical Comparison of Machine Learning Algorithms for Predicting Breast Cancer. Bilge International Journal of Science and Technology Research, 3(Special Issue): 9-20.

Next, the experimental setup and results with a thorough discussion is provided in Section 4 and Section 5 respectively. Finally, conclusions and future works are outlined in Section 6.

2. Literature Review

Numerous studies have been published and various classification techniques were developed for predicting breast cancer through Machine Learning. Most of the works evaluated their proposed models using the dataset taken from the UCI machine-learning repository.

Polat and Güneş (2007) conducted breast cancer diagnosis by using Least Square Support Vector Machines (LS-SVM). They evaluated the robustness of their model via k-fold cross validation with accuracy, sensitivity and specify metrics. They obtained classification accuracy of 98.53%. Akay (2009) employed an SVM-based method combined with feature selection. He obtained an accuracy of 99.52% with his proposed model containing five features. Sadhukan (2020) and Upadhyay compared KNN and SVM to predict breast cancer and analyzed digital image of a fine needle aspirate (FNA) of breast tissue with image processing to extract features of kernel of the cells. Sri et al (2019) proposed SVM and Neural Network models for tumor prognosis. By using WEKA tool, they applied 10-fold and 5-fold cross validation for high precision results. Kadam et al (2019) proposed feature ensemble learning based on Sparse Autoencoders and Softmax Regression for classification of Breast Cancer into benign or malignant. They obtained 98.60% true accuracy with their proposed model. Sethi (2018) compared evolutionary algorithms and machine learning predicting breast cancer in three different datasets. Jain et al (2018) presented a hybrid machine learning framework for the diagnosis of breast cancer and diabetes using feature selection and classification techniques. Their model identified significant risk factors related to both chronic disease datasets by applying different feature selection techniques and hybridization of Relief Feature Ranking with Principal Component Analysis (PCA) method. Rustam and Hartini (2019) proposed a new ML method based on kernel, which is a modification of KC-Means combining K-Means and Fuzzy C-Means algorithms together with kernel function. They applied C-Means algorithm on the centers of a fixed number of groups founded by K-Means, in order to improve the accuracy of classification. Rashed et al (2019) developed a novel network architecture with an inspiration from U-net structure to predict breast cancer in early stages. Omondiagbe (2019) investigated classification performance of Support Vector Machine (using radial basis kernel), Artificial Neural Networks and Naïve Bayes for breast cancer prediction, focusing on integrating machine learning techniques with feature selection and extraction methods. They proposed a hybrid approach by reducing the number of features with linear discriminant analysis (LDA).

3. Methodology

Literature on the subject of breast cancer prediction is mostly based on traditional methods. As a fairly new discipline, data science takes advantage of vast amounts of data at our disposal today and availability of advanced computational power. These factors make it possible the improvement of existing prediction methods and contribute to the development of new and better algorithms. In this section, we introduce several popular machine learning algorithms for prediction of breast cancer.

3.1. Dataset

The dataset used in this study is publicly available and was created by Dr. William H. Wolberg, physician at the University of Wisconsin Hospital at Madison, Wisconsin, USA. To create the dataset Dr. Wolberg used fluid samples, taken from patients with solid breast masses and a user-friendly graphical software called Xcyt, which is capable of perform the analysis of cytological features based on a digitized image of a fine needle aspiration (FNA) procedure of a breast mass.

The program describes the characteristics of the cell nuclei present in the image and uses a curve-fitting algorithm, to compute ten features from each one of the cells in the sample, than it calculates the mean value, extreme value and standard error of each feature for the image, returning a 30 real-valuated vector. Dataset consists of 569 instances of which 357 instances are benign and 212 are malignant cases. A Digitized Image of FNA is depicted in Figure 1.

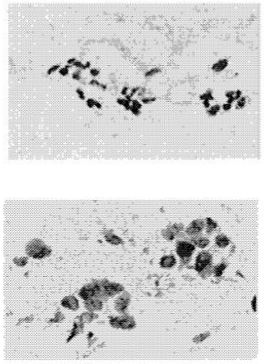

Figure 1. Digitized Image of FNA. Benign (top) and Malignant (bottom).

3.2. Feature selection and preprocessing

Feature Selection is the process of automatically or manually selecting features which contribute most to model prediction. Having irrelevant features in data can decrease the accuracy of the models and make the model learn based on irrelevant features. Feature selection is often confused with dimensionality reduction. The purpose of both methods is to simplify the data that feeds the algorithm. However, while the feature selection inputs the data to the model without altering it, the dimensionality reduction can process the data to obtain data of different structures and sizes.

An important feature of decision tree-based classifiers is that they can analyze the attributes in the dataset well and prioritize the data columns that yield the best results. Using this feature in the Extreme Gradient Boosting algorithm, we extracted the 10 most important features in the Wisconsin Breast Cancer Dataset (shown on Fig.2). This allowed us to simplify the model make better predictions in a reasonable amount of time.

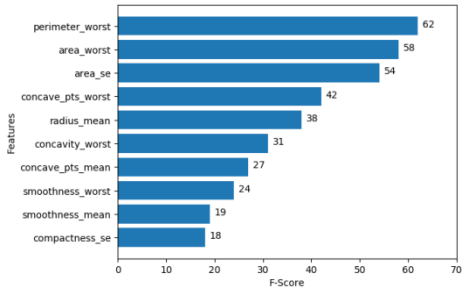

Figure 2. Feature Importance Table for Wisconsin Breast Cancer Dataset

3.3. ML Algorithms

Machine learning models have been employed in the last decade as serious competitors to classical statistical algorithms for prediction (Tokmak & Küçüksille). In machine learning, the ability of a model to predict categorical values based on a training dataset is called classification (ŞENOL & MUSAYEV). In this paper, we used Logistic Regression (Hosmer Jr, Lemeshow, & Sturdivant, 2013; Kleinbaum, Dietz, Gail, Klein, & Klein, 2002; Wright, 1995), K-Nearest Neighbors (Cover & Hart, 1967; Han, Kamber, & Pei, 2011; Ho, 1998), Support Vector Machines (Boser, Guyon, & Vapnik, 1992; Cortes & Vapnik, 1995; Vapnik, 1998), Classification and Regression Tress (Breiman, Friedman, Olshen, & Stone, 1984; Morgan & Sonquist, 1963; Timofeev, 2004), Naïve Bayes (Clark & Niblett, 1989; Frank, Hall, & Pfahringer, 2002; Zheng & Webb, 2000), Support Vector Machines (Boser et al., 1992; Cortes & Vapnik, 1995; Vapnik, 1998), ensemble techniques like Adaboost Classifier (Freund & Schapire, 1997; Li, Wang, & Sung, 2008), Gradient Boosting Classifier (Friedman, 2001, 2002), Random Forest (Breiman, 2001; Liaw & Wiener, 2002), Extreme Gradient Boosting (Chen & Guestrin, 2016; Chen, He, Benesty, Khotilovich, & Tang, 2015; Friedman, 2001) and finally Artificial Neural Networks with Multilayer Perceptron (Hecht-Nielsen, 1992; Mitchell, 1997; Rosenblatt, 1958; Tekin & Çan)

4. Experimental Setup

In order to evaluate the performance of given models, a series of experiments have been conducted. The models have been implemented with Python 3.7 programming language, using Keras framework and Tensorflow as a backend, running on Google Colaboratory Notebook. It is powered by single Tesla K80 GPU on free cloud service.

Initially, we load the dataset and make an exploratory data analysis to extract best features for determining major reasons of malignant tumors. Later, we modify data structure to prepare training on machine learning models. Finally, we apply selected algorithms and record results of their performance for prediction.

We used various advanced performance metrics to evaluate our model. The main score is based on

the accuracy of the model, which basically shows the number of successful predictions. Precision (sensitivity) gives the percentage of the positive predictions that were correctly identified. Recall (specificity) which is another performance metric is the percentage of correctly predicted positive cases. F-measure metric is the harmonic average of the precision and recall. Calculation of those metrics is given in equation 1-4.

$$Accuracy = \frac{TN + FP}{FN + FP + TN + FP} \quad (1)$$

$$F - Measure = \frac{2\ x\ Precision\ x\ Recall}{Precision + Recall} \quad (2)$$

$$Precision = \frac{TP}{FP + TP} \quad (3)$$

$$Recall = \frac{TP}{FN + TP} \quad (4)$$

True Positive (TP): Benign samples classified as benign.
True Negative (TN): Malignant samples classified as malignant.
False Positive (FP): Benign samples classified as malignant.
False Negative (FN): Malignant samples classified as benign.

Confusion Matrix: The confusion matrix provides statistics about correct and incorrect predictions. It makes a comparison of expected values within the test set with the predicted values in the training set. The columns represent the predictions, while the rows indicate actual labels. The chart gives an idea about the performance of the classifier algorithm. Elements of a typical Confusion Matrix are given in Table 1.

Table 1. Elements of Confusion Matrix

	Actual Class		
		Positive (P)	Negative (N)
Predicted Class	True (T)	True Positive (TP)	True Negative (TN)
	False (F)	False Positive (FP)	False Negative (FN)

Cross-Validation (CV): Cross-validation is a technique used for making sure that our model is well trained, without using the test set. It consists in partition data into *k* portions of equal length. For each portion, we train the model on the remaining *k-1* parameters and evaluate it on partition *i*. The overall score is the mean of the *K* scores calculated.

There are two types of cross validation splits:
- Leave one out cross validation
- K-fold cross validation

Leave one out CV cycles over the dataset and removes one test group per iteration that will not be included in the training set but instead will be used to test the model's performance.

K-fold CV takes a K variable as an input, partition the dataset into K parts, cycles over the parts and for each cycle leaves the single portion out of training and use it as a test set.
By using k-fold validation we make sure that the model uses all the training data available for tuning the model, it can be computationally expensive but allows to train models even if little data is available. The main purpose of k-fold validation is to get an unbiased estimate of model generalization on new data.

Stratified k-Fold: In stratified k-fold, the aim is to include the same proportion of data labels for each test portion. For example, if the data has %75 Benign and %25 malignant samples, every fold contains the same percentage of benign and malignant samples.

Repeated k-fold: In repeated cross-validation, the cross-validation procedure is repeated n times, giving n random partitions of the original sample. Mean values of results for each n partition produce a single prediction.

5. Results and Discussion

The results were achieved using 10 fold cross-validation for each model, and are based on the average results obtained. Table 2 shows the complete set of results in a tabular format.

Cross-validation results were auspicious. The results indicate that Support Vector Machines gained top performance when compared to other

nine models. Neural Networks, KNN and Logistic Regression Models have also demonstrated significant success when predicting breast cancer. Naïve Bayes and CART showed relatively poor performance but the prediction rates are at an acceptable level for our problem.

Table 2. Experiment Results

Algorithms	**Cross Validation Accuracy (Mean)**	**Std. (+/- %)**
Logistic Regression (LR)	0.9772	0.0207
K-Nearest Neighbors (KNN)	0.9701	0.0236
Decision Trees (CART)	0.9349	0.0197
Naïve Bayes (NB)	0.9332	0.0376
Support Vector Machines (SVM)	0.9789	0.0131
Adaboost Classifier (ADB)	0.9649	0.0157
Gradient Boosting Classifier (GRAD)	0.9612	0.0307
Random Forests (RF)	0.9613	0.0324
Extreme Gradient Boosting (XGB)	0.9630	0.0269
Neural Networks (MLP)	0.9772	0.0175

Comparison of ML Algorithms has been depicted in Figure 3. Detailed cross validation results for all algorithms have been tabulated at Table 3.

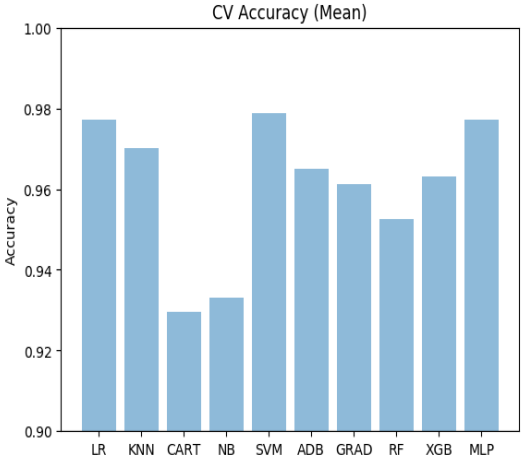

Figure 3. ML Comparison Chart

Table 3. Cross Validation Results for All Algorithms

LOGISTIC REGRESSION (LR)						
Confusion Matrix			Precision	Recall	F1 Score	Acc.
35	1	B	0.9459	0.9722	0.9589	0.9483
2	20	M	0.9523	0.9090	0.9302	
36	0	B	1.0000	1.0000	1.0000	1.0000
0	22	M	1.0000	1.0000	1.0000	
36	0	B	0.9473	1.0000	0.9730	0.9649
2	19	M	1.0000	0.9048	0.9500	
36	0	B	1.0000	1.0000	1.0000	1.0000
0	22	M	1.0000	1.0000	1.0000	
35	1	B	0.9722	0.9722	0.9722	0.9649
1	10	M	0.9524	0.9524	0.9524	
36	0	B	1.0000	1.0000	1.0000	1.0000
0	22	M	1.0000	1.0000	1.0000	
34	2	B	0.9714	0.9444	0.9577	0.9474
1	20	M	0.9091	0.9524	0.9302	
34	1	B	1.0000	0.9714	0.9855	0.9821
0	21	M	0.9545	1.0000	0.9767	
35	0	B	1.0000	1.0000	1.0000	1.0000
0	21	M	1.0000	1.0000	1.0000	
35	0	B	0.9459	1.0000	0.9722	0.9643
2	19	M	1.0000	0.9048	0.9500	
Mean Accuracy :						**0.9772**
Std (+/-) % :						**0.0207**

K-NEAREST NEIGHBOR (KNN)						
Confusion Matrix			Precision	Recall	F1 Score	Acc
35	1	B	0.9211	0.9722	0.9459	0.9310
3	19	M	0.9500	0.8636	0.9048	
36	0	B	0.9730	1.0000	0.9863	0.9828
1	21	M	1.0000	0.9545	0.9767	
35	1	B	0.9722	0.9722	0.9722	0.9649
1	20	M	0.9524	0.9524	0.9524	
36	0	B	0.9730	1.0000	0.9863	0.9825
1	20	M	1.0000	0.9524	0.9756	
36	0	B	0.9730	1.0000	0.9863	0.9825
1	20	M	1.0000	0.9524	0.9756	

36	0	B	1.0000	1.0000	1.0000	1.0000
0	21	M	1.0000	1.0000	1.0000	
36	0	B	0.9474	1.0000	0.9730	0.9649
2	19	M	1.0000	0.9048	0.9500	
35	0	B	1.0000	1.0000	1.0000	1.0000
0	21	M	1.0000	1.0000	1.0000	
35	0	B	0.9459	1.0000	0.9722	0.9643
2	19	M	1.0000	0.9048	0.9500	
34	1	B	0.9189	0.9714	0.9444	0.9286
3	18	M	0.9474	0.8571	0.9000	
Mean Accuracy :						**0.9701**
Std (+/-) % :						**0.0236**

DECISION TREES (CART)						
Confusion Matrix			Precision	Recall	F1 Score	Acc.
35	1	B	0.9459	0.9722	0.9589	0.9483
2	20	M	0.9524	0.9091	0.9302	
34	2	B	0.9444	0.9444	0.9444	0.9310
2	20	M	0.9091	0.9091	0.9091	
33	3	B	0.9429	0.9167	0.9296	0.9123
2	19	M	0.8636	0.9048	0.8837	
35	1	B	0.9459	0.9722	0.9589	0.9474
2	19	M	0.9500	0.9048	0.9268	
33	3	B	0.9706	0.9167	0.9429	0.9298
1	20	M	0.8696	0.9524	0.9091	
33	3	B	1.0000	0.9167	0.9565	0.9474
0	21	M	0.8750	1.0000	9333	
36	0	B	0.9474	1.0000	0.9730	0.9649
2	19	M	1.0000	0.9048	0.9500	
32	3	B	1.0000	0.9143	0.9552	0.9464
0	21	M	0.8750	1.0000	0.9333	
32	3	B	0.9697	0.9143	0.9412	0.9286
1	20	M	0.8696	0.9524	0.9091	
33	2	B	0.8919	0.9429	0.9167	0.8929
4	17	M	0.8947	0.8095	0.8500	
Mean Accuracy :						**0.9349**
Std (+/-) % :						**0.0197**

NAIVE BAYES CLASSIFIER (NB)						
Confusion Matrix			Precision	Recall	F1 Score	Acc
34	2	B	0.9444	0.9444	0.9444	0.9310
2	20	M	0.9091	0.9091	0.9091	
34	2	B	0.9444	0.9444	0.9444	0.9310
2	20	M	0.9091	0.9091	0.9091	
33	3	B	0.9429	0.9167	0.9296	0.9123
2	19	M	0.8636	0.9048	0.8837	
34	2	B	0.9714	0.9444	0.9577	0.9474
1	20	M	0.9091	0.9524	0.9302	
33	3	B	0.8684	0.9167	0.8919	0.8596
5	16	M	0.8421	0.7619	0.8000	
36	0	B	1.0000	1.0000	1.0000	1.0000
0	21	M	1.0000	1.0000	1.0000	
36	0	B	0.9474	1.0000	0.9730	0.9649
2	19	M	1.0000	0.9048	0.9500	
33	2	B	1.0000	0.9429	0.9706	0.9643
0	21	M	0.9130	1.0000	0.9545	
34	1	B	0.9189	0.9714	0.9444	0.9286
3	18	M	0.9474	0.8571	0.9000	
33	2	B	0.8919	0.9429	0.9167	0.8929
4	17	M	0.8947	0.8095	0.8500	
Mean Accuracy :						**0.9332**
Std (+/-) % :						**0.0376**

SUPPORT VECTOR MACHINES (SVM)						
Confusion Matrix			Precision	Recall	F1 Score	Acc.
35	1	B	0.9722	0.9722	0.9722	0.9655
1	21	M	0.9545	0.9545	0.9545	
36	0	B	1.0000	1.0000	1.0000	1.0000
0	22	M	1.0000	1.0000	1.0000	
35	1	B	0.9722	0.9722	0.9722	0.9649
1	20	M	0.9524	0.9524	0.9524	
36	0	B	0.9730	1.0000	0.9863	0.9825
1	20	M	1.0000	0.9524	0.9756	
35	1	B	0.9722	0.9722	0.9722	0.9649
1	20	M	0.9524	0.9524	0.9524	
36	0	B	1.0000	1.0000	1.0000	1.0000

0	21	M	1.0000	1.0000	1.0000	
36	0	B	0.9730	1.0000	0.9863	0.9825
1	20	M	1.0000	0.9524	0.9756	
34	1	B	1.0000	0.9714	0.9855	0.9821
0	21	M	0.9545	1.0000	0.9767	
35	0	B	0.9722	1.0000	0.9859	0.9821
1	20	M	1.0000	0.9524	0.9756	
35	0	B	0.9459	1.0000	0.9722	0.9643
2	19	M	1.0000	0.9048	0.9500	
Mean Accuracy :						**0.9789**
Std (+/-) % :						**0.0131**

ADABOOST CLASSIFIER (ADB)						
Confusion Matrix			Precision	Recall	F1 Score	Acc
35	1	B	0.9459	0.9722	0.9589	0.9483
2	20	M	0.9524	0.9091	0.9302	
35	1	B	0.9722	0.9722	0.9722	0.9655
1	21	M	0.9545	0.9545	0.9545	
35	1	B	0.9459	0.9722	0.9589	0.9474
2	19	M	0.9500	0.9048	0.9268	
36	0	B	0.9730	1.0000	0.9863	0.9825
1	20	M	1.0000	0.9524	0.9756	
35	1	B	0.9459	0.9722	0.9589	0.9474
2	19	M	0.9500	0.9048	0.9268	
35	1	B	1.0000	0.9722	0.9859	0.9825
0	21	M	0.9545	1.0000	0.9767	
35	1	B	1.0000	0.9722	0.9859	0.9825
0	21	M	0.9545	1.0000	0.9767	
34	1	B	1.0000	0.9714	0.9855	0.9821
0	21	M	0.9545	1.0000	0.9767	
35	0	B	0.9459	1.0000	0.9722	0.9643
2	19	M	1.0000	0.9048	0.9500	
34	1	B	0.9444	0.9714	0.9577	0.9464
2	19	M	0.9500	0.9048	0.9268	
Mean Accuracy :						**0.9649**
Std (+/-) % :						**0.0157**

GRADIENT BOOSTING CLASSIFIER (GRAD)					
Confusion Matrix		Precision	Recall	F1 Score	Acc.

35	1	B	0.9722	0.9722	0.9722	0.9655
1	21	M	0.9545	0.9545	0.9545	
35	1	B	0.9722	0.9722	0.9722	0.9655
1	21	M	0.9545	0.9545	0.9545	
36	0	B	0.9730	1.0000	0.9863	0.9825
1	20	M	1.0000	0.9524	0.9756	
35	1	B	0.9722	0.9722	0.9722	0.9649
1	20	M	0.9524	0.9524	0.9524	
35	1	B	0.9459	0.9722	0.9589	0.9474
2	19	M	0.9500	0.9048	0.9268	
36	0	B	1.0000	1.0000	1.0000	1.0000
0	21	M	1.0000	1.0000	1.0000	
35	1	B	0.9722	0.9722	0.9722	0.9649
1	20	M	0.9524	0.9524	0.9524	
35	0	B	1.0000	1.0000	1.0000	1.0000
0	21	M	1.0000	1.0000	1.0000	
35	0	B	0.8974	1.0000	0.9459	0.9286
4	17	M	1.0000	0.8095	0.8947	
33	2	B	0.8919	0.9429	0.9167	0.8929
4	17	M	0.8947	0.8095	0.8500	
Mean Accuracy :						**0.9612**
Std (+/-) % :						**0.0307**

RANDOM FOREST (RF)						
Confusion Matrix			Precision	Recall	F1 Score	Acc
35	1	B	0.9211	0.9722	0.9459	0.9310
3	19	M	0.9500	0.8636	0.9048	
36	0	B	0.9474	1.0000	0.9730	0.9655
2	20	M	1.0000	0.9091	0.9524	
36	0	B	0.9730	1.0000	0.9863	0.9825
1	20	M	1.0000	0.9524	0.9756	
36	0	B	1.0000	1.0000	1.0000	1.0000
0	21	M	1.0000	1.0000	1.0000	
35	1	B	0.9211	0.9722	0.9459	0.9298
3	18	M	0.9474	0.8571	0.9000	
36	0	B	1.0000	1.0000	1.0000	1.0000
0	21	M	1.0000	1.0000	1.0000	
36	0	B	0.9730	1.0000	0.9863	0.9825
1	20	M	1.0000	0.9524	0.9756	

33	2	B	1.0000	0.9429	0.9706	0.9643
0	21	M	0.9130	1.0000	0.9545	
35	0	B	0.9459	1.0000	0.9722	0.9643
2	19	M	1.0000	0.9048	0.9500	
33	2	B	0.8919	0.9429	0.9167	0.8929
4	17	M	0.8947	0.8095	0.8500	
Mean Accuracy :						**0.9613**
Std (+/-) % :						**0.0324**

EXTREME GRADIENT BOOSTING (XGB)						
Confusion Matrix			Precision	Recall	F1 Score	Acc.
35	1	B	0.9722	0.9722	0.9722	0.9655
1	21	M	0.9545	0.9545	0.9545	
34	2	B	0.9714	0.9444	0.9577	0.9483
1	21	M	0.9130	0.9545	0.9333	
36	0	B	0.9730	1.0000	0.9863	0.9825
1	20	M	1.0000	0.9524	0.9756	
36	0	B	0.9730	1.0000	0.9863	0.9825
1	20	M	1.0000	0.9524	0.9756	
35	1	B	0.9459	0.9722	0.9589	0.9474
2	19	M	0.9500	0.9048	0.9268	
36	0	B	1.0000	1.0000	1.0000	1.0000
0	21	M	1.0000	1.0000	1.0000	
36	0	B	0.9730	1.0000	0.9863	0.9825
1	20	M	1.0000	0.9524	0.9756	
34	1	B	1.0000	0.9714	0.9855	0.9821
0	21	M	0.9545	1.0000	0.9767	
35	0	B	0.8974	1.0000	0.9459	0.9286
4	17	M	1.0000	0.8095	0.8947	
34	1	B	0.8947	0.9714	0.9315	0.9107
4	17	M	0.9444	0.8095	0.8718	
Mean Accuracy :						**0.9630**
Std (+/-) % :						**0.0269**

NEURAL NETWORK (MLP)						
Confusion Matrix			Precision	Recall	F1 Score	Acc
35	1	B	0.9459	0.9722	0.9589	0.9483
2	20	M	0.9	0.9091	0.930	
			524		2	
36	0	B	1.0000	1.0000	1.0000	1.0000
0	22	M	1.0000	1.0000	1.0000	
36	0	B	0.9474	1.0000	0.9730	0.9649
2	19	M	1.0000	0.9048	0.9500	
36	0	B	1.0000	1.0000	1.0000	1.0000
0	21	M	1.0000	1.0000	1.0000	
35	1	B	0.9722	0.9722	0.9722	0.9649
1	20	M	0.9524	0.9524	0.9524	
35	1	B	1.0000	0.9722	0.9859	0.9825
0	21	M	0.9545	1.0000	0.9767	
35	1	B	0.9722	0.9722	0.9722	0.9649
1	20	M	0.9524	0.9524	0.9524	
34	1	B	1.0000	0.9714	0.9855	0.9821
0	21	M	0.9545	1.0000	0.9767	
35	0	B	1.0000	1.0000	1.0000	1.0000
0	21	M	1.0000	1.0000	1.0000	
35	0	B	0.9459	1.0000	0.9722	0.9643
2	19	M	1.0000	0.9048	0.9500	
Mean Accuracy :						**0.9772**
Std (+/-) % :						**0.0175**

In order to evaluate overall performance of an algorithm, learning curves can be utilized to measure how many training sample is required to reach optimum performance. Learning curves depict the test and training score of a classifier for various lengths of training samples. It is a visual indicator of how the performance is increased by adding new training samples and whether the classifier is adversely affected from a variance error or a bias error. Learning curves for the algorithms are depicted on Figure 4.

Gap between the two curves shown above, determines the interpretation of the models in the bias-variance landscape. A narrow distance shows

low variance. On the contrary, a wide gap indicates that validation error will generally be higher. If we change the training set sizes, the pattern will likely to continue, and the value between training and validation errors will draw that distance between the two learning curves. If a model performs better on the training set and poor on the test set, overfitting will occur.

Learning curves of above models clearly demonstrate that KNN and Logistic Regression show significant performance with less training examples. Although, performing best among the other models, SVM needs more samples to reach best accuracy.

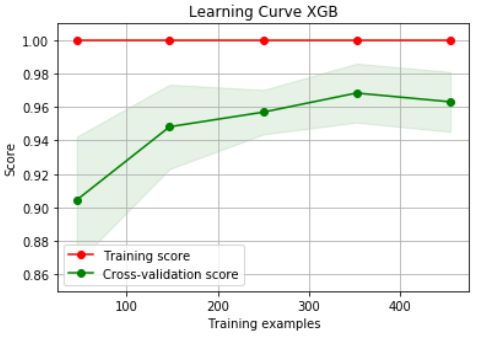

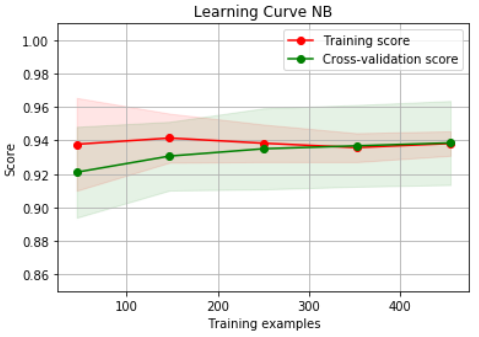

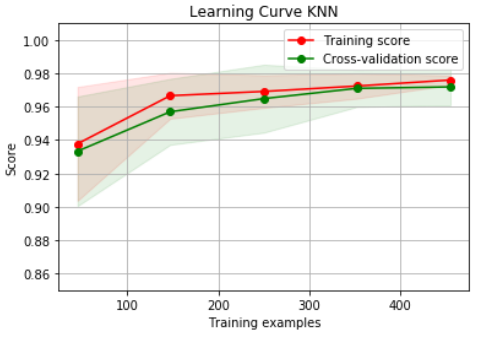

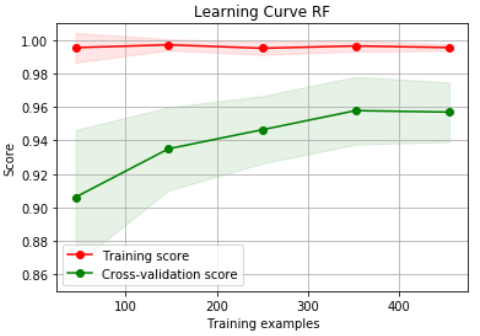

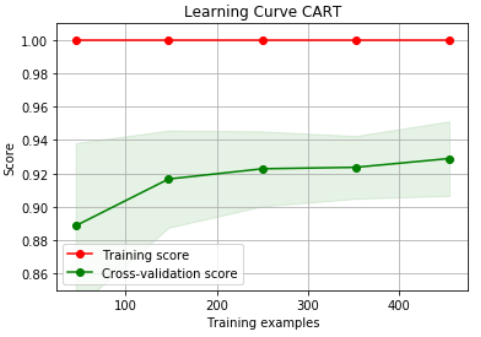

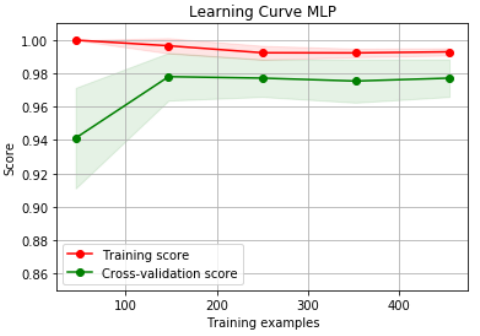

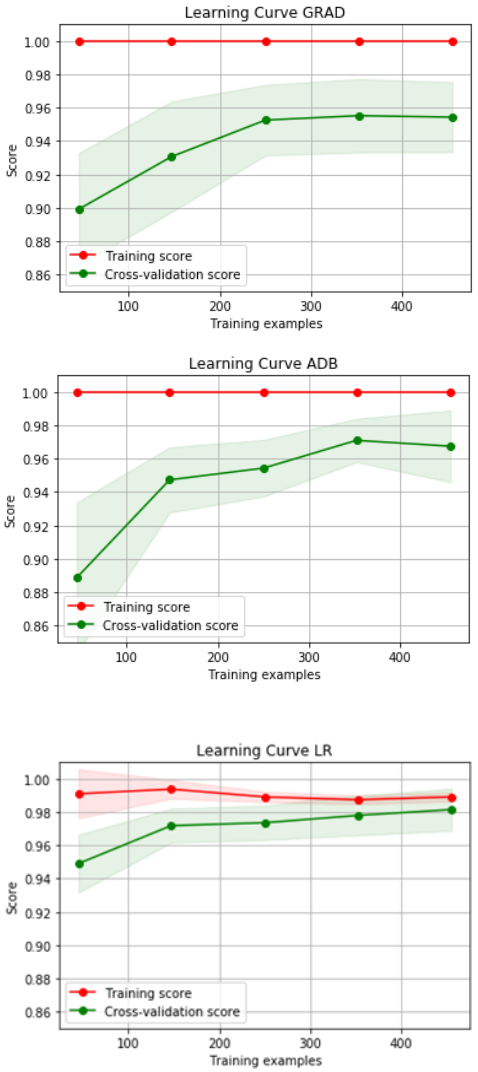

Figure 4. Learning Curves for ML Algorithms

6. Conclusions and Future Work

This paper presented a comparison between several classification techniques in machine learning (Logistic Regression, K-Nearest Neighbors (KNN), Decision Trees (CART), Naïve Bayes, Support Vector Machines (SVM), Adaboost Classifier, Gradient Boosting Classifier, Random Forests, Extreme Gradient Boosting and Neural Networks), for the prediction of breast cancer. The selected techniques were applied to the well-known 'Wisconsin Breast Cancer dataset' as a part of UCI data repository. The results showed that all methods performed remarkable performance, while LR, SVM and MLP gained the best metrics.

We also have identified which features contribute to predict breast cancer by using tree based classifiers. Application of data visualization and data analytics techniques, together with the application of data science tools, allowed the understanding of feature's predictive relevance.

Our ongoing research efforts are geared toward applying advanced Machine Learning techniques to recent real world problems on various domains and increasing the prediction performance with fine-tuning of hyper parameters.

Code for the models can be found on Github repository:
https://github.com/htanerunal/breast_cancer/blob/master/breast_cancer_ML_comparison.ipynb

Acknowledgment

We would like to express gratitude to our families for their patience and continuous support.

References

Agarap, A. F. M. (2018). *On breast cancer detection: an application of machine learning algorithms on the wisconsin diagnostic dataset.* Paper presented at the Proceedings of the 2nd International Conference on Machine Learning and Soft Computing.

Akay, M. F. (2009). Support vector machines combined with feature selection for breast cancer diagnosis. *Expert Systems with Applications*, *36*(2), 3240-3247.

American Cancer Society. (2018). "Cancer Facts & Figures 2018". *Atlanta, American Cancer Society*.

Boser, B. E., Guyon, I. M., & Vapnik, V. N. (1992). *A training algorithm for optimal margin classifiers.* Paper presented at the Proceedings of the fifth annual workshop on Computational learning theory.

Breiman, L. (2001). Random forests. *Machine learning*, *45*(1), 5-32.

Breiman, L., Friedman, J., Olshen, R., & Stone, C. (1984). Classification and regression trees. Wadsworth Int. *Group*, *37*(15), 237-251.

Chen, T., & Guestrin, C. (2016). *Xgboost: A scalable tree boosting system.* Paper presented at the Proceedings of the 22nd

acm sigkdd international conference on knowledge discovery and data mining.

Chen, T., He, T., Benesty, M., Khotilovich, V., & Tang, Y. (2015). Xgboost: extreme gradient boosting. *R package version 0.4-2*, 1-4.

Clark, P., & Niblett, T. (1989). The CN2 induction algorithm. *Machine learning*, *3*(4), 261-283.

Cortes, C., & Vapnik, V. (1995). Soft margin classifiers. *Machine learning*, *20*, 273-297.

Cover, T. M., & Hart, P. (1967). Nearest neighbor pattern classification. *IEEE transactions on information theory*, *13*(1), 21-27.

Frank, E., Hall, M., & Pfahringer, B. (2002). *Locally weighted naive bayes.* Paper presented at the Proceedings of the Nineteenth conference on Uncertainty in Artificial Intelligence.

Freund, Y., & Schapire, R. E. (1997). A decision-theoretic generalization of on-line learning and an application to boosting. *Journal of computer and system sciences*, *55*(1), 119-139.

Friedman, J. H. (2001). Greedy function approximation: a gradient boosting machine. *Annals of statistics*, 1189-1232.

Friedman, J. H. (2002). Stochastic gradient boosting. *Computational statistics & data analysis*, *38*(4), 367-378.

Han, J., Kamber, M., & Pei, J. (2011). Data mining concepts and techniques third edition. *The Morgan Kaufmann Series in Data Management Systems*, 83-124.

Hecht-Nielsen, R. (1992). Theory of the backpropagation neural network. In *Neural networks for perception* (pp. 65-93): Elsevier.

Ho, T. K. (1998). *Nearest neighbors in random subspaces.* Paper presented at the Joint IAPR International Workshops on Statistical Techniques in Pattern Recognition (SPR) and Structural and Syntactic Pattern Recognition (SSPR).

Hosmer Jr, D. W., Lemeshow, S., & Sturdivant, R. X. (2013). *Applied logistic regression* (Vol. 398): John Wiley & Sons.

Jain, D., & Singh, V. (2018). *Diagnosis of Breast Cancer and Diabetes using Hybrid Feature Selection Method.* Paper presented at the 2018 Fifth International Conference on Parallel, Distributed and Grid Computing (PDGC).

Kadam, V. J., Jadhav, S. M., & Vijayakumar, K. (2019). Breast Cancer Diagnosis Using Feature Ensemble Learning Based on Stacked Sparse Autoencoders and Softmax Regression. *Journal of medical systems*, *43*(8), 263.

Kleinbaum, D. G., Dietz, K., Gail, M., Klein, M., & Klein, M. (2002). *Logistic regression*: Springer.

Li, X., Wang, L., & Sung, E. (2008). AdaBoost with SVM-based component classifiers. *Engineering Applications of Artificial Intelligence*, *21*(5), 785-795.

Liaw, A., & Wiener, M. (2002). Classification and regression by randomForest. *R news*, *2*(3), 18-22.

Mitchell, T. M. (1997). Machine learning. 1997. *Burr Ridge, IL: McGraw Hill*, *45*(37), 870-877.

Morgan, J. N., & Sonquist, J. A. (1963). Problems in the analysis of survey data, and a proposal. *Journal of the American statistical association*, *58*(302), 415-434.

Omondiagbe, D. A., Veeramani, S., & Sidhu, A. S. (2019). *Machine Learning Classification Techniques for Breast Cancer Diagnosis.* Paper presented at the IOP Conference Series: Materials Science and Engineering.

Polat, K., & Güneş, S. (2007). Breast cancer diagnosis using least square support vector machine. *Digital signal processing*, *17*(4), 694-701.

Rashed, E., & El Seoud, M. (2019). *Deep learning approach for breast cancer diagnosis.* Paper presented at the Proceedings of the 2019 8th International Conference on Software and Information Engineering.

Rosenblatt, F. (1958). The perceptron: a probabilistic model for information storage and organization in the brain. *Psychological review*, *65*(6), 386.

Rustam, Z., & Hartini, S. (2019). *Classification of Breast Cancer using Fast Fuzzy Clustering based on Kernel.* Paper presented at the IOP Conference Series: Materials Science and Engineering.

Sadhukhan, S., Upadhyay, N., & Chakraborty, P. (2020). Breast Cancer Diagnosis Using Image Processing and Machine Learning. In *Emerging Technology in Modelling and Graphics* (pp. 113-127): Springer.

Sethi, A. (2018). *Analogizing of Evolutionary and Machine Learning Algorithms for Prognosis of Breast Cancer.* Paper presented at the 2018 7th International Conference on Reliability, Infocom Technologies and Optimization (Trends and Future Directions)(ICRITO).

Siegel, R., & Jemal, A. (2015). Cancer facts & figures 2015. *American Cancer Society Cancer Facts & Figures*.

Sri, M. N., Sailaja, D., Priyanka, J. H., Chittineni, S., & RamaKrishnaMurthy, M. (2019). *Performance Evaluation of SVM and Neural Network Classification Methods for Diagnosis of Breast Cancer.* Paper presented at the International Conference on E-Business and Telecommunications.

ŞENOL, Ü., & MUSAYEV, Z. Estimating Wind Energy Potential by Artificial Neural Networks Method. *Bilge International Journal of Science and Technology Research, 1*(1), 23-31.

Tekin, S., & Çan, T. Yapay Sinir Ağları Yöntemi ile Ermenek Havzası'nın (Karaman) Kayma Türü Heyelan Duyarlılık Değerlendirmesi. *Bilge International Journal of Science and Technology Research, 3*(1), 21-28.

Timofeev, R. (2004). Classification and regression trees (CART) theory and applications. *Humboldt University, Berlin*.

Tokmak, M., & Küçüksille, E. U. Kötü Amaçlı Windows Çalıştırılabilir Dosyalarının Derin Öğrenme İle Tespiti. *Bilge International Journal of Science and Technology Research, 3*(1), 67-76.

Vapnik, V. (1998). Statistical Learning Theory Wiley-Interscience. *New York*.

Wright, R. E. (1995). Logistic regression.

Yue, W., Wang, Z., Chen, H., Payne, A., & Liu, X. (2018). Machine learning with applications in breast cancer diagnosis and prognosis. *Designs, 2*(2), 13.

Zheng, Z., & Webb, G. I. (2000). Lazy learning of Bayesian rules. *Machine learning, 41*(1), 53-84.

Bilge International Journal of Science and Technology Research

Web : http://dergipark.gov.tr/bilgesci - **E-mail:** kutbilgescience@gmail.com

Received: 12.11.2019
Accepted: 25.12.2019
DOI: 10.30516/bilgesci.646126

ISSN: 2651-401X
e-ISSN: 2651-4028
3(Special Issue), 21-34, 2019

Classification of the Monolithic Columns Produced in Troad and Mysia Region Ancient Granite Quarries in Northwestern Anatolia via Soft Decision-Making

Serdar Enginoğlu[1*], Murat Ay[2], Naim Çağman[3], Veysel Tolun[2]

Abstract: Ay and Tolun [An Archaeometric Approach on the Distribution of Troadic Granite Columns in the Western Anatolian Coasts. Journal of Archaeology & Art, 156, 2017, 119-130 (In Turkish)] have analysed the distribution of the monolithic columns produced in the ancient granite quarries, located in Troad Region and Mysia Region in Northwestern Anatolia, by archaeometric analyses. Moreover, they have achieved some results by interpreting the prominent data obtained therein. In this study, we propose a novel soft decision-making method, i.e. Monolithic Columns Classification Method (MCCM), constructed via fuzzy parameterized fuzzy soft matrices (*fpfs*-matrices) and Prevalence Effect Method (PEM). MCCM provides an outcome by interpreting all the results of the analyses mentioned above. We then apply the method to the problem of monolithic columns classification. Finally, we discuss the need for further research.

Keywords: Ancient Granite Quarries, Classification, *fpfs*-matrices, Monolithic Columns, Soft Decision-Making

1. Introduction

In the Roman Imperial Period, Troad Region and Mysia Region are two essential regions contained ancient granite quarries (Figure 1. a.) (Galetti et al., 1992; Williams-Thorpe and Thorpe, 1993; Williams-Thorpe and Henty, 2000) such as Koçali (Figure 1. b.), Akçakeçili (Figure 1. c.), and Kozak (Figure 1. d.) which known to be produced monolithic granite columns in Anatolia. While Koçali and Akçakeçili ancient granite quarries in Troad Region (Ponti, 1995; Ay, 2017; Ay and Tolun, 2017a, b) are located in Ezine/Çanakkale, Kozak ancient granite quarry in Mysia Region (Williams-Thorpe et al., 2000) is located in Bergama/Izmir.

However, there are not exist a sufficient number of an archaeological document about some subjects such as the exportation of the columns produced in these centres located in Troad and Mysia Region.

[1]Department of Mathematics, Faculty of Arts and Sciences, Çanakkale Onsekiz Mart University, Çanakkale, Turkey
[2]Department of Archaeology, Faculty of Arts and Sciences, Çanakkale Onsekiz Mart University, Çanakkale, Turkey
[3]Department of Mathematics, Faculty of Arts and Sciences, Tokat Gaziosmanpaşa University, Tokat, Turkey
*Corresponding author (İletişim yazarı): serdarenginoglu@gmail.com

For this reason, to locate the source of a column considered in an ancient city, the method commonly used is to compare some archaeological samples taken from this city and some geological samples taken from the granite quarries by using mineralogical-petrographic and geochemical analyses (Williams-Thorpe and Thorpe, 1993; Williams-Thorpe and Henty, 2000; Williams-Thorpe et al., 2000; Potts, 2002; Williams-Thorpe, 2008; Ay, 2017; Ay and Tolun, 2017b).

The mineralogical-petrographic analyses are an examination of the samples in a microscopic environment using their thin sections. These analyses carry out to determine the types, quantities, sizes, and shapes of the minerals forming the rock types, main and secondary components of the samples (Galetti et al., 1992; Williams-Thorpe, 2008; Ay, 2017; Ay and Tolun,

Citation (Atıf): Enginoğlu, S., Ay, M., Çağman, N., Tolun, V. (2019). Classification of the Monolithic Columns Produced in Troad and Mysia Region Ancient Granite Quarries in Northwestern Anatolia via Soft Decision-Making. Bilge International Journal of Science and Technology Research, 3(Special Issue):21-34.

2017b). The geochemical analyses perform in determining the type and number of major elements contained in the samples (Galetti et al., 1992; Potts, 2002; Williams-Thorpe, 2008).

Recently, Ay and Tolun have examined the distribution in Northwestern Anatolia of the monolithic columns produced in the ancient granite quarries, located in Troad Region and Mysia Region, by using archaeometric methods (Ay, 2017; Ay and Tolun, 2017b). For this aim, by using the qualitative mineralogical-petrographic and geochemical analyses, they have compared the geological samples taken from Koçali-Akçakeçili ancient quarries in Troad Region and Kozak ancient quarry in Mysia Region with the archaeological samples taken from Smintheion (Smintheion 1, Smintheion 2), Pergamon Red Hall/Serapeion, Smyrna Agora (Smyrna Agora 1, Smyrna Agora 2), Tlos Stadium, Tlos Theatre, and Side Theatre.

Moreover, Ay and Tolun have divided the samples into two groups as ancient granite quarries and ancient city (Figure 2). They first have compared the results of each group in itself. Afterwards, they have compared separately the archaeological samples with the geological samples and have revealed which archaeological samples are more similar to which geological.

The results show that the granite columns in Smintheion 1, Smintheion 2, Smyrna Agora 2, Tlos Stadium, and Side Theatre may originate from the Koçali-Akçakeçili granite quarries located in Troad Region while the others may originate from Kozak quarry located in Mysia Region.

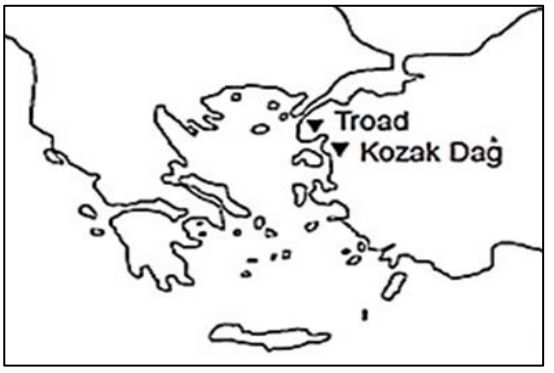

a.

b.

c.

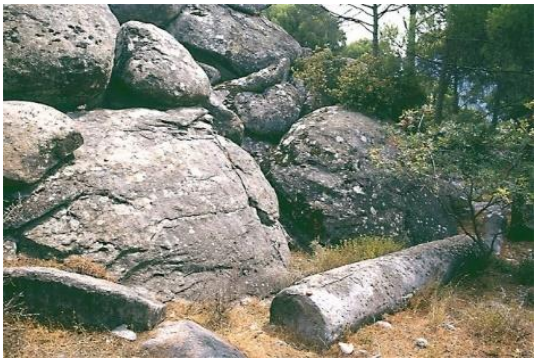

d.

Figure 1. a. Troad and Kozak ancient quarries in the Roman period (Williams-Thorpe, 2008) b. Akçakeçili quarry c. Koçali quarry d. Kozak quarry (De Vecchi et al., 2000)

The concept of soft sets was introduced by Molodtsov (1999) to cope with uncertainty and have been applied to many areas from analysis to decision-making problems (Maji et al., 2001; Çağman and Enginoğlu, 2010; Çağman et al., 2010; Çağman et al., 2011a; Çağman and Deli, 2012; Deli and Çağman, 2015; Enginoğlu and Demiriz, 2015; Enginoğlu and Dönmez, 2015; Enginoğlu et al., 2015; Karaaslan, 2016; Şenel, 2016; Zorlutuna and Atmaca, 2016; Atmaca, 2017; Bera et al., 2017; Çıtak and Çağman, 2017; Şenel, 2017; Çıtak, 2018; Enginoğlu and Memiş,

2018a, b, c, d; Enginoğlu et al., 2018a, b, c, d; Gulistan et al., 2018; Mahmood et al., 2018; Riaz and Hashmi, 2018; Riaz et al., 2018; Şenel, 2018; Ullah et al., 2018). Recently, some soft decision-making methods constructed by fuzzy parameterized fuzzy soft matrices (*fpfs*-matrices) have enabled data processing in many problems containing uncertainty. Being one of these methods, Prevalence Effect Method (PEM) (Enginoğlu and Çağman, In Press) has been applied to a performance-based value assignment to some methods used in noise removal so that the methods can be ordered in terms of performance. We use this method for classification the monolithic columns mentioned in (Ay, 2017; Ay and Tolun, 2017b). The results show that Monolithic Columns Classification Method (MCCM) is successfully model the monolithic columns classification (MCC) problem. Here, *fpfs*-matrices have a row consisting of the significance degrees (membership degrees) of the parameters. These values are usually determined by consulting an expert.

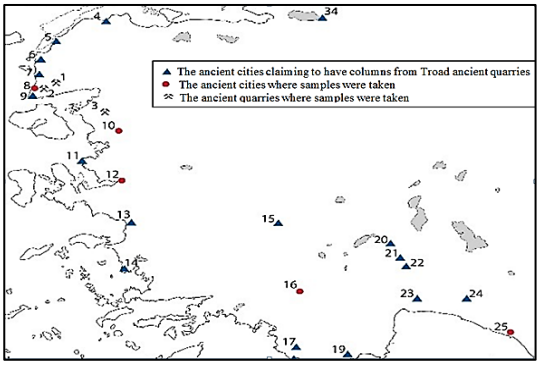

Figure 2. The estimated-distribution of Troad granite columns in Western Anatolia (Ay and Tolun, 2017b)

In this study, we have identified the values, that is, the weights of archaeometric and geochemical parameters, concerning the opinions mentioned in (Ay, 2017; Ay and Tolun, 2017b). Moreover, Ay and Tolun have considered of more effective the geochemical data than the archaeometric data. Therefore, we set a higher value to geochemical data than archaeometric data in the final decision step.

In Section 2 of the present study, we present the concept of *fpfs*-matrices and PEM. In Section 3, we give all the results of the qualitative mineralogical-petrographic and geochemical analyses provided in (Ay, 2017; Ay and Tolun, 2017b). In Section 4, we propose a new method, i.e. MCCM. In section 5, we apply MCCM to the MCC problem. Finally, we discuss the need for further research.

2. Preliminaries

In this section, we first present the concept of fuzzy soft matrices (*fs*-matrices) (Çağman and Enginoğlu, 2012). Throughout this paper, let U be universal set, E be a parameter set, $F(E)$ be the set of all fuzzy sets over E, and $\mu \in F(E)$. Here, a fuzzy set is denoted by $\left\{{}^{\mu(x)}x : x \in E\right\}$.

Definition 2.1. (Çağman et al., 2011b) Let U be a universal set, E be a parameter set, and α be a function from E to $F(U)$. Then, the set $\{(x, \alpha(x)) : x \in E\}$ being the graphic of α is called a fuzzy soft set (*fs*-set) parameterized via E over U (or briefly over U).

In the present paper, the set of all *fs*-sets over U is denoted by $FS_E(U)$. In $FS_E(U)$, since the graphic of α $(graph(\alpha))$ and α generate each other uniquely, the notations are interchangeable. Therefore, as long as it does not cause any confusion, we denote an *fs*-set $graph(\alpha)$ by α.

Example 2.1. Let $E = \{x_1, x_2, x_3, x_4\}$ and $U = \{u_1, u_2, u_3, u_4, u_5\}$. Then,

$$\alpha = \{(x_1, \{{}^{0.9}u_1, {}^{0.5}u_4\}), (x_2, \{{}^{0.3}u_2, {}^{0.5}u_3\}), (x_3, \{{}^{0.7}u_1, {}^{0.8}u_3, {}^{0.6}u_4\}), (x_4, \{u_3, {}^{0.9}u_5\})\}$$

is an *fs*-set over U. Here, for brevity, the notation u_3 is used instead of ${}^{1}u_3$ and also the elements which have zero membership value such as ${}^{0}u_3$ does not show in the sets containing them.

Definition 2.2. (Çağman and Enginoğlu, 2012) Let $\alpha \in FS_E(U)$. Then, $[a_{ij}]$ is called the matrix representation of α (or briefly *fs*-matrix of α) and is defined by

$$[a_{ij}] := \begin{bmatrix} a_{11} & a_{12} & a_{13} & \dots & a_{1n} & \dots \\ a_{21} & a_{22} & a_{23} & \cdots & a_{2n} & \cdots \\ \vdots & \vdots & \vdots & \ddots & \vdots & \vdots \\ a_{m1} & a_{m2} & a_{m3} & \dots & a_{mn} & \dots \\ \vdots & \vdots & \vdots & \ddots & \vdots & \ddots \end{bmatrix}$$

such that for $i \in \{1,2,\cdots\}$ and $j \in \{1,2,\cdots\}$, $a_{ij} := \alpha(x_j)(u_i)$, where $\alpha(x_j)(u_i)$ refers to the membership degree of u_i in the fuzzy set $\alpha(x_j)$.Here, if $|U| = m$ and $|E| = n$, then $[a_{ij}]$ has order $m \times n$.

From now on, the set of all *fs*-matrices parameterized via E over U is denoted by $FS_E[U]$.

Example 2.2. The *fs*-matrix of α provided in Example 2.1 is as follows:

$$[a_{ij}] = \begin{bmatrix} 0.9 & 0 & 0.7 & 0 \\ 0 & 0.3 & 0 & 0 \\ 0 & 0.5 & 0.8 & 1 \\ 0.5 & 0 & 0.6 & 0 \\ 0 & 0 & 0 & 0.9 \end{bmatrix}$$

Secondly, we present the concept of *fpfs*-matrices.

Definition 2.3. (Çağman et al., 2010; Enginoğlu, 2012) Let U be a universal set, $\mu \in F(E)$, and α be a function from μ to $F(U)$. Then, the set $\{({}^{\mu(x)}x, \alpha({}^{\mu(x)}x)) : x \in E\}$ being the graphic of α is called a fuzzy parameterized fuzzy soft set (*fpfs*-set) parameterized via E over U (or briefly over U).

In the present paper, the set of all *fpfs*-sets over U is denoted by $FPFS_E(U)$. In $FPFS_E(U)$, since the $graph(\alpha)$ and α generate each other uniquely, the notations are interchangeable. Therefore, as long as it does not cause any confusion, we denote an *fpfs*-set $graph(\alpha)$ by α.

Example 2.3. Let $E = \{x_1, x_2, x_3, x_4\}$ and $U = \{u_1, u_2, u_3, u_4, u_5\}$. Then,

$\alpha = \{({}^{0.8}x_1, \{{}^{0.9}u_1, {}^{0.5}u_4\}), ({}^{0}x_2, \{{}^{0.3}u_2, {}^{0.5}u_3\}), ({}^{0.1}x_3, \{{}^{0.7}u_1, {}^{0.8}u_3, {}^{0.6}u_4\}), ({}^{1}x_4, \{{}^{1}u_3, {}^{0.9}u_5\})\}$ is an *fpfs*-set over U.

Definition 2.4. (Enginoğlu, 2012; Enginoğlu and Çağman, In Press) Let $\alpha \in FPFS_E(U)$. Then, $[a_{ij}]$ is called the matrix representation of α (or briefly *fpfs*-matrix of α) and is defined by

$$[a_{ij}] \coloneqq \begin{bmatrix} a_{01} & a_{02} & a_{03} & \dots & a_{0n} & \dots \\ a_{11} & a_{12} & a_{13} & \dots & a_{1n} & \dots \\ \vdots & \vdots & \vdots & \ddots & \vdots & \vdots \\ a_{m1} & a_{m2} & a_{m3} & \dots & a_{mn} & \dots \\ \vdots & \vdots & \vdots & \ddots & \vdots & \ddots \end{bmatrix}$$

such that for $i \in \{0,1,2,\cdots\}$ and $j \in \{1,2,\cdots\}$,

$$a_{ij} \coloneqq \begin{cases} \mu(x_j), & i = 0 \\ \alpha({}^{\mu(x_j)}x_j)(u_i), & i \neq 0 \end{cases}$$

Here, if $|U| = m - 1$ and $|E| = n$, then $[a_{ij}]$ has order $m \times n$.

Herein, the set of all *fpfs*-matrices parameterized via E over U is denoted by $FPFS_E[U]$.

Example 2.4. The *fpfs*-matrix of α provided in Example 2.3 is as follows:

$$[a_{ij}] = \begin{bmatrix} 0.8 & 0 & 0.1 & 1 \\ 0.9 & 0 & 0.7 & 0 \\ 0 & 0.3 & 0 & 0 \\ 0 & 0.5 & 0.8 & 1 \\ 0.5 & 0 & 0.6 & 0 \\ 0 & 0 & 0 & 0.9 \end{bmatrix}$$

Definition 2.5. (Enginoğlu, 2012; Enginoğlu and Çağman, In Press) Let $[a_{ij}] \in FPFS_E[U]$. For all i and j, if $a_{ij} = \lambda$, then $[a_{ij}]$ is called λ-*fpfs*-matrix and is denoted by $[\lambda]$. Here, $[0]$ is called empty *fpfs*-matrix and $[1]$ is called universal *fpfs*-matrix.

Definition 2.6. (Enginoğlu, 2012; Enginoğlu and Çağman, In Press) Let $[a_{ij}], [b_{ij}], [c_{ij}] \in FPFS_E[U]$. For all i and j, if $c_{ij} \coloneqq |a_{ij} - b_{ij}|$, then $[c_{ij}]$ is called symmetric difference between $[a_{ij}]$ and $[b_{ij}]$ and is denoted by $[a_{ij}]\tilde{\Delta}[b_{ij}]$.

Finally, we present the soft decision-making method PEM provided in (Enginoğlu and Çağman, In Press). Throughout this paper, $I_n \coloneqq \{1,2,\dots,n\}$ and $I_n^* \coloneqq \{0,1,2,\dots,n\}$.

PEM Algorithm Steps

Step 1. Construct an *fpfs*-matrix $[a_{ij}]_{(m+1)\times n}$ such that $i \in I_m^*$ and $j \in I_n$

Step 2. Obtain a matrix $[s_{i1}]$ defined by

$$s_{i1} \coloneqq \sum_{j=1}^{n} \left[\left(\frac{1}{m} \sum_{k=1}^{m} a_{kj} \right) \left(\frac{1}{n} \sum_{t=1}^{n} a_{it} \right) a_{0j} a_{ij} \right], i \in I_m$$

Step 3. Obtain a decision set $\left\{ \frac{s_{i1}}{\max_k s_{k1}} u_i \mid u_i \in U \right\}$

3. The Qualitative Mineralogical-Petrographic and Geochemical Analyses Results

In this section, we give tables of the results of the qualitative mineralogical-petrographic and geochemical analyses provided in (Ay, 2017; Ay and Tolun, 2017b). The qualitative mineralogical-petrographic analyses result from Koçali and Akçakeçili are the same, and the geochemical analyses results are close to each other. Since Koçali and Akçakeçili ancient quarries are the same structure, Ay and Tolun have compared eight samples with two sources: Bergama Kozak and Koçali-Akçakeçili in (Ay, 2017; Ay and Tolun, 2017b). Therefore, in the next section, we use the mean results from Koçali and Akçakeçili.

Table 1. Results of the mineralogical-petrographic analyses of alkali feldspars in thin sections

Alkali Feldspars	*Coarse–Medium–Fine*	*Coarse –Medium*	*Medium–Fine*	*Fine*	*Chloritised*	*Sericitised*	*Pertitic*	*Mirmekitic*	*Carbonated*	*Clayed*	*Idiomorphic*	*Hypidiomorphic*	*Xenomorphic*	*Homogeneous*	*Recrystallised*	*Prismatic*	*Flat Prismatic*	*Clean-Surfaced*	*Twinning*
Side Theatre	0	0	1	0	0	0	0	0	0	0	0	0	1	0	0	0	0	0	0
Tlos Theatre	0	0	1	0	0	0	0	0	0	0	0	0	1	0	0	0	0	0	0
Tlos Stadium	1	0	0	0	0	0	0	0	0	0	0	0	1	0	0	0	0	0	0
Smyrna Agora 1	0	0	1	0	0	0	0	0	0	0	0	0	1	0	0	0	0	0	0
Smyrna Agora 2	1	0	0	0	0	0	1	0	0	1	0	0	1	1	0	0	0	0	0
Pergamon Red Hall	1	0	0	0	0	0	0	1	0	1	0	0	1	1	0	0	0	0	0
Smintheion 1	0	0	1	0	0	0	0	0	0	1	0	1	0	0	0	0	0	0	0
Smintheion 2	0	1	0	0	0	0	1	0	0	1	0	1	0	0	0	0	0	0	0
Bergama Kozak	0	0	1	0	0	0	1	1	0	1	0	0	1	1	0	0	0	0	0
Koçali	1	0	0	0	0	0	1	1	0	1	0	1	1	1	0	0	0	0	1
Akçakeçili	1	0	0	0	0	0	1	1	0	1	0	1	1	1	0	0	0	0	1

Table 2. Results of the mineralogical-petrographic analyses of amphiboles in thin-sections

Amphiboles	*Coarse–Medium–Fine*	*Coarse –Medium*	*Medium–Fine*	*Fine*	*Chloritised*	*Sericitised*	*Pertitic*	*Mirmekitic*	*Carbonated*	*Clayed*	*Idiomorphic*	*Hypidiomorphic*	*Xenomorphic*	*Homogeneous*	*Recrystallised*	*Prismatic*	*Flat Prismatic*	*Clean-Surfaced*	*Twinning*
Side Theatre	0	0	0	1	0	0	0	0	0	0	1	1	0	0	0	0	0	0	0
Tlos Theatre	0	0	0	1	0	0	0	0	0	0	1	1	0	0	0	0	0	0	0
Tlos Stadium	0	0	1	0	0	0	0	0	0	0	1	1	0	0	0	0	0	0	0
Smyrna Agora 1	0	0	0	1	0	0	0	0	0	0	0	1	0	0	0	0	0	0	0
Smyrna Agora 2	1	0	1	0	0	0	0	0	0	0	0	1	0	1	0	1	0	0	0
Pergamon Red Hall	1	0	1	0	1	0	0	0	1	0	0	1	0	1	0	1	0	0	0
Smintheion 1	0	0	0	1	0	0	0	0	0	0	0	1	0	0	0	0	0	0	0
Smintheion 2	0	0	1	0	0	0	0	0	0	0	0	1	0	0	0	0	0	0	0
Bergama Kozak	0	0	1	0	0	0	0	0	1	0	1	1	0	1	0	1	0	0	0
Koçali	0	0	1	0	0	0	0	0	1	0	0	1	0	1	0	1	0	0	0
Akçakeçili	0	0	1	0	0	0	0	0	1	0	0	1	0	1	0	1	0	0	0

Table 3. Results of the mineralogical-petrographic analyses of biotite in thin-sections

Biotite	*Coarse–Medium–Fine*	*Coarse –Medium*	*Medium–Fine*	*Fine*	*Chloritised*	*Sericitised*	*Pertitic*	*Mirmekitic*	*Carbonated*	*Clayed*	*Idiomorphic*	*Hypidiomorphic*	*Xenomorphic*	*Homogeneous*	*Recrystallised*	*Prismatic*	*Flat Prismatic*	*Clean-Surfaced*	*Twinning*
Side Theatre	0	0	0	1	0	0	0	0	0	0	1	0	0	0	0	0	0	0	0
Tlos Theatre	0	0	1	0	0	0	0	0	0	0	1	0	0	0	0	0	0	0	0
Tlos Stadium	0	0	0	1	0	0	0	0	0	0	1	0	0	0	0	0	0	0	0
Smyrna Agora 1	0	0	0	1	0	0	0	0	0	0	1	1	0	0	0	0	0	0	0
Smyrna Agora 2	0	0	1	0	1	0	0	0	0	0	1	1	0	1	0	0	0	0	0
Pergamon Red Hall	0	0	1	0	1	0	0	0	0	0	1	1	0	1	0	0	0	0	0
Smintheion 1	0	0	0	1	0	0	0	0	0	0	0	1	0	0	0	0	0	0	0
Smintheion 2	0	0	0	1	0	0	0	0	0	0	0	1	0	0	0	0	0	0	0
Bergama Kozak	0	0	1	0	1	0	0	0	0	0	1	1	0	1	0	0	0	0	0
Koçali	0	0	1	0	1	0	0	0	0	0	1	1	0	1	0	0	0	0	0
Akçakeçili	0	0	1	0	1	0	0	0	0	0	1	1	0	1	0	0	0	0	0

Table 4. Results of the mineralogical-petrographic analyses of plagioclase in thin-sections

Plagioclase	*Coarse–Medium–Fine*	*Coarse –Medium*	*Medium–Fine*	*Fine*	*Chloritised*	*Sericitised*	*Pertitic*	*Mirmekitic*	*Carbonated*	*Clayed*	*Idiomorphic*	*Hypidiomorphic*	*Xenomorphic*	*Homogeneous*	*Recrystallised*	*Prismatic*	*Flat Prismatic*	*Clean-Surfaced*	*Twinning*
Side Theatre	0	0	1	0	0	0	0	0	0	0	1	1	0	0	0	0	0	0	0
Tlos Theatre	0	0	1	0	0	0	0	0	0	0	1	1	0	0	0	0	0	0	0
Tlos Stadium	0	0	1	0	0	0	0	0	0	0	1	1	0	0	0	0	0	0	0
Smyrna Agora 1	0	0	1	0	0	0	0	0	0	0	1	1	0	0	0	0	0	0	0
Smyrna Agora 2	1	0	0	0	0	1	0	0	1	1	0	1	0	1	0	0	1	0	0
Pergamon Red Hall	0	0	1	0	0	1	0	0	1	0	0	1	0	1	0	0	1	0	0
Smintheion 1	0	0	1	0	0	1	0	0	0	0	0	1	0	0	0	0	0	0	1
Smintheion 2	0	1	0	0	0	0	0	0	0	0	0	1	0	0	0	0	0	0	1
Bergama Kozak	0	0	1	0	0	1	0	0	1	0	0	1	0	1	0	0	1	0	0
Koçali	1	0	0	0	0	1	0	0	0	0	0	1	0	1	0	0	1	0	1
Akçakeçili	1	0	0	0	0	1	0	0	0	0	0	1	0	1	0	0	1	0	1

Table 5. Results of the mineralogical-petrographic analyses of quartz in thin-sections

Quartz	*Coarse–Medium–Fine*	*Coarse –Medium*	*Medium–Fine*	*Fine*	*Chloritised*	*Sericitised*	*Pertitic*	*Mirmekitic*	*Carbonated*	*Clayed*	*Idiomorphic*	*Hypidiomorphic*	*Xenomorphic*	*Homogeneous*	*Recrystallised*	*Prismatic*	*Flat Prismatic*	*Clean-Surfaced*	*Twinning*
Side Theatre	0	0	0	1	0	0	0	0	0	0	0	0	1	0	0	0	0	0	0
Tlos Theatre	0	0	0	1	0	0	0	0	0	0	0	0	1	0	0	0	0	0	0
Tlos Stadium	0	0	0	1	0	0	0	0	0	0	0	0	1	0	0	0	0	0	0
Smyrna Agora 1	0	0	0	0	0	0	0	0	0	0	0	0	0	0	0	0	0	0	0
Smyrna Agora 2	0	0	1	0	0	0	0	0	0	0	0	0	1	1	0	0	0	0	0
Pergamon Red Hall	0	0	1	0	0	0	0	0	0	0	0	0	1	1	1	0	0	0	0
Smintheion 1	0	0	0	1	0	0	0	0	0	0	0	0	1	0	1	0	0	1	0
Smintheion 2	0	0	0	1	0	0	0	0	0	0	0	0	1	0	1	0	0	1	0
Bergama Kozak	0	0	1	0	0	0	0	0	0	0	0	0	1	1	1	0	0	0	0
Koçali	0	0	1	0	0	0	0	0	0	0	0	0	1	1	1	0	0	1	0
Akçakeçili	0	0	1	0	0	0	0	0	0	0	0	0	1	1	1	0	0	1	0

Table 6. Results of the geochemical analyses of thin-sections

Geochemical Analyses	CaO	Fe_2O_3	MgO	P_2O_5	SiO_2	Al_2O_3	K_2O	MnO	Na_2O	TiO_2
Side Theatre	5.9	5.0	2.0	0.7	59.5	16.3	5.1	0.2	3.4	0.8
Tlos Theatre	5.0	4.5	2.2	0.3	63.5	15.8	3.7	0.1	3.2	0.7
Tlos Stadium	5.3	4.9	1.9	0.6	60.5	16.6	5.1	0.1	3.5	0.7
Smyrna Agora 1	4.4	3.9	1.0	0.1	67.4	15.7	2.8	0.1	3.4	0.5
Smyrna Agora 2	5.7	5.2	2.3	0.5	59.6	16.8	4.1	0.1	3.6	0.9
Pergamon Red Hall	5.5	4.6	2.1	0.3	61.9	16.3	3.4	0.1	3.3	0.7
Smintheion 1	4.6	3.8	1.7	0.4	63.6	15.9	4.4	0.1	3.5	0.6
Smintheion 2	4.8	3.9	1.7	0.4	63.8	15.8	4.3	0.1	3.5	0.6
Bergama Kozak	4.7	4.2	2.0	0.3	64.2	15.9	3.7	0.1	3.4	0.7
Koçali	5.0	4.6	1.9	0.5	61.5	16.4	4.5	0.1	3.6	0.7
Akçakeçili	5.0	4.4	1.9	0.5	61.6	16.1	4.7	0.1	3.5	0.7
Koçali-Akçakeçili	5.0	4.5	1.9	0.5	61.55	16.25	4.6	0.1	3.55	0.7

Table 7. Results of the geochemical analyses of thin-sections (normalised via maximum value in Table 6)

Geochemical Analyses (Normalised)	CaO	Fe_2O_3	MgO	P_2O_5	SiO_2	Al_2O_3	K_2O	MnO	Na_2O	TiO_2
Side Theatre	0.0875	0.0742	0.0297	0.0104	0.8828	0.2418	0.0757	0.0030	0.0504	0.0119
Tlos Theatre	0.0742	0.0668	0.0326	0.0045	0.9421	0.2344	0.0549	0.0015	0.0475	0.0104
Tlos Stadium	0.0786	0.0727	0.0282	0.0089	0.8976	0.2463	0.0757	0.0015	0.0519	0.0104
Smyrna Agora 1	0.0653	0.0579	0.0148	0.0015	1.0000	0.2329	0.0415	0.0015	0.0504	0.0074
Smyrna Agora 2	0.0846	0.0772	0.0341	0.0074	0.8843	0.2493	0.0608	0.0015	0.0534	0.0134
Pergamon Red Hall	0.0816	0.0682	0.0312	0.0045	0.9184	0.2418	0.0504	0.0015	0.0490	0.0104
Smintheion 1	0.0682	0.0564	0.0252	0.0059	0.9436	0.2359	0.0653	0.0015	0.0519	0.0089
Smintheion 2	0.0712	0.0579	0.0252	0.0059	0.9466	0.2344	0.0638	0.0015	0.0519	0.0089
Bergama Kozak	0.0697	0.0623	0.0297	0.0045	0.9525	0.2359	0.0549	0.0015	0.0504	0.0104
Koçali-Akçakeçili	0.0742	0.0668	0.0282	0.0074	0.9132	0.2411	0.0682	0.0015	0.0527	0.0104

4. Research Method

In this section, we first present MCCM and which also uses the abilities of PEM (Enginoğlu and Çağman, In Press).

Algorithm Steps of MCCM

Pre-processing Steps for Archaeometric Data

Step 1. Construct *fs*-matrices $\left[a_{ij}^{z}\right]_{m\times n}$ for archaeological samples, for all $z \in I_w$

Step 2. Construct *fs*-matrices $\left[b_{kj}^{z}\right]_{r\times n}$ for geological samples, for all $z \in I_w$

Step 3. Obtain $\left[c_{ij}^{zk}\right]_{m\times n}$ defined by $c_{ij}^{zk} \coloneqq b_{kj}^{z}$ such that $z \in I_w$ and $k \in I_r$

Step 4. Obtain $\left[d_{ij}^{zk}\right]_{m\times n}$ defined by $\left[d_{ij}^{zk}\right] \coloneqq [1] - \left[c_{ij}^{zk}\right]\tilde{\Delta}\left[a_{ij}^{z}\right]$ such that $z \in I_w$ and $k \in I_r$

Main Steps for Archaeometric Data

Step 1. Construct *fpfs*-matrices $\left[e_{ij}^{zk}\right]_{(m+1)\times n}$ such that $i \in I_m^*$, $j \in I_n$, and $i \neq 0 \Rightarrow e_{ij}^{zk} \coloneqq d_{ij}^{zk}$

Step 2. Apply PEM to $\left[e_{ij}^{zk}\right]$ for all $z \in I_w$ and $k \in I_r$. That is, obtain $[f_{ik}^{z}]_{m\times r}$ defined by

$$f_{ik}^{z} \coloneqq \left(\frac{1}{n}\sum\nolimits_{l=1}^{n} e_{il}^{zk}\right)\sum\nolimits_{j=1}^{n}\left[\left(\frac{1}{m}\sum\nolimits_{p=1}^{m} e_{pj}^{zk}\right)e_{0j}^{zk}e_{ij}^{zk}\right]$$

such that $z \in I_w$ and $k \in I_r$

Step 3. Obtain $[g_{ik}]_{m\times r}$ defined by $g_{ik} \coloneqq \frac{1}{w}\sum_{z=1}^{w} f_{ik}^{z}$

Step 4. Obtain $[s_{ik}^{1}]_{m\times r}$ defined by

$$s_{ik}^{1} \coloneqq \begin{cases} \dfrac{g_{ik}}{\max\limits_{t\in I_r} g_{it}}, & \max\limits_{t\in I_r} g_{it} \neq 0 \\ g_{ik}, & \max\limits_{t\in I_r} g_{it} = 0 \end{cases}$$

Pre-processing Steps for Geochemical Data

Step 1. Construct *fs*-matrices $\left[a_{ij}\right]_{m\times n}$ for archaeological samples

Step 2. Construct *fs*-matrices $\left[b_{ij}\right]_{m\times n}$ for geological samples

Step 3. Obtain *fs*-matrices $\left[c_{ij}^{k}\right]_{m\times n}$ defined by $c_{ij}^{k} \coloneqq b_{kj}$ such that $k \in I_r$

Step 4. Obtain *fs*-matrices $\left[d_{ij}^{k}\right]_{m\times n}$ defined by $\left[d_{ij}^{k}\right] \coloneqq [1] - \left[c_{ij}^{k}\right]\tilde{\Delta}\left[a_{ij}\right]$ such that $k \in I_r$

Main Steps for Geochemical Data

Step 1. Construct *fpfs*-matrices $\left[e_{ij}^{k}\right]_{(m+1)\times n}$ such that $i \in I_m^*$, $j \in I_n$, and $i \neq 0 \Rightarrow e_{ij}^{k} \coloneqq d_{ij}^{k}$

Step 2. Apply PEM to $\left[e_{ij}^{k}\right]$ for all $k \in I_r$. That is, obtain $[f_{ik}]_{m\times r}$ defined by

$$f_{ik} \coloneqq \left(\frac{1}{n}\sum\nolimits_{l=1}^{n} e_{il}^{k}\right)\sum\nolimits_{j=1}^{n}\left[\left(\frac{1}{m}\sum\nolimits_{p=1}^{m} e_{pj}^{k}\right)e_{0j}^{k}e_{ij}^{k}\right]$$

such that $i \in I_m$ and $k \in I_r$

Step 3. Obtain $[s_{ik}^{2}]_{m\times r}$ defined by

$$s_{ik}^{2} \coloneqq \begin{cases} \dfrac{f_{ik}}{\max\limits_{t\in I_r} f_{it}}, & \max\limits_{t\in I_r} f_{it} \neq 0 \\ f_{ik}, & \max\limits_{t\in I_r} f_{it} = 0 \end{cases}$$

Output Steps

Step 1. Obtain the decision matrix $[s_{ik}]_{m\times r}$ such that $s_{ik} = 0.25s_{ik}^{1} + 0.75s_{ik}^{2}$

Step 2. Obtain the decision sets $D_k \coloneqq \{u_i \,|s_{ik} = \max\limits_{p} s_{ip}\}$ such that $k, p \in I_r$

Secondly, we illustrate MCCM for $z = k = 2$, that is, for the Amphibols data given in the previous. Faithfully to the Ay and Tolun's opinions, we set

[0.01, 0.01, 0.01, 0.01, 1, 1, 1, 1, 1, 1, 0.01, 0.01, 0.01, 0.01, 0.01, 0.01, 0.01, 0.01]

and

[0.6, 0.6, 0.01, 0.7, 1, 0.8, 1, 0.01, 0.7, 0.01]

to the weights of the archaeometric and geochemical parameters, respectively. Moreover, Ay and Tolun (2017b) consider more effective the geochemical data than archaeometric data. Therefore, we set 0.25 and 0.75 values to these data as weights, respectively, in the final decision stage.

Pre-process Steps for Archaeometric Data

Step 1. and Step 2.

Let $U = \{u_i : i \in I_8\}$, $V = \{v_k : k \in I_2\}$, and $E_1 = \{x_j : j \in I_{19}\}$ such that u_1 =*Side Theatre*, u_2 =*Tlos Theatre*, u_3 =*Tlos Stadium*, u_4 =*Smyrna Agora 1*, u_5 =*Smyrna Agora 2*, u_6 =*Pergamon Red Hall / Serapeion*, u_7 =*Smintheion 1*, u_8 =*Smintheion 2*, v_1 =*Bergama Kozak*, v_2 =*Koçali-Akçakeçili*, x_1 = *Coarse-Medium-Fine*, x_2 = *Coarse - Medium*, x_3 = *Medium-Fine*, x_4 = *Fine*, x_5 = *Chloritised*, x_6 = *Sericitised*, x_7 = *Pertitic*, x_8 = *Mirmekitic*, x_9 = *Carbonated*, x_{10} = *Clayed*, x_{11} =*Idiomorphic (Self-Shaped)*, x_{12} =*Hypidiomorphic (Semi-Self-Shaped)*, x_{13} =*Xenomorphic (Self-Shapeless)*, x_{14} = *Homogeneous*, x_{15} =*Recrystallised (Wavy)*, x_{16} =*Prismatic*, x_{17} =*Flat Prismatic*, x_{18} =*Clean Surfaced, and* x_{19} =*Twinning.*

Therefore, the *fs*-sets of the Amphiboles data are as follows:

$$\alpha = \{ (x_1, \{u_5, u_6\}), (x_3, \{u_3, u_5, u_6, u_8\}), (x_4, \{u_1, u_2, u_4, u_7\}), (x_5, \{u_6\}), (x_9, \{u_6\}), (x_{11}, \{u_1, u_2, u_3\}), (x_{12}, U), (x_{14}, \{u_5, u_6\}), (x_{16}, \{u_5, u_6\})\}$$

$$\beta = \{(x_3, V), (x_9, V), (x_{11}, \{v_1\}), (x_{12}, V), (x_{14}, V), (x_{16}, V)\}$$

where $\emptyset$ denotes empty fuzzy set. Here, for brevity, the notation u_3 has been used instead of ${}^1u_3$. Also, the elements such ${}^0u_3$ and $(x_4, \emptyset)$ have not been shown in the sets containing them.

The *fs*-matrices corresponded to the *fs*-sets α and β, respectively, are as follows:

$$[a_{ij}^2] = \begin{bmatrix} 0&0&0&1&0&0&0&0&0&0&1&1&0&0&0&0&0&0&0 \\ 0&0&0&1&0&0&0&0&0&0&1&1&0&0&0&0&0&0&0 \\ 0&0&1&0&0&0&0&0&0&0&1&1&0&0&0&0&0&0&0 \\ 0&0&0&1&0&0&0&0&0&0&0&1&0&0&0&0&0&0&0 \\ 1&0&1&0&0&0&0&0&0&0&0&1&0&1&0&1&0&0&0 \\ 1&0&1&0&1&0&0&0&1&0&0&1&0&1&0&1&0&0&0 \\ 0&0&0&1&0&0&0&0&0&0&0&1&0&0&0&0&0&0&0 \\ 0&0&1&0&0&0&0&0&0&0&0&1&0&0&0&0&0&0&0 \end{bmatrix}$$

$$[b_{ij}^2] = \begin{bmatrix} 0&0&1&0&0&0&0&0&1&0&1&1&0&1&0&1&0&0&0 \\ 0&0&1&0&0&0&0&0&1&0&0&1&0&1&0&1&0&0&0 \end{bmatrix}$$

Step 3.

$$[c_{ij}^{22}] = \begin{bmatrix} 0&0&1&0&0&0&0&0&1&0&0&1&0&1&0&1&0&0&0 \\ 0&0&1&0&0&0&0&0&1&0&0&1&0&1&0&1&0&0&0 \\ 0&0&1&0&0&0&0&0&1&0&0&1&0&1&0&1&0&0&0 \\ 0&0&1&0&0&0&0&0&1&0&0&1&0&1&0&1&0&0&0 \\ 0&0&1&0&0&0&0&0&1&0&0&1&0&1&0&1&0&0&0 \\ 0&0&1&0&0&0&0&0&1&0&0&1&0&1&0&1&0&0&0 \\ 0&0&1&0&0&0&0&0&1&0&0&1&0&1&0&1&0&0&0 \\ 0&0&1&0&0&0&0&0&1&0&0&1&0&1&0&1&0&0&0 \end{bmatrix}$$

Step 4.

$$[d_{ij}^{22}] = \begin{bmatrix} 1 & 1 & 0 & 0 & 1 & 1 & 1 & 1 & 0 & 1 & 0 & 1 & 1 & 0 & 1 & 0 & 1 & 1 & 1 \\ 1 & 1 & 0 & 0 & 1 & 1 & 1 & 1 & 0 & 1 & 0 & 1 & 1 & 0 & 1 & 0 & 1 & 1 & 1 \\ 1 & 1 & 1 & 1 & 1 & 1 & 1 & 1 & 0 & 1 & 0 & 1 & 1 & 0 & 1 & 0 & 1 & 1 & 1 \\ 1 & 1 & 0 & 0 & 1 & 1 & 1 & 1 & 0 & 1 & 1 & 1 & 1 & 0 & 1 & 0 & 1 & 1 & 1 \\ 0 & 1 & 1 & 1 & 1 & 1 & 1 & 1 & 0 & 1 & 1 & 1 & 1 & 1 & 1 & 1 & 1 & 1 & 1 \\ 0 & 1 & 1 & 1 & 0 & 1 & 1 & 1 & 1 & 1 & 1 & 1 & 1 & 1 & 1 & 1 & 1 & 1 & 1 \\ 1 & 1 & 0 & 0 & 1 & 1 & 1 & 1 & 0 & 1 & 1 & 1 & 1 & 0 & 1 & 0 & 1 & 1 & 1 \\ 1 & 1 & 1 & 1 & 1 & 1 & 1 & 1 & 0 & 1 & 1 & 1 & 1 & 0 & 1 & 0 & 1 & 1 & 1 \end{bmatrix}$$

Main Steps for Archaeometric Data

Step 1.

$$[e_{ij}^{22}] = \begin{bmatrix} 0.01 & 0.01 & 0.01 & 0.01 & 1 & 1 & 1 & 1 & 1 & 1 & 0.01 & 0.01 & 0.01 & 0.01 & 0.01 & 0.01 & 0.01 & 0.01 & 0.01 \\ 1 & 1 & 0 & 0 & 1 & 1 & 1 & 1 & 0 & 1 & 0 & 1 & 1 & 0 & 1 & 0 & 1 & 1 & 1 \\ 1 & 1 & 0 & 0 & 1 & 1 & 1 & 1 & 0 & 1 & 0 & 1 & 1 & 0 & 1 & 0 & 1 & 1 & 1 \\ 1 & 1 & 1 & 1 & 1 & 1 & 1 & 1 & 0 & 1 & 0 & 1 & 1 & 0 & 1 & 0 & 1 & 1 & 1 \\ 1 & 1 & 0 & 0 & 1 & 1 & 1 & 1 & 0 & 1 & 1 & 1 & 1 & 0 & 1 & 0 & 1 & 1 & 1 \\ 0 & 1 & 1 & 1 & 1 & 1 & 1 & 1 & 0 & 1 & 1 & 1 & 1 & 1 & 1 & 1 & 1 & 1 & 1 \\ 0 & 1 & 1 & 1 & 0 & 1 & 1 & 1 & 1 & 1 & 1 & 1 & 1 & 1 & 1 & 1 & 1 & 1 & 1 \\ 1 & 1 & 0 & 0 & 1 & 1 & 1 & 1 & 0 & 1 & 1 & 1 & 1 & 0 & 1 & 0 & 1 & 1 & 1 \\ 1 & 1 & 1 & 1 & 1 & 1 & 1 & 1 & 0 & 1 & 1 & 1 & 1 & 0 & 1 & 0 & 1 & 1 & 1 \end{bmatrix}$$

Step 2.

$$[f_{ik}^{2}] = \begin{bmatrix} 3.6520 & 3.3886 \\ 3.6520 & 3.3886 \\ 4.1821 & 3.9178 \\ 3.3886 & 3.6538 \\ 4.1768 & 4.4435 \\ 3.5453 & 3.7724 \\ 3.3886 & 3.6538 \\ 3.9178 & 4.1842 \end{bmatrix}$$

Step 3.

$$[g_{ik}] = \begin{bmatrix} 3.5157 & 3.2720 \\ 3.6240 & 3.3803 \\ 3.5548 & 3.4438 \\ 3.5167 & 3.3788 \\ 4.2189 & 4.1625 \\ 4.4318 & 4.1732 \\ 3.6016 & 3.7574 \\ 3.5155 & 3.8252 \end{bmatrix}$$

Step 4.

$$[s_{ik}^{1}] = \begin{bmatrix} 0.7933 & 0.7383 \\ 0.8177 & 0.7627 \\ 0.8021 & 0.7771 \\ 0.7935 & 0.7624 \\ 0.9519 & 0.9392 \\ 1.0000 & 0.9416 \\ 0.8127 & 0.8478 \\ 0.7932 & 0.8631 \end{bmatrix}$$

Pre-process Steps for Geochemical Data

Step 1. and Step 2.

Let $U = \{u_i : i \in I_8\}$, $V = \{v_k : k \in I_2\}$, and $E_2 = \{y_l : l \in I_{10}\}$ such that u_1 =*Side Theatre*, u_2 =*Tlos Theatre*, u_3 =*Tlos Stadium*, u_4 =*Smyrna Agora 1*, u_5 =*Smyrna Agora 2*, u_6 =*Pergamon Red Hall / Serapeion*, u_7 =*Smintheion 1*, u_8 =*Smintheion 2*, v_1 =*Bergama Kozak*, v_2 =*Koçali-Akçakeçili*, $y_1 = CaO$, $y_2 = Fe_2O_3$, $y_3 = MgO$, $y_4 = P_2O_5$, $y_5 = SiO_2$, $y_6 = AlO_3$, $y_7 = K_2O$, $y_8 = MnO$, $y_9 = Na_2O$, *and* $y_{10} = TiO_2$. Therefore, the *fs*-sets of the Amphiboles data are as follows:

$$\begin{aligned}\gamma = \; & \{(y_1, \{^{0.0875}u_1, {}^{0.0742}u_2, {}^{0.0786}u_3, {}^{0.0653}u_4, {}^{0.0846}u_5, {}^{0.0846}u_6, {}^{0.0682}u_7, {}^{0.0712}u_8\}), \\ & (y_2, \{^{0.0742}u_1, {}^{0.0668}u_2, {}^{0.0727}u_3, {}^{0.0579}u_4, {}^{0.0772}u_5, {}^{0.0682}u_6, {}^{0.0564}u_7, {}^{0.0579}u_8\}), \\ & (y_3, \{^{0.0297}u_1, {}^{0.0326}u_2, {}^{0.0282}u_3, {}^{0.0148}u_4, {}^{0.0341}u_5, {}^{0.0312}u_6, {}^{0.0252}u_7, {}^{0.0252}u_8\}), \\ & (y_4, \{^{0.0104}u_1, {}^{0.0045}u_2, {}^{0.0089}u_3, {}^{0.0015}u_4, {}^{0.0074}u_5, {}^{0.0045}u_6, {}^{0.0059}u_7, {}^{0.0059}u_8\}), \\ & (y_5, \{^{0.8828}u_1, {}^{0.9421}u_2, {}^{0.8976}u_3, {}^{1,0000}u_4, {}^{0.8843}u_5, {}^{0.9184}u_6, {}^{0.9436}u_7, {}^{0.9466}u_8\}), \\ & (y_6, \{^{0.2418}u_1, {}^{0.2344}u_2, {}^{0.2463}u_3, {}^{0.2329}u_4, {}^{0.2493}u_5, {}^{0.2418}u_6, {}^{0.2359}u_7, {}^{0.2344}u_8\}), \\ & (y_7, \{^{0.0757}u_1, {}^{0.0549}u_2, {}^{0.0757}u_3, {}^{0.0415}u_4, {}^{0.0608}u_5, {}^{0.0504}u_6, {}^{0.0653}u_7, {}^{0.0638}u_8\}), \\ & (y_8, \{^{0.0030}u_1, {}^{0.0015}u_2, {}^{0.0015}u_3, {}^{0.0015}u_4, {}^{0.0015}u_5, {}^{0.0015}u_6, {}^{0.0015}u_7, {}^{0.0015}u_8\}), \\ & (y_9, \{^{0.0504}u_1, {}^{0.0475}u_2, {}^{0.0519}u_3, {}^{0.0504}u_4, {}^{0.0534}u_5, {}^{0.0490}u_6, {}^{0.0519}u_7, {}^{0.0519}u_8\}), \\ & (y_{10}, \{^{0.0119}u_1, {}^{0.0104}u_2, {}^{0.0104}u_3, {}^{0.0074}u_4, {}^{0.0134}u_5, {}^{0.0104}u_6, {}^{0.0089}u_7, {}^{0.0089}u_8\})\}\end{aligned}$$

$$\begin{aligned}\delta = \; & \{(y_1, \{^{0.0697}v_1, {}^{0.0742}v_2\}), (y_2, \{^{0.0623}v_1, {}^{0.0668}v_2\}), (y_3, \{^{0.0297}v_1, {}^{0.0282}v_2\}), \\ & (y_4, \{^{0.0045}v_1, {}^{0.0074}v_2\}), (y_5, \{^{0.9525}v_1, {}^{0.9132}v_2\}), (y_6, \{^{0.2359}v_1, {}^{0.2411}v_2\}), \\ & (y_7, \{^{0.0549}v_1, {}^{0.0682}v_2\}), (y_8, \{^{0.0015}v_1, {}^{0.0015}v_2\}), (y_9, \{^{0.0504}v_1, {}^{0.0527}v_2\}), \\ & (y_{10}, \{^{0.0104}v_1, {}^{0.0104}v_2\})\}\end{aligned}$$

The *fs*-matrices corresponded to the *fs*-sets γ and δ, respectively, are as follows:

$$[a_{ij}] = \begin{bmatrix} 0.0875 & 0.0742 & 0.0297 & 0.0104 & 0.8828 & 0.2418 & 0.0757 & 0.0030 & 0.0504 & 0.0119 \\ 0.0742 & 0.0668 & 0.0326 & 0.0045 & 0.9421 & 0.2344 & 0.0549 & 0.0015 & 0.0475 & 0.0104 \\ 0.0786 & 0.0727 & 0.0282 & 0.0089 & 0.8976 & 0.2463 & 0.0757 & 0.0015 & 0.0519 & 0.0104 \\ 0.0653 & 0.0579 & 0.0148 & 0.0015 & 1.0000 & 0.2329 & 0.0415 & 0.0015 & 0.0504 & 0.0074 \\ 0.0846 & 0.0772 & 0.0341 & 0.0074 & 0.8843 & 0.2493 & 0.0608 & 0.0015 & 0.0534 & 0.0134 \\ 0.0816 & 0.0682 & 0.0312 & 0.0045 & 0.9184 & 0.2418 & 0.0504 & 0.0015 & 0.0490 & 0.0104 \\ 0.0682 & 0.0564 & 0.0252 & 0.0059 & 0.9436 & 0.2359 & 0.0653 & 0.0015 & 0.0519 & 0.0089 \\ 0.0712 & 0.0579 & 0.0252 & 0.0059 & 0.9466 & 0.2344 & 0.0638 & 0.0015 & 0.0519 & 0.0089 \end{bmatrix}$$

$$[b_{ij}] = \begin{bmatrix} 0.0697 & 0.0623 & 0.0297 & 0.0045 & 0.9525 & 0.2359 & 0.0549 & 0.0015 & 0.0504 & 0.0104 \\ 0.0742 & 0.0668 & 0.0282 & 0.0074 & 0.9132 & 0.2411 & 0.0682 & 0.0015 & 0.0527 & 0.0104 \end{bmatrix}$$

Step 3.

$$[c_{ij}^2] = \begin{bmatrix} 0.0742 & 0.0668 & 0.0282 & 0.0074 & 0.9132 & 0.2411 & 0.0682 & 0.0015 & 0.0527 & 0.0104 \\ 0.0742 & 0.0668 & 0.0282 & 0.0074 & 0.9132 & 0.2411 & 0.0682 & 0.0015 & 0.0527 & 0.0104 \\ 0.0742 & 0.0668 & 0.0282 & 0.0074 & 0.9132 & 0.2411 & 0.0682 & 0.0015 & 0.0527 & 0.0104 \\ 0.0742 & 0.0668 & 0.0282 & 0.0074 & 0.9132 & 0.2411 & 0.0682 & 0.0015 & 0.0527 & 0.0104 \\ 0.0742 & 0.0668 & 0.0282 & 0.0074 & 0.9132 & 0.2411 & 0.0682 & 0.0015 & 0.0527 & 0.0104 \\ 0.0742 & 0.0668 & 0.0282 & 0.0074 & 0.9132 & 0.2411 & 0.0682 & 0.0015 & 0.0527 & 0.0104 \\ 0.0742 & 0.0668 & 0.0282 & 0.0074 & 0.9132 & 0.2411 & 0.0682 & 0.0015 & 0.0527 & 0.0104 \\ 0.0742 & 0.0668 & 0.0282 & 0.0074 & 0.9132 & 0.2411 & 0.0682 & 0.0015 & 0.0527 & 0.0104 \end{bmatrix}$$

Step 4.

$$[d_{ij}^2] = \begin{bmatrix} 0.9867 & 0.9926 & 0.9985 & 0.9970 & 0.9696 & 0.9993 & 0.9925 & 0.9985 & 0.9977 & 0.9985 \\ 1 & 1 & 0.9956 & 0.9971 & 0.9711 & 0.9933 & 0.9867 & 1 & 0.9948 & 1 \\ 0.9956 & 0.9941 & 1 & 0.9985 & 0.9844 & 0.9948 & 0.9925 & 1 & 0.9992 & 1 \\ 0.9911 & 0.9911 & 0.9866 & 0.9941 & 0.9132 & 0.9918 & 0.9733 & 1 & 0.9977 & 0.9970 \\ 0.9896 & 0.9896 & 0.9941 & 1 & 0.9711 & 0.9918 & 0.9926 & 1 & 0.9993 & 0.9970 \\ 0.9926 & 0.9986 & 0.9970 & 0.9971 & 0.9948 & 0.9993 & 0.9822 & 1 & 0.9963 & 1 \\ 0.9940 & 0.9896 & 0.9970 & 0.9985 & 0.9696 & 0.9948 & 0.9971 & 1 & 0.9992 & 0.9985 \\ 0.9970 & 0.9911 & 0.9970 & 0.9985 & 0.9666 & 0.9933 & 0.9956 & 1 & 0.9992 & 0.9985 \end{bmatrix}$$

Main Steps for Geochemical Data

Step 1.

$$[e_{ij}^2] = \begin{bmatrix} 0.6 & 0.6 & 0.01 & 0.7 & 1 & 0.8 & 1 & 0.01 & 0.7 & 0.01 \\ 0.9867 & 0.9926 & 0.9985 & 0.9970 & 0.9696 & 0.9993 & 0.9925 & 0.9985 & 0.9977 & 0.9985 \\ 1 & 1 & 0.9956 & 0.9971 & 0.9711 & 0.9933 & 0.9867 & 1 & 0.9948 & 1 \\ 0.9956 & 0.9941 & 1 & 0.9985 & 0.9844 & 0.9948 & 0.9925 & 1 & 0.9992 & 1 \\ 0.9911 & 0.9911 & 0.9866 & 0.9941 & 0.9132 & 0.9918 & 0.9733 & 1 & 0.9977 & 0.9970 \\ 0.9896 & 0.9896 & 0.9941 & 1 & 0.9711 & 0.9918 & 0.9926 & 1 & 0.9993 & 0.9970 \\ 0.9926 & 0.9986 & 0.9970 & 0.9971 & 0.9948 & 0.9993 & 0.9822 & 1 & 0.9963 & 1 \\ 0.9940 & 0.9896 & 0.9970 & 0.9985 & 0.9696 & 0.9948 & 0.9971 & 1 & 0.9992 & 0.9985 \\ 0.9970 & 0.9911 & 0.9970 & 0.9985 & 0.9666 & 0.9933 & 0.9956 & 1 & 0.9992 & 0.9985 \end{bmatrix}$$

Step 2.

$$[f_{ik}] = \begin{bmatrix} 5.1804 & 5.2810 \\ 5.3326 & 5.2865 \\ 5.2087 & 5.3150 \\ 5.2470 & 5.1519 \\ 5.1927 & 5.2767 \\ 5.2773 & 5.3157 \\ 5.3211 & 5.2906 \\ 5.3276 & 5.2869 \end{bmatrix}$$

Step 3.

$$[s_{ik}^2] = \begin{bmatrix} 0.9715 & 0.9903 \\ 1.0000 & 0.9913 \\ 0.9768 & 0.9967 \\ 0.9840 & 0.9661 \\ 0.9738 & 0.9895 \\ 0.9896 & 0.9968 \\ 0.9978 & 0.9921 \\ 0.9991 & 0.9914 \end{bmatrix}$$

Output Steps

Step 1.

$$[s_{ik}] = \begin{bmatrix} 0.9269 & 0.9273 \\ 0.9544 & 0.9342 \\ 0.9331 & 0.9418 \\ 0.9363 & 0.9152 \\ 0.9683 & 0.9769 \\ 0.9922 & 0.9830 \\ 0.9516 & 0.9560 \\ 0.9476 & 0.9594 \end{bmatrix}$$

Step 2.

Side Theatre	*Koçali-Akçakeçili*
Tlos Theatre	*Bergama Kozak*
Tlos Stadium	*Koçali-Akçakeçili*
Smyrna Agora 1	*Bergama Kozak*
Smyrna Agora 2	*Koçali-Akçakeçili*
Pergamon Red Hall	*Bergama Kozak*
Smintheion 1	*Koçali-Akçakeçili*
Smintheion 2	*Koçali-Akçakeçili*

5. Conclusion

We, in this paper, proposed a novel method MCCM to model an MCC problem. We then applied MCCM to the data provided in (Ay, 2017; Ay and Tolun, 2017b). The results affirmed those obtained by archaeometric analyses. Since this method is the first, it could not be compared with other methods for now. Soon, however, if another soft decision-making method that differs from PEM is applied to this problem, then a comparison of these methods can be given.

Acknowledgements

We thank Ayten Çalık (PhD) and Ömer Can Yıldırım (MA) for technical support. The archaeological portion of this work was supported by the Office of Scientific Research Projects Coordination at Çanakkale Onsekiz Mart University, Grant number: SYL-2015-521. The mathematical portion of this work was supported by the Office of Scientific Research Projects Coordination at Tokat Gaziosmanpaşa University, Grant numbers: 2009-72 and 2010/89.

References

Atmaca, S. (2017). Relationship between fuzzy soft topological spaces and (X, τ_e) parameter spaces. Cumhuriyet Science Journal, 38(4), 77-85.

Ay, M. (2017). Distribution of the granite columns from the Troadic quarries in Western Anatolia an archaeometric approach, Master's Thesis, Çanakkale Onsekiz Mart University, Çanakkale, Turkey (In Turkish).

Ay, M., Tolun, V. (2017a). Ancient granite quarries in Troad: New findings. The Turkish Yearbook of Çanakkale Studies, 15(23), 265-295 (In Turkish).

Ay, M., Tolun, V. (2017b). An archaeometric approach on the distribution of Troadic granite columns in the Western Anatolian coasts. Journal of Archaeology & Art, 156, 119-130 (In Turkish).

Bera, S., Roy, S. K., Karaaslan, F., Çağman, N. (2017). Soft congruence relation over lattice. Hacettepe Journal of Mathematics and Statistics, 46(6), 1035-1042.

Çağman, N., Çıtak, F., Enginoğlu, S. (2010). Fuzzy parameterized fuzzy soft set theory and its applications. Turkish Journal of Fuzzy Systems, 1(1), 21-35.

Çağman, N., Çıtak, F., Enginoğlu, S. (2011a). FP-soft set theory and its applications. Annals of Fuzzy Mathematics and Informatics, 2(2), 219-226.

Çağman, N., Deli, İ. (2012). Means of FP-soft sets and their applications. Hacettepe Journal of Mathematics and Statistics, 41(5), 615-625.

Çağman, N., Enginoğlu, S. (2010). Soft set theory and uni-int decision making. European Journal of Operational Research, 207, 848-855.

Çağman, N., Enginoğlu, S. (2012). Fuzzy soft matrix theory and its application in decision making. Iranian Journal of Fuzzy Systems, 9(1), 109-119.

Çağman, N., Enginoğlu, S., Çıtak, F. (2011b). Fuzzy soft set theory and its applications. Iranian Journal of Fuzzy Systems, 8(3), 137-147.

Çıtak, F. (2018). Soft k-uni ideals of semirings and its algebraic applications. Journal of the Institute of Science and Technology, 8(4), 281-294.

Çıtak, F., Çağman, N. (2017). Soft k-int-ideals of semirings and its algebraic structures. Annals of Fuzzy Mathematics and Informatics, 13(4), 531-538.

De Vecchi, G., Lazzarini, L., Lünel, T., Mignucci, A., Visonà, D. (2000). The genesis and characterisation of marmor misium from Kozak (Turkey) a granit used antiquity. Journal of Cultural Heritage, 1, 145-153.

Deli, İ., Çağman, N. (2015). Relations on FP-soft sets applied to decision making problems. Journal of New Theory, (3), 98-107.

Enginoğlu, S. (2012). Soft matrices, PhD Dissertation, Gaziosmanpaşa University, Tokat, Turkey, (In Turkish).

Enginoğlu, S., Çağman, N. Fuzzy parameterized fuzzy soft matrices and their application in decision-making. TWMS Journal of Applied and Engineering Mathematics, (In Press).

Enginoğlu, S., Çağman, N., Karataş, S., Aydın, T. (2015). On soft topology. El-Cezerî Journal of Science and Engineering, 2(3), 23-38.

Enginoğlu, S., Demiriz, S. (2015). A comparison with the convergent, Cesàro convergent and Riesz convergent sequences of fuzzy numbers. In: The 4th International Fuzzy Systems Symposium, 5-6 November 2015 İstanbul, Turkey, pp. 413-416.

Enginoğlu, S., Dönmez, H. (2015). An application on decision making problem by using intuitionistic fuzzy parameterized intuitionistic fuzzy soft expert sets. In: The 4th International Fuzzy Systems Symposium, 5-6 November 2015 İstanbul, Turkey, pp. 413-415.

Enginoğlu, S., Memiş, S. (2018a). Comment on fuzzy soft sets [The Journal of Fuzzy Mathematics, 9(3), 2001, 589-602]. International Journal of Latest Engineering Research and Applications, 3(9), 1-9.

Enginoğlu, S., Memiş, S. (2018b). A review on an application of fuzzy soft set in multicriteria

decision making problem. In: Proceedings of The International Conference on Mathematical Studies and Applications, pp. 173-178.

Enginoğlu, S., Memiş, S. (2018c). A configuration of some soft decision-making algorithms via *fpfs*-matrices. Cumhuriyet Science Journal, 39(4), 871-881.

Enginoğlu, S., Memiş, S. (2018d). A review on some soft decision-making methods. In: Proceedings of The International Conference on Mathematical Studies and Applications, pp. 437-442.

Enginoğlu, S., Memiş, S., Arslan, B. (2018a). A fast and simple soft decision-making algorithm: EMA18an. In: Proceedings of The International Conference on Mathematical Studies and Applications, pp. 426-438.

Enginoğlu, S., Memiş, S., Arslan, B. (2018b). Comment (2) on soft set theory and uni-int decision making [European Journal of Operational Research, (2010) 207, 848-855]. Journal New Theory, (25), 84-102.

Enginoğlu, S., Memiş, S., Öngel, T. (2018c). A fast and simple soft decision-making algorithm: EMO18o. In: Proceedings of The International Conference on Mathematical Studies and Applications, pp. 179-187.

Enginoğlu, S., Memiş, S., Öngel, T. (2018d). Comment on soft set theory and uni-int decision-making [European Journal of Operational Research, (2010) 207, 848-855]. Journal of New Results in Science, 7(3), 28-43.

Galetti, G., Lazzarini, L., Maggetti, M. (1992). A first characterization of the most important granites used in antiquity. In Ancient Stones: Quarrying, Trade and Provenance. Acta Archaeologica Lovaniensia Monographia, pp. 167-178.

Gulistan, M., Feng, F., Khan, M., Sezgin, A. (2018). Characterizations of right weakly regular semigroups in terms of generalized cubic soft sets. Mathematics, 6(293), 20 pages.

Karaaslan, F. (2016). Soft classes and soft rough classes with applications in decision making. Mathematical Problems in Engineering, Article ID 1584528, 11 pages.

Mahmood, T., Rehman, Z. U., Sezgin, A. (2018). Lattice ordered soft near rings. Korean Journal of Mathematics, 26(3), 503-517.

Maji, P. K., Biswas, R., Roy, A. R. (2001). Fuzzy soft sets. The Journal of Fuzzy Mathematics, 9(3), 589-602.

Molodtsov, D. (1999). Soft set theory-first results. Computers and Mathematics with Applications, 37(4-5), 19-31.

Ponti, G. (1995). Granite quarries in the troad. a preliminary survey. In Studia Troica, pp. 291-320.

Potts, P. J. (2002). Geochemical and magnetic provenancing of Roman granite columns from Andalucia. Oxford Journal of Archaeology, 21(2), 167-194.

Riaz, M., Hashmi, M. R. (2018). Fuzzy parameterized fuzzy soft topology with applications. Annals of Fuzzy Mathematics and Informatics, 13(5), 593-613.

Riaz, M., Hashmi, M. R., Farooq, A. (2018). Fuzzy parameterized fuzzy soft metric spaces. Journal of Mathematical Analysis, 9(2), 25-36.

Şenel, G. (2016). A new approach to Hausdorff space theory via the soft sets. Mathematical Problems in Engineering, Article ID 2196743, 6 pages.

Şenel, G., 2017. The parameterization reduction of soft point and its applications with soft matrix. International Journal of Computer Applications, 164(1), 1-6.

Şenel, G. (2018). Analyzing the locus of soft spheres: Illustrative cases and drawings. European Journal of Pure and Applied Mathematics, 11(4), 946-957.

Ullah, A., Karaaslan, F., Ahmad, I. (2018). Soft uni-Abel-Grassmann's groups. European Journal of Pure and Applied Mathematics, 11(2), 517-536.

Williams-Thorpe, O. (2008). A thousand and one columns: Observations on the roman granite trade in the Mediterranean area. Oxford Journal of Archaeology, 27(1), 73-89.

Williams-Thorpe, O., Henty, M. M. (2000). The sources of Roman granite columns in Israel. Levant, 32, 155-170.

Williams-Thorpe, O., Thorpe, R. S. (1993). Magnetic susceptibility used in non-destructive provenancing of Roman granite columns. Archaeometry, 35(2), 185-195.

Williams-Thorpe, O., Webb, P. C., Thorpe, R. S. (2000). Non-destructive portable gamma ray spectrometry used in provenancing Roman granitoid columns from Leptis Magna, North Africa. Archaeometry, 42(1), 77-99.

Zorlutuna, İ., Atmaca, S. (2016). Fuzzy parametrized fuzzy soft topology. New Trends in Mathematical Sciences, 4(1), 142-152.

Bilge International Journal of Science and Technology Research

Web : http://dergipark.gov.tr/bilgesci - **E-mail:** kutbilgescience@gmail.com

Received: 18.11.2019
Accepted: 23.12.2019
DOI: 10.30516/bilgesci.647923

ISSN: 2651-401X
e-ISSN: 2651-4028
3(Special Issue), 35-39, 2019

Controlling Structural and Electronic Properties of ZnO NPs: Density-Functional Tight-Binding Method

Mustafa Kurban[1*], Hasan Kurban[2], Mehmet Dalkılıç[2]

Abstract: We carried out a thorough examination of the structural and electronic features of undoped and Nitrogen (N)-doped ZnO nanoparticles (NPs) by the density-functional tight-binding (DFTB) method. By increasing the percent of N atoms in undoped ZnO NPs, the number of bonds (n), order parameter (R) and radial distribution function (RDF) of two-body interactions such as Zn-Zn, N-N, O-O, N-O, etc. were investigated using novel algorithms. Our results show that the total n of Zn-Zn interactions is greater than that of Zn-Zn, N-N, N-O, and O-O; thus, it means that Zn atoms have a greater preference for N or O atoms. The RDFs of Zn and O atoms increase based on the increase in the content of N atoms. The R of Zn, O and N atoms demonstrate that O and N atoms tend to locate at the center, whereas Zn atoms tend to reside on the surface. The density of state (DOS) indicates that the undoped and N-doped ZnO NPs demonstrate a semiconductor-like behavior that is coherent with measured data. The HOMO-LUMO energy gap decreases from -4.717 to -0.853 eV. n increase in the content of N atoms contributes to the destabilization of ZnO NPs due to a decrease in the energy gap.

Keywords: Productivity, Nanoparticle, N-doped ZnO, Electronic Structure, Data Science

1. Introduction

Nanoparticles (NPs), tiny objects whose sizes are lay between 1 and 100 nanometers, are finding use in diverse areas including energy, electronics, biomedical and optical fields due to their shape dependence properties as opposed to their bulk structure. More specifically, metallic NPs exhibit properties useful as both insulators and semiconductors and have been widely investigated (Wang, 2007; Yang, et al. 2008; Kushwaha, 2012). ZnO and its NPs, in particular, have been an area of intense scrutiny (Koç, et al. 2019; Rezkallah, et al. 2017; Caglar, et al. 2019; Coşkun, et al. 2018), because they have a wide bandgap and excellent optical properties for optoelectronics applications, being widely studied in various fields as photodetectors (Chang, et al. 2012), energetic materials (Barziniy, et al. 2019), and biomedical agents (Zhang, 2013).

This study aims at investigating the effect of Nitrogen (N) on ZnO NPs using the density-functional tight-binding (DFTB) method. Among the analyses, we conduct are studies of the HOMO, LUMO and HOMO-LUMO gap (E_g), total energies, density of states (DOS), as well as, the structural analysis such as radial distribution functions (RDFs), order parameter (R) to learn about how behave Zinc (Zn), Oxygen (O) and N atoms and the number of bonds (n) of two-body interactions in the undoped and doped ZnO NPs. To supplement our work on structural changes, we implemented programs in R code (https://github.com/hasankurban/Structural-Analysis-NanoParticles) to analyze the RDF, n and R.

2. Material and Method

We used the DFTB+ code (Aradi, et al. 2007), which is an implementation of DFTB method, with the 3ob/3ob-3-1 (Gaus, et al. 2013; Kubillus, et al. 2015) set of Slater Koster parameters to

[1]Kırşehir Ahi Evran University, Department of Electronics and Automation, 40100, Kırşehir, Turkey
[2]Indiana University, Bloomington, Computer Science Department, 47405, IN, USA.
*Corresponding author (İletişim yazarı): mkurbanphys@gmail.com

Citation (Atıf): Kurban, M., Kurban, H., Dalkılıç, M., (2019). Controlling Structural and Electronic Properties of ZnO NPs: Density-Functional Tight-Binding Method. Bilge International Journal of Science and Technology Research, 3(Special Issue): 35-39.

compare the structural features and electronic structure of studied ZnO NPs.

To make the program more accessible to non-computational scientists, we have also ensured that the programs are simple to use. Additionally, we have added functionality to include analysis of the *n*, *R*, and RDF of the ZnO NPs in terms of an increase in the N content. The code is open source and it is freely available online, thus, researchers can visualize their data using the code.

3. Results

3.1. Structural analysis

The initial structure of undoped ZnO NP with n = 258 atoms is indicated in Fig. 1. All of the ZnO NPs were characterized by 30×30×30 supercells of the hexagonal crystal structure (wurtzite, space group *P6₃mc*). We *carved* a spherical ZnO NP from this bulk hexagonal *supercell*. The radius of the NP is set to the desired value (0.9 nm) and only atoms within that sphere are considered, whereas those outside the sphere are removed. All calculations are carried out at constant volume.

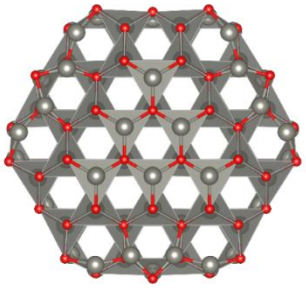

Figure 1. Initial structure (polyhedral) of undoped ZnO NP with 258 atoms. (Red is Oxygen, grey is Zinc).

The n_{ij} represents the nearest neighbor contacts number, which is also the number of bonds, and usually used to distinguish the degree of packing, a significant property of NP. The n_{ij} (Wu, et al. 2016) for the NPs is given by

$$n_{ij} = \sum_{i<j} \delta_{ij} \qquad (1)$$

where $\delta_{ij} = \begin{cases} 1, r_{ij} \leq 1.2 r_{ij}^{(0)} \\ 0, r_{ij} > 1.2 r_{ij}^{(0)} \end{cases}$ $i, j =$ Zn, O or N, r_{ij} is the distance between i and j atoms and $r_{ij}^{(0)}$ is obtained by fitting the experimental data and represents a nearest neighbor criterion (NIST, 2019; Czajkowski, et al. 1999). Fig. 2 indicates the total n in the ZnO NP with 258 atoms. The curve of ZnO NP in Fig. 2 reveals that the n of N-N and N-O interactions increases gradually in terms of increase in the content of N. Moreover, the total n of Zn-Zn interactions is comparatively smaller than the total n, while the n of N-N is the smallest. These results show that N atoms incline to make more bonds with O atoms: that Zn_2 tends to locate at the surface. Additionally, the total n of Zn-Zn bonds is larger than that of N-N, N-O, O-O and Zn-Zn. it means that Zn atoms have a higher priority for N or O atoms than for Zn atoms based on the increase of N content. Here, it is interesting to note that there is no experimental data on the Zn-O and Zn-N two-body interactions, thus, Zn atoms probably adhere to N or O atoms.

R_{T_i} represents the order parameter and is used to find a stable structure in the NP. One needs to calculate R_{T_i} (Kurban, et al. 2016) which helps to investigate the segregation of atoms in the NP. R_{T_i} is the average distance of a type T_i atoms according to a center of a NP,

$$R_{T_i} = \frac{1}{n_{T_i}} \sum_{i=1}^{n_{T_i}} r_i \qquad (2)$$

where is the number of T_i type atoms, and r_i is the distance of the atoms to the coordinate center . We define a distance from the center of NP to a reference point as ϵ to indicate the location of atoms; if $R_{T_i} < \epsilon_{min}$ (a "small" value), the T_i type atoms are assumed to be at the center, and if $R_{T_i} > \epsilon_{max}$ (a "large" value), the T_i type atoms are assumed to be at the surface region of NP. If neither is true, *i.e.*, if $\epsilon_{min} \leq R_{T_i} \leq \epsilon_{max}$ (a "medium" value), it is assumed a well-mixed NP.

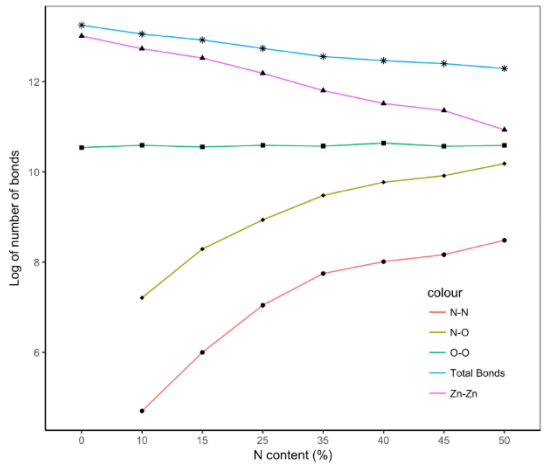

Figure 2. The number of bonds of binary N-N, N-O, O-O and Zn-Zn interactions based on an increase in the content of N atoms.

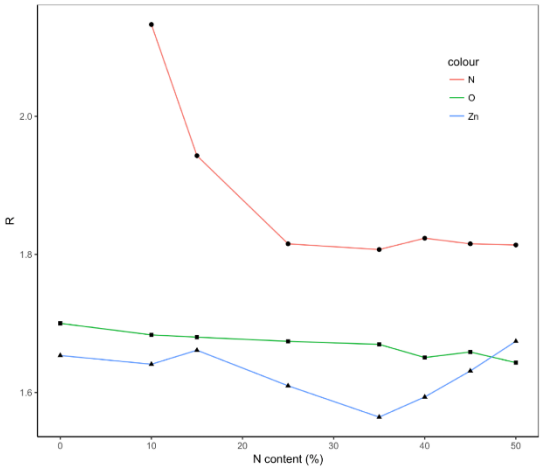

Figure 3. The order parameter of Zn, O and N atoms in the ZnO NPs.

Fig. 3 demonstrates the *R* of Zn, O and N atoms based on the N content in the ZnO NPs. Here, the *R* shows the changes in the structural properties of ZnO NP with a change N-doped ZnO NPs. The *R* of Zn, O and N atoms indicate that N atoms incline to locate at the center, while Zn atoms tend to occupy the surface. The *R* of N atoms to the surface is related to its lower cohesive energy. Besides, the *R* demonstrates different features when it comes to an increase in the content of N atoms. For example, R_{Zn} values sharply increase after doping 35% N, and R_O smoothly decrease.

The Radial Distribution Function (RDF), a significant parameter, is known as the probability of finding a particle at a distance *r* from another tagged particle. The RDF is mathematically shown as follows:

$g_{(r_i)} = n_{(r_i)}/(|\Delta| \times V_s \times V_d)$ where $n_{(r_i)}$ represents the mean number of atoms in a shell of width dr at distance r_i, $|\Delta|$ is the total atom number and V_s is the volume of the spherical shell and V_d is the mean atom density.

Fig. 4 indicates the RDF Zn-Zn, O-O and N-N two-body interactions in the studied ZnO NPs. The RDFs are searched for each interactions of optimized NPs. Zn-Zn has a narrower and higher distribution than O-O interactions. With regards to an increase in the content of N, the peaks for both pairs increase. Moreover, the fluctuations were observed in obvious peaks of N-N interactions with raising the content of N.

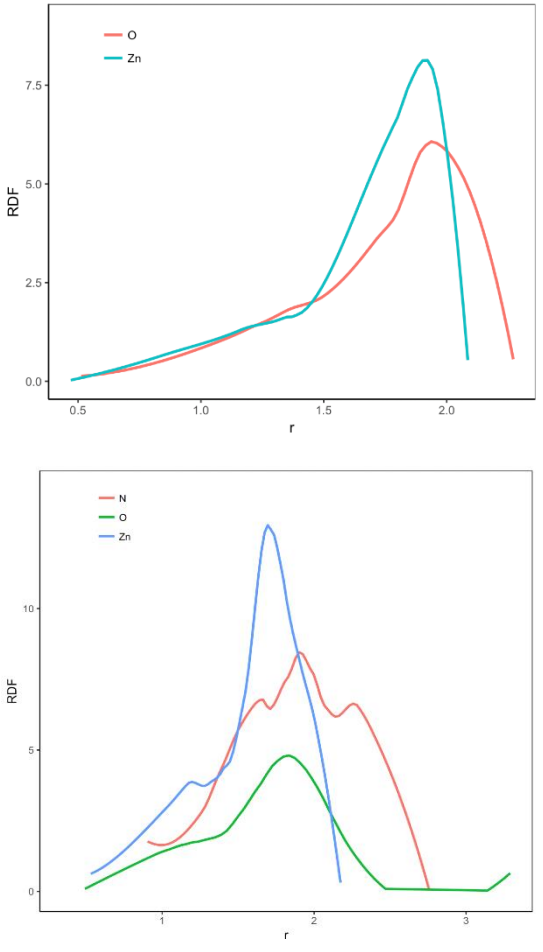

Figure 4. Radial distribution function of undoped (up) and doped (down) ZnO NPs.

3.2. Electronic structure

In Fig. 5, we demonstrate the results of the HOMO, LUMO and Fermi levels with respect to N content to acquire detailed information on electronic states in the undoped and N-doped ZnO NPs. When it comes to an increase in the content of N, the density of localized states concomitantly decreases, thus the greatest contribution comes from the undoped ZnO NPs and then these fluctuations progressively also disappear. It has a sharply increasing tendency to occur in the region of between -10 and -15 eV. The DOS figures also demonstrate that the studied ZnO NPs have the energy gap, so, all the NPs indicate semiconductor character. With increasing the content of N, the changes in HOMO, LUMO and Fermi energy were predicted in a different manner like an increase and a decrease.

The HOMO energy level for undoped ZnO NP is -7.89 eV, *i.e.*, about 0.97 eV higher than that of the 50% N-doped NP (-6.91 eV) which is the lowest HOMO level among the other NPs models and thus it is less reactive, but more stable (see Fig. 6, Table 1). On the other hand, Fermi energies are in the middle of the valence and conduction band. The HOMO-LUMO energy gap of undoped ZnO NP is 4.71 eV, which decreases from -4.717 to -0.853 eV. It is clear then that an increase in the content of N atoms contributes to the destabilization of ZnO NPs due to a decrease in the energy gap.

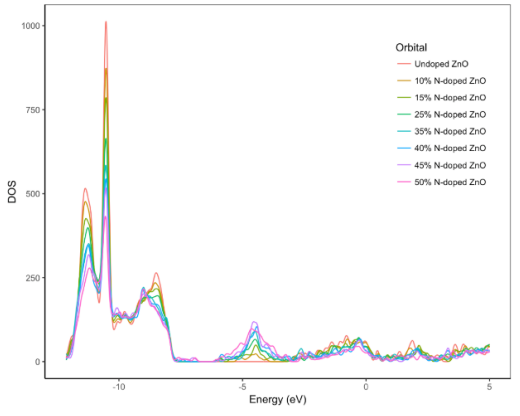

Figure 5. The total density of states (DOS) of undoped and N-doped ZnO NPs.

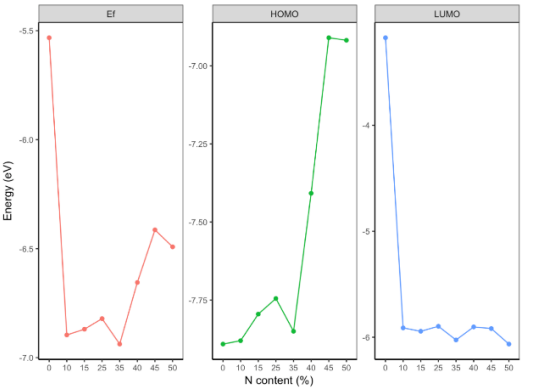

Figure 6. HOMO, LUMO and Fermi energies of undoped and N-doped ZnO NPs.

Table 1. The electronic properties such as HOMO (H), LUMO (L), Energy gap (E_g), and Fermi energy (E_F) of undoped and N-doped ZnO NPs.

	H	L	E_g	E_F
Undoped ZnO	-7.89	-3.17	4.71	-5.53
10% N-doped	-7.88	-5.91	1.96	-6.89
15% N-doped	-7.79	-5.94	1.85	-6.86
25% N-doped	-7.74	-5.89	1.84	-6.82
35% N-doped	-7.85	-6.02	1.82	-6.93
40% N-doped	-7.40	-5.90	1.50	-6.65
45% N-doped	-6.91	-5.91	0.99	-6.41
50% N-doped	-6.91	-6.06	0.85	-6.49

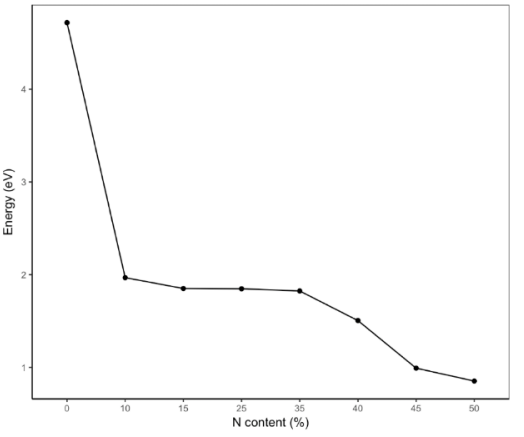

Figure 7. HOMO-LUMO energy gap of undoped and N-doped ZnO NPs.

4. Discussion and Conclusions

In this study, we use the DFTB method and study electronic structural features of undoped and Nitrogen (N)- doped ZnO NPs with 258 atoms. To carry out structural analysis, we developed a

new code in R code to conduct structural analysis, i.e., analyzing the RDF, *n* and *R* of two-body interactions of atoms in the ZnO NPs. Our results show that the total *n* of Zn-Zn two-body interactions is larger than that of N-N, N-O, O-O, and Zn-Zn; thus, it means that Zn atoms have a higher priority for N or O atoms. N atoms contribute to the stabilization of the ZnO NPs. The *R* of Zn, O and N atoms indicate that N atoms tend to locate at the center, while Zn atoms incline to occupy the surface. The HOMO decreases; however, the LUMO increase, thus the HOMO-LUMO band gap declines from 4.717 to 0.853 eV. The decline in the HOMO value contributes to the stabilization of the ZnO NPs. The DOS analysis also shows that ZnO NPs exhibits a semiconductor-like character.

Acknowledgements

The calculations were partially carried out at TUBITAK ULAKBIM, High Performance and Grid Computing Centre (TRUBA resources), Turkey.

Kaynaklar

Aradi, B., Hourahine, B., Frauenheim, T. (2007). DFTB+, a Sparse Matrix-Based Implementation of the DFTB Method. J. Phys. Chem. A 111, 5678-5684.

Barzinjy, A. A., Mustafa, S., Ismael, H. H. J. (2019). Characterization of ZnO NPs Prepared from Green Synthesis Using Euphorbia Petiolata Leaves. EAJSE 4, 74-83.

Caglar, M., Ilican, S., Caglar, Y., Yakuphanoglu F. (2019). Electrical conductivity and optical properties of ZnO nanostructured thin film. Appl. Surf. Sci. 255, 4491-4496.

Chang S-P., Chen, K-J. (2012). Zinc Oxide NP Photodetector. J. Nanomater. 2012, 1-5.

Coşkun, B., Mensah-Darkwa, K., Soylu, M., Al-Sehemi, A. G., Dere, A., Al-Ghamdi, A., Gupta, R.K., Yakuphanoglu, F. (2018). Optoelectrical properties of Al/p-Si/Fe:N doped ZnO/Al diodes. Thin Solid Films 653, 236-248.

Czajkowski, M. A., Koperski, J. (1999). The Cd2 and Zn2 van der Waals dimers revisited. Correction for some molecular potential parameters. Spectrochim. Acta, Part A 55, 2221-2229.

Gaus, M., Goez, A., & Elstneri, M. (2013). Parametrization and Benchmark of DFTB3 for Organic Molecules. J. Chem. Theory Comput. 9, 338-354.

Koç, M. M., Aslan, N., Erkovan, M., Aksakal, B., Uzun, O., Farooq, W. A., Yakuphanoğlu, F. (2019). Electrical characterization of solar sensitive zinc oxide doped-amorphous carbon photodiode. Optik 178, 316-326.

Kubillus, M., Kubař, T., Gaus, M., Řezáč, J., & Elstner, M. (2015). Parameterization of the DFTB3 Method for Br, Ca, Cl, F, I, K, and Na in Organic and Biological Systems. J. Chem. Theory Comput. 11, 332–342.

Kurban, M. (2018). Size and composition dependent structure of ternary Cd-Te-Se nanoparticles. Turk. J. Phys. 42, 443-454.

Kurban, M. Malcıoğlu, O. B. Erkoç Ş. (2016). Structural and thermal properties of Cd-Zn-Te ternary NPs: Molecular-dynamics simulations. Chem. Phys. 464, 40-45.

Kushwaha, A. K. (2012). Lattice dynamical calculations for HgTe, CdTe and their ternary alloy CdxHg1−xTe. Comp. Mater Sci. 65, 315-319.

NIST Standard Reference Database (2019). Experimental bond lengths. https://cccbdb.nist.gov/expbondlengths1.asp. (Access Date: 10.05.2019).

Rezkallah, T., Djabri, I., Koç, M. M., Erkovan, M., Chumakov, Yu., Chemam, F. (2017). Investigation of the electronic and magnetic properties of Mn doped ZnO using the FP-LAPW method. Chin. J. Phys. 55, 1432-1440.

Wang, CL., Zhang, H., Zhang, JH., Li, MJ., Sun, HZ., Yang, B. (2007). Application of Ultrasonic Irradiation in Aqueous Synthesis of Highly Fluorescent CdTe/CdSCore-Shell Nanocrystals. J. Phys. Chem. C111, 2465-2469.

Wu, X., Wei, Z., Liu, Q., Pang, T., Wu, G. (2016). Structure and bonding in quaternary Ag-Au-Pd-Pt clusters. J Alloy. Compd. 687, 115-120.

Yang, P., Tretiak, S., Masunov, A. E., Ivanov, S. (2008). Quantum chemistry of the minimal CdSe clusters. J. Chem. Phys. 129, 074709-1—074709-12.

Zhang, Y., Nayak, TR., Hong, H., Cai, W. (2013). Biomedical applications of zinc oxide nanomaterials. Curr. Mol. Med. 13(10), 1633-1645.

Bilge International Journal of Science and Technology Research

Web : http://dergipark.gov.tr/bilgesci - **E-mail:** kutbilgescience@gmail.com

Received: 17.11.2019
Accepted: 23.12.2019
DOI: 10.30516/bilgesci.647894

ISSN: 2651-401X
e-ISSN: 2651-4028
3(Special Issue), 40-44, 2019

The Effects of A Single Atom Substitution and Temperature on Electronic and Photophysical Properties F8t2 Organic Material

Mustafa Kurban[1*]

Abstract: The electronic and photophysical features of F8T2 organic semiconductor-based on a single atom substitution and temperature have been carried out by the self-consistent charge density-functional based tight-binding (SCC-DFTB) which is based on the density functional theory (DFT) and molecular dynamics (MD) methods. First of all, the heat treatment was carried out on the F8T2 from 50 K to 600 K. After that, the optoelectronic features of F8T2 by substitution of some nonmetallic single atoms, such as Fluorine (F), Bromine (Br) and Iodine (I) was studied. Herein, the dipole moments, HOMO, LUMO, bandgap and Fermi energies were searched. Also, the absorbance has been examined by time-dependent (TD)-DFTB. The obtained results of F8T2 were compared to experimental results. The HOMO value was found as -5.045 eV, which is compatible with its experimental value (-5.44 eV); the LUMO value was found -2.729 eV, which is coherent with the experimental LUMO value (-2.95 eV). Similarly, the bandgap of F8T2 (2.32 eV) was found to be compatible with measured result (2.49 eV). The bandgap for F8T2 increased from 2.32 eV (at 0 K) to 3.03 K (at 663.38 K) which is about 0.71 eV wide than that of F8T2 at 0 K. The maximum absorbance is found as 437 nm which is very well matched with experimental value (465 nm).

Keywords: F8T2, Absorbance, Electronic structure, TD-DFTB.

1. Introduction

Recently, organic semiconductors have been of significant attention in many applications such as electronic and photonic applications (Cheng, et al. 2019; Zhang, et al. 2018). Among them, poly[(9,9-dioctylfluorenyl-2,7-diyl)-co-bithiophene] (F8T2) which has high ionization potential (5.5 eV), is a significant category in organic field-effect phototransistors as the active material (Whang, et al. 2010; Sirringhaus, et al. 2000). Besides, the transistors demonstrate a highly stable and reproducible response when exposed to temperature (Whang, et al. 2010).

The photophysical features of materials are highly tunable with a change in temperature and an atom doped on it (Kurban, 2018; Kurban, et al. 2016). Herein, the electronic structure and photophysical features of organic F8T2 semiconductor have been studied by the self-consistent charge density-functional based tight-binding (SCC-DFTB) which is based on the density functional theory (DFT) and molecular dynamics (MD) methods in this study (Aradi, et al. 2007; Elstner, et al. 1998). First of all, the heat treatment was carried out on the F8T2 from 50 K to 600 K. After that, the properties mentioned above of F8T2 by substitution of some nonmetallic single atoms, such as Fluorine (F), Bromine (Br) and Iodine (I), was performed. The dipole moments to understand the interactions in F8T2 molecule, as well as, HOMO, LUMO, bandgap energies and Fermi energies were investigated. Also, the absorbance spectra were carried out time-dependent (TD)-DFTB.

2. Material and Method

The electronic and photophysical properties of undoped and Br-, I- and F-doped F8T2 have been examined using SCC-DFTB implemented in DFTB+ code (Aradi, et al. 2007) with the 3ob/3ob-

[1]Kırşehir Ahi Evran University, Department of Electronics and Automation, 40100, Kırşehir, Turkey
* Corresponding author (Mustafa Kurban): *mkurbanphys@gmail.com

Citation (Atıf): Kurban, M. (2019). The Effects of A Single Atom Substitution and Temperature on Electronic and Photophysical Properties F8t2 Organic Material. Bilge International Journal of Science and Technology Research, 3(Special Issue): 40-44.

3-1 (Gaus, et al. 2013; Kubillus, et al. 2015) set of Slater Koster parameters. On the other hand, DFTB approximates a Taylor series expansion of the total energy density functional theory (DFT). The SCC-DFTB includes a self-consistent charge step, optimizing the (Mulliken) charges, thus it improves very much the accuracy of the DFTB method. MD method was used to search temperature dependence properties in the frame of DFTB+ code. Besides, the absorption spectra were calculated by the TD-DFTB method based on Casida's approach (Andersen, 1980).

3. Results

The different views obtained from the optimized geometry of F8T2 organic molecule are indicated in Fig. 1.

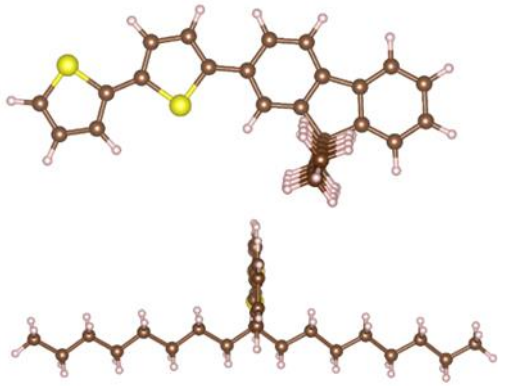

Figure 1. Different views obtained from the optimized geometry of F8T2 organic molecule. (Yellow is Sulfur, purple is Hydrogen and brown is Carbon).

To get more information on electronic states in undoped F8T2 organic semiconductor, firstly, a deep analysis has been performed on the electronic total DOS at different temperatures and doped single atoms (see Fig. 2). The density of localized states decreases in terms of an increase in temperature where the greatest contribution comes from F8T2 at 0 K and Br-doped F8T2. These oscillating behaviors progressively continue based on the increase in temperature, but there is a shift in energy values. The density of localized states shows a sharp increase between -8 and -7 eV. Besides, the DOS analysis demonstrates that F8T2 have the bandgap, so, all the nanoparticles show semiconductor character. There is an increase in HOMO, and a decrease in LUMO and Fermi energy is slightly increasing with increasing temperature in the range of 0-600 K.

The HOMO value for F8T2 organic semiconductor is -5.04 eV wide, i.e., about 0.40 eV smaller than the experimental data (-5.44) (Kettner, et al. 2016), which is more reactive, while being less stable than F8T2 at high temperatures (see Fig. 3). Fermi energies are in the middle of the valence and conduction band. The HOMO-LUMO energy gap of F8T2 is 2.31 eV, which increases from 2.31 to 3.03 eV in the range of 0-600 K (see Fig. 4), because of the interatomic spacing increases. It is clear then that a rise in the temperature contributes to the stabilization of F8T2 because of an increase in the bandgap. The total energy (per/atom), which is the sum of potential and kinetic energy, also increases under heat treatment (see Fig. 4).

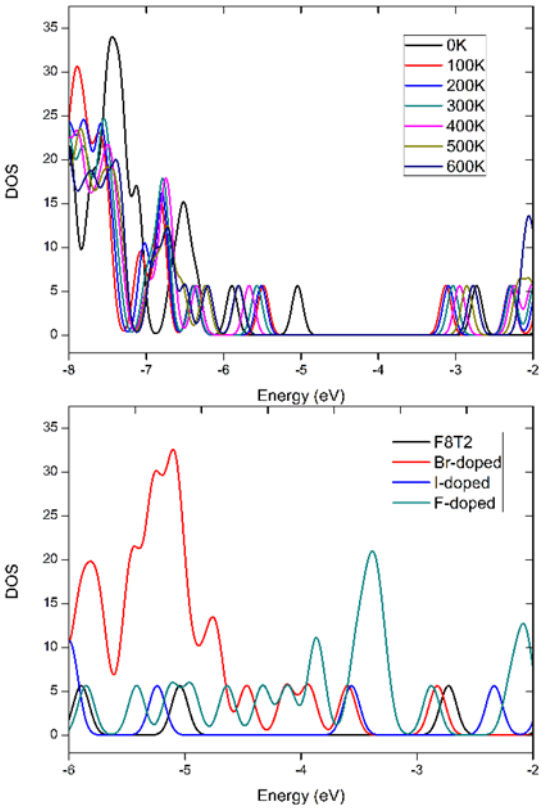

Figure 2. The total density of states (DOS) under heat treatment and atom doped F8T2.

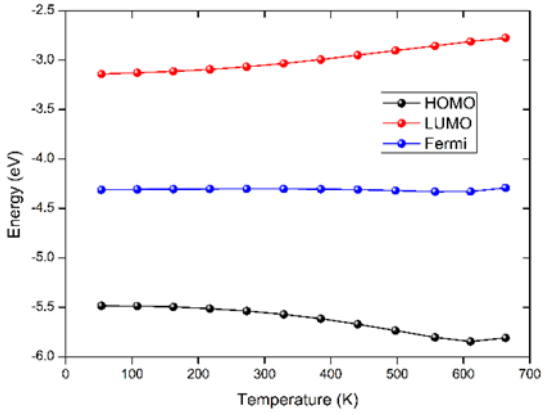

Figure 3. The HOMO, LUMO and Fermi energy levels of F8T2 under heat treatment.

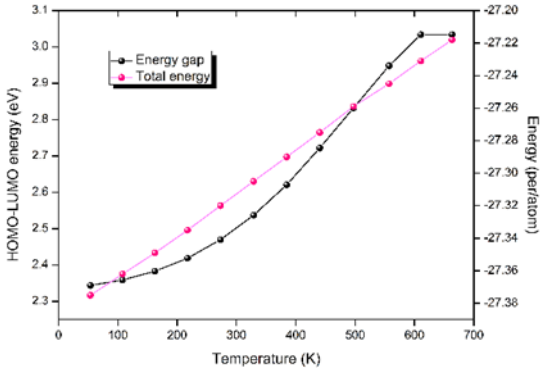

Figure 4. The variations of the HOMO-LUMO energy gap and total energy (per/atom) of F8T2 under heat treatment.

On the other hand, the energetic properties of Br, I and F doped-F8T2 have been investigated. The HOMO, LUMO, bandgap and Fermi energies were given in Table 1. The bandgap of pure F8T2 are in the following decreasing order: F8T2> I-doped F8T2> F-doped F8T2> Br-doped F8T2 (see Table 1). The experimental energy gap value of F8T2 is 2.49 eV wide (Kettner, et al. 2016), i.e., about 0.17 eV greater than that of DFTB calculations which are very compatible with experimental data. The HOMO value for Br-doped F8T2 organic semiconductor is -3.78 eV wide, i.e., about 1.26 eV smaller than that of undoped F8T2 (-5.04 eV). The HOMO value for I-doped F8T2 is -5.17 eV wide, i.e., about 0.12 eV greater than undoped F8T2. This also indicates that the transfer of the electrons from HOMO to LUMO for Br-doped F8T2 is easier that of undoped and I and F-doped F8T2.

Table 1. The HOMO (H), LUMO(L), Energy gap (Eg) and Fermi Energy (EF) of undoped and Br-, I- and F-doped F8T2.

Structures	H	L	E_g	E_F
F8T2-DFTB	-5.04	-2.72	2.31	-3.88
F8T2-Exp.	-5.44	-2.95	2.49	-
I-doped	-5.17	-3.49	1.67	-4.33
F-doped	-4.79	-3.13	1.66	-3.96
Br-doped	-3.78	-2.68	1.09	-3.23

The dipole moment (D_M) is related to differences in electronegativity. The bigger D_M corresponds to stronger intermolecular force. Herein, the D_M in x-, y- and z-directions as a function of temperature was shown in Fig. 5. Our results show that the *Dx* (-0.48 Debye) at 0 K for F8T2 causes the largest negative charge separation in the x-direction. D_M decreases in terms of temperature along x-directions; it increases along y and z directions. After 500 K, it started increasing up to almost 663 K. When it comes to Br, I and F doped F8T2, the biggest component of DM for Br-doped F8T2 is found to be along the x-axis (-1.39 Debye) which

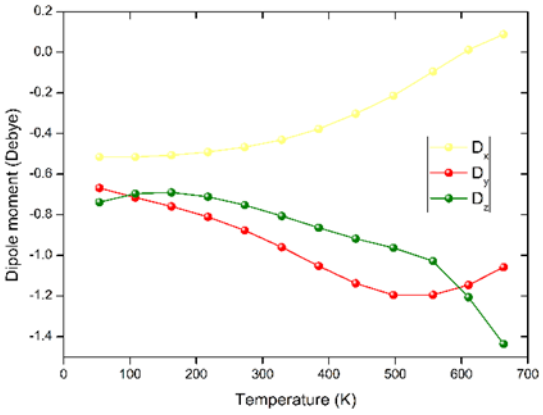

Figure 5. The variations of dipole moments of F8T2 in different x, y, z directions under heat treatment.

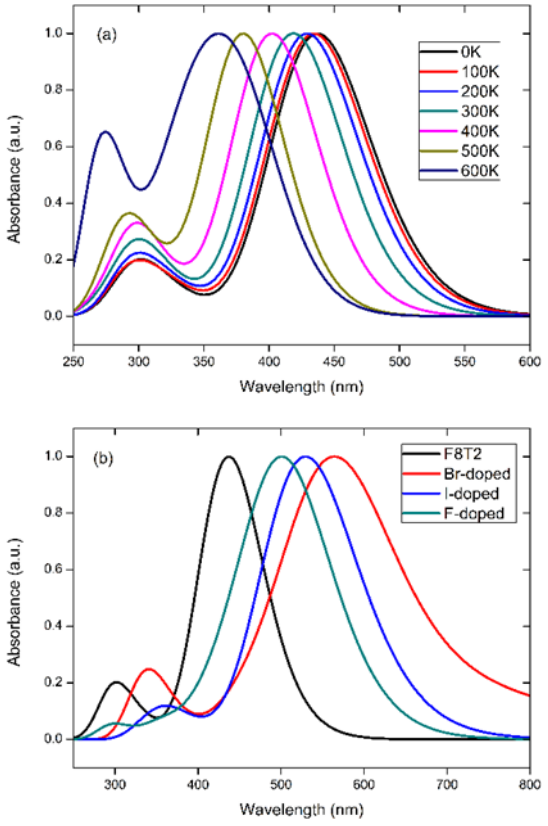

Figure 6. Absorbance spectra of (a) undoped F8T2 under heat treatment and (b) atom doped F8T2.

means large negative charge separation in the x-direction.

The biggest value of DM for Br-doped F8T2 corresponds to the stronger interaction among the atoms in the molecule. These results are compatible with the bandgap because the lowest bandgap of Br-doped F8T2 infers that electrons easily jump from HOMO to LUMO. Herein, there is a correlation between DM and the bandgap of the undoped and doped FT82. Thus, it can be expressed that the large DM has small bandgap.

Absorbance spectra of F8T2 at different temperatures and Br, I and F-doped F8T2 were depicted in Fig. 6 (a, b). The F8T2 exhibits the maximum peaks 2.84 eV (436 nm) for undoped F8T2 corresponds to the ultraviolet (UV) region, which is very well matched with experimental data 2.66 eV (465 nm) (Kettner, et al. 2016). The absorbance spectrum of F8T2 decreases concomitantly with an increase in temperature where the maximum spectra of F8T2 (361 nm; 3.43 eV) are smallest at 600K. The absorption peaks are getting narrower and have smaller magnitude from 0 K to 600 K. It is also clear from the spectra that the structures are shifted towards higher energy in going from 0 K to 600 K. Absorbance spectra of Br-, I- and F-doped F8T2 are 2.20 eV (563 nm), 2.34 eV (529 nm) and 2.38 eV (501 nm), respectively. The obtained results show that a single atom substitution significantly improves the photophysical properties of F8T2.

4. Discussion and Conclusions

The electronic and photophysical properties of F8T2 organic semiconductor-based on a single atom substitution and temperature have been researched by the DFTB approach. The predicted HOMO (-5.045 eV) and LUMO (-2.729 eV) energies were compatible with measured HOMO (-5.44 eV) and LUMO (-2.95 eV) energies. Besides, the bandgap (2.32 eV) is compatible with measured result (2.49 eV). The bandgap of F8T2 increased from 2.32 eV (at 0 K) to 3.03 K (at 663.38 K) which is about 0.71 eV wide than that of F8T2 at 0 K. The biggest component of dipole moment for Br-doped F8T2 is along the x-axis (-1.39 Debye), thus there is a large negative charge separation in the x-direction. Besides, there is a correlation between D_M and the energy gap of the undoped and doped FT82. The maximum absorbance is 437 nm which is very well matched with experimental value (465 nm). Br-, I- and F- were doped on F8T2; such doping procedure significantly improves the photophysical properties of F8T2.

Acknowledgements

The numerical calculations were also partially carried out at TUBITAK ULAKBIM, High Performance and Grid Computing Centre (TRUBA resources), Turkey.

References

Andersen, H.C. (1980). Molecular Dynamics Simulations at Constant Pressure and/or Temperature. J. Chem. Phys. 72(4), 2384-2393.

Aradi, B., Hourahine, B., Frauenheim, T. (2007). DFTB+, a Sparse Matrix-Based Implementation of the DFTB Method. J. Phys. Chem. A 111, 5678-5684.

Cheng, Z., Wang, Y., O'Carol, D. M. (2019). Influence of Partially-Oxidized Silver Back Electrodes on the Electrical Properties and Stability of Organic Semiconductor Diodes. Org. Electron. 70, 179-185.

Elstner, M., Porezag, D., Jungnickel, G., Elsner, J., Haugk, M., Frauenheim Th., Suhai, S. Seifert G. (1998). Self-Consistent-Charge Density-Functional Tight-Binding Method for Simulations of Complex Materials Properties. Phys. Rev. B 58, 7260-7268.

Gaus, M., Goez, A., & Elstneri, M., (2013). Parametrization and Benchmark of DFTB3 for Organic Molecules. J. Chem. Theory Comput. 9, 338-354.

Kettner, O., Pein, A., Trimmel, G., Christian, P., Röthel, C., Salzmann, I., Resel, R., Lakhwani, G., Lombeck, F., Sommer, M., Friedel, B. (2016). Mixed Side-Chain Geometries for Aggregation Control of Poly(Fluorene- Alt-Bithiophene) and Their Effects on Photophysics and Charge Transport. Synth. Met. 220, 162–173.

Kubillus, M. Kubař, T., Gaus, M., Řezáč, J., Elstner, M., (2015). Parameterization of the DFTB3 Method for Br, Ca, Cl, F, I, K, and Na in Organic and Biological Systems. J. Chem. Theory Comput. 11, 332–342.

Kurban, M. (2018). Electronic Structure, Optical and Structural Properties of Si, Ni, B and N-Doped A Carbon Nanotube: Dft Study. Optik 172, 295-301.

Kurban, M. (2018). Size and Composition Dependent Structure of Ternary Cd-Te-Se Nanoparticles. Turk. J. Phys. 42, 443-454.

Kurban, M., Malcıoğlu, O. B., Erkoç, Ş. (2016). Structural and Thermal Properties of Cd–Zn–Te Ternary Nanoparticles: Molecular-Dynamics Simulations. Chem. Phys. 464, 40-45.

Sirringhaus, H., Kawase, T., Friend, R. H., Shimoda, T., Inbasekaran, M., Wu, W., Woo, E. P. (2000). High-Resolution Inkjet Printing of All-Polymer Transistor Circuits. Science 290, 2123-2126.

Wang, X., Wasapinyokul, K., Tan, W. D., Rawcliffe, R. Campbell, A. J., Bradley, D. D.C. (2010). Device Physics of Highly Sensitive Thin Film Polyfluorene Copolymer Organic Phototransistors. J. Appl. Phys. 107, 024509 (1-10).

Zhang, X., Dong, H., Hu, W. (2018). Organic Semiconductor Single Crystals for Electronics and Photonics. 30, 1801048 (1-34).

Bilge International Journal of Science and Technology Research

Web : http://dergipark.gov.tr/bilgesci - **E-mail:** kutbilgescience@gmail.com

Received: 18.11.2019
Accepted: 25.12.2019
DOI: 10.30516/bilgesci.648096

ISSN: 2651-401X
e-ISSN: 2651-4028
3(Special Issue), 45-57, 2019

Numerical Simulation of Annular Flow boiling in Millimeter-scale Channels and Investigation of Design Parameters Using Taguchi Method

Aliihsan Koca[1]*, Mansour Nasiri Khalajı[2]

Abstract: As the technology progresses, the electronic components become smaller and at the same time continue to produce more heat, and therefore development of new high heat-flux cooling technologies have become obligatory. The mini and millimeter-scale phase change cooling systems, which have a reduced size and a large surface area where heat transfer can take place, have become an integral part of advanced cooling systems. When comparing phase-change cooling systems with other cooling systems, a relatively low flow rate of very high evaporation heat, which is associated with the phase change for most fluids, allows large amounts of heat to dissipate with flow boiling and substantially solves the many problems. The two-phase cooling technologies used for critical applications include; heat pipes, loop heat pipes and capillary pumped loops which are all passive hence very reliable solutions relying on only capillary effects. Though this passive device cannot meet future high cooling demands because of the limitations of the capillary pumping in terms of heat flux, transport distance and multiple heat source capabilities. On the other hand, in boiling and condensing flows functionality problems arise since at the micrometer and millimeter-scale, shear/pressure forces dominate over gravitational forces and cause thermally hydro-dynamically ineffective/problematic liquid-vapor configurations – such as plug/slugs flow regimes. For this reason, to overcome the requirement of large amounts of heat transfer from limited spaces and resolving the above problem, novel millimeter-scale phase-change devices should be developed. In this study, for the design of millimeter-scale boilers a 3D Ansys-Fluent© simulation model was developed and numerical simulations were conducted for two different cooling fluids (water and FC-72), different mass flow rates and two different channel heights. Moreover, to examine the simulation results Taguchi method was used. In order to realize thin film annular flow over the boiler surface, employed specific boundary conditions in the 3D simulation model were obtained by means of one dimensional Matlab© simulation code. By means of utilizing the evaluated numerical results, distribution of heat transfer coefficient, vapor quality and pressure drop over the heat transfer surfaces were reported.

Keywords: Heat Transfer, Boiling flow, Phase Change, Computational Fluid Dynamics, Taguchi Method.

1. Introduction

The rapid improvements in the performance of miniature and electronic devices have resulted in a significant challenge in the thermal management of these devices. The heat dissipation from these high-performance and compact devices has reached great values, and as a result traditional cooling methods such as air cooling have become ineffective. The heat transfer coefficient in applications such as high-power lasers, microwave devices and radars is about 10 MW/m^2 (Lee and Mudawar, 2008). However, overpressure drop and uneven temperature distribution can be accompanied by electronic chips. In contrast, flow boiling in mini and millimeter channel heat sinks

[1]Fatih Sultan Mehmet Vakif University, Faculty of Engineering, 34445, Istanbul, Turkey
[2]Ataturk University, Faculty of Engineering, 25240, Erzurum/Turkey
* Corresponding author: * ihsankoca@hotmail.com

Citation (Atıf): Koca, A., Khalaji, M.N. (2019). Numerical Simulation of Annular Flow boiling in Millimeter-scale Channels and Investigation of Design Parameters Using Taguchi Method. Bilge International Journal of Science and Technology Research, 3(Special Issue): 45-57.

can achieve higher heat transfer rates, better axial temperature homogeneity, lower mass flow rates, and lower pressure differential or less pumping power than single-phase flow (Consolini and Thome, 2009; Karayiannis et al., 2010).

The increasing development of electronical systems has become an increasing trend among the separate branches of the Defense industry (Park and Vallury, 2006; Park and Jaura, 2002; Kuszewski and Zerby 2012; Ponnappan et al., 2002; Park and Zuo, 2004).

In the defense industry of many developed countries, research has been conducted to increase the power density while reducing the size of the hybrid electric vehicle, electrical electronic subsystems, and the component parts to increase the component power that supports this strategy (Moore, 1993; Urciuoli et al., 2012). However, the new generation of electronic systems produces multiple kilowatt waste heat with heat fluxes at a predicted future device level up to 1000 W/cm² (Lee and Mudawar, 2009). To achieve this, innovative condensers and boilers operating in the cyclic regime and interrupted by the negligible effect of gravity must be developed (Kivisalu et al., 2014). The advantages of operating these capacitors in pulsatile mode are also discussed. Such millimeter-scale capacitors (Kivisalu et al., 2014) are of great value in the design of new generation space-based thermal systems and gravity insensitive aircraft-based systems (including avionics cooling).

The application of various micro and mini channel designs has started to gain considerable importance (Tuckerman and Pease, 1981; Sullivan, et al., 1992; Hall and Mudawar, 1995). Regardless of a particular heat sink configuration, critical cooling options carried out beyond a laboratory environment are based on almost single-phase liquid flow designs (Mudawar, 2009). But with the ever-increasing electronic heat flows and the installation of single-phase thermal management problems, cooling schemes using liquid-vapor phase change (two-phase cooling) have been examined as a new generation cooler superior to single-phase cooling systems that are practical and cost-conscious. In many studies, it has already well-known two-phase flow technologies as an appropriate solution to meet the stringent demands for high cooling needs requirements (Kuszewski and Zerby 2012; Ponnappan et al., 2002). In the two-phase cooling cycle, when it exceeds the boiling point, a portion of it is obtained in a gas/liquid mixture and at least a portion of the liquid is converted into vapor upon heating. This generally means that the temperature of the heat-collecting surface is called the saturation temperature of the liquid or boiling and the use of a cooling fluid. At this temperature, the vapor pressure of the liquid is equal to the ambient pressure, thus causing vapor bubbles to form, grow and eventually detach from the surface at the solid and liquid interface. As shown in Figure 1, the heat transfer coefficients obtained from the two-phase flow may have a greater heat transfer than equivalent single-phase forced or natural heat convection (Mudawar, 2001).

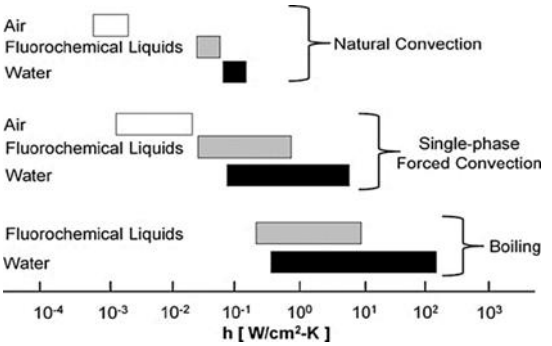

Figure 1. Heat transfer coefficients for various fluids (Mudawar, 2001).

Two-phase mini and millimeter channel systems have received great interest as a method for electronic cooling with high heat flux. Although it has been shown that flow in the large surface area of the microchannels increases the heat transfer coefficient in single-phase flow (Tuckerman and Pease, 1981; Phillips, 1990). Additional gains in heat transfer coefficient can be obtained by allowing the liquid to evaporate along the mini and millimeter channel walls. For these reasons, recent research has focused on two-phase cooling and mini and millimeter channel flow boiling. The controlled heat transfer mechanism in the mini and millimeter channels is thought to be the evaporation of the thin liquid film around the bubbles in the micro-channels (Chen, et al., 2013; Mersen, 2017). There are several general literature reviews of one-dimensional and two-dimensional FC-72 flow boiling and heat transfer, depending on channel geometry (Pereira et al., 2017; Ansys, 2017; Kivisalu et al., 2014; Naik, et al.2014).

In this study, we will examine the numerical heat transfer with different ducts at different heights,

refrigerants with different properties, different flow rates, different vapor qualities, fluid pressures and different heat fluxes with Taguchi method.

2. Material and Method

2.1. Taguchi method

The Taguchi method is an experimental design method that tries to minimize the number of experiments by selecting the most optimal combination of levels of factors that can be controlled against uncontrollable factors that consist of variables and levels before conducting experiments (Canıyılmaz, 2001; Ömeroğlu, 2018).

In this method, one of the ranking method, observation method, variance method, analysis of factor effects, column differences method and graphical representation methods are applied to determine factor levels (Ross, 1989). In another study (Caliskan, et al., 2015), using the Taguchi method, Reynolds's number and jet-plate distances performed heat transfer measurements on the surface for a sequential jet array.

In this study, by means of using Taguchi experimental design method, optimum levels of parametric values were applied in order to examine the in heat transfer characteristics in a millimeter channel.

Taguchi analysis was carried out by using Minitab 18.0©, which has a capability to evaluate the statistical functions. In the Minitab software, orthogonal array (OA) designs for the array design, whose degrees of freedom should be greater than or at least equal to those of the design parameters, generated. Therefore, L8 corresponds to the design considered and the factors are shown in Table 1. The main target is to increase the bubbles and therefore maximum heat transfer. The performance statistics were preferred as the optimization measure and implemented for the "large is better" condition and determined by means of the below equation.

$$Z_L = -10\log\left(\frac{1}{n}\sum_{i=0}^{n}\frac{1}{Y_i^2}\right) \quad (1)$$

Where, Y is the performance value of the experiments and Z shows the performance statistics, while n is the repetition number in the experiments.

Table 1. Parameters and their values corresponding to their levels

Parameters	Levels	
Channel height	5mm	8mm
Fluid Material	Water	FC-72
Heat flux	107 w/m^2	200 w/m^2
Pressure	1.5 bar	3 bar
Total Mass flow rate	140 kg/m^{2}s	200 kg/m^{2}s
Steam quality	0.61	0.67

In the test plan, optimum operating conditions for optimum values of parameters affecting system performance may not be always available. Ideal operating conditions which correspond to performance could be evaluated by means using the Orthogonal Array (OA) balanced character.

In Table 2 and Table 3, the contributing ratios of all factors on the performance are specified based on the SNR values. In the tables ideal combination of the important parameters can be estimated. For implementing the reproducibility approval procedure, the deviation of the SNR between the current and ideal conditions after the first prediction was attained. From the SNR deviations, the ideal parameters estimated from the parameter design can be validated.

The levels of the process parameters and factors are given in Table 2, and Table 3 shows the orthogonal sequence L8 of the desired experimental design.

Table 2. Experimental L8 (2 ^ 6) orthogonal sequence and SNR values plan

Ex no	Channel height (A)	Fluid Material (B)	Heat flux (C)	Pressure (D)	Mass flow rate (E)	Steam quality (F)
1	1	1	1	1	1	1
2	1	1	1	2	2	2
3	1	2	2	1	1	2
4	1	2	2	2	2	1
5	2	1	2	1	2	1
6	2	1	2	2	1	2
7	2	2	1	1	2	2
8	2	2	1	2	1	1

Table 3. Numerical plan of L8 (2 ^ 6) orthogonal sequence and SNR values

Plane Vapor Quality	SNR1	Outlet Vapor Quality	SNR2	Plane Thermal Conductivity	SNR3
0.67	-3.4785	0.65	-3.7417	0.21	-13.5556
0.72	-2.8533	0.7	-3.0980	0.18	-14.8945
0.69	-3.2230	0.69	-3.2230	16.5	24.3496
0.64	-3.8764	0.66	-3.6091	21.12	26.4938
0.64	-3.8764	0.65	-3.7417	0.23	-12.7654
0.69	-3.2230	0.68	-3.3498	0.21	-13.5556
0.69	-3.2230	0.68	-3.3498	22.18	26.1945
0.62	-4.1521	0.63	-4.0131	24	27.6042

Tables 4, 5 and 6 and Figures 2, 3 and 4 show the S/N or signal to noise ratio and variable level. High delta refers to the high S/N ratio variation of the design parameter. Sequence refers to the surface area, which is the most important design parameter.

Table 4. Contribution ratio and factorial effect for vapor volume fraction

Response Table for Signal to Noise Ratios for plane Vapor friction						
Level	A	B	C	D	E	F
1	-3.36	-3.36	-3.43	-3.45	-3.52	-3.85
2	-3.62	-3.62	-3.55	-3.53	-3.46	-3.13
Delta	0.261	0.261	0.12	0.07	0.06	0.71
Rank	3	2	4	5	6	1

As shown in the figure 2, 3 and 4, the millimeter channel heat exchanger is open with all three effective parameters, increasing the channel height, the type of fluid flowing, and the mass efficiency as well as increasing efficiency.

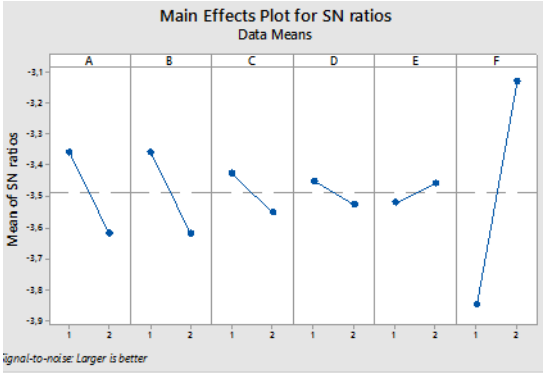

Figure 2. The Effect of the Parameter On Performance Statistics (For vapor quality in the plate).

Table 5. Factorial effect and contribution ratio for projected outlet vapor volume fraction

Response Table for Signal to Noise Ratios for plane Vapor friction						
Level	A	B	C	D	E	F
1	-3.42	-3.48	-3.55	-3.51	-3.58	-3.78
2	-3.61	-3.55	-3.48	-3.52	-3.45	-3.25
Delta	0.20	0.07	0.07	0.003	0.132	0.52
Rank	2	5	4	6	3	1

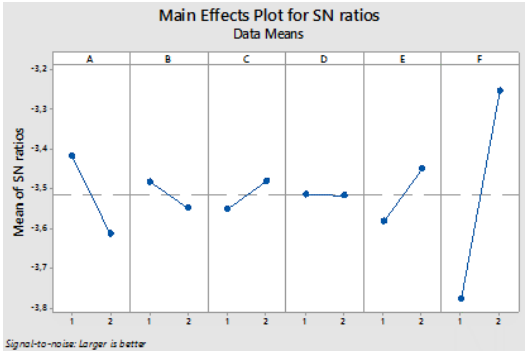

Figure 3. The Effect of the Parameter on Performance Statistics (for vapor quality in outlet).

Table 6. Contribution ratio and factorial effect for thermal conductivity

Response Table for Signal to Noise Ratios for plane Vapor friction						
Level	A	B	C	D	E	F
1	5.598	-13.7	6.52	6.24	6.21	6.94
2	7.051	26.34	6.13	6.41	6.44	5.70
Delta	1.452	40.03	0.39	0.17	0.23	1.24
Rank	2	1	4	6	5	3

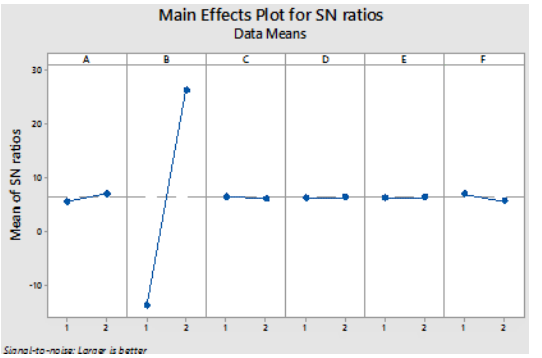

Figure 4. The effect of the parameter on performance statistics (for thermal conductivity in plate).

Taguchi analysis is also useful for predicting the best case from selected experimental cases. In this study, a response named outlet temperature was selected and the S/N ratio results discussed in the previous sections. Figures 2, 3 and 4 are 5 millimeters away from the x, y plane and the z plane, respectively. The steam quality value shows the average ratio and S/N ratio results for responses with the value of the steam quality at the outlet and the thermal conductivity value. As it can be seen from the tables and figures, for both fluid flow steam quality plays an important role in the measurement of vapor volume fraction and fluid material is considered as one of the most important and effective parameters in heat transfer coefficient.

2.1. Flow boiling in mini and millimeter Channels

In two-phase heat transfer systems, it can operate at lower flow rates and lower pumping power than single-phase forced convection heat exchangers based on latent heat of the working fluid. A single-phase liquid system with a temperature increase limited to 25 ° C will require approximately seven times the flow rate of a two-phase system to reject the same amount of heat (Agostini, 2007; Hannemann, et al., 2004; Marcinichen and Thome, 2010; Pan, et al. 2015). It also ensures lower flow rates and smaller thermal management systems (Mudawar, 2001; Willingham and Mudawar, 1992). In a study related to this, (Mishima and Hibiki, 1996) examined the air/water flow of the vertical and horizontally directed capillary tubes connected to the closed rings and found that these same capillary forces affect the bubble dynamics and the flow regime of the air/water mixture.

Based on the analysis of data from various sources (Tran, et al.1996; Lazarek and Black, 1982; Cooper, 1984; Cooper, 1989; Liu and Winterton, 1991), they proved that the micro-regime had begun if the number of limitations was greater than 0.5 in another study (Kuznetsov, 2013), when the width of the channel falls below the capillary constant (δc), it points to a similar criterion at which the mini and millimeter regime begin:

$$\delta_c = \sqrt{\frac{2\sigma}{g(\rho_1-\rho_2)}} \quad (2)$$

They investigated three micro, mini and macro regimes on Bond number (Bo), which is also related to surface tension, gravity and hydraulic diameter (Cheng, et al. 2007).

$$Bo = \frac{g(\rho_1-\rho_2)D_h^2}{\sigma} \quad (3)$$

They also investigated that the gravitational effects of the mini and millimeter channels and that the Bond number is less than 0.05 can be overlooked in this region, but in small channels the Bond number (Bo) is between 5 and 30 and proved that the surface tension and gravitational effects are small but still present. These results are shown in Figure 2a (Harirchian and Garimella, 2009a; Harirchian and Garimella, 2009b; Thome, et al., 2013). They proposed the convective limiting number as a combination of the Bond number and the Reynolds number, and this is the correct method to define the flow limitation.

$$Bo^{1/2} \times Re = \frac{GL_c^2}{\mu_1}\left(\frac{g(\rho_1-\rho_2)D_h^2}{\sigma}\right)^{1/2} \quad (4)$$

Here the viscosity (μ) is the mass flux (G) and the characteristic length (Lc) is the square root of the cross-sectional area of the channel as opposed to the normal hydraulic diameter. Two simulation tools and mathematical models for the definition of the above were proposed in separate articles (Narain, et al. 2004; Liang, et al., 2004).

The limitation is a feature of mini and millimeter channel flow, which can be regarded as decisive criteria between mini, millimeter or macro. In many studies, the authors compared these transition criteria with other experimental data using different fluids, and all made good estimates. (Figure 2b). In Figure 2-b, the researchers emphasize that the cross-sectional area rather than the hydraulic diameter or aspect ratio is important in this determination. Although there is no clear consensus as to what distinguishes the mini and millimeter channel from a conventional channel, it is clear that there are significant differences between the two dimensions.

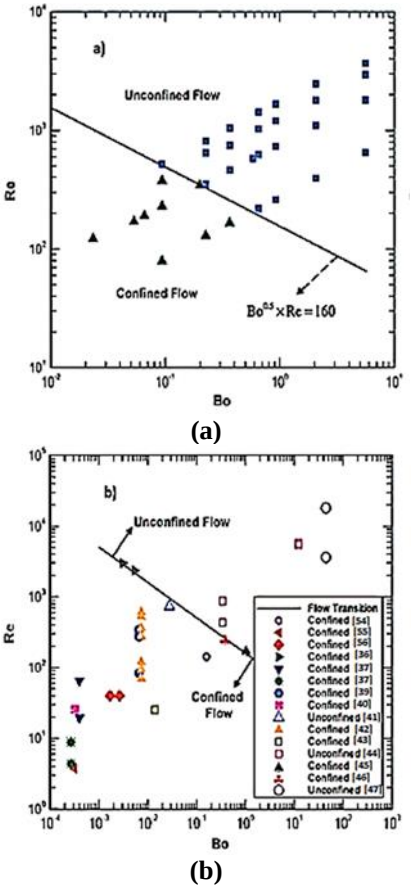

Figure 5. (a) A combination of the convective limiting number, the Bond number and the Reynolds number (Harirchian and Garimella, 2009b; Thome, et al., 2013). (b) The transition from various other studies to the unrestricted flow

Three boundary conditions are required to fully uncover the mini and millimeter channel problem and solve the equations. Each channel has its boundary conditions are set in Fluent. Boundary conditions include:

• Mass flow rate (depends on the input limit of mini and spindle channel)
• Output pressure (depends on mini and spindle channel output limit)
• Wall temperature (depends on mini and spindle channel wall limit)

Basic equations are discretized using finite difference schemes.

We first designed the geometry using drawing programs such as SolidWorks. Typically, the CAD geometry consists solely of the solid body structure from which the design is produced.

Figure 6a shows a millimeter channel heat exchanger which is used as the CFD model. In the model, two-phase liquid fields were formed along with the heat-exchanger by means of the thermal energy supplied from the bottom wall. Each phases (liquid and vapor) enter the system from different inlets and exit from two different outlets.

Figure 6b shows a schematic dual phase heat exchanger of the same millimeter channel which were used to develop simple dual input and dual output.

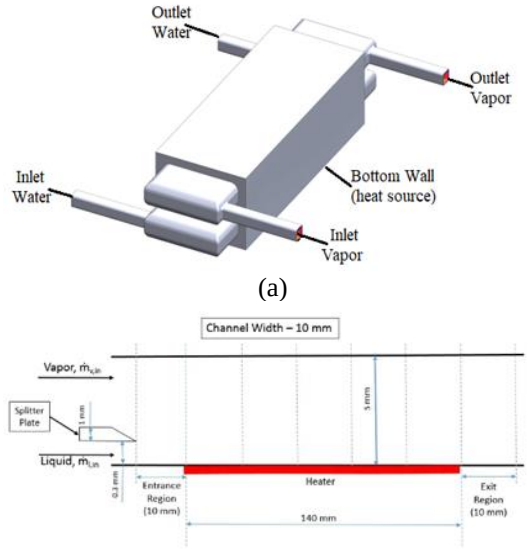

Figure 6. Two-input and two-output dual-phase heat exchanger (a) 3D view (b) cross-section view (Soroush, 2019)

In further applications of CFD, geometric simplifications were made during geometry generation by methods such as 3D or symmetrical to reduce the complexity of areas that do not affect the physics of the overall solution. For conjugate heat transfer problems, such as heat exchanger modelling, it is important to construct the geometry of the liquid areas in such a way that the solid boundaries in contact with the liquid are perfect and matched. The stability of the solutions were obtained from two different methods (1-D and 2-D) is given in (Naik, et al. 2015) and the stability of gravity-driven and shear-driven flows is given in (Naik, et al. 2015), respectively.

After the geometry is created for both the gas and liquid areas, the calculation area in which the CFD simulation is solved was created. By using ANSYS Mesher©, the best mesh was produced using different mesh configurations. For conjugate heat transfer problems, it is common practice to connect solid and fluid areas to mesh using appropriate methods, and to provide a unity between areas (providing a one-to-one mesh face). Conformal meshes eliminate any interpolation found in incompatible meshes, providing accuracy for improved mesh production. In all simulation cases, the solution is highly dependent on the mesh resolution. To understand this situation, it is useful to complete a network convergence study and a mesh validation test must be performed in this. For this reason, a mesh independency study was performed.

Then, for an optimal solution, simulations were carried out under predefined initial and boundary conditions, which depend on the desired operating conditions of the design. Main boundary conditions for heat exchangers are energy operating conditions, such as flow conditions passing through each fluid area, such as mass flow rates and pressure properties, or initial temperatures of liquids entering the heat exchanger. This study only deals with steady-state cases, but it is necessary to establish initial conditions for transient cases in other CFD problems.

Simulation with appropriate mesh and initial and boundary conditions can now be approached for simulation resolution, with conditions set in the CFD solvent. Under start-up conditions, a desired mass flow of liquid at a given temperature can be performed in many ways using manual initiation or automatic methods. With the combined algorithm, the iterative decoding process provides the temperature, speed and pressure profiles for each of the channel flows by solving the annular flow model using the current conditions of the CFD simulation and the solution was initiated. The linked algorithm is iterative and each of the solutions for the model and CFD simulation will be interconnected, and once a repetition is complete, the channel outlet pressure, wall temperature profile, and mass flow rates through the channels

are updated according to the flow model. ANSYS Fluent was used to perform numerical functions and the liquid-vapor interface in this simulation was solved by accepting a finite volume (VOF) model. In this model, by solving an additional continuity-like equation for the volume fraction, it is assumed and realized that the two-phases are incompressible and do not penetrate each other. The sum of the volume fractions of the two-phases in each cell is combined and the properties of a single liquid are calculated based on the volume weight fraction of each phase in the cell. In this study, a group of mathematical models, conservation laws for mass, momentum and energy were solved.

In the current analysis study, the VOF model was used to simulate multiphase flow, while gravitational acceleration was given on the minus y axis and its value was taken as 9.813 m/s2. Furthermore, water and FC-72 were used as the working fluid, and the thermophysical properties of the fluids at the saturation temperature corresponding to the fluid 1bar are shown in Table 1 from the Fluent© substance database.

The liquid water was selected as the secondary phase (liquid phase) and, due to the dynamic behaviour of the two-phase flow, a transient solution with a period time of 0.001 s was used for the all cases. A combination of the SIMPLE algorithm for pressure-speed coupling and the calculation of momentum and energy and the standard k-ε model were used to model turbulence. Table 7 shows the thermodynamic properties of both fluids and the calculations were made by means using the default data in this table.

Table 7. Properties of working fluids used in simulation

Features	Water (L)	Water (V)	FC-72 (L)	FC-72 (V)
Density (kg/m^3)	1000	0.5542	1674.75	13.01
Cp (J/kg*K)	4182	2014	1052.85	1100.24
Thermal Conductivity (W/m*K)	0.6	0.0261	0.05725	0.0536
Viscosity (kg/m*s)	0.009	13e-6	0.00064	0.00043
Molecular Weight (kg/kmol)	18.01	18.0152	340	340
Reference Temperature (K)	298.15	298.15	329.15	329.15

In order to reduce the simulation time of the boiling process, the initial temperature of both the boiling surface and the liquid was selected above the boiling point. As the coolant fluid, perfluorohexane, a Fluorinert™, commercially as FC-72 was used. The basic physical properties of this dielectric fluid are reported in Table 1. FC-72 is thermally and chemically stable, compatible with sensitive materials, flammable, non-toxic, colorless and has no ozone depletion potential. This combination of features makes the FC-72 particularly suitable for applications such as heat sinks for electronic components in combination with low viscosity. It should be also noted that the latent heat of the FC-72 is significantly higher (88 kJ/kg) than the specific heat capacity (1.1 kJ/kgK).

3. Results and Discussion

In the project a one-dimensional Matlab© simulation code was developed using existing theories/correlations in the literature in order to design a boiler. Using this simulation code, evaporator designs can be realized for different fields of application and operating conditions. Afterwards 3D simulation studies were carried out for the boiler geometry which was designed by means of using the developed one-dimensional Matlab© simulation code. In this study, as refrigerant; FC-72 (Fluorinert™) and water were used. then, using the Taguchi (L8) method, after eight analyzes, as shown in T0able 3, the S/N numbers were calculated and tabulated, and finally the heat transfer coefficient and steam quality for both fluids were calculated and compared to the values obtained in the Matlab© code.

By the proposed new method (continuous steam recirculation), the thin film was provided for different thermal boundary conditions of the continuous flow regime, eliminating hydrodynamic and other thermally inefficient flow regimes.

Figures 7 and 9 illustrate their effect on heat transfer coefficients and steam quality for each experiment. The heat transfer coefficients of the 8 mm milichannel are approximately 12% lower than that of the 5 mm millimeter channel. This may be due to an increase in perimeter which contributes to the effective distribution of the heat load to each channel (5 and 8 mm). In addition, the heat transfer coefficients of steam quality in the 8 mm millimeter channel are smaller than those in

the 5 mm millimeter channel. As a result, the height of the channel causes an adverse effect.

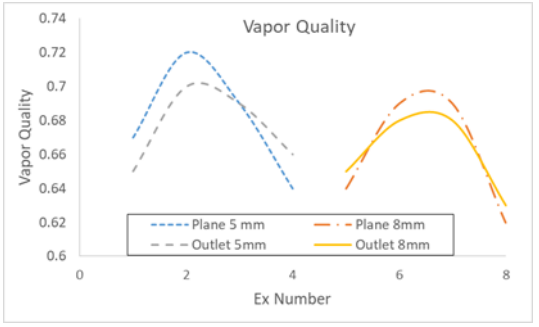

Figure 7. Vapor quality value for each experiment

Figures of 8, 11 and 12, illustrates the calculated thermal conductivity values of the fluids for different cases.

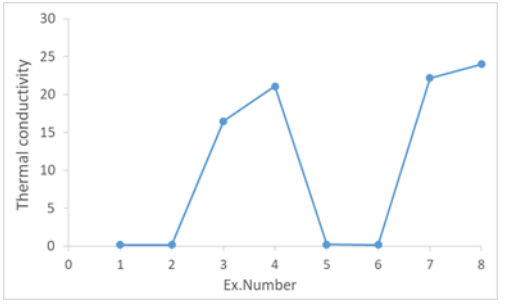

Figure 8. Thermal conductivity value for each experiment

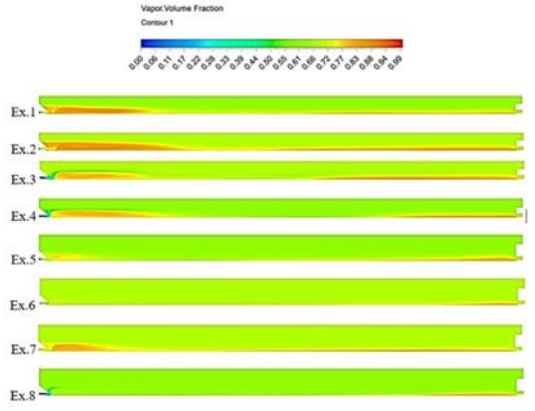

Figure 9. Vapor volume fraction contours for each experiment

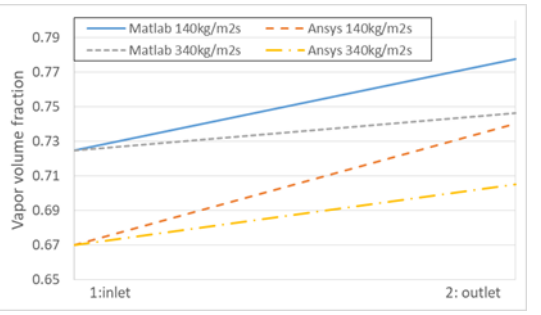

Figure 10. Vapor volume fraction value for water each experiment

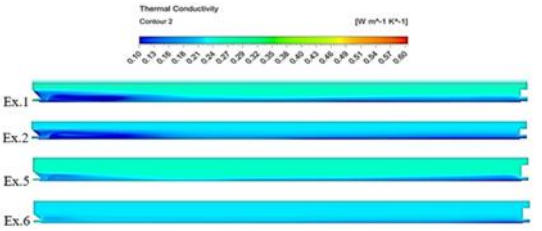

Figure 11. Thermal conductivity contours for water each experiment

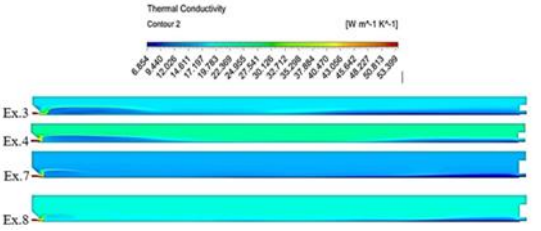

Figure 12. Thermal conductivity contours for FC-72 each experiment

Figures 13 and 14 show the velocity vector of the millimeter channels of fluids near the inlet having both heights (5mm and 8mm). In the 5mm channel, the steam flow enters having higher velocity than the 8mm channel, which can cause a high pressure difference.

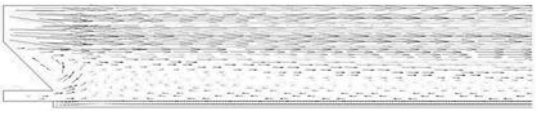

Figure 13. Fluid flow vector for 5 mm channel

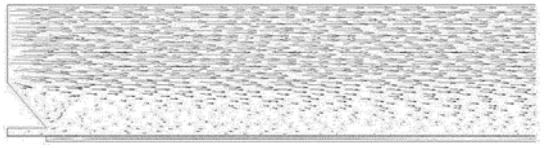

Figure 14. Fluid flow vector for 8 mm channel

4. Conclusions

Numerical research has been conducted to investigate the flow boiling of water vapor and FC-72 at different flow rates, heat fluxes, pressures, vapor qualities. The effect these parameters on heat system performance were discussed. Finally, the main results are plotted as follows:

• Vapor quality increases with the increase of steam flow and hence the Reynolds number, but as millimeter channel height increases, the heat transfer coefficient decreases.

• Depending on the hydraulic diameter of the mini channel, the Reynolds number of high inlet vapor and the boiling in the millimeter channel for the external heat flux will be greater than necessary conditions.

• Wall temperature decreases along the flow direction to increase thin film thicknesses. This may result in increased thermal resistance in the wall. However, in order to avoid dry-out instability at the outlet, film thickness was maintained at certain values (minimum 30 μm).

Acknowledgements

This work was supported by the Scientific and Technological Research council of Turkey (TUBITAK). The study was a part of the TUBITAK 3501 project with the number of 118M457.

References

Agostini, B., et al. (2007). State of the Art of High Heat Flux Cooling Technologies. Heat Transf. Eng., 28(4), pp. 258-281.

Ansys, (2017, October.). Electromagnetic simulation products [Online]. Avaible: http://www.ansys.com/products/electronics

Bevis, T.A. (2016). High Heat Flux Phase Change Thermal Management of Laser Diode Arrays. Colorado State University, PhD Thesis.

Caliskan S., Nasiri Khalaji M., Baskaya S., Kotcioglu I. (2015). Design Analysis of Impinging Jet Array Heat Transfer from a Surface with V-shaped and Convergent-divergent Ribs by Taguchi Method. Heat Transfer Engineering 37(15), pp1252-1266.

Cheng, P., Wu, H.Y., and Hong, F.J. (2007). Phase-Change Heat Transfer in Microsystems. J. Heat Transfer, 129(2), p. 101.

Canıyılmaz, E. (2001). Kalite Geliştirmede Taguchi Metodu ve Bir Uygulama, Yüksek Lisans Tezi, Gazi Üniversitesi.

Chen, Z. et al. (2013). Development of a 1200 V, 120 A SiC MOSFET Module for High-temperature and High-frequency Applications. In the 1st IEEE Workshop on Wide Bandgap Power Devices and Applications, pp.52-59.

Cooper, M.G. (1984). Saturated Nucleate Pool Boiling – a Simple Correlation. Proc. Of the 1st UK National Heat Transfer Conference, IChemE Symposium, pp. 785-793.

Cooper, M.G. (1989). Flow Boiling-the 'apparently Nucleate Regime. Int. J. Heat Mass Transf., 32(3). 459-464.

Consolini, L., Thome J.R. (2009). Microchannel Flow Boiling Heat Transfer of R134a. R236fa and R245fa, Microfluidics and Nanofluid, 6 731-746.

Hall, D.D., Mudawar, I. (1995). Experimental and Numerical Study of Quenching Complex-Shaped Metallic Alloys with Multiple, Overlapping Sprays. International Journal of Heat and Mass Transfer, 38, 1201-1216.

Hannemann, R., Joseph, M., Pitasi, M. (2004). Pumped Liquid Multiphase Cooling. IMECE, pp. 3-7.

Garimella, S.V, Yeh, L., and Persoons, T. (2012). Thermal Management Challenges in Telecommunication Systems and Data Centers. IEEE Trans. Components, 2(8), pp. 1307- 1316.

Garimella, S.V, Persoons, T., Weibel, J., Yeh, L.T. (2013). Technological Drivers in Data Centers and Telecom Systems: Multiscale Thermal, Electrical, and Energy Management. Appl. Energy, 107, pp. 66-80.

Harirchian, T., and Garimella, S.V. (2009a). The Critical Role of Channel Cross-Sectional Area in Microchannel Flow Boiling Heat Transfer. Int. J. Multiph. Flow, 35, pp. 904-913.

Harirchian, T., and Garimella, S.V. (2009b). Effects of Channel Dimension, Heat Flux, and Mass Flux on Flow Boiling Regimes in Microchannels. Int. J. Multiph. Flow, 35(4), pp. 349-362.

Karayiannis, T.G., et al. (2010). Flow pattern and heat transfer for flow boiling in small to micro diameter tubes. Heat Transfer Engineering, 31, 257-275.

Karayiannis, T.G., and Mahmoud, M.M. (2017). Flow Boiling in Microchannels: Fundamentals and Applications. Appl. Therm. Eng., 115, pp.1372-1397.

Kandlikar, S.G., and Grande, W.J., (2003). Evolution of Microchannel Flow Passages-Thermohydraulic Performance and Fabrication Technology. Heat Transf. Eng., 24(1), pp. 3-17.

Kandlikar, S.G. (2012). History, Advances, and Challenges in Liquid Flow and Flow Boiling Heat Transfer in Microchannels: A Critical Review. J. Heat Transfer, 134 (3).

Kew, P. A., and Cornwell, K. (1997). Correlations for the Prediction of Boiling Heat Transfer in Small Diameter Channels. Appl. Therm. Eng., 17, pp. 705-715.

Kivisalu, M.T., Gorgitrattanagul, P., and Narain, A. (2014). Results for high heat-flux flow realizations in innovative operations of milli-meter scale condensers and boilers. International Journal of Heat and Mass Transfer, 75, p. 381-398.

Kuznetsov, V.V. (2013). Correlation of the Flow Pattern and Flow Boiling Heat Transfer in Microchannels. Heat Transf. Eng., 34(2-3), pp. 235-245.

Kuszewski, M., Zerby, M. (2012). Next Generation Navy Thermal Management Program. CARDIVNSWC-TR-82-(2002)/12.

Lazarek, G.M., Black, S.H. (1982). Evaporative Heat Transfer, Pressure Drop and Critical Heat Flux in a Small Vertical Tube with R-113. Int. J. Heat Mass Transf., 25(7), pp. 945-960.

Lee, J., Mudawar, I. (2008). Fluid Flow and Heat Transfer Characteristics of Low Temperature Two- Phase Microchannel Heat Sink-Part I: Experimental Methods and Flow Visualization Results. International Journal of Heat and Mass Transfer, 51, 4315-4326.

Lee, J., Mudawar, I. (2009). Low-Temperature Two-Phase Microchannel Cooling for High- heatFlux Thermal Management of Defense Electronics. IEEE Transactions on Components and Packaging Technologies June, 2.

Liang, Q.X. Wang and Narain, A. (2004). Effects of Gravity, Shear and Surface Tension in Internal Condensing Flows: Results from Direct Computational Simulations. Journal of Heat Transfer, 126(5), p. 676-686.

Liu, Z., Winterton, R.H.S. (1991). A General Correlation for Saturated and Subcooled Flow Boiling in Tubes and Annuli, Based on a Nucleate Pool Boiling Equation. Int. J. Heat Mass Transf., 34(11), pp. 2759-2766.

Marcinichen, J.B., and Thome, J.R. (2010). New Novel Green Computer Two-Phase Cooling Cycle: A Model for Its Steady-State Simulation. Proc. 23rd Int. Conf. Effic. Cost, Optim. Simulation, Environ. Impact Energy Syst. ECOS, 3, January.

Mersen (2017, October.), R-Tools [Online]. Avaible:http://epus.mersen.com/solutions/cooling-of-power-electronics/r-tools2/

Mehendale, S.S., Jacobi, M.A., and Shah, R.K. (2000). Fluid Flow and Heat Transfer at Micro- and Meso-Scales with Application to Heat Exchanger Design. Appl. Mech. Rev., 53(7), pp. 175-193.

Moore, B.R. (1993). Ideas from Future Technologies Workshop. Held by ARL/TARDEC, ARLSR

Mishima, K., Hibiki, T. (1996). Some Characteristics of Air-Water Two-Phase Flow in Small Diameter Vertical Tubes. Int. J. Multiph. Flow, 22(4), pp. 703-712.

Mudawar, I., Bharathan, D., Kelly, K., Narumanchi, S. (2009). Two-Phase Spray Cooling of Hybrid Vehicle Electronics. IEEE Transactions on Components and Packaging Technologies, June, 32 (2).

Mudawar, I. (2001). Assessment of High-Heat-Flux Thermal Management Schemes. IEEE Transactions on Components and Packaging Technologies, June, 24 (2).

Mudawar, I. (2001). Assessment of High-Heat-Flux Thermal Management Schemes. Components Packag. Technol. IEEE Trans., 24(2), pp. 122-141.

Naik, R., Mitra, S., and Narain, A. (2015). Steady and Unsteady Simulations that Elucidate Flow Physics and Instability Mechanisms for Annular/Stratified Internal Condensing Flows inside a Channel. Journal of Computational Physics,

Naik, R., Mitra, S., and Narain, A. (2014). Steady and Unsteady Computational Simulations for Annular Internal Condensing Flows in a Channel, in Proceedings of 2014 ASME International Mechanical Engineering Congress and Exposition: Montreal, Canada.

Narain, A., et al. (2004). Direct Computational Simulations for Internal Condensing Flows and Results on Attainability/Stability of Steady Solutions, Their Intrinsic Waviness, And Their Noise Sensitivity. Journal of Applied Mechanics, 71(1), p. 69-88.

Ömeroğlu, G . (2018). Investigation In Electrical And Thermal Efficiency Of An Active Cooling Photovoltaic Thermal (Pv/T) Solar System With Taguchi Method. Bilge International Journal of Science and Technology Research , 2 (1) , 47-55 . DOI: 10.30516/bilgesci.406359

Pan, Z., Weibel, J.A., Garimella, S.V. (2015). A Cost-Effective Modeling Approach for Simulating Phase Change and Flow Boiling in Microchannels. Proc. of ASME 2015 Int'l Technical Conf. and Exhibition on Packaging and Integration of Electronic and Photonic Microsystems, San Francisco, CA, pp. 1-9.

Park, C., Zuo, J. (2004). Hybrid Loop Thermal Bus Technology for Vehicle Thermal Management. Advanced Cooling Technologies Inc., Lancaster, PA.

Park, C., Vallury, A. (2006). Advanced Hybrid Cooling Loop Technology for High Performance Thermal Management. 4th International Energy Conversion Engineering Conference, San Diego, California, 26-29.

Park, C., Jaura, A.K. Thermal Analysis of Cooling System in Hybrid Electric Vehicles. SAE Transactions, SAE-2002-01-0710.

Phillips, R.J. (1990). Microchannel Heat Sinks; In: A Bar-Cohen and A. D. Krous, Editors, Advances in Thermal Modeling of Electronic Components and Systems, Vol.2, ASME, New York.

Pereira A., et al. (2017). Comparison Between Numerical and Analytical Methods of AC Resistance Evaluation for Medium-Frequency Transformers: Validation on a Prototype and Thermal Impact Analysis. Canadian Journal of Electrical and Computer Engineering, vol. 40, no.2, pp. 101-109.

Ponnappan, R., Donovan, B., Chow, L. (2002). High power thermal management issues in spacebased systems. Space Technology and Applications International Forum-STAIF, Albuquerque, New Mexico, February 3-6.

Ross, P.J. (1989). Taguchi Techniques for Quality Engineering, McGraw-Hill, Singapure.

Sepahyar, S. (2019). Influence of Micro-Nucleate Boiling On Annular Flow Regime Heat Transfer Coefficient Values and Flow Parameters–For High Heat-Flux Flow Boiling of Water, PhD thesis, Michigan Technological University.

Sullivan, P.F., Ramadhyani, S., Incropera, F.P. (1992). Extended Surfaces to Enhance Impingement Cooling with Single Circular Liquid Jets. In Proceedings of ASME/JSME Joint Conference on Electronic Packages, 207-215.

Thome, J.R. (2006). State-of-the-Art Overview of Boiling and Two-Phase Flows in

Microchannels. Heat Transf. Eng., 27(9), pp. 4–19.

Thome, J.R., Bar-Cohen, A., Revellin, R., and Zun, I. (2013). Unified Mechanistic Multiscale Mapping of Two-Phase Flow Patterns in Microchannels. Exp. Therm. Fluid Sci., 44, pp. 1-22.

Tran, T.N., Wambsganss, M.W., France, D.M. (1996). Small Circular and Rectangular Channel Boiling with Two Refrigerants. Int. J. Multiph. Flow, 22, pp. 485-498.

Triplett, K.A., et al. (1999). Gas–liquid Two-Phase Flow in Microchannels Part I: Two-Phase Flow Patterns. Int. J. Multiph. Flow, 25(3), pp. 377-394.

Tuckerman, D.B., Pease, R.F.W. (1981). High Performance Heat Sinking for VLSI. IEEE Electron Device Letters, May, 2 (5).

Urciuoli, D., Tipton, C.W., Porschet, D. (2012). Development of a 90 kW, Two-Phase, BiDirectional DC-DC Converter for Power Dense Applications. U.S. Army Research Laboratory, #ADA433112, Adelphi, MD

Willingham, T.C., Mudawar, I. (1992). Forced-Convection Boiling and Critical Heat Flux from a Linear Array of Discrete Heat Sources. Int. J. Heat Mass Transf., 35(11), pp. 2879-2890.

Bilge International Journal of Science and Technology Research

Web : http://dergipark.gov.tr/bilgesci - **E-mail:** kutbilgescience@gmail.com

Received: 23.11.2019
Accepted: 23.12.2019
DOI: 10.30516/bilgesci.650160

ISSN: 2651-401X
e-ISSN: 2651-4028
3(Special Issue), 58-76, 2019

Review of Traditionally Consumed Antidiabetic Fruits in the Diet

Pınar Ünsal, Ebru Aydın[1*], Gülcan Özkan[1]

Abstract: According to the WHO's report, the risk of diabetes is increasing and one in eleven people now have diabetes. By 2030 the patients with diabetes will increase in a sharp manner like doubling the number nowadays, and so 90% will carry type-2 diabetes. To put the blood glucose level under control, in a stable level with low deviations is the effective way to prevent or delay type-2 diabetes. Hence, the use of traditional herbal supplements and fruit-vegetable extracts stands out and commonly used all over the world in high volumes. The use of traditional herbs has advantage on the lowering the cost of medication, and one another advantage is the avoiding the side effects such as flatulence, diarrhoea, tiredness and upset stomach.

The objective of this review was to evaluate in vitro and in vivo studies (animal and human) of some antidiabetic fruits. Health benefits of the antidiabetic fruits is well-recognized and traditionally consumption of some fruits draw attention for the prevention of type-2 diabetes due to their active hyperglycemic constituents.

The publications cited originate from electronic databases such as Google Scholar, Pubmed, Web of Science, Scopus, Wiley-Blackwell and Springer. Scientific name of the fruits, the words antidiabetic, hypoglycemic and type 2 diabetes were used as keywords for search.

Certain fruits may be used in the management of diabetes (acarbose-like activity) due to some bioactive compounds of fruits such as polyphenols and essential oils, which inhibit digestive enzymes or act as insulin like molecules. This review highlights the benefits of antidiabetic fruits, and active chemical constituents of them. These fruits have significant role in the control of type-2 diabetes.

Keywords: Antidiabetic Fruit; Hypoglycemic; Type 2 Diabetes; Phenolics; Essential oil

1. Introduction

Carbohydrates cover about 56% of the usable energy in the diet (Paulev & Zubieta, 2004). Two or more mono-saccharides combine to synthesize oligo- and polysaccharides. While generating energy oligo- and polysaccharides are catabolized to the monosaccharides. Sucrose is a disaccharide and synthesized by the reaction between glucose and fructose (Figure 1).

Sucrase (EC 3.2.1.48) is an enzyme that catalyze the enzymatic hydrolysis of sucrose in humans. In the studies it was reported that sucrase locates in the intestinal surface of enterocytes and is released by intestinal microvillus cells (Marieb, 2004). The α-1,2 and α-1,4 glycosidic bonds of sucrose are hydrolysed by the active site of sucrase.

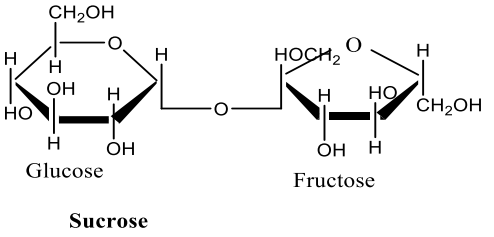

Figure 1: Structure of sucrose, maltose and isomaltose.

[1]Suleyman Demirel Universty, Department of Food Engineering.
*Corresponding author (İletişim yazarı): ebruaydin@sdu.edu.tr

Citation (Atıf): Ünsal, P., Aydın, E., Özkan, G. (2019). Review of Traditionally Consumed Antidiabetic Fruits in the Diet. Bilge International Journal of Science and Technology Research, 3(Special Issue): 58-76.

There are some transporters which is responsible from transport of liberated glucose and fructose from sucrose. These transporters are the sodium-dependent glucose transporter SGLT1 (active transport) and sodium-independent transporter GLUT2 (facilitated) (Goodman, 2010). Two Na^+ molecules are to be connected to SGLT1, to permit glucose binding to allow glucose to enter the enterocytes (Figure 2). Glucose is also able to be transported through GLUT2 that is present at the basal surface of the intestine. Following that glucose sustains to enter the blood circulation and fructose follows the same path to enter and exit the cells via GLUT2. Following the absorption of postprandial glucose in the blood, it is transported to body cells via the bloodstream (Figure 2). Insulin is secreted from the pancreatic β-cells to maintain the glucose homeostasis in the body and insulin allows uptake of glucose to the muscle and adipose tissues (Leney and Tavare, 2009; Govers, 2014). After hydrolysis of glucose from sucrose post-prandial blood glucose level starts to increase and hydrolyzed fructose is utilized in the liver to generate components such as glucose, glycogen and pyruvate (Törrönen et al., 2010). Hence those metabolism steps may have role in the improvement type-2 diabetes.

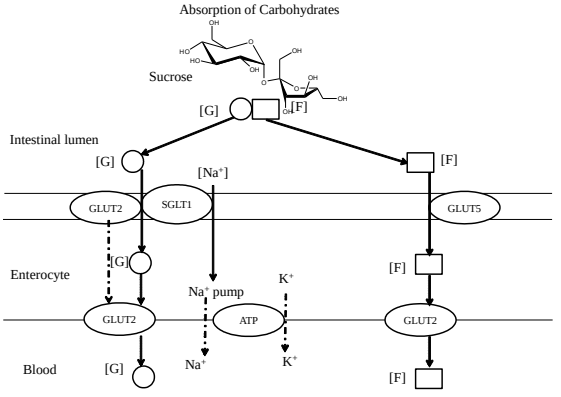

Figure 2 Carbohydrate absorption (Paulev & Zubieta, 2004). G: glucose

In the development of diabetes glucose has significant role. Deficient or impaired insulin signaling results in high blood glucose level hence insulin resistance/deficiency cause type-2 diabetes. The expected glucose level of human is ~4 mM (72 mg/dl). After food intake such as a proper meal, temporarily it may get higher to level <7.8 mM (140 mg/dl) (NICE, 2011). The raise of the blood glucose level has influence on the secretion of the insulin, there after the muscle cells absorb the excess glucose and store as glycogen (Nelson and Cox, 2000). Accordingly, if the blood glucose becomes to the normal level, the insulin begins to reduce. Because of the shortage in the insulin production or enough production level but ineffective feature of the insulin stimulates the type-2 diabetes. The ineffective insulin is conceptualized as insulin resistance and high blood glucose level is conceptualized as hyperglycemia (Nelson and Cox, 2000).

The International Diabetes Federation (2016) reported that more than 371 million people suffer from the diabetes. Moreover, it is projected that more than 550 million people by 2030 which means 9,5 % of the world population will be having type-2 diabetes (Ogurtsova et al., 2016). One another issue in academic research sheds light onto the medical costs of the type-2 diabetes patients. In the European countries 1/10 of the healthcare costs are for the diabetes (196 billion USD in 2010), and the 2030 projection for these costs are to be 235 billion USD in 2030 (Zhang et al., 2010).

The medication used for the treatment of the diabetes are most commonly drug intake. However, the drugs are used in high amounts all around the world, there are many side effects such as flatulence, diarrhea, tiredness and upset stomach. Acarbose, metformin, sulphonylureas, and glitazones are major components in the chemical drugs which are intaken by the patients. These components have different impact on the blood glucose level. For instance, acarbose puts the control on the glucose level to rise in high level after meals; metformin affects the liver to avoid releasing glucose to the blood; sulphonylureas has impact on the pancreas; and glitazones has impact on the body cells sensitivity.

Herbal treatment is opening another way for the diabetes to avoid the side effects aforementioned. Dabaghian and colleagues (2012) reported that around 3 million diabetic patients in the USA utilized herbal remedies and supporting this case WHO reported that approximately ¾ of the world population prefer traditional herbal remedies for health issues arise. In these cases, daily dietary intake of the humans may help to prevent type-2 diabetes. As the blood glucose level has impact on the diabetes, for the treatment or prevention of the type-2 diabetes, the blood glucose level must be regulated. To decrease the blood glucose level

two different processes can be followed: digestive enzymes for disaccharides can be inhibited and/or inhibition of the glucose transporters (GLUTs and SGLT1) to stop/decrease glucose absorption in the intestine.

Thus, controlling the blood glucose level will decrease the risk of diabetes and related diseases such as obesity, heart disease, damage the kidney, retina and peripheral nerves (Williamson and Carughi, 2010; Hauner et al., 2012).

Most of the people prefer to use plants as they are safer (as they have no side effects compared to synthetic drugs), cheaper and more efficient (Durmuskahya and Ozturk, 2013). Depending on the region different plants and its parts (the whole plant, flower, leaf, bark or fruit) may be used for the treatment of diabetes.

In this review, it was aimed to report antidiabetic activity of fruits that analyzed through *in vitro* and/or *in vivo* methods in the literature. It was discovered that polyphenols and essential oils of some fruits have effect on regulating the sugar level in the blood, and so they can be used to prevent type-2 diabetes. For instance *Sarcopoterium spinosum*, Japanese apricot, *Ficus deltoidea*, *Passiflora ligularis*, *Persea Americana*, *Rosa canina*, *Vaccinium myrtillus*, *Terminalia catappa* L., *Myristica fragrans*, *Pimenta dioica*, *Momordica charantia*, *Sarcopoterium spinosum*, Mango, *Pyracantha fortuneana*, *Chrysophyllum cainito* L., *Pometia pinnata*, *Malus communis* L., *Empetrum nigrum* L., *Momordica charantia*, *Zizyphus lotus*, *Xylopia aethiopica*, *Morinda Citrifolia* L., *Malus communis L.*, *Coriandrum sativum* L., *Juglans regia* L., *Sorbus umbellate*, *Fritsch var. Cretica*, *Schneider* and encapsulated *Citrus limon Osbeck* were reported for their inhibitory activity on α-amylase and α-glucosidase enzymes (Smirin et al., 2010; Park et al., 2012; Misbah et al., 2013; Saravanan and Parimelazhagan, 2014; Oboh et al., 2014; Asghari et al., 2015; Guder et al., 2015; Adefegha et al., 2016; Loizzo et al., 2016; Khatib et al., 2017; Elyasiyan et al., 2017; Sekar et al., 2017; Putri et al., 2017; Wei et al., 2017; Doan et al., 2018; Sukiman et al., 2018; Yegin et al., 2018; Hyun and Kim 2018; Hwang, 2018; Yegin et al., 2018; Deniz et al., 2018; Raimov and Fakir., 2018; Incegul et al., 2018; Marmouzi et al., 2019; Mohammed et al., 2019; Simomara et al., 2019). *Juniperus communis*, *Eugenia jambolana*, *Foeniculum vulgare*, *Secale cereale* L., *Carum carvi and Capparis spinosa* L., *Rosa canina* L., *Rhus coriaria* L., *Phaleria macrocarpa*, *Persea americana* Mil., *Pithecellobium dulcee* Benth, *Carum carvi*, *Vacciniummyrtillus*, *Backhousia citriodora* oil, *Vanilla planifolia* Andrews were analyzed for their antidiabetic effects using STZ or alloxan induced rats (Medina et al., 1993; Kelkar and Kaklij (1997); Ozbek, 2002; Ozbek et al., 2002; Eddouks et al., 2004; Orhan et al., 2009; Mohammadi et al., 2010; Rabyah et al., 2012; Thenmozhi et al., 2012; Pradeepa et al., 2013; El-Soudi et al., 2014; Erjaee et al., 2015; Asgary et al., 2015; Mishra et al., 2019; Kanedi et al., 2019). There are also some clinical studies reported about the antidiabetic effects of fruits such as *Sumac Rhuscoriaria* L., Berberis fruit, *Rosa canina* L., *Citrus junos* Tanaka, *Balanites aegyptiaca* Del., Cambuci, cagaita, camu-camu, jaboticaba juices (Shidfar et al., 2013; Moazezi and Qujeq, 2014; Dabaghian et al., 2015; Hwang et al., 2015; Rashad et al., 2017; Balisteiro et al., 2017).

2. Antidiabetic Activity of Dietary Fruits in In-vitro Studies

The effect of dietary components in lifestyle in the prevention and management of type 2 diabetes has been getting attention for long time. Most of the in-vitro studies indicate that intake of fruits and their polyphenol or essential oil compounds have antidiabetic effects which are listed in Table 1 and then briefly explained.

Table 1. Summary of antidiabetic activity of dietary fruits *in-vitro* studies

Analysed/ major polyphenols	Plant Food	Experimental model	Effect	Reference
Catechin and epicatechin	*Sarcopoterium spinosum*	Adipose tissue and hepatocytes cells	Increased insulin secretion	Smirin et al., 2010
Hydroxycinnamic acid, chlorogenic acids	Japanese apricot	α-Glucosidase enzymes, murine 3T3-L1 fibroblasts cells	20% inihibition of α-glucosidase activity, insulin-like activity	Park et al., 2012
Flavan-3-ol monomers, proanthocyanidins, and C-linked flavone glycosides	*Ficus deltoidea*	Rat intestinal α-glucosidase	IC_{50} : 0.473 mg/ml	Misbah et al., 2013
Ellagic acid, gallic acid, and rutin.	*Passiflora ligularis*	α-Amylase and α-glucosidase enzymes	Inihibition of α-amylase: 82.56 % α-glucosidase: 75.36 %	Saravanan and Parimelazhagan, 2014
Syringic acid, eugenol, vanillic acid, isoeugenol, guaiacol, kaemferol, catechin	*Persea Americana*	α-Amylase and α-glucosidase enzymes	IC_{50} mg/ml: α-amylase 0.057 and α-glucosidase 0.241	Oboh et al., 2014
Daucosterol and D-glucono-1,4-lactone	*Rosa canina*	Yeast α-glucosidase	IC_{50}: 0.3 µg/ml	Asghari et al., 2015
Antochyanins, malvidin-3-*O*-glucoside	*Vaccinium myrtillus*	α-Amylase and α-glucosidase enzymes	IC_{50} µg/ml: α-amylase 61.3 and α-glucosidase 128.9	Guder et al., 2015
Chlorogenic acid, ellagic acid and kaempferol	*Terminalia catappa* L.	α-Amylase and α-glucosidase enzymes	IC_{50} µg/ml: α-amylase 510.11 and α-glucosidase 583.33 µg/ml	Adefegha et al., 2016
Rhamnetin, lutein, ferulic acid, quercetin-3-O-glucoside and rutin	*Myristica fragrans*	α-Amylase and α-glucosidase enzymes	IC_{50} of α-amylase 62.1 and α-glucosidase 75.7 µg/ml The IC_{50} of acarbose for α-amylase 50.0 and α-glucosidase 35.5 µg/ml	Loizzo et al., 2016
	Pimenta dioica			

			α-Amylase 147.9 and α-glucosidase 152.8 μg/ml	
Coumarin, alkaloid, steroid and phenols	*Momordica charantia*	Intestinal α-glucosidase	Low inhibition of α-glucosidase activity	Khatib et al., 2017
Catechins and phenolics	*Sarcopoterium spinosum*	inhibition activity of α-amylase and α-glucosidase enzymes	IC_{50} μg/ml: α-amylase 0.29 and α-glucosidase 0.125 mg/ml	Elyasiyan et al., 2017
		3T3-L1 adipocytes cells	Increased insulin secretion and improved the transmission of insulin signalling	
Magniferin	Mango	α-Amylase and α-glucosidase enzymes	IC_{50} of : mango, magniferin and acarbose is 112.8, 36.84 and 21.33 μg/ml	Sekar et al., 2017
			Acarbose: 0.064 ppm Mango: 64.71 ppm	Putri et al., 2017
Proanthocyanidin	*Pyracantha fortuneana*	Intestinal α-glucosidase	IC_{50}: 0.15 μg/mL	Wei et al., 2017
Phenols, tannin, glycosides, terpenoids, and saponin	*Chrysophyllum cainito* L	α-Amylase and α-glucosidase enzymes	IC_{50} (μg/ml) of : fruit 1.20 and acarbose 198.17	Doan et al., 2018
Tannins and saponins	*Pometia pinnata*	Intestinal α-glucosidase	IC_{50} of methanol extract 169.81 μg/ml	Sukiman et al., 2018
Quercetin glycosides, procyanidin B2, chlorogenic acid, epicatechin, phloretin glycosides	*Malus communis* L.	Inhibition of α-amylase and α-glucosidase	IC_{50} (μg/ml) of α-amylase 501.08 and α-glucosidase 924.93	Yegin et al., 2018
Anthocyanins, proanthocyanidins and flavonoids	*Empetrum nigrum* L.	Inhibition of α-amylase and α-glucosidase	IC_{50} (μg/ml) α-glucosidase 0.5 and α-amylase 100	Hyun and Kim 2018
Catechin, flavonoids,	*Momordica*	Intestinal α-	At 100 μg/ml of	Hwang, 2018

caffeic acid, p-coumarc acid, ferrulic acid, isoflavones, terpenes, and glucosinolates	*charantia*	glucosidase	inhibition of α-glucosidase (%) bitter melon 30.0 and acorbose 22.6	
Gallic acid, ferulic and vanillic acids, rutin, catechin and epicatechin	*Zizyphus lotus*	Inhibition of α-amylase and α-glucosidase	IC_{50} (μg/ml) α-amylase 31.9 and α-glucosidase 27.95	Marmouzi et al., 2019
Oleanolic acid, sesquiterpenoids, diterpenoids, triterpenoids	*Xylopia aethiopica*	Inhibition of α-amylase and α-glucosidase	IC_{50} values (α-amylase: 89.02 ± 1.12 mM, α-glucosidase: 46.05 ± 0.25 mM	Mohammed et al., 2019
α-Ketoglutaric acid and malic acid	*Morinda Citrifolia* L.	Intestinal α-glucosidase	IC_{50} 28.99 μg GAE/ml	Simomara et al., 2019

Smirin and colleagues (2010) studied the effect of *Sarcopoterium spinosum* extract (SSE) in the management of diabetes employing *in vitro* and *in vivo* methods. They discovered that due to catechin and epicatechin content of SSE, the root extract of Sarcopoterium spinosum indicated insulin-like effect in skeletal muscle, adipose tissue and hepatocytes cells and increased insulin secretion *in vitro*. It was also reported that SSE improved glucose tolerance but did not affect fasting glucose level of genetically diabetic male KK-Ay mice when they fed in short term period with the extract. In addition, chronic administration of SSE decreased blood glucose level, plasma insulin and free fatty acid and was reported as beneficial for hypoglycemic effect.

Park and colleagues (2012) investigated the antidiabetic effect of 50 commonly consumed fruit and vegetables in Korea either in whole juice (WJ) samples or ethanolic extract (EE). Firstly, inhibition of α-glucosidase enzymes was investigated in the presence of commonly consumed fruits and vegetables. Japanese apricot (20.0 %) showed the highest inhibition activity within the WJ fruits. Among ethanolic extract of the fruits; pear (28.3%), Japanese apricot (17.4%), cucumber (13%) and plum (8%) had better α-glucosidase inhibitory activity compared to other EE fruits. Following those analyses to obtain the insulin-like activity of those fruits, murine 3T3-L1 fibroblasts cells were used with/without insulin. From WJ fruits only Japanese apricot demonstrated insulin-like activity but EE fruit cucumber, pear and plum indicated insulin-like activity with insulin sensitizing ability.

To regulate the blood glucose level, the use of tea bags and/or capsules of *Ficus deltoidea* is getting popular in Malaysia. Water and ethyl acetate fraction of the fruit was investigated for its antidiabetic activity with *in vitro* methods. In contrast to above researches, Misbah and colleagues (2013) did not observe any corelation between phenolic content and antidiabetic activity of the fruit. The IC_{50} value of rat intestinal α-glucosidase inhibition of the fruit's water extraction was detected as 0.473 mg/ml. It was concluded that the antidiabetic activity of the fruit may be about other polar plant components and phenolics together (Misbah et al., 2013).

Antidiabetic activity of *Passiflora ligularis* fruits were analyzed using various solvents extractions. Acetone extract of the fruit exhibited the highest phenolic compound and showed significant inhibitory activity on α-amylase (82.56 %) and α-glucosidase (75.36 %) enzymes (Saravanan and Parimelazhagan, 2014).

Persea americana (avocado) fruit and leaf were reported due to its inhibitory activity on α-amylase and α-glucosidase enzymes (Oboh et al., 2014). The research reported that the inhibition of α-amylase with fruit is higher than the leaf. In contrast the inhibitory activity of leaf on α-glucosidase was better than fruit. The inhibition activity of fruit may be related to rich constituent of phenolics such as syringic acid,

epigallocatechin, isoeugenol, kaemferol, catechin, ferulic acid, apigenin, and epigallocatechin-3-O-gallate.

Asghari and colleagues (2015) investigated the inhibitory activity of *Rosa canina* fruit on yeast α-glucosidase with different extraction methods. Solvents used in those methods are n-hexane, ethyl acetate, acetone and methanol. The acetone extract showed the highest inhibition with an IC_{50} value of 0.3 μg/ml. The fruit contains high amount of phytosterols (daucosterol and D-glucono-1,4-lactone) and their IC_{50} values of yeast α-glucosidase activity were calculated as 13.3 and 6.5 μM respectively which is lower than acarbose (IC_{50} 16.1 μM).

A research analyzed the antidiabetic activity of bilberry (*Vaccinium myrtillus* L.) fruit using different extraction solvents. Bilberry is rich in anthocyanin constituent and this can influence its inhibitory activity. The inhibition of α-amylase was found highest for methanol extraction with an IC_{50} value of 61.3 μg/ml and for α-glucosidase activity IC_{50} value was detected highest for ethanolic extraction as 128.9 μg/ml (Guder et al., 2015).

Adefegha and colleagues (2016) investigated the effect of almond (*Terminalia catappa* L.) fruit parts (hull and drupe) extracts on α-amylase and α-glucosidase enzymes. For both α-amylase and α-glucosidase the drupe extract exhibited the highest inhibition with an IC_{50} value of 510.11 and 583.33 μg/ml, respectively. The major components of the fruit were identified as chlorogenic acid, ellagic acid and kaempferol and the result of this study indicated that the antidiabetic activity might be related with those phenolic contents.

In recent years dried powder of nutmeg mace (*Myristica fragrans*) and pimento (*Pimenta dioica*) is using as spice and functional ingredient due to its effect on carbohydrate digestive enzymes; α-amylase and α-glucosidase. Loozio and colleagues found that mace inhibited α-amylase and α-glucosidase with an IC_{50} value of 62.1 and 75.7 μg/ml, respectively. While acarbose inhibited α-amylase and α-glucosidase activity 50.0 and 35.5 μg/ml respectively, pimento inhibited them 147.9 and 152.8 μg/ml, respectively (Loozio et al., 2016).

Ethanolic and aqueous extracts of *Momordica charantia* fruit was tested for its α-glucosidase inhibitory activity and phytochemicals screening (coumarin, alkaloid, steroid and phenol) (Khatib et al., 2017). Both extracts showed low inhibition effect on α-glucosidase activity however previous study of the authors tested *in vivo* activity of the fruit and found that fruit was indicated high antidiabetic activity. Therefore, it was concluded that its antidiabetic activity is not related with the inhibition of digestive enzymes, but it might be about the carbohydrate transport or uptake mechanism (Khatib et al., 2017).

Elyasiyan and colleagues (2017) analyzed the antidiabetic effect of *Sarcopoterium spinosum* (S. spinosum) rich in catechins and phenolics. Firstly, they measured the inhibition activity of α-amylase and α-glucosidase enzymes and reported the IC_{50} values as 0.29 and 0.125 mg/ml respectively. Then glucose uptake into 3T3-L1 adipocytes showed that it also increased insulin secretion and improved the transmission of insulin signaling that leads to the induction of glucose uptake.

Ripe and unripe mango fruit contains magniferin which is a xanthone glycoside and may decrease blood glucose level due to its inhibitory activity on carbohydrate digestive enzymes. The IC_{50} value of α-glucosidase enzymes with mango, magniferin and acarbose was found as 112.8, 36.84 and 21.33 μg/ml respectively (Sekar et al., 2017). In another study Putri and colleagues (2017) also observed the antidiabetic activity of peel, flesh, endosperm, and endocarp of the 4 type of mango fruits. While the IC_{50} value of acarbose was found as 0.064 ppm, the ethanolic extract of the *manalagi* endosperm had the highest inhibitory activity with IC_{50} value of 64.71 ppm. Therefore, as well as the fruit the peel of the fruit may be also used as an alternative to control blood glucose level even it did not indicate as good inhibitory activity as positive control (acarbose).

Pyracantha fortuneana fruit (PFF) is a fruit which is rich in proanthocyanin. The results of the research indicated that PFF inhibited α-glucosidase in a non-competitive type with the IC_{50} value of 0.15 μg/ml (Wei et al., 2017). The study also demonstrated the inhibitory mechanism of proanthocyanins on α-glucosidase.

Doan and colleagues (2018) analyzed the hypoglycemic activity of *Chrysophyllum cainito*

L with both *in vitro* and *in vivo* methods. The inhibition of α-glucosidase activity of the extract and acarbose were found as IC_{50} 1.20 and 198.17 μg/ml respectively. The extract was administered to normal and alloxan-induced diabetic mice at 500 mg/kg and found that fasting blood glucose level significantly reduced in diabetic mice. Thus, antidiabetic activity of the fruit comes from its effect on glucose uptake stimulation and α-glucosidase inhibition due to its phenols, tannin, glycosides, terpenoids, and saponin content.

In a recent research, antidiabetic activity of *Pometia pinnata* was studied using various solvents (methanol, ethyl acetate, n-hexane) for the fruits extraction (Sukiman et al., 2018). It was reported that the IC_{50} values of α-glucosidase for the methanol, ethyl acetate, n-hexane extract of the *P. pinnata* was obtained as 169.81 μg/mL, 505.55 μg/mL and 263.18 μg/mL respectively. The phenolic content of the methanolic extraction was higher than other solvent extractions therefore this may be related with better inhibitory activity on α-glucosidase enzyme.

Yegin and colleagues (2018) investigated the inhibition of α-amylase and α-glucosidase activity by *Malus communis* L. (Piraziz apple). The authors analyzed the antidiabetic activity by spectrophotometry. Piraziz apple inhibited α-amylase and α-glucosidase with IC_{50} values of 501.08 and 924.93 μg/ml respectively. When they used acarbose as a positive control, they found that the inhibition of α-amylase and α-glucosidase with IC_{50} values of 94.35 and 75.20 μg /ml respectively. They concluded that the inhibition activity of acarbose was higher than Piraziz apple for both α-amylase and α-glucosidase enzymes.

Crowberry (*Empetrum nigrum* L.) has been traditionally used due to its rich anthocyanins content, together with proanthocyanins and flavonoids (Hyun and Kim 2018). Ethyl-acetate fraction of the fruit extract exhibited significant inhibition of α-glucosidase and α-amylase activities with an IC_{50} of 0.5 and 100 μg/ml respectively. The correlation analysis indicated that the significant inhibition of α-glucosidase and α-amylase activities by the ethyl acetate fraction was due to the presence of polyphenolic compounds.

Bitter melon (*Momordica charantia*) is a phenolic rich fruit and there are some researches about its antidiabetic activities. The taste of bitterness comes from catechin, flavonoids, caffeic acid, p-coumaric acid, ferulic acid, isoflavones, terpenes, and glucosinolates content of the fruit. The inhibitory activity of bitter melon and acarbose was discovered for α-glucosidase enzyme. At 100 μg/ml of bitter melon extract and acarbose concentration the percentage inhibition was found as 30.0 and 22.6, respectively (Hwang, 2018).

Marmouzi and colleagues (2019) investigated the antidiabetic activity of *Zizyphus lotus* (Rhamnaceae) fruit. The major components of the fruit were gallic acid, ferulic and vanillic acids, rutin, catechin and epicatechin. The fruit demonstrated inhibition activity against α-amylase and α-glucosidase enzymes with an IC_{50} value of 31.9 and 27.95 μg/ml respectively.

Ethiopian pepper (*Xylopia aethiopica* (Dunal) A. Rich) is a type of fruit which is used as spice in West and Central Africa. The major constituents of the fruit were oleanolic acid, sesquiterpenoids, diterpenoids, triterpenoids and polyphenol. Oleanolic acid (OA) indicated a significant inhibition effect with lower IC_{50} values (α-amylase: 89.02 ± 1.12 mM, α-glucosidase: 46.05 ± 0.25 mM) than other fractions and the acarbose (Mohammed et al., 2019).

Morinda citrifolia L. is a fruit which is used as nutraceutical beverage due to its antidiabetic and antioxidant activities. In one of the recent papers, the antidiabetic activity of fermented Morinda fruit juice was tested and its IC_{50} value calculated as 28.99 μg GAE/ml. It was concluded that the antidiabetic activity may be due to the organic acid (α-ketoglutaric acid and malic acid) composition of the fermented fruit (Simomara et al., 2019).

3. Antidiabetic Activity of Dietary Fruits in In-vivo Studies

Animal Studies:

Antidiabetic activities of commonly consumed fruits, rich in phenolics and volatiles, in animal studies were presented in Table 2.

Table 2. Summary of antidiabetic activity of dietary fruits in animal studies

Analysed/ major polyphenols	Plant Food	Experimental model	Type of interaction	Effect	Reference
α-Pinene, sabinene, quercetin-hexoside, isoscutellarein-8-O-hexoside	*Juniperus communis*	STZ-induced female Wistar rats	250 mg/kg bw (body weight) of fruit administration for 24 days	Decreased blood glucose level and body weight	Medina et al., 1993
Flavones, saponins, proteins and tannins	*Eugenia jambolana*	STZ-induced Wistar rats	1.25 mg/kg bw	Blood glucose level decreased 50 %	Kelkar and Kaklij (1997)
Trans-anethol, fenchon, limonen, methyl chavicol, α-felandren	*Foeniculum vulgare*	Alloxan induced diabetic rats	Saline: 0.2 ml glibenclamide: 3 mg/kg Foeniculum vulgare Mill. essential oil: 5 ml/kg	Blood glucose level significantly reduced at 4h Glibenclamide reduced the blood glucose level significantly at 1, 2, and 24h.	Ozbek, 2002
Ferulic acid dehydrodimer (diFA), caffeic acid, sinapic acid	*Secale cereale* L.	Alloxan induced diabetic and normal rats	Saline: 0.2 ml Glibenclamide: 3 mg/kg Extract: 5 ml/kg	Extract indicated lower antidiabetic activity compared to glibenclamide Decreased blood glucose level only between 0-4 h.	Ozbek et al., 2002
Rutin, carvone, limonene, carveol, dihydrocarveol, thymol	*Carum carvi* and *Capparis spinosa* L.	Healthy and STZ induced diabetic rats	20 mg/kg of extract administered to rats for 14 days	Blood glucose level reduced Plasma insulin concentrations did not change	Eddouks et al., 2004
Anthocyanin, several glycosides of quercetin	*Rosa canina* L.	Healthy and STZ induced diabetic rats	Different solvent extracts of the fruit were administered 250 mg/kg for 7 days	The extract (water fraction) that has the lowest phenolic content exhibited the highest reduction of blood glucose level Reduction may be due to oligosaccharide rich of water fraction	Orhan et al., 2009
Gallic acid, protocatechuic acid, *p*-OH-benzoic acid and vanillic acid	*Rhus coriaria* L.	Alloxan induced diabetic wistar rats	Ethanolic extract of fruit were given to rats at a dose of 200 mg/kg for 21 day	Blood glucose level of the diabetic rats decreased 26% compared to control group.	Mohammadi et al., 2010
Kaempferol, myricetin, naringin, and rutin	*Phaleria macrocarpa*	STZ induced diabetic male Sprague Dawley rats	Different extraction fractions of extract given	Methyl and n-butanol fractions lowered plasma	Rabyah et al., 2012

			to rats at a dose of 1 g/kg for 12 days	insulin level significantly Dose-dependently inhibited glucose transport across isolated rat jejunum	
Hydroxybenzoic and hydroxycinnamic acids and procyanidins	*Persea americana* Mil.	STZ induced diabetic and normal male Wistar Albino rats	Rats were treated for 8 weeks at a dose of 300 mg/kg bw hydro-methanolic extract and its sub fractions	n-Hexane fractions of the extract exhibited the highest antidiabetic activity	Thenmozhi et al., 2012
Quercitrin, rutin, kaempferol, naringin and daidzein	*Pithecellobium dulcee* Benth	STZ induced diabetic and normal male Wistar Albino rats	Rats were fat orally with 300 mg/kg bw of extract for 30 days.	Significant reduction in blood glucose level, glycosylated hemoglobin, urea and creatinine.	Pradeepa et al., 2013
Carvone, γ – Terpinene and Limonene	*Carum carvi*	STZ-induced diabetic and normal rats	Rats were administered with 10 mg/kg bw caraway essential oil	*Carum carvi* essential oil exhibited renoprotection against diabetic nephropathy due to its essential oil. *Carum carvi* seed oil supplementation decreased blood glucose level in diabetic rats.	El-Soudi et al., 2014 Erjaee et al., 2015
Anthocyanins	*Vacciniummyrtillus*	Diabetic alloxan rats	Rats were administered with bilberry (2 g/d) and glibenclamide (0.6 mg/kg bw) for 4 weeks.	Extract decreased plasma glucose level better than glibenclamide.	Asgary et al., 2015
Citral	*Backhousia citriodora* oil	High-fat diet (HFD) and streptozotocin (STZ) induced diabetic rats	Rats were treated with 45 mg/kg bw of citral for 28 days	Citral and glibenclamide decreased blood glucose level at 55.3% and 58.7%, respectively.	Mishra et al., 2019
o-Guaiacol, *p*-creosol, *p*-vinylguaiacol, *p*-hydroxybenzaldehyde, vanillic acid and vanillin	*Vanilla planifolia* Andrews	Diabetic alloxan male mice	150 mg/ml of extract were administered to mice for 20 days	Decreased blood glucose level	Kanedi et al., 2019

Juniperus communis is a type of berry reported as antidiabetic fruit. The researchers administered the healthy and STZ-induced female Wistar rats with the fruit and observed that 250 mg/kg body weight (bw) of fruit administration for 24 days decreased blood glucose level and body weight significantly (Medina et al., 1993).

In another study antidiabetic compound was extracted from the fruit of *Eugenia jambolana* and then analyzed for its antidiabetic activity. Kelkar and Kaklij (1997) analyzed the effect of *Eugenia jambolana* on the blood glucose levels of STZ-induced Wistar rats. The identified antidiabetic compounds were peptidyl glycan and an oligosaccharide (Mw 6.0 and 1.2 kD). It was observed that loading peptidyl glycan preparation to rats at a dose of 1.25 mg/kg body weight (bw) decreased the blood glucose level by 50 % and oligosaccharide (8.0 mg/kg bw) reduced 30%.

Foeniculum vulgare (fennel) essential oil (FEO) was analyzed for its hypoglycemic activity using alloxan induced diabetic rats. Glibenclamide was used as positive control and saline was used as a control. The blood glucose level of rats was analyzed at 0, 1, 2, 4 and 24 hours after administration of FEO, glibenclamide and saline. It was discovered that FEO only significantly decreased the blood glucose level at 4h but glibenclamide reduced the blood glucose level significantly at 1, 2, and 24h. The lethal dose (LD_{50}) of FEO was found as 6.149 ml/kg (Ozbek, 2002).

Ozbek and colleagues (2002) analyzed the effect of *Secale cereale* L. fruit decotation extracts in alloxan diabetic and healthy rats. The blood glucose level of rats was analyzed at 0, 1, 2, 4 and 24 hours after administration of extract, glibenclamide, and saline as a control. It was observed that *Secale cereale* L. extract decreased blood glucose level between 0-4 h but observed lower antidiabetic activity compared to glibenclamide.

The essential oil content of Cuminum cyminum L. fruit indicated similar hypoglycemic effect with reference drug glibenclamide in the alloxan induced diabetic and healthy rats (Ceylan et al., 2003). The lethal dose (LD50) of fruit was 0.780 ml/kg.

In another study, the hypoglycaemic effects of aqueous extracts of *Carum carvi* (CC) and *Capparis spinosa* L. (CS) fruit were investigated in healthy and STZ induced rats. It was observed that administration of CC and CS aqueous extracts (20 mg/kg) to rats for 14 days decreased the blood glucose level in STZ rats but did not change normal rats. Also, the basal plasma insulin concentrations of both groups remained same in both acute and chronic treatments (Eddouks et al., 2004).

Fruit of *Rosa canina* L. is used traditionally in the management of diabetes in Anatolia. The ethanol extract of fruit was administered (250 mg/kg) to normal and STZ induced rats for 7 days. Also, different fractions of ethanolic extracts were administered to rats as well as EtOAc, n -BuOH, R-H_2O. It was observed that antidiabetic activity of fruit was not related with phenolic content as R-H_2O fraction demonstrates the highest inhibitory activity on blood glucose level (Orhan et al., 2009).

Mohammadi and colleagues (2010) studied fruits of *Rhus coriaria* L. (Anacardiaceae) which is traditionally used to treat diabetes in Iran. The ethanolic extract of fruit was analyzed with *in vitro* and *in vivo* studies. Alloxan induced wistar rats were fed with 200 mg extract/kg body weight. In the first day, postprandial blood glucose level was decreased by 24% and after 21-day, blood glucose level was decreased by 26% compared to control group. The maltase and sucrase activities were inhibited by 44 and 27% respectively by using extract. However, there were not any changes observed on the transcription level of INS (mRNA levels of insulin) and GLUT-4 genes. The authors concluded that the fruits of *Rhus coriaria* L. may improve the life of type 2 diabetic patients.

Anti-hyperglycemic activity of *Phaleria macrocarpa* (PM) fruit was studied with methanolic extract which was further fractionated with chloroform (CF), ethyl acetate (EAF), n-butanol (NBF) and aqueous (AF) fractions (Rabyah et al., 2012). STZ induced male Sprague Dawley (SD) rats were administered with 1 g/kg of above fractions and postprandial glucose levels were observed with intraperitoneal glucose tolerance test. While NBF fraction decreased the blood glucose level, other fractions did not affect. In addition, the rats were treated with the fractions

(1 g/kg) for 12 days and ME and NBF fractions lowered plasma insulin level significantly and dose-dependently inhibited glucose transport across isolated rat jejunum which implies an extra-pancreatic mechanism.

In one of the researches the hydro-methanolic (2:3) extract of the *Persea americana* Mil. (avacado) was administered to both STZ induced and normal male Wistar Albino rats for 8 weeks at a dose of 300 mg/kg bw. It was reported that n-hexane fraction of the extract exhibited the highest antidiabetic activity in STZ-induced rats and concluded that avocado may be beneficial to control blood glucose level (Thenmozhi et al., 2012).

Pradeepa and colleagues (2013) assessed the antidiabetic activity of polyphenol rich *Pithecellobium dulcee* Benth. (Leguminosae) fruits and treated STZ induced and normal male Wistar Albino rats with 300 mg/kg bw of extract orally for 30 days. It was found that the extract rich in phenolic compounds such as quercitrin, rutin, kaempferol, naringin and daidzein may influence amorilate of blood glucose level. It was reported that the fruit is none toxic and significantly reduced the levels of blood glucose.

Carum carvi (caraway) is an aromatic plant and traditionally used for the treatment of metabolic disorders. El-Soudi and colleagues (2014) analyzed the renoprotective effect of caraway essential oil in male albino rats. The major essential oil of the caraway was Carvone (70.1%), and it was followed by γ –Terpinene (12.6%) and Limonene (5.5%). The STZ-induced and normal rats were treated with 10 mg/kg bw caraway essential oil orally for 3 weeks. The morphological examination of the kidneys is a key factor to observe diabetic nephropathy. It was showed that diabetic rats which fed with *Carum carvi* oil has an improvement with minor pathological changes in their kidneys compare to diabetic rats which were not administered with *Carum carvi* oil. Therefore, it was reported that *Carum carvi* essential oil exhibited renoprotection against diabetic nephropathy due to its essential oil. There was another study about the effect of *Carum carvi* oil on STZ-induced Wistar male rats. The results of this study was also in agreement with Neveen and collagues (2014) as it was reported caraway seed oil supplementation decreased blood glucose level in diabetic rats (Erjaee et al., 2015).

It is believed that *Vacciniummyrtillus* (bilberry) has antidiabetic activity and therefore it is used traditionally within the prediabetics and diabetic patients. The researchers treated the diabetic alloxan rats with bilberry (2 g/d) and glibenclamide (0.6 mg/kg bw) for 4 weeks. It was found that bilberry supplementation decreased plasma glucose level better than glibenclamide and this effect might be related with anthocyanin content of the fruit (Asgary et al., 2015).

Anti-diabetic activity of citral was studied recently using high-fatdiet (HFD) and streptozotocin (STZ) induced diabetic rats. The study revealed the effect of citral on carbohydrate metabolic regulatory enzymes in the liver. Rats were treated with 45 mg/kg bw of citral for 28 days and it was discovered that citral and glibenclamide decreased blood glucose level in a percentage of 55.3 and 58.7 respectively (Mishra et al., 2019).

Kanedi and colleagues discovered whether the ethanolic extract of vanillin (*Vanilla planifolia* Andrews) has hyperglycemic effect in alloxan induced rats. The ethanolic extract of vanillin contains bioactive compounds of flavonoids, antioxidants, and phenols. 150 mg/ml of extract was administered to mice for 20 days. On the 20th day it was found that vanilla fruit extract decreased blood glucose level better than that glibenclamide did.

Clinical Trials:

Antidiabetic activity of dietary fruits such as Sumac *Rhuscoriaria*, berberis fruit, *Rosa canina*, *Citrus junos*, *Balanites aegyptiac*, cambuci, cagaita, maracujá-alho, cupuaçu, camu-camu and jaboticaba in clinical trials were presented in Table 3.

Table 3. Summary of antidiabetic activity of dietary fruits in clinical trials

Analysed/ major polyphenols	Plant Food	Experimental model	Type of interaction	Effect	Reference
Gallic acid, methyl gallate, kaempferol, and quercetin	Sumac *Rhuscoriaria* L.	Type-2 diabetic patients	Double blind randomized clinical study	Plasma glucose and HbA1c (Glycosylated hemoglobin) level significantly decreased compared to control	Shidfar et al., 2013
Anthocyanins, (delphinidin, cyanidin)	Berberis fruit	Type-2 diabetic patients	Randomized, double-blind, and placebo-controlled study	Serum glucose HbA1c level reduced compared to control	Moazezi and Qujeq, 2014
Proanthocyanidin aglycones	*Rosa canina* L.	Type-2 diabetic patients	Randomized controlled cross-over	Fasting blood glucose level significantly decreased HbA1c level did not changed	Dabaghian et al., 2015
Rutin, quercetin, tangeretin, naringin, and hesperidin	*Citrus junos* Tanaka	Prediabetic patients	Double-blind, crossover, placebo controlled	Fasting blood glucose level significantly decreased Postprandial glucose level slightly reduced	Hwang et al., 2015
Furostanol saponins, rutin, quercetin, syringic acid	*Balanites aegyptiaca* Del.	Type-2 diabetic patients	Randomised controlled cross-over	Reduced postprandial blood glucose level 26.9%	Rashad et al., 2017
Syringic acid Quercetin derivates Catechin Epicatechin Kaempferol derivates Free ellagic acid Total ellagic acid Myricetin derivates	Cambuci, cagaita, camu-camu jaboticaba juices	Healthy humans	Randomised controlled cross-over	Reduced blood glucose	Balisteiro et al., 2017

Forty-two patients of type-2 diabetics were fed with Sumac *Rhuscoriaria* L. for 3 months to analyze the effect of Sumac on serum glycemic status (Shidfar et al., 2013). This clinical trial was controlled as double-blind randomized study and volunteers were fed with 3 g/day sumac powder (n=22) or placebo (n=19) every day. Blood samples were collected before and after the intervention and it was found that serum glucose and HbA1c (Glycosylated hemoglobin) levels were decreased significantly in volunteers fed with sumac powder.

Moazezi and Qujeq, (2014) studied with 30 type-2 diabetic patients and fed them with berberis fruit extract for 8 weeks with a dose of 2 mg/day. The serum glucose HbA1c level of the volunteers who consumed barberry fruit had a significant decrease compare to group consumed placebo.

Rosa canina L. (rose hip) fruit extract have been traditionally used as antidiabetic fruit in Iran. Type-2 diabetic patients took rose hip fruit extract and toast powder capsule (placebo) for 3 months. Blood samples were collected before and after the intervention. It was reported that while the fasting blood glucose level significantly decreased in fruit extract consumed group, HbA1c group was not significantly more than placebo group. Therefore, the researchers suggested repeating the clinical study with larger dose of the fruit (Dabaghian et al., 2015).

Hwang and colleagues (2015) studied 40 prediabetic patients fed with the ethanol extracts of *Citrus junos Tanaka* peel (YE-4250 mg/day) for 16 weeks. The intervention study was conducted in double-blind, crossover, placebo controlled. Fasting plasma glucose, postprandial glucose, and fasting plasma insulin concentrations were assessed after end of each 8 weeks. It was found that while fasting plasma glucose level significantly reduced in YE group postprandial glucose slightly decreased and results supported that YE might be a useful supplement for prediabetic patients.

The effect of ethanol extract of *Balanites aegyptiaca* Del. (BE) (Zygophyllaceae) fruits on glucose control in elderly 30 type-2 diabetic people was evaluated in a recent study. Two groups were assigned for the intervention: placebo control and BE group. During 8 weeks of the study volunteers were fed with 400 mg/day BE fruit extract capsule or placebo test. The results of the 8 weeks treatment indicated that BE fruit extract reduced postprandial blood glucose level by 26.9% (Rashad et al., 2017).

Balisteiro and colleagues (2017) studied with 23 healthy subjects and fed them with different traditionally consumed fruit juices (or cambuci, cagaita, maracujá-alho, cupuaçu, camu-camu and jaboticaba) in Brazilian. On the first visit the participants fed with 50 g white bread plus 300 mL of water (control meal) and after 1-week interval they consumed 50 g white bread plus 300 mL fruit juices (test meal). The results indicated that cambuci, cagaita, camu-camu and jaboticaba juices reduced blood glucose level compared to control.

4. Conclusion

In this review, the antidiabetic potential of the selected fruits was summarized. The present data demonstrated the short and/or long-term potential and traditional usage of the antidiabetic fruits using *in vitro* and *in vivo* studies. The present studies indicated that due to phenolic and volatile contents of the fruits, they may inhibit digestive enzymes, improve insulin sensitivity, stimulate insulin secretion, decrease carbohydrate absorption and/or increase peripheral glucose uptake. *In vitro* studies explained the mechanism of action on the inhibition of α-glucosidase and α-amylase enzymes, cell culture experiments provide more details about fruits action to the transport or uptake of glucose and stimulation of insulin secretion. However, there are only limited *in vivo* studies about their antidiabetic effect. Therefore, to promote rational use of these fruits it is needed to have more biological knowledge on the specific mechanism for treatment of diabetes. Further *in vivo* studies are necessary to elucidate the effect of fruits and its active constituent on carbohydrate mechanism.

References

Abou El-Soud, N. H., El-Lithy, N. A., El-Saeed, G., Wahby, M. S., Khalil, M. Y., Morsy, F., & Shaffie, N. (2014). Renoprotective effects of Caraway (Carum carvi L.) essential oil in streptozotocin induced diabetic rats. Journal of Applied Pharmaceutical Science, 4(2), 27–33. https://doi.org/10.7324/JAPS.2014.40205

Adefegha, S. A., Oboh, G., Oyeleye, S. I., & Ejakpovi, I. (2017). Erectogenic, Antihypertensive, Antidiabetic, Anti-Oxidative Properties and Phenolic Compositions of Almond Fruit (Terminalia catappa L.) Parts (Hull and Drupe) – in vitro. Journal of Food Biochemistry, 41(2), 1–12. https://doi.org/10.1111/jfbc.12309

Adefegha, S. A., Oyeleye, S. I., & Oboh, G. (2015). Distribution of Phenolic Contents, Antidiabetic Potentials, Antihypertensive Properties, and Antioxidative Effects of Soursop (Annona muricata L.) Fruit Parts in Vitro. Biochemistry Research International, 2015. https://doi.org/10.1155/2015/347673

Al-Gubory, K. H., & Laher, I. (2018). Preface. Nutritional Antioxidant Therapies: Treatments and Perspectives, v–vi. https://doi.org/10.1007/978-3-319-67625-8

Ali, R. B., Atangwho, I. J., Kaur, N., Abraika, O. S., Ahmad, M., Mahmud, R., & Asmawi, M. Z. (2012). Bioassay-guided antidiabetic study of Phaleria macrocarpa fruit extract. Molecules, 17(5), 4986–5002. https://doi.org/10.3390/molecules17054986

Altun, M. L., Çitoğlu, G. S., Yilmaz, B. S., Özbek, H., Bayram, I., & CengIz, N. (2010). Hepatoprotective and hypoglycemic activities of Viburnum

opulus L. Turkish Journal of Pharmaceutical Sciences, 7(1), 35–48.

Andersson, U., Berger, K., Högberg, A., Landin-Olsson, M., & Holm, C. (2012). Effects of rose hip intake on risk markers of type 2 diabetes and cardiovascular disease: A randomized, double-blind, cross-over investigation in obese persons. European Journal of Clinical Nutrition, 66(5), 585–590. https://doi.org/10.1038/ejcn.2011.203

Anwer, T., Sharma, M., Khan, G., Iqbal, M., Ali, M. S., Alam, M. S., … Gupta, N. (2013). Rhus coriaria ameliorates insulin resistance in non-insulin-dependent diabetes mellitus (NIDDM) rats. Acta Poloniae Pharmaceutica - Drug Research, 70(5), 861–867.

Asgary, S., Rafieiankopaei, M., Sahebkar, A., Shamsi, F., & Goli-malekabadi, N. (2016). Anti-hyperglycemic and anti-hyperlipidemic effects of Vaccinium myrtillus fruit in experimentally induced diabetes (antidiabetic effect of Vaccinium myrtillus fruit). Journal of the Science of Food and Agriculture, 96(3), 764–768. https://doi.org/10.1002/jsfa.7144

Asgary, S., Rafieiankopaei, M., Sahebkar, A., Shamsi, F., & Goli-malekabadi, N. (2016). Anti-hyperglycemic and anti-hyperlipidemic effects of Vaccinium myrtillus fruit in experimentally induced diabetes (antidiabetic effect of Vaccinium myrtillus fruit). Journal of the Science of Food and Agriculture, 96(3), 764–768. https://doi.org/10.1002/jsfa.7144

Asghari, B., Salehi, P., Farimani, M. M., & Ebrahimi, S. N. (2015). α-Glucosidase Inhibitors from Fruits of Rosa canina L. Records of Natural Products, 9(3), 276–283.

Atal, S., Atal, S., Vyas, S., & Phadnis, P. (2016). Bio-enhancing effect of Piperine with Metformin on lowering blood glucose level in Alloxan induced diabetic mice. Pharmacognosy Research, 8(1), 56–60. https://doi.org/10.4103/0974-8490.171096

Balisteiro, D. M., Araujo, R. L. de, Giacaglia, L. R., & Genovese, M. I. (2017). Effect of clarified Brazilian native fruit juices on postprandial glycemia in healthy subjects. Food Research International, 100(May), 196–203. https://doi.org/10.1016/j.foodres.2017.08.044

Buah, E., Boerl, S., & Daun, D. A. N. (2016). Combination of ethanolic extract of α-glucosidase inhibitory activity of Phaleria macrocarpa (Scheff.) Boerl. Fruits and Annona muricata L. Leaves. Majalah Obat Tradisional, 21(2), 63–68. https://doi.org/10.22146/tradmedj.12819

Ceylan, E., Özbek, H., & Ağaoğlu, Z. (2003). Cuminum cyminum L. (Kimyon) Meyvesi Uçucu Yağının Median Lethal Doz (LD 50) Düzeyi ve Sağlıklı ve Diyabetli Farelerde Hipoglisemik Etkisinin Araştırılması, 10(2), 29–35.

Dabaghian, F. H., Kamalinejad, M., & Shojaei, A. (2012). Presenting anti-diabetic plants in Iranian traditional medicine, 3(November), 70–76. https://doi.org/10.5897/JDE12.004

De Medina, F. S., Gamez, M. J., Jimenez, I., Jimenez, J., Osuna, J. I., & Zarzuelo, A. (1994). Hypoglycemic activity of juniper "berries." Planta Medica, 60(3), 197–200. https://doi.org/10.1055/s-2006-959457

Debeljak, J., Ferk, P., Čokolič, M., Zavratnik, A., Tavčar Benković, E., Kreft, S., & Štrukelj, B. (2016). Randomised, double blind, cross-over, placebo and active controlled human pharmacodynamic study on the influence of silver fir wood extract (Belinal) on post-prandial glycemic response. Pharmazie, 71(10), 566–569. https://doi.org/10.1691/ph.2016.6658

Doan, H. Van, Riyajan, S., Iyara, R., & Chudapongse, N. (2018). Antidiabetic activity, glucose uptake stimulation and α-glucosidase inhibitory effect of Chrysophyllum cainito L. stem bark extract. BMC Complementary and Alternative Medicine, 18(1), 1–10. https://doi.org/10.1186/s12906-018-2328-0

Donado-Pestana, C. M., Moura, M. H. C., de Araujo, R. L., de Lima Santiago, G., de Moraes Barros, H. R., & Genovese, M. I. (2018). Polyphenols from Brazilian native Myrtaceae fruits and their potential health benefits against obesity and its associated complications. Current Opinion in Food

Science, 19, 42–49. https://doi.org/10.1016/j.cofs.2018.01.001

Eddouks, M., Lemhadri, A., & Michel, J. B. (2004). Caraway and caper: Potential anti-hyperglycemic plants in diabetic rats. Journal of Ethnopharmacology, 94(1), 143–148. https://doi.org/10.1016/j.jep.2004.05.006

Elyasiyan, U., Nudel, A., Skalka, N., Rozenberg, K., Drori, E., Oppenheimer, R., Rosenzweig, T. (2017). Anti-diabetic activity of aerial parts of Sarcopoterium spinosum. BMC Complementary and Alternative Medicine, 17(1), 1–12. https://doi.org/10.1186/s12906-017-1860-7

Erjaee, H., Rajaian, H., Nazifi, S., & Chahardahcherik, M. (2015). The effect of caraway (Carum carvi L.) on the blood antioxidant enzymes and lipid peroxidation in streptozotocin-induced diabetic rats. Comparative Clinical Pathology, 24(5), 1197–1203. https://doi.org/10.1007/s00580-014-2060-1

Raimov, R., Fakir, Hüseyin. (2018). Orman Köylülerinin Odun Dışı Orman Ürünlerini Kullanım Olanakları (Eğirdir Yöresi Örneği). Bilge International Journal of Science and Technology Research, 2, 132–144. https://doi.org/10.30516/bilgesci.490659

Giancarlo, S., Rosa, L. M., Nadjafi, F., & Francesco, M. (2006). Hypoglycaemic activity of two spices extracts: Rhus coriaria L. and Bunium persicum Boiss. Natural Product Research, 20(9), 882–886. https://doi.org/10.1080/14786410500520186

Güder, A., Gür, M., & Engin, M. S. (2015). Antidiabetic and Antioxidant Properties of Bilberry (Vaccinium myrtillus Linn.) Fruit and Their Chemical Composition. Journal of Agricultural Science and Technology, 17(2), 401–414.

Hashem Dabaghian, F., Abdollahifard, M., Khalighi Sigarudi, F., Taghavi Shirazi, M., Shojaee, A., Sabet, Z., & Fallah Huseini, H. (2015). Effects of Rosa canina L. fruit on glycemia and lipid profile in type 2 diabetic patients: A randomized, double-blind, placebo-controlled clinical trial. Journal of Medicinal Plants, 14(55), 95–104.

Hwang, E. S. (2018). Comparison of antioxidant capacity and α -glucosidase inhibitory activity between bitter melon (Momordica charanti) fruit and leaf extract. Asian Pacific Journal of Tropical Biomedicine, 8(4), 189–193. https://doi.org/10.4103/2221-1691.231280

Hwang, J. T., Yang, H. J., Ha, K. C., So, B. O., Choi, E. K., & Chae, S. W. (2015). A randomized, double-blind, placebo-controlled clinical trial to investigate the anti-diabetic effect of Citrus junos Tanaka peel. Journal of Functional Foods, 18, 532–537. https://doi.org/10.1016/j.jff.2015.08.019

Hyun, T. K., Ra, J. H., Han, S. H., & Kim, J. S. (2018). Antioxidant, antimicrobial, and antidiabetic activities of crowberry fruits. Indian Journal of Pharmaceutical Sciences, 80(3), 489–495. https://doi.org/10.4172/pharmaceutical-sciences.1000382

Ibitoye, O. B., Uwazie, J. N., & Ajiboye, T. O. (2018). Bioactivity-guided isolation of kaempferol as the antidiabetic principle from Cucumis sativus L. fruits. Journal of Food Biochemistry, 42(4), 1–7. https://doi.org/10.1111/jfbc.12479

İncegül, Y., Karaboyacı, M., Aydın, E., Özçelik, M. M., Özkan, G. (2018). Production and characterization of natural lemonade powder using β-Cyclodextrin particles. Bilge International Journal of Science and Technology Research, 2, 10–18. https://doi.org/10.30516/bilgesci.480942

Jyothsna, D. K. (2017). The Study of Effect of Pomegranate Juice on Type 2 Diabetes Mellietus. IOSR Journal of Dental and Medical Sciences, 16(04), 28–30. https://doi.org/10.9790/0853-1604032830

Kaleem, M., Medha, P., Ahmed, Q. U., Asif, M., & Bano, B. (2008). Beneficial effects of Annona squamosa extract in streptozotocin-induced diabetic rats. Singapore Medical Journal, 49(10), 800–804.

Kaleem, M., Sheema, Sarmad, H., & Bano, B. (2005). Protective effects of Piper nigrum

and Vinca rosea in alloxan induced diabetic rats. Indian Journal of Physiology and Pharmacology, 49(1), 65–71.

Kanedi, M. (2019). Fruit Extract of Vanilla (Vanilla planifolia Andrews) Lowers Total Blood Glucose in Alloxan-Induced Hyperglycemic Mice. European Journal of Pharmaceutical and Medical Research, 6(9), 314–316. Retrieved from https://www.researchgate.net/publication/336936580

Kelkar, S. M., & Kaklij, G. S. (1997). A simple two-step purification of antidiabetic compounds from Eugenia jambolana fruit-pulp: proteolytic resistance and other properties. Phytomedicine, 3(4), 353–359. https://doi.org/10.1016/s0944-7113(97)80009-8

Khaliq, T., Sarfraz, M., & Ashraf, M. A. (2015). Recent progress for the utilization of Curcuma longa, Piper nigrum and Phoenix dactylifera Seeds against type 2 diabetes. West Indian Medical Journal, 64(5), 527–532. https://doi.org/10.7727/wimj.2016.176

Khatib, A., Perumal, V., Ahmed, Q., Uzir, B., & Murugesu, S. (2017). Low inhibition of alpha-glucosidase and xanthine oxidase activities of ethanol extract of Momordica charantia fruit. Journal of Pharmaceutical Negative Results, 8(1), 20–24. https://doi.org/10.4103/0976-9234.204906

Lerman-garber, I., Ichazo-cerro, S., Zamora-gonzalez, J., & Posadas-romero, C. (1994). Monounsaturated Fat Diet, 17(4), 311–315.

Loizzo, M. R., Sicari, V., Tenuta, M. C., Leporini, M. R., Falco, T., Pellicanò, T. M., Tundis, R. (2016). Phytochemicals content, antioxidant and hypoglycaemic activities of commercial nutmeg mace (Myristica fragrans L.) and pimento (Pimenta dioica (L.) Merr.). International Journal of Food Science and Technology, 51(9), 2057–2063. https://doi.org/10.1111/ijfs.13178

Mahadeva Rao, U. S. (2018). In vitro free radical scavenging and reducing potentials as well as inhibitory potential on α-amylase and α-glucosidase activities of fruit of Morinda citrifolia (Rubiaceae). Research Journal of Pharmacy and Technology, 11(9), 4135–4142. https://doi.org/10.5958/0974-360X.2018.00760.6

Marmouzi, I., Kharbach, M., El Jemli, M., Bouyahya, A., Cherrah, Y., Bouklouze, A., … Faouzi, M. E. A. (2019). Antidiabetic, dermatoprotective, antioxidant and chemical functionalities in Zizyphus lotus leaves and fruits. Industrial Crops and Products, 132(June 2018), 134–139. https://doi.org/10.1016/j.indcrop.2019.02.007

Misbah, H., Aziz, A. A., & Aminudin, N. (2013). Antidiabetic and antioxidant properties of Ficus deltoidea fruit extracts and fractions. BMC Complementary and Alternative Medicine, 13. https://doi.org/10.1186/1472-6882-13-118

Mishra, C., Khalid, M. A., Fatima, N., Singh, B., Tripathi, D., Waseem, M., & Mahdi, A. A. (2019). Effects of citral on oxidative stress and hepatic key enzymes of glucose metabolism in streptozotocin/high-fat-diet induced diabetic dyslipidemia rats. Iranian Journal of Basic Medical Sciences, 22(1), 49–57. https://doi.org/10.22038/ijbms.2018.26889.6574

Moazezi, Z., & Qujeq, D. (2014). Berberis Fruit Extract and Biochemical Parameters in Patients with Type II Diabetes. Jundishapur, 9(2), 1–4.

Mohammadi, S., Kouhsari Montasser, S., & Feshani Monavar, A. (2010). Antidiabetic properties of the ethanolic extract of Rhus coriaria fruits in rats. DARU, Journal of Pharmaceutical Sciences, 18(4), 270–275.

Mohammed, A., Victoria Awolola, G., Ibrahim, M. A., Anthony Koorbanally, N., & Islam, M. S. (2019). Oleanolic acid as a potential antidiabetic component of Xylopia aethiopica (Dunal) A. Rich. (Annonaceae) fruit: bioassay guided isolation and molecular docking studies. Natural Product Research, 0(0), 1–4. https://doi.org/10.1080/14786419.2019.1596094

Nabi, S. A., Kasetti, R. B., Sirasanagandla, S., Tilak, T. K., Kumar, M. V. J., & Rao, C. A. (2013). Antidiabetic and antihyperlipidemic activity of Piper longum root aqueous extract in STZ

induced diabetic rats. BMC Complementary and Alternative Medicine, 13. https://doi.org/10.1186/1472-6882-13-37

Nowicka, P., Wojdyło, A., & Samoticha, J. (2016). Evaluation of phytochemicals, antioxidant capacity, and antidiabetic activity of novel smoothies from selected Prunus fruits. Journal of Functional Foods, 25, 397–407. https://doi.org/10.1016/j.jff.2016.06.024

Oboh, G., Isaac, A. T., Akinyemi, A. J., & Ajani, R. A. (2014). Inhibition of key enzymes linked to type 2 diabetes and sodium nitroprusside induced lipid peroxidation in rats' pancreas by phenolic extracts of avocado pear leaves and fruit. International Journal of Biomedical Science, 10(3), 210–218.

Ogurtsova, K., Rocha, J. D., Huang, Y., Linnenkamp, U., & Guariguata, L. (2017). IDF Diabetes Atlas: Global estimates for the prevalence of diabetes for 2015 and 2040. Diabetes Research and Clinical Practice, 128, 40–50. https://doi.org/10.1016/j.diabres.2017.03.024

Orhan, N., Aslan, M., Hoşbaş, S., & Deliorman Orhan, D. (2009). Antidiabetic effect and antioxidant potential of Rosa canina fruits. Pharmacognosy Magazine, 5(20), 309–315. https://doi.org/10.4103/0973-1296.58151

Özbek, H. (2002). Foeniculum Vulgare Miller (Rezene) Meyvesi Uçucu Yağının Lethal Doz 50 (LD50) Düzeyi ve Sağlıklı ve Diyabetli Farelerde Hipoglisemik Etkisinin Araştırılması. Van Tıp Dergisi, 9(4), 98–103.

Özbek, H., Özgökçe, F., Ceylan, E., & Ta, A. (2002). Secale cereale L. (Çavdar) Meyvesi Dekoksiyon Ekstresinin Sağlıklı ve Diyabetli Farelerde Hipoglisemik Etkisinin Araştırılması, 9(3), 73–77.

Park, J. H., Kim, R. Y., & Park, E. (2012). Antidiabetic activity of fruits and vegetables commonly consumed in Korea: Inhibitory potential against α-glucosidase and insulin-like action in vitro. Food Science and Biotechnology, 21(4), 1187–1193. https://doi.org/10.1007/s10068-012-0155-5

Pradeepa, S., Subramanian, S., & Kaviyarasan, V. (2013). Biochemical evaluation of antidiabetic properties of Pithecellobium dulce fruits studied in streptozotocin induced experimental diabetic rats. International Journal of Herbal Medicine, 1(4), 21–28. Retrieved from https://pdfs.semanticscholar.org/5b3a/7af005fd589792f943102c710067e78483b6.pdf

Putri, N. P., Nursyamsi, K. S., Prayogo, Y. H., Sari, D. R., Budiarti, E., & Batubara, I. (2017). Exploration of Mango Fruits (Mangifera indica) as α-Glucosidase Inhibitors. Biosaintifika: Journal of Biology & Biology Education, 9(3), 554. https://doi.org/10.15294/biosaintifika.v9i3.10516

Rashad, H., Metwally, F. M., Ezzat, S. M., Salama, M. M., Hasheesh, A., & Motaal, A. A. (2017). Randomized double-blinded pilot clinical study of the antidiabetic activity of Balanites aegyptiaca and UPLC-ESI,MS-MS identification of its metabolites. Pharmaceutical Biology, 55(1), 1954–1961. https://doi.org/10.1080/13880209.2017.1354388

Sancheti, S., Sancheti, S., & Seo, S. Y. (2013). Antidiabetic and antiacetylcholinesterase effects of ethyl acetate fraction of Chaenomeles sinensis (Thouin) Koehne fruits in streptozotocin-induced diabetic rats. Experimental and Toxicologic Pathology, 65(1–2), 55–60. https://doi.org/10.1016/j.etp.2011.05.010

Saravanan, S., & Parimelazhagan, T. (2014). In vitro antioxidant, antimicrobial and anti-diabetic properties of polyphenols of Passiflora ligularis Juss. fruit pulp. Food Science and Human Wellness, 3(2), 56–64. https://doi.org/10.1016/j.fshw.2014.05.001

Sekar, V., Chakraborty, S., Mani, S., Sali, V. K., & Vasanthi, H. R. (2019). Mangiferin from Mangifera indica fruits reduces post-prandial glucose level by inhibiting α-glucosidase and α-amylase activity. South African Journal of Botany, 120(2017), 129–134. https://doi.org/10.1016/j.sajb.2018.02.001

Shidfar, F., Rahideh, S. T., Rajab, A., Khandozi, N., Hosseini, S., Shidfar, S., & Mojab, F. (2014). The effect of Sumac rhuscoriaria L. Powder on serum glycemic status, ApoB, ApoA-I and total antioxidant capacity in type 2 diabetic patients. Iranian Journal of Pharmaceutical Research, 13(4), 1249–1255. https://doi.org/10.22037/ijpr.2014.1585

Simamora, A., Santoso, A. W., & Timotius, K. H. (2019). A-Glucosidase Inhibitory Effect of Fermented Fruit Juice of Morinda citrifolia L and Combination Effect with Acarbose. Current Research in Nutrition and Food Science, 7(1), 218–226. https://doi.org/10.12944/CRNFSJ.7.1.21

Smirin, P., Taler, D., Abitbol, G., Brutman-Barazani, T., Kerem, Z., Sampson, S. R., & Rosenzweig, T. (2010). Sarcopoterium spinosum extract as an antidiabetic agent: In vitro and in vivo study. Journal of Ethnopharmacology, 129(1), 10–17. https://doi.org/10.1016/j.jep.2010.02.021

Studies, M. (2013). Diversity of Ethno – Medicinal Plants for Diabetes from Bahraich (U.P.) India, 1(1), 13–23.

Sukiman, M., Margaretha, J. A., & Irawan, C. (2018). Evaluation of antidiabetes activity of matoa seed extract (Pometia pinnata) using enzym α -glucosidase, 7(5), 10–12.

Takahashi, K., Yoshioka, Y., Kato, E., Katsuki, S., Iida, O., Hosokawa, K., & Kawabata, J. (2010). Methyl caffeate as an α-glucosidase inhibitor from Solanum torvum fruits and the activity of related compounds. Bioscience, Biotechnology and Biochemistry, 74(4), 741–745. https://doi.org/10.1271/bbb.90789

Thenmozhi, A., Shanmugasundaram, C., & Mahadeva Rao, U. S. (2012). Biochemical evaluation of anti-diabetic Phytomolecule through bioactivity guided solvent fractionation and sub-fractionation from hydro-methanolic (2:3) extract of alligator pear fruit in streptozotocin induced diabetic rats. Journal of Applied Pharmaceutical Science, 2(1), 61–69.

Ulutaş Deniz, E., Yeğenoğlu, S., Sözen Şahne, B., & Gençler Özkan, A. M. (2018). Kişniş (Coriandrum sativum L.) üzerine bir derleme. Marmara Pharmaceutical Journal, 22(1), 15–28. https://doi.org/10.12991/mpj.2018.36

Vahid, H., Rakhshandeh, H., & Ghorbani, A. (2017). Antidiabetic properties of Capparis spinosa L. and its components. Biomedicine and Pharmacotherapy, 92, 293–302. https://doi.org/10.1016/j.biopha.2017.05.082

Wei, M., Chai, W. M., Yang, Q., Wang, R., & Peng, Y. (2017). Novel Insights into the Inhibitory Effect and Mechanism of proanthocyanins from Pyracantha fortuneana Fruit on α-Glucosidase. Journal of Food Science, 82(10), 2260–2268. https://doi.org/10.1111/1750-3841.13816

Yeğin, S. Ç., Güder, A., Kılıç, A., & Aydın, H. (2018). New Apple Culture: Investigation of Antioxidant Contents and Antidiabetic Effect of Piraziz Apple (Malus communis L.). Journal of the Institute of Science and Technology, 8(3), 237–242. https://doi.org/10.21597/jist.458644

Bilge International Journal of Science and Technology Research

Web : http://dergipark.gov.tr/bilgesci - **E-mail:** kutbilgescience@gmail.com

Received: 11.11.2019
Accepted: 29.12.2019
DOI: 10.30516/bilgesci.645588

ISSN: 2651-401X
e-ISSN: 2651-4028
3(Special Issue), 77-88, 2019

Topografik Özellikleri Kullanarak Arazi Morfolojisi Analizi: Uşak Ulubey Kanyonu Örneği

Ahmet Çilek[1]*, Süha Berberoğlu[1], Müge Ünal Çilek[1], Cenk Dönmez[1]

Özet: Yeryüzü şekilleri, geçmişte fizyografik ve morfometrik haritalar el yöntemleri ile çizilerek konumsal teknolojilerin gelişmesiyle arazi formlarının otomatik üretilmesi, veri tabanlarında depolanması kolaylaşarak, jeomorfoloji, toprak, ekoloji, peyzaj mimarlığı gibi fiziki planlarla ilgilenen pek çok bilim dalı tarafından daha etkin kullanılmaya başlamıştır. Bu çalışmada Ulubey Kanyonlarının arazi formlarını Coğrafi Bilgi Sistemleri aracılığıyla Topografik Pozisyon İndeksi (TPI) ile morfolojik analizler yaparak sınıflandırmak amaçlanmıştır. Uşak Ulubey Kanyonu, Amerika Birleşik Devletleri'nin Arizona eyaletinde bulunan Büyük Kanyon'dan (Grand Canyon) sonra dünyanın en büyük ikinci kanyonu unvanına sahiptir. Uşak'ın Ulubey ilçesinde yer alan kanyon, Ulubey ve Banaz çayları boyunca devam eden bir ana kanyon ve buna bağlanan onlarca büyük yan kanyonlardan oluşmaktadır. Morfolojik sınıflandırmaların oluşturulmasında 30 m çözünürlükte ASTER Sayısal Yükseklik Modeli (SYM) kullanılmıştır. Arazi morfolojisinin oluşturulmasında SYM verilerinden üretilen eğim, eğrisellik, yükseklik farkı, topografik açıklık vb. morfolojik parametreler kullanılmaktadır. TPI hesaplanmasında kullanılan Jennes algoritması, en küçük kareleri kullanarak belirlenen pencere boyutuna ikinci dereceden bir polinom yerleştirerek çok ölçekli bir yaklaşım kullanmaktadır. Araştırmada farklı ölçekteki SYM verileri için 300 m ve 2000 m pencere genişliği kullanılarak sonuçlar karşılaştırılmıştır. Oluşturulan morfolojk sınıflar kanyonlar, sığ vadiler, yaylalar, tabanlı vadiler, ovalar, açık yamaçlar, dik yamaçlar, vadilerde tepeler, orta eğimli sırtlar veya ovalardaki küçük tepeler, zirveler olmak üzere 10 sınıfta toplanmaktadır.

Bu çalışmadan elde edilen bilgiler, farklı özelliklere sahip arazi değişkenleri (toprak, bitki örtüsü, yükseklik vb.) için doğal sınırlar olarak kabul edilen yüzey morfolojisinin sınıflandırılması özellikle arazi bozulması ve jeomorfolojide belirlenmesinde faydalı olacaktır.

Anahtar Kelimeler: Arazi Formu, Ulubey Kanyonu, Topografik Pozisyon İndeksi, CBS

Landform Analysis using Topographic Characteristics: An Example of Usak Ulubey Canyon

Abstract: Earth shapes, physiographic and morphometric maps have been drawn by hand in the past. With the development of spatial technologies, automatic production of landforms and storage in databases has become easier and has been used more effectively by many disciplines interested in physical plans such as geomorphology, soil, ecology and landscape planning. This study aims to classify the landforms of Ulubey Canyons by morphological analysis with Topographic Positions Index (TPI) using Geographical Information Systems. Usak Ulubey Canyon is the second largest canyon in the world after the Grand Canyon in Arizona, USA. The canyon, located in the Ulubey district of Usak, consists of a main canyon along the Ulubey and Banaz streams and dozens of large side canyons connected to it. ASTER Digital

[1]Cukurova University, Landscape Architecture Department, Adana, Turkey
*Corresponding author (İletişim yazarı): acilek@cu.edu.tr

Citation (Atıf): Çilek, A., Berberoğlu, S., Ünal Çilek, M., Dönmez, C., (2019). Topografik Özellikleri Kullanarak Arazi Morfolojisi Analizi: Uşak Ulubey Kanyonu Örneği. Bilge International Journal of Science and Technology Research, 3(Special Issue): 77-88.

Elevation Model (DEM) with 30 m resolution was used to form the morphological classifications. Morphological parameters such as slope, curvature, height difference, topographic aperture, etc. are used to generate the land morphology. The Jennes algorithm used in the TPI calculation uses a multi-scale approach by placing a quadratic polynomial in the specified window size using the least squares. In this study, 300 m and 2000 m window widths were combined for landform classification. The morphological classes are classified into 10 class including i) canyons, deeply incised streams ii) mid-slope drainages, shallow valleys iii) upland drainages, headwaters iv) U-shape valleys v) plains vi) open slopes vii) upper slopes, mesas viii) local ridges/hills in valleys ix) mid-slope ridges, small hills in plains x) mountain tops, high ridges. The information obtained from this study, classification of surface morphology considered as natural boundaries for land variables (soil, vegetation, height, etc.) with different characteristics will be useful in determining land degradation and geomorphology.

Keywords: Landform, Ulubey Canyon, Topographic Position Index, GIS

1. Giriş

Son yıllarda arazi formunun sınıflandırılması için otomatik tekniklerin uygulanması çok yaygın hale gelmiştir (De Reu vd. 2013; Grohmann ve Riccomini 2009; Han vd. 2011; Ilia vd. 2017; Ilia I vd. 2013; Mokarram vd. 2015; Mokarram ve Sathyamoorthy 2018; Rigol-Sanchez vd. 2015; Seif 2014; Skentos ve Ourania 2017; Tagil ve Jenness 2008). Arazi formu sınıflandırması yer bilimleri ile sınırlı olmayıp özellikle arkeoloji, ekoloji, tarım, ormancılık, kırsal peyzaj planlama, afet yönetimi gibi bir bilim dalı için de önemli bir veri kaynağı olduğu kanıtlanmıştır (Ho ve Umitsu 2011; Hoersch vd. 2002; Mac Millan vd. 2003; Martín-Duque vd. 2003; McNab 2007; Mert vd. 2013; Oruç vd. 2017; Özdemir ve Özkan 2016; Verhagen ve Drâguţ 2012; Şentürk vd. 2019; Tekin ve Çan, 2019). Morfometri, yer şekillerinin kantitatif bir tanımı sağlar ve matematik, mühendislik ve son yıllarda bilgisayar bilimi kombinasyonunu kullanarak türetilmektedir. Blaszczynski'ye (1997) göre arazi morfolojisi yer şekilleri, ovalar, dağ silsileleri gibi büyük ölçekli özelliklerden bireysel tepeler ve vadiler gibi küçük ölçeklere kadar değişen dünyanın yüzeyindeki spesifik jeomorfolojik özellikler olarak tanımlanmaktadır. Tepe, ova, vadi gibi topografik özellikler eğim, derinlik ve engebelilik hakkında bilgiler verdiği için peyzajı etkileyen fiziksel ve biyolojik işlemler için önemlidir. Bitkilerin doğal habitatları, erozyon potansiyeli ve güneş radyasyonu arazi formu ve konumu ile doğrudan ilgilidir.

Sayısal yükseklik modelleri (SYM) topografyanın digital olarak temsil edilmektedir ve 1970'lerin başından beri her alanda kullanılmaktadır. SYM'ler ve ğim, bakı, gölgeli yamaçlar, hidrolojik yapı gibi bu veriden üretilen veriler jeomorfolojik ve jeomorfometrik çalışmalar için araştırmacılar tarafından kullanılmıştır. Jeomorfolojik araştırmalarda, arazinin morfometrik parametrelerinin incelenmesi, arazi formunun yorumlanması için büyük önem taşımaktadır. Arazi morfolojisi verisi multispektral görüntüler ile birlikte kullanıldığında jeoloji, litoloji, toprak, arazi örtüsü/kullanımı, fay hatları gibi birçok yersel bilgi içim hızlı ve faydalı bilgiler sağlamaktadır.
Bu çalışmada da SYM verilerine gelişmiş konumsal istatistik ve görüntü işleme algoritmaları uygulayarak Uşak Ulubey Kanyonunda arazi formlarını topografik poziyon indeksi (TPI) yardımıyla arazi formlarınnı yarı otomatik olarak tanımlamak ve sınıflandırmaktır.

2. Materyal ve Yöntem

2.1. Çalışma alanı

Çalışma alanı, Ege Denizi'ne akan Büyük Menderes Nehri'nin başlıca kollarından olan Banaz çayı ve Ulubey Deresi'nin geçtiği alanı kapsayan Ulubey kanyonları 500-1000 m genişliğe, 135-170 m derinliğe ve 40-45 km uzunluğa sahip olup Banaz-Ulubey akarsuları boyunca uzanmaktadır. Dikey tektonik hareketlerden etkilenerek Büyük Menderes Grabeninin çökmesiyle Horst-Graben sistemi şeklini alarak karstik bir oluşum meydana getirmiştir. 27 Haziran 2013 tarihinde tabiat parkı olarak ilan edilen Ulubey Kanyonu ve çevresi jeolojik, jeomorfolojik, bilimsel ve kültürel açıdan ender özelliklere sahiptir. Ege ve İç Anadolu bölgeleri arasında bir geçiş alanı üzerinde bulunması sebebiyle her iki bölgenin iklim özelliklerini bir arada gösterir. Ege kıyılarına göre yazları sıcak ve kurak geçen, kışları ise İç Anadolu Bölgesi'ne göre daha ılıman geçen bir geçiş iklimine sahiptir. Ege Denizi üzerinden

gelen hava kütlelerinin getirdiği yağışlar bölgenin iklimini nemli hale getirir. Yıllık ortalama yağış miktarı 551.0 mm'dir ve aylara-mevsimlere göre düzensiz bir dağılış göstermektedir.

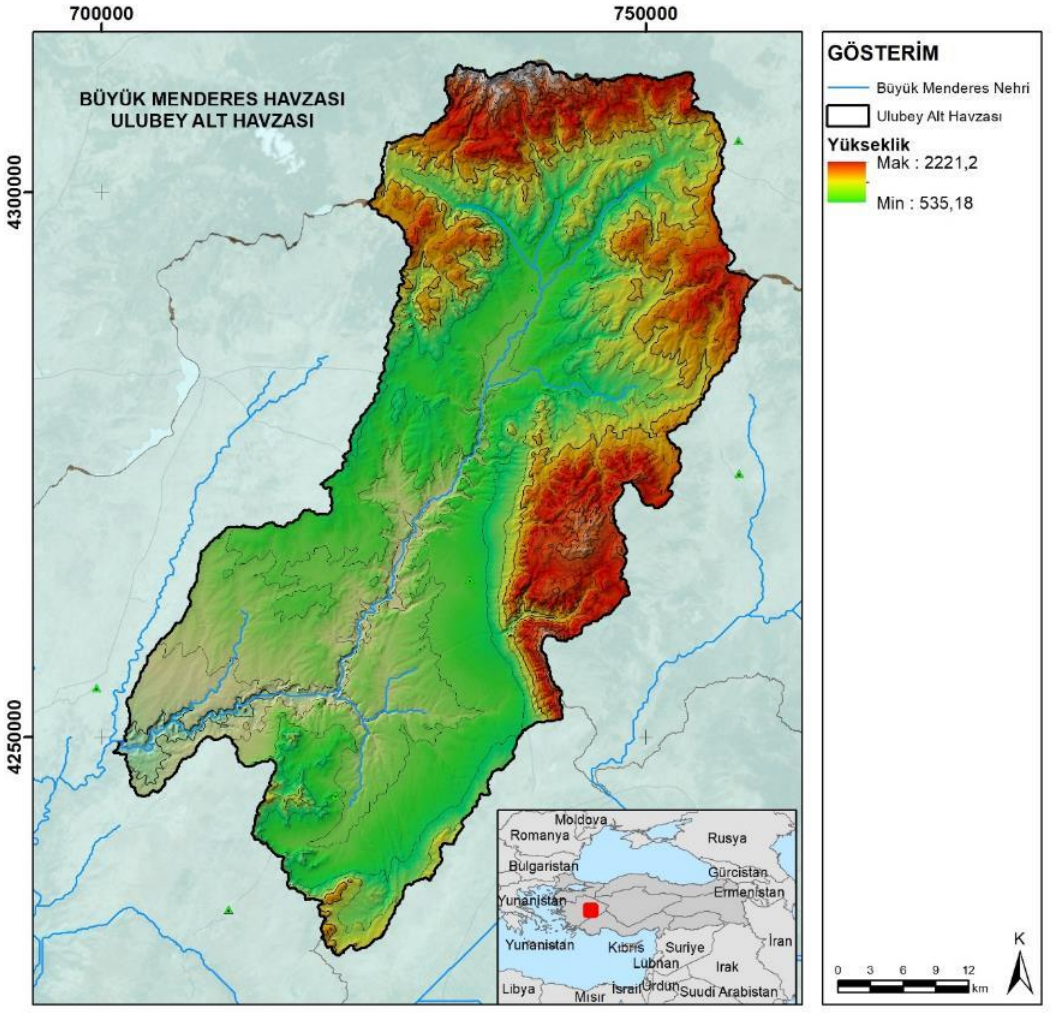

Şekil 1. Çalışma alanı ve yükseklik haritası

2.2. Metod

2.2.1. Topografik Pozisyon İndeksi (TPI)

Andrew Weiss TPI kavramını ve nasıl hesaplanacağını ESRI Uluslararası Kullanıcı Konferansında bir poster sunum ile ortaya çıkarmıştır (Guisan vd. 1999; Jones vd. 2000; Weiss 2001). TPI'yi farklı ölçeklerde ve eğim verisini kullanarak bir alanı hem eğim durumuna (sırt, vadi tabanı, orta eğim vb.) hem de arazi formuna göre (dik dar kanyonlar, geniş vadiler, ovalar, açık yamaçlar vb.) sınıflamaktadır. Geliştirilen algoritma sisteminin basitçe temeli bir pikselin yükseklik değeri ile o hücrenin etrafındaki komşu piksellerin ortalama değeri dikkat alır. Çıkan değer pozitif ise o pikselin diğer piksellerden yüksek olduğu, negatif ise de düşük olduğu anlamına gelmektedir. Ayrıca pikselin eğim derecesi de bazı sınıflarda dikkate alınmaktadır. Eğer bir hücre komşu hücrelerinden önemli oranda yüksek ise o bölgeler tepe veya sırt olarak sınıflandırılmaktadır. Komşu hücrelere göre önemli derecede düşük değerler ise o hücrenin vadi tabanı veya tabana yakın olduğunu göstermektedir. Sıfıra yakın değerler ise düz alanları veya orta eğimli alanlar olarak sınıflandırılır. Bu durumda eğim derecesi de hesaba dahil edilerek düz alanlar ile orta eğimli alanlar ayırt edilmektedir (Şekil 2).

Şekil 2. TPI değerlerinin arazi formunun belirlenmesindeki durumu (Jenness 2006)

TPI hesaplaması doğal olarak büyük oranda ölçeğe bağlıdır. Bir sıra dağlardaki tepe noktası bir otoyol inşaat ekibine açılan sırt veya bir fareye ise düz bir alan olarak algılanabilir (Jenness 2006). Böylece üretilen sınıflandırmalar tamamen peyzaj analizinde kullandığınız ölçeğe bağlıdır. Örneğin Şekil 3 de verilen çizimde TPI üç farklı ölçek kullanılarak aynı nokta için hesaplanmıştır. Kullanıcılar kendi çalışmalarında hangi ölçeğin en uygun olduğunu dikkatlice düşünmelidir. Büyük habitatların özellikleri hakkında bir çalışmada büyük ve belirgin bir arazi formu tanımlanabilir.

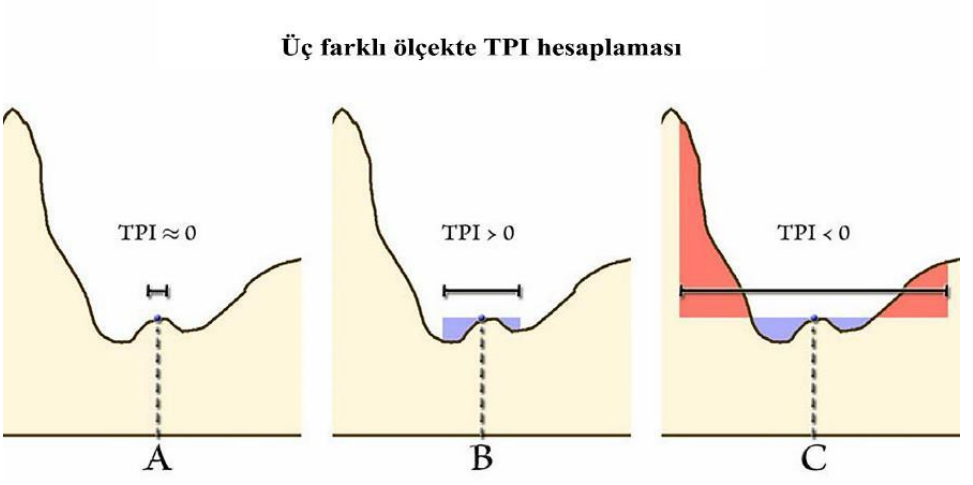

Şekil 3. Farklı ölçeklerde TPI hesaplaması (Jenness 2006)

Örneğin bir dağ aslanı çevresindeki yüzlerce metre yüksekliğindeki sırt çizgisi küçük tepeler ve engebelilikten daha fazla etkileneceği muhtemeldir. Diğer bir örnekte kanyonun dibindeki küçük bir tepenin üstündeki nokta bir ölçekte kanyon olarak sınıflandırılırken, başka ölçekte tepe olarak sınıflandırılabilir. Uygulamada her ikisi de doğru ve geçerli bir sınıflandırmadır. Kullanıcılar hangi ölçeğin çalışmasında uygun olduğunu belirlemesi gerekmektedir. Ölçek TPI analizinde kullanılan komşu pikseller tarafından belirlenmektedir. Az komşu piksellerin dahil edilmesi ile küçük ve yerel tepeler, vadiler; çok komşu piksellerin dahil edilmesi büyük ölçekli özellikler sınıflanır (Şekil 4). Her iki komşuluk sınıflandırmalarının ve eğim durumunun kullanılması ile Weiss (2001) tarafından yaklaşım geliştirilerek 10 sınıflı arazi formu sınıfları meydana gelmiştir.

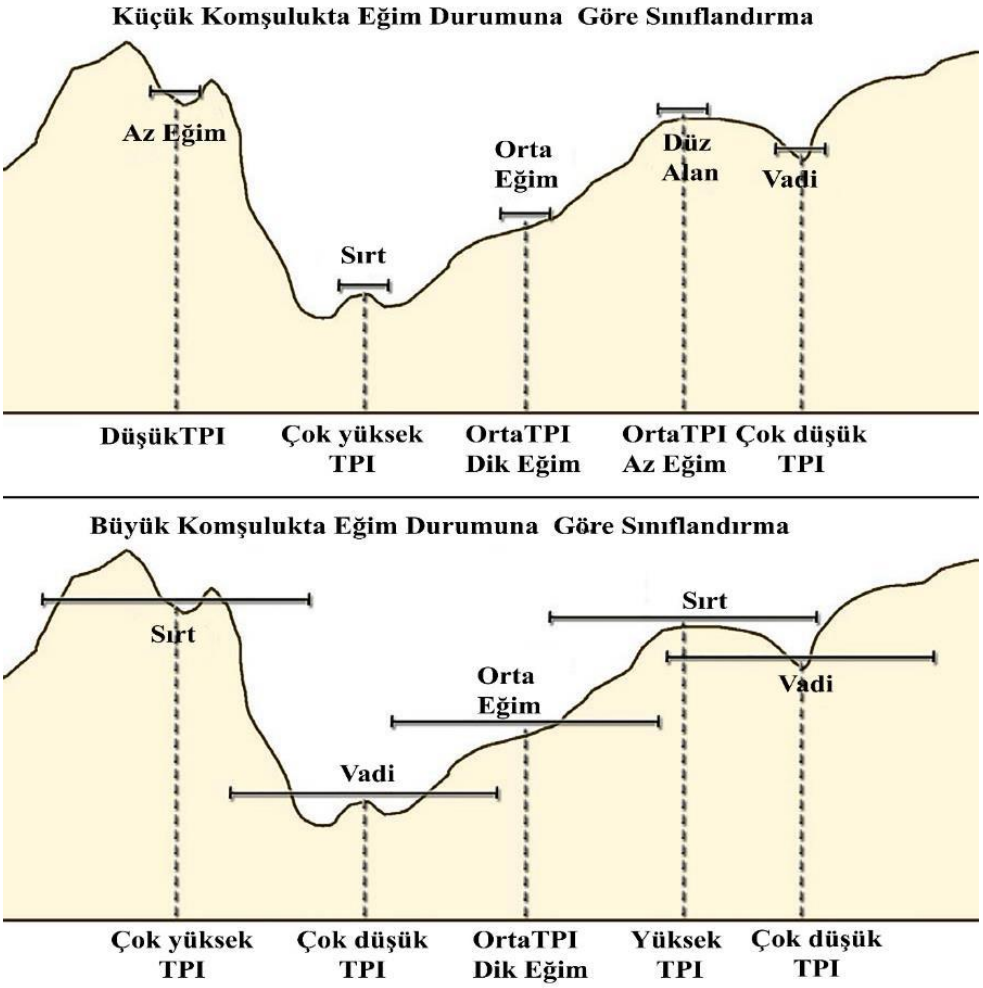

Şekil 4. Farklı komşuluk hesaplamalarında TPI ve arazi formu sınıflandırması (Jenness 2006)

3. Bulgular

TPI değerleri iki farklı komşuluk mesafesi kullanılarak hesaplanmıştır. 300 m yarıçaplı dairesel komşulukta 10 piksel yarıçapında hücrelerin değerleri hesaba dahil edilerek yapılmaktadır. 2000 m yarıçaplı dairesel komşulukta ise 67 piksel yarıçapında komşu hücrelerin değeri hesaplanmıştır. 300 m yarıçaplı veriden kanyonlar ve yan bağlantıları detaylı bir şekilde çıkartılırken, 2000 m yarıçapı veri ile genel kanyon sistemi (Şekil 5) ortaya konulmuştur.

Şekil 5. Ulubey kanyonları

TPI değerleri 300 m komşulukta 141 ile -183 arasında, 2000 m komşulukta ise 660 ile -487 arasında bulunmuştur. Sıfıra yakın alanlar düz alanları (eğimin sıfıra yakın olduğu yerler) ve orta eğimli alanları, yüksek değerler zirve ve sırtları, eksi değerler ise vadi ve kanyonları göstermektedir (Şekil 6).

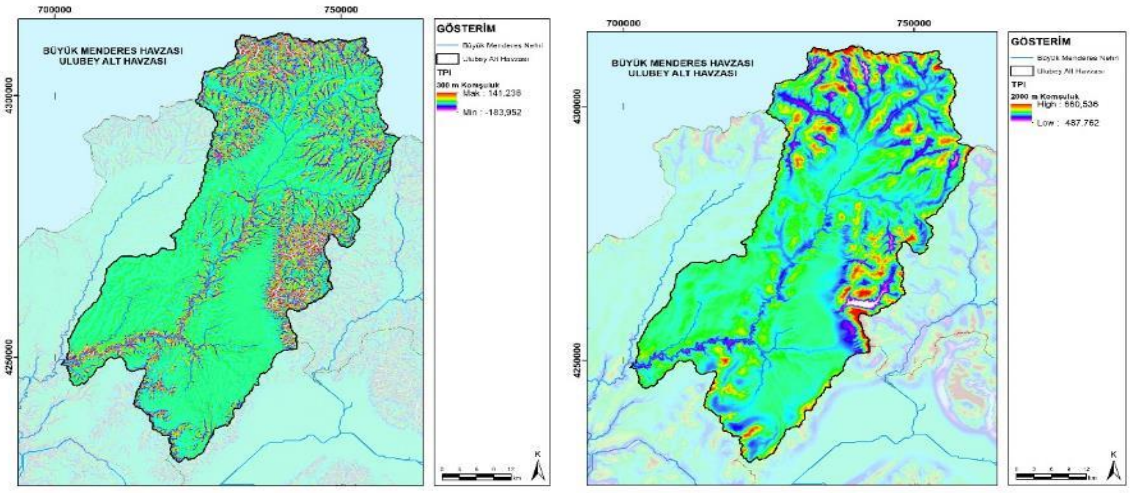

Şekil 6. Farklı komşuluklarda (300m ve 2000m) TPI verisi üretimi

TPI verileri üretildikten sonra CBS yazılımları kullanılarak arazi formu verisi üretilmiştir (Şekil 8). Çizelge 1'de belirtilen TPI değer aralıkları Model Maker kullanılarak otomatik sınıflayıcı modeli uygulanmıştır. Bu model içerisine çalışma alanı sınırı, TPI 300, TPI 2000 ve SYM verileri dahil edildiğinde otomatik olarak hesaplamalar yapılacak ve arazi formu sonuç haritası 10 sınıfta sınıflanacaktır. Böylelikle işlemler arasında üretilecek veri (Şekil 7'da yeşil renkli veriler) kalabalığı ve olası yanlış değerler girilme hatası önlenecektir. Model istenildiği takdirde ise TPI değer eşikleri değişikliğine olanak sağlamaktadır.

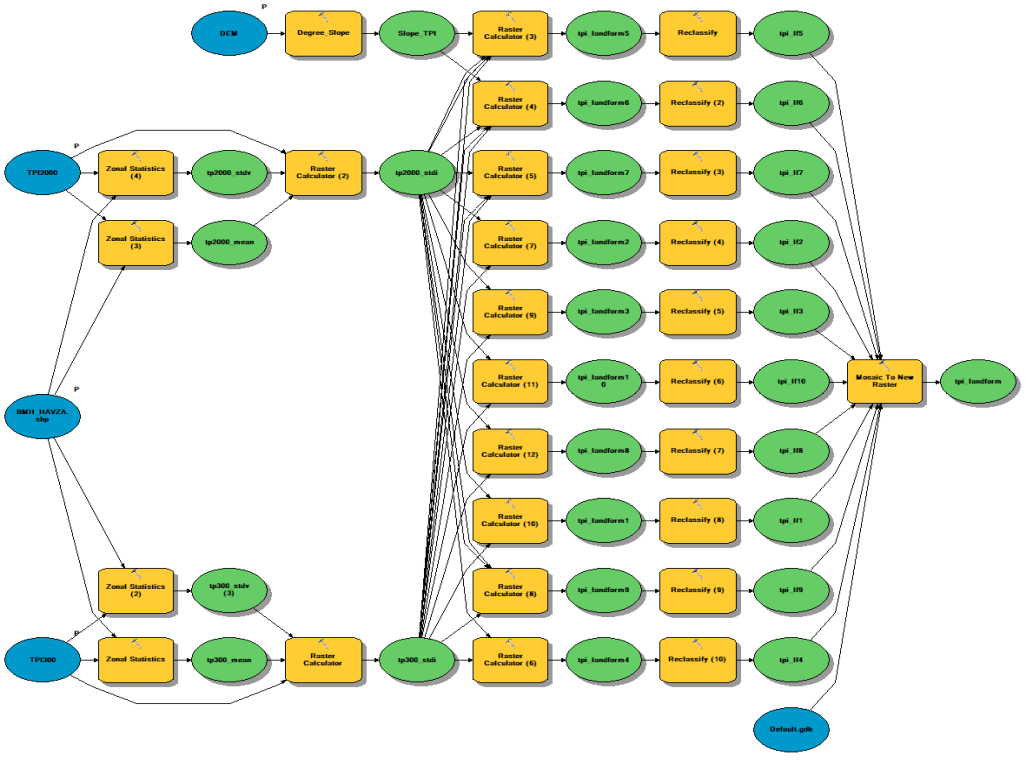

Şekil 7. TPI verisinden arazi formu üretilmesinde ArcGIS yazılımıyla modelin uygulanması

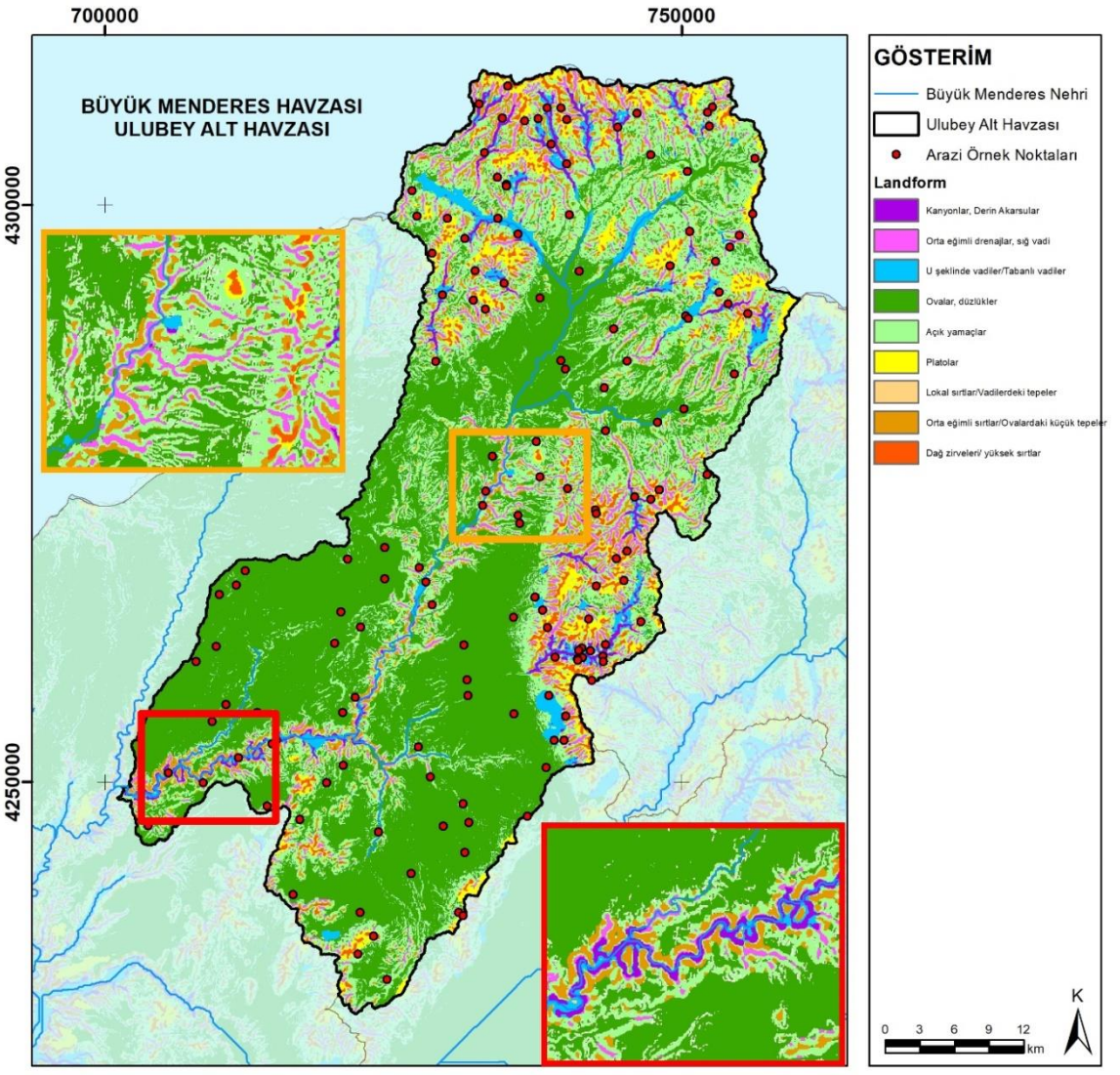

Şekil 8. Ulubey alt havzası Arazi formu sınıfları haritası

TPI değerleri ve eğim derecesi dikkate alınarak çalışma alanı için arazi form sınıfları üretilmiştir. Toplamda on farklı sınıf her hücredeki iki farklı komşuluktaki TPI değerlerinden eşik değerler kullanılarak sınıflandırılmaktadır. Örneğin kanyon alanlar küçük ve büyük komşulukta -1 değerine eşit veya küçük olması gerekmektedir. Ovalar/düzlük alanlar ise küçük ve büyük komşulukta -1 ile 1 arasında ve eğim derecesi de 5 dereceden düşük olması gerekmektedir. Oluşturulan arazi formlarının alan ve yüzde dağılımı Çizelge 1'de verilmiştir. Özellikle ovalar ve açık yamaçların çalışma alanında baskın sınıflar olarak görülmektedir. Ancak kanyonlarında önemli miktarda alan kapladığı dikkat çekmektedir.

Çizelge 1. Çalışma alanı arazi formları sınıfları, kapladığı alanlar ve TPI değerleri (Weiss, 2001)

Arazi formu Sınıfları	**Alan**		**Sınıflama tanımları**		
	Ha	**%**	**Eğim**	**Küçük Komşuluk (300 m)**	**Büyük Komşuluk (2000 m)**
Kanyonlar, Derin Akarsular	4510.17	2.1	-	TPI ≤ -1	TPI ≤ -1
Orta eğimli drenajlar, sığ vadi	11523.87	5.3	-	TPI ≤ -1	-1 < TPI < 1
Yüksek drenajlar, Üst nehir kolları	-		-	TPI ≤ -1	TPI ≥ 1
U Şeklinde vadiler (Tabanlı vadiler)	6677.37	3.1	-	-1 < TPI < 1	TPI ≤ -1
Ovalar, düzlükler	107510.76	49.3	≤5	-1 < TPI < 1	-1 < TPI < 1
Açık yamaçlar	60353.19	27.7	>5	-1 < TPI < 1	-1 < TPI < 1
Platolar	8445.06	3.9	-	-1 < TPI < 1	TPI ≥ 1
Lokal sırtlar/Vadilerdeki tepeler	303.39	0.1	-	TPI ≥ 1	TPI ≤ -1
Orta eğimli sırtlar/Ovalardaki küçük tepeler	12482.37	5.7	-	TPI ≥ 1	-1 < TPI < 1
Dağ zirveleri/ yüksek sırtlar	6084.09	2.8	-	TPI ≥ 1	TPI ≥ 1

Üretilen verilerde doğruluma verileri, yüksek çözünürlüklü görüntüler, mevcut sınıflandırılmış görüntüler veya CBS veri katmanlarından elde edilerek test edilebilir. Sınıflandırılmış bir haritanın doğruluğunu değerlendirmenin en yaygın yolu, yer gerçeği verilerinden bir dizi rastgele nokta oluşturmak ve bunu bir hata matrisindeki sınıflandırılmış verilerle karşılaştırmaktır. Bu amaçla üretilen haritanın doğruluk değerlendirmesi için çalışma alanında alansal büyüklüklere göre orantılı rastgele 147 nokta seçilmiş ve her bir noktanın yer gerçeği verileri karşılaştırılmıştır. Hata matrisleri oluşturularak her bir arazi formu sınıfı için doğruluk değerlendirme sonuçları Çizelge 2'de verilmiştir. Doğruluk analizinde, her bir sınıf için kullanıcının doğruluğu ve üreticinin doğruluğunun yanı sıra genel kappa istatistiği hesaplanmıştır.

Çizelge 2. Arazi formları sınıfları doğruluk analizi matrisi (Weiss, 2001)

Arazi Formu Sınıfları	Kanyonlar, Derin Akarsular	Orta eğimli drenajlar, sığ vadi	U Şeklinde vadiler	Ovalar, düzlükler	Açık yamaçlar	Platolar	Lokal sırtlar/ Vadilerdeki tepeler	Orta eğimli sırtlar/ Ovalardaki küçük tepeler	Dağ zirveleri/ yüksek sırtlar	Kullanıcı Doğruluğu
Kanyonlar, Derin Akarsular	**8**	1	1	0	0	0	0	0	0	0.80
Orta eğimli drenajlar, sığ vadi	1	**9**	0	0	0	0	0	0	0	0.90
U Şeklinde vadiler	1	1	**8**	0	0	0	0	0	0	0.80
Ovalar, düzlükler	0	0	0	**46**	1	2	0	0	0	0.94
Açık yamaçlar	0	0	0	0	**25**		1	1	0	0.89
Platolar	0	0	0	1	1	**8**	0	0	0	0.80
Lokal sırtlar/Vadilerdeki tepeler	0	0	0	0	0	0	**9**	1	0	0.90
Orta eğimli sırtlar/Ovalardaki küçük tepeler	0	0	0	0	0	0	1	**9**		0.90
Dağ zirveleri/ yüksek sırtlar	0	0	0	0	0	0	0	1	**9**	0.90
Üretici Doğruluğu	0.80	0.82	0.89	0.98	0.93	0.80	0.82	0.75	1.00	**0.89**
									Kappa İstatistiği	**0.87**

Hata matrisi sınıflamanın % 89 doğruluğunu ve genel kappa istatistik değerini 0.87 olarak hesaplamaktadır. Foody (2002)'ye göre % 85'in üzerinde doğruluk olan sınıflandırmaların kabul edilebilir değerde olduğunu ifade etmektedir.

4. Tartışma ve Sonuçlar

Jeomorfolojik analizlere dayanan CBS ve uzaktan algılama teknikleri ile birlikte peyzaj analizi ve haritalama teknikleri doğal kaynakların yönetimi için faydalı araçlardır. Bu çalışmada yarı otomatik bir arazi formu sınıflarını üretmek için TPI indeksi kullanılmıştır. Weiss (2001) tarafından geliştirilen yöntem kullanılarak ekoloji, toprak, jeoloji, planlama gibi konularda çalışan araştırmacılar için önemli olabilecek ve çok çeşitli peyzaj morfolojik özellikleri sağlayacak yaklaşım Büyük Menderes Havzası Ulubey kanyonlarında TPI'nin topografik özellikleri tanımlamak için güçlü bir araç olduğu ortaya konulmuştur.

Sonuç olarak, kanyonların hem jeolojik ortamın hem de topografyanın jeomorfolojik gelişimine katkıda bulunan faktörler olduğu görülmektedir. Alanın büyük bir bölümünü ova/düzlük alanlar oluştururken, nehir ağları etrafında çok sayıda kanyonlar meydana geldiği görülmektedir. Arazi formunun oluşturulması ile böylesi farklı arazi tiplerinin tespit edilmesi öne çıkmaktadır. Otomatik olarak arazi formu sınıflandırmasının morfoloji ile ilgilenen bilim dalları için güçlü bir coğrafi işlem tekniği olduğunu göstermektedir. Arazi formu sınıflarının jeolojik birimler ile ilişkilendirilmesi ise jeomorfolojik yapı ve jeolojik yapının oluşumu hakkında anlamlı bilgiler için kullanılabilmektedir. Ayrıca bu verilere ek olarak SYM'lerden üretilmiş arazi rölyefi, eğrisellik, topografik açıklık, eğim, vadi derinliği, yüzey pürüzlülüğü gibi verilerle daha detaylı morfometrik analizler yapılabilir.

Kaynaklar

Blaszczynski, J. S. (1997). Landform characterization with geographic information systems. *Photogrammetric Engineering and Remote Sensing*.

De Reu, J., Bourgeois, J., Bats, M., Zwertvaegher, A., Gelorini, V., De Smedt, P., vd. (2013). Application of the topographic position index to heterogeneous landscapes. *Geomorphology*. doi:10.1016/j.geomorph.2012.12.015

Foody, G. M. (2002). Status of land cover classification accuracy assessment. *Remote Sensing and Environment*, 80 (2002) 185-201

Grohmann, C. H., & Riccomini, C. (2009). Comparison of roving-window and search-window techniques for characterising landscape morphometry. *Computers and Geosciences*. doi:10.1016/j.cageo.2008.12.014

Guisan, A., Weiss, S. B., & Weiss, A. D. (1999). GLM versus CCA spatial modeling of plant species distribution. *Plant Ecology*. doi:10.1023/A:1009841519580

Han, H., Jang, K., Song, J., Seol, A., Chung, W., & Chung, J. (2011). The effects of site factors on herb species diversity in Kwangneung forest stands. *Forest Science and Technology*, *7*(1), 1–7. doi:10.1080/21580103.2011.559942

Ho, L. T. K., & Umitsu, M. (2011). Micro-landform classification and flood hazard assessment of the Thu Bon alluvial plain, central Vietnam via an integrated method utilizing remotely sensed data. *Applied Geography*. doi:10.1016/j.apgeog.2011.01.005

Hoersch, B., Braun, G., & Schmidt, U. (2002). Relation between landform and vegetation in alpine regions of Wallis, Switzerland. A multiscale remote sensing and GIS approach. *Computers, Environment and Urban Systems*. doi:10.1016/S0198-9715(01)00039-4

Ilia, I., Rozos, D., & Koumantakis, I. (2017). Landform classification using GIS techniques. The case of Kimi municipality area, Euboea Island, Greece. *Bulletin of the Geological Society of Greece*, *47*(1), 264. doi:10.12681/bgsg.10940

Ilia I, Rozos D, & Koumantakis I. (2013). LANDFORM CLASSIFICATION USING GIS TECHNIQUES. THE CASE OF KIMI MUNICIPALITY AREA, EUBOEA ISLAND, GREECE. *Bulletin of the Geological Society of Greece*.

Jenness, J. (2006). Topographic Position Index (tpi_jen.avx) extension for ArcView 3.x, v. 1.2. *Jenness Enterprises*.

Jones, K. B., Heggem, D. T., Wade, T. G., Neale, A. C., Ebert, D. W., Nash, M. S., vd. (2000). Assessing landscape condition relative to water resources in the western united states: A strategic approach. Içinde *Environmental Monitoring and Assessment*. doi:10.1023/A:1006448400047

Mac Millan, R. A., Martin, T. C., Earle, T. J., & Mc Nabb, D. H. (2003). Automated analysis and classification of landforms using high-resolution digital elevation data: Applications and issues. *Canadian Journal of Remote Sensing*. doi:10.5589/m03-031

Martín-Duque, J. F., Pedraza, J., Sanz, M. A., Bodoque, J. M., Godfrey, A. E., Díez, A., & Carrasco, R. M. (2003). Landform Classification for Land Use Planning in Developed Areas: An Example in Segovia Province (Central Spain). *Environmental Management*. doi:10.1007/s00267-003-2848-2

McNab, W. H. (2007). A topographic index to quantify the effect of mesoscale landform on site productivity. *Canadian Journal of Forest Research*. doi:10.1139/x93-140

Mert, A., Şentürk, Ö., Güney, C. O., Akdemir, D., & Özkan, K. (2013). Mapping of Some Distal Variables Available for Mapping Habitat Suitabilities of The Species . A Case Study from Buldan District. Içinde *3rd International Geography Symposium - GEOMED 2013* (ss. 489–497).

Mokarram, M., Roshan, G., & Negahban, S. (2015). Landform classification using topography position index (case study: salt dome of Korsia-Darab plain, Iran). *Modeling Earth Systems and Environment*, *1*(4), 1–7. doi:10.1007/s40808-015-0055-9

Mokarram, M., & Sathyamoorthy, D. (2018). A review of landform classification methods. *Spatial Information Research*, *26*(6), 647–660. doi:10.1007/s41324-018-0209-8

Oruç, M. S., Mert, A., & Özdemir, İ. (2017). Modelling Habitat Suitability for Red Deer (Cervus elaphus L .) Using Environmental Variables in Çatacık Region, Eskişehir. *Bilge International Journal of Science and Technology Research*, *1*(2), 135–142.

Özdemir, S., & Özkan, K. (2016). Ecological properties of Turkish Oregano (Origanum onites L.) and balsamic sage (Salvia tomentosa Miller) in the Ovacık Mountain district of the Mediterranean region. *İstanbul Üniversitesi Orman Fakültesi Dergisi*, *66*(1), 264–277. doi:10.17099/jffiu.39407

Rigol-Sanchez, J. P., Stuart, N., & Pulido-Bosch, A. (2015). ArcGeomorphometry: A toolbox for geomorphometric characterisation of DEMs in the ArcGIS environment. *Computers and Geosciences*. doi:10.1016/j.cageo.2015.09.020

Seif, A. (2014). Using Topography Position Index for Landform Classification (Case study: Grain Mountain). *BEPLS Bull. Env. Pharmacol. Life Sci*, *311*(311), 33–39. http://www.bepls.com/october2014bepls/6.pdf

Skentos, A., & Ourania, A. (2017). Landform Analysis Using Terrain Attributes. A Gis Application on the Island of Ikaria (Aegean Sea, Greece). *Annals of Valahia University of Targoviste, Geographical Series*, *17*(1), 90–97. doi:10.1515/avutgs-2017-0009

Şentürk, Ö., Negis M.G. & Gülsoy, S. (2019). Alpha Species Diversity and Ecological Site Factor Relations in Brutian Pine Forests: A Case Study From Gölhisar District. *Bilge International Journal of Science and Technology Research*, *3*(2), 178-188.

Tekin, S. & Çan, T. (2019). Slide Type Landslide Susceptibility Assessment of the Ermenek River Watershed (Karaman) Using Artificial Neural Network. *Bilge International Journal of Science and Technology Research*, *3*(1), 21-28.

Tagil, S., & Jenness, J. (2008). GIS-based automated landform classification and topographic, landcover and geologic attributes of landforms around the Yazoren Polje, Turkey. *Journal of Applied Sciences*. doi:10.3923/jas.2008.910.921

Verhagen, P., & Drâguţ, L. (2012). Object-based landform delineation and classification from DEMs for archaeological predictive mapping. *Journal of Archaeological Science*. doi:10.1016/j.jas.2011.11.001

Weiss, A. (2001). Topographic position and landforms analysis (Poster presentation). Içinde *ESRI User Conference, San Diego, CA, July 9-13*.

Bilge International Journal of Science and Technology Research

Web : http://dergipark.gov.tr/bilgesci - **E-mail:** kutbilgescience@gmail.com

Received: 11.11.2019
Accepted: 29.12.2019
DOI: 10.30516/bilgesci.645595

ISSN: 2651-401X
e-ISSN: 2651-4028
3(Special Issue), 89-105, 2019

Adana Katı Atık Toplama Tesisinin Mevcut Yer Seçim Uygunluğunun Konumsal Bilgi Teknolojileri ile Değerlendirilmesi

Müge Ünal Çilek[1]*, Ahmet Çilek[1], Esra Deniz Güner[2]

Özet: Belediye katı atık tesisleri dünyadaki kentleşme, sanayileşme, nüfus artışı ve teknolojik gelişmelerin sonucu karar vericilerin (mimarlar, şehir plancıları, yerel makamlar, bakanlar vb.) en uygun yer seçmesine önem kazandırmaktadır. Ancak, uygun depolama alanını belirlemek ve değerlendirmek için çevresel, sosyal, ekonomik ve teknik faktörleri içeren çok disiplinli çalışmalara ihtiyaç vardır. Bu nedenle, bu çalışma Adana'daki çevresel ve sosyo-ekonomik kısıtlamaları dikkate alarak mevcut belediye katı atık tesisinin alan uygunluğu değerlendirmek için çok kriterli bir model geliştirmeyi amaçlamaktadır. Bu bağlamda öncelikle depolama sahası uygunluk kriterleri literatür araştırması ile belirlenmiştir. İkinci aşamada her kriter katman olarak belirlendi ve uygun ve uygun olmayan alanlar Coğrafi Bilgi Sistemleri ortamında analiz edilmiştir. Üçüncü aşamada ise kriterlerin değer aralıkları fuzzy (bulanık mantık) yöntemiyle standardize edilmiştir. Son olarak standardize edilen katmanlar çakıştırılarak uygunluk haritası elde edilmiştir. Sonuç olarak, karar vericiler katı atık depolama sahası için uygun yerin değerlendirilmesi ve seçilmesi gerekliliği ile karşı karşıya kalarak bu çok kriterli analiz yönteminden faydalanabilir. Mevcut katı atık depolama alanının çevre ve sosyal yaşam üzerindeki olumsuz etkilerden dolayı en uygun alan olmadığını göstermektedir, ancak bu çalışma yeni katı atık depolama alanlarının seçiminde ekonomik ve ekolojik faydalar sağlayacaktır.

Anahtar Kelimeler: Katı Atık Depolama Alanı, CBS, Çok Kriterli Analizler, Fuzzy Logic

Evaluation of the Location Selection Suitability of Adana Municipality Solid Waste Facility with Spatial Information Technologies

Abstract: Municipal solid waste (MSW) gain importance for decision maker (architects, city planners, local authorities, ministries, etc.) to select suitable location, as a results of the rapid urbanization, industrialization, population growth, and technological development in the world. However, multidisciplinary studies involving environmental, social, economic and technical factors are required to decide and evaluate suitable landfill location. Therefore, this study aims to develop a multi-criteria model for evaluating the land use suitability for existing MSW considering environmental and socio-economic constraints in Adana, Turkey. In order to achieve this goal, firstly landfill suitability criteria and their evaluated values were defined by literature review. Secondly, each criteria were defined as a layer and then suitable and unsuitable area were analysed by Geographic Information Systems (GIS). Thirdly, the criteria were standardized to equalize the value ranges with each other by Fuzzy method. Finally, the

[1]Cukurova University, Landscape Architecture Department, Adana, Turkey
*Corresponding author (İletişim yazarı): mugeunal23@gmail.com

Citation (Atıf): Ünal Çilek, M., Çilek, A., Güner, E. D., (2019). Adana Katı Atık Toplama Tesisinin Mevcut Yer Seçim Uygunluğunun Konumsal Bilgi Teknolojileri ile Değerlendirilmesi. Bilge International Journal of Science and Technology Research, 3(Special Issue): 89-105.

standardized criteria maps were overlaid and MSW suitability class were determined in the result map. Consequently, the decision-makers, faced with the need of evaluating and selecting the suitable location for MSW landfill can benefit from this multi-criteria model. The findings of the research indicate that existing MSW landfill is not the best suitable area due to the negative effect on environment and social life, however, this study will provide economic and ecological benefits in the selection of new MSW storage sites.

Keywords: Siting MSW Landfills, GIS, Multi Criteria Decision Making, Fuzzy Logic

1. Giriş

Dünyada teknolojik gelişmeler ile birlikte kentleşme ve endüstrileşme hız kazanmış ve bu durum hem çevre üzerinde hem de insan sağlığı üzerinde olumsuz etkilerini göstermeye başlamıştır. Son yıllarda gerek sivil toplum kuruluşlarının gerekse kent üzerinde söz sahibi olan karar vericilerin (mimarlar, şehir plancıları, yerel yönetimler, bakanlıklar, vb.) çalışmaları ile sürdürülebilir çevre ve kamusal alan planları önem kazanmıştır. Sürdürülebilirliğin sağlanması için karar vericilerin sadece kamu yararı göz önünde bulundurması yeterli olmadığı günümüz şartları, çevresel, sosyal, ekonomik ve teknik konularının da dahil edildiği bütüncül bir yaklaşım gerektiren ve farklı meslek disiplinlerinin de dahil olduğu planların üretilmesini zorunluluk haline dönüştürmüştür (Torabi-Kaveh vd., 2016; Khan vd., 2018; Demesouka vd., 2019, Unal vd. 2019). Katı atık entegre tesisleri bu tür planların üretilmesi gereken ve son yıllarda karar vericilerin üzerinde durduğu çalışma konularından birisidir. Çünkü katı atık tesisleri yapım ve işletme aşamalarında çevre (su kirliliği, toprak kirliliği, hava kirliliği vb.) ve toplum sağlığını (koku etkisi, sağlığa zararlı gazların salınımı, vb.) etkilemekte, kısıtlı alan kullanımına sahip olunmasından dolayı kamulaştırmada ekonomik sınırlayıcılarla karşılaşmaktadır. Katı atık depolama alanının uygun yer seçim kararları sadece ulusal değil uluslararası düzenlemelere de uymak zorundadır (Demesouka vd., 2019). Bu yüzden karar vericiler iyi seçim ve yönetim stratejine sahip olmayan depolama tesislerinin çevre ve halk sağlığı üzerindeki olumsuz etkilerinin bilincinde olmalı ve uygun depolama alanı seçim kararı verilirken bu risklerin en düşük seviyede olmasına özen göstermelidirler (Önüt ve Soner, 2008; Gbanie vd., 2013; Soltani vd., 2015; Torabi-Kaveh vd., 2016; Khan vd., 2018).

Katı atık depolama sahasının uygun yer seçim kararının verilmesi karmaşık ve çok disiplinli bir süreçtir. Katı atık depolama sahası seçim probleminin konumsal olması gerekliliği Coğrafi Bilgi Sistemleri (CBS) kullanımını gerektirir. McHarg'ın harita katmanlama fikrine dayanarak (McHarg, 1992), konumsal bilgilerin yönetimi, detaylandırılması ve performansının desteklenmesi için desteklenen prosedürler, konumlandırma analizindeki rollerini arttırır. CBS tabanlı çok kriterli analiz (MCDA) yöntemi, mekansal ve mekansal olmayan pek çok veriyi dikkate alarak kullanılabilecek bilgilere dönüştüren ve uygun yer şeçim kararlarının belirlenmesinde kritik unsurları göz önünde bulunduran ve pek çok çalışmanın konusunu oluşturan akıllı bir sistemdir (Malczewski, 2004; Sumathi vd., 2008). Literatür incelemeleri sonucunda Analytic Hierarchical Process (AHP), Analytic Network Process (ANP), Weighted Linear Combination (WLC) veya Simple Additive Method (SAM) ve Fuzzy Logic süreçlerini içerebilen çok kriterli analizler uygun alan seçimi belirlemede en çok kullanılan yöntemlerdir. Katı atık entegre tesisleri için uygun yer seçim kararının verilmesinde çok kriterli analiz yöntemini kullanan ve ilk olabilecek çalışmalardan Vuk vd., (1991), Cheng vd., (2002, 2003) ve Queiruga vd., (2008) önceden belirlenmiş aday sahaların değerlendirilmesinde kullanmışlardır. Alumur ve Kara (2007), Emek ve Kara (2007) ve Colebrook ve Sicilia (2007) diğer yazarlardan farklı olarak, yer seçim kararı alınmasında önceden belirlenen aday alanları değerlendirmemiş, çalışma sınırları içerisindeki tüm alanlarda çok kriterli analiz yöntemi aracılığıyla uygun aday alanları belirlemişlerdir. Erkut ve Newman (1989), Khan ve Faisal (2008) ve Aragonés-Beltrán vd. (2010) katı atık entegre tesisleri için uygun yer seçim kararında bilgi ve deneyime göre belirlenen kriterler ve alternatifler arasındaki etki ve etkileşimleri dikkate alan AHP sürecini ele almışlardır.

Hızlı kentleşme sonucunda potansiyel alan kullanımlarına dikkat etmeyen gelişmekte olan ülkelerde, çevre mevzuatının geliştirilmesi katı atık depolama alanının uygun yer seçim kararının alınabilmesinde uygun alan kullanım optimizasyonunu sağlayacaktır. Gelişmekte olan

ülkeler arasında yer alan Türkiye'de katı atık üretimi son 10 yılda 25.373.000 tondan 31.584.000 tona yükselmiş, kontrollü katı atık depolama alanları ise yaklaşık % 60 artmıştır (TÜİK, 2018). Çalışma alanını oluşturan Adana kentinde ise hızlı nüfus artışı çöp üretiminin artmasına, hızlı kentleşme ise mevcut katı atık entegre tesisinin yerleşim alanı içerisinde kalmasına ve koku etkisinin kentin sağlık ve sosyal yaşamını olumsuz etkilemesine sebep olmuştur. Bu bağlamda çalışmanın amacı, coğrafi bilgi sistemleri ve çok kriterli analiz yöntemi kombinasyonu ile katı atık tesisleri uygun yer seçimin değerlendirilmesi için bir metodoloji ortaya koymaktır. Çalışma ile pek çok çevresel ve sosyo-ekonomik faktör sistematik olarak değerlendirilmiştir. Çalışma sonucunda ise karar vericilerin doğru alan kullanım kararlarını verebilmeleri için güvenilir, uygun ve uygulanabilir somut verilerin elde edilmesi hedeflenmiştir.

2. Materyal ve Yöntem

2.1. Çalışma alanı

Türkiye'nin nüfusu en yüksek 5. kenti olan Adana, Çukurova metropoliten alanının da merkezi konumundadır (37°00′N 35°19′E). Bu alan ülkenin en verimli tarım arazilerini kapsadığından tarım ve tarımsal sanayi gelişmiştir. Bu gelişme önemli düzeyde istihdam kapasitesi yarattığından kırsal kesimden kente yoğun bir iç göç oluşmuştur. Böylece 1980'lerin başında 500.000 olan kent nüfusu 2018 yılında yaklaşık 2.220.125'e yükselmiştir. Kent, aralarındaki sınırları Seyhan nehri ve ana sulama kanalının belirlediği ve 2018 nüfusları parantez içinde belirtilen dört ilçeye ayrılmıştır: Çukurova (365.735), Sarıçam (173.154), Seyhan (793.480) ve Yüreğir (415.198) (TUİK, 2018) (Şekil 1). Adana'nın 1985-2015 döneminde hazırlanan imar plan ve iyileştirmelerinde dört ilçe merkezinde de artan nüfusun konut gereksiniminin karşılanmasına öncelik verilmiştir. Bu durum, hızlı kentleşme ve nüfus artışı ile birlikte kentsel atıkların miktarının artmasına yol açmış ve kentsel atıkların depolanma gereksinimini ortaya çıkarmıştır.

Adana Büyükşehir Belediyesi sınırları içerisinde; 15 adet ilçe belediyesi yer almaktadır. Bu belediyelerin sorumluluğunda olan yerleşim yerlerinden kaynaklı katı atıklar 2011 yılından itibaren Adana Entegre Katı Atık Bertaraf Tesisi'nde toplanmaktadır. Bu tesis ile ilgili bazı sayısal veriler şunlardır: 1.800 ton/gün evsel katı atık, 4 adet aktarma istasyonu, 15 adet Semitrey ile (her birinin kapasitesi ortalama 25 ton), hizmet verdiği nüfus 2.149.260 kişi, ve 2013 yılı verilerine göre atık miktarı 519.140,440 ton/yıldır. Fakat son yıllarda mevcut katı atık tesisinin yerleşim alanları içerisinde kalması, çevreye ve kent yaşamına olumsuz etkilerinin bulunmasından dolayı mevcut yer seçiminin değerlendirilmesi ihtiyacı ortaya çıkmıştır.

Araştırma alanı olarak mevcut katı atık depolama alanının seçilmesinin ana nedenleri;

- Adana Sarıçam ilçesinde yapılaşmaya öncelik tanınmasından dolayı mevcut tesisin yerleşim alanı içerinde kalması,
- Depolama alanından kaynaklı gazların kent sağlığını olumsuz yönde etkilemesi,
- Koku etkisinin kentin sosyal yaşantısını olumsuz etkilemesi olarak sıralanabilir.

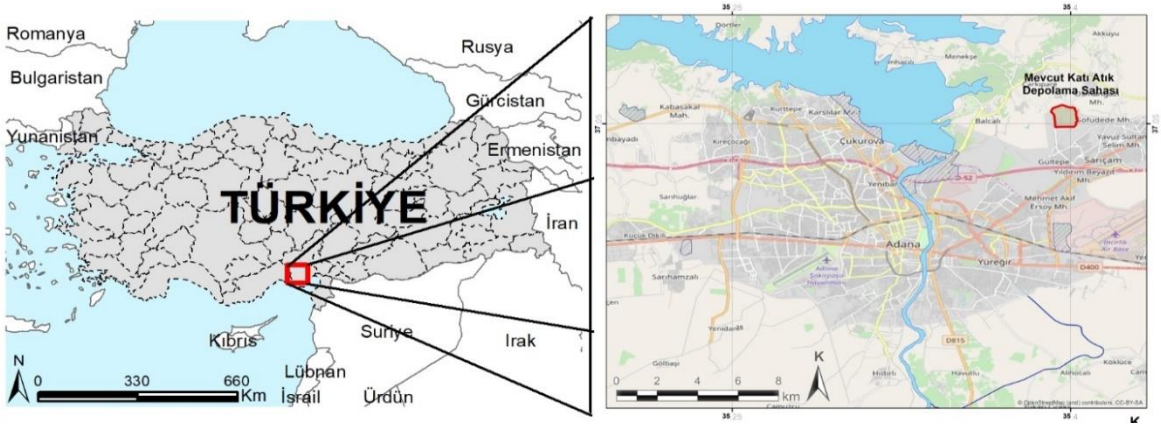

Şekil 1. Çalışma alanı sınırları, Adana/Türkiye

2.2. Yöntem

Çalışmanın yöntemi beş aşamadan oluşmaktadır (Şekil 2):

- Katı atık tesisinin yer seçimin uygunluğunun belirlenebilmesi için gerekli kriterlerin literatür araştırması ve uzman görüşleri doğrultusunda belirlenmesi
- Coğrafi Bilgi Sistemleri tabanlı Çok Katmanlı Analiz yönteminin uygulanması
  - Gerekli katmanların belirlenmesi,
  - Uygun ve uygun olmayan alanları belirtecek şekilde sınıflandırma yapılması,
  - Standardizasyon (Fuzzy yöntemi ile haritaların aynı birime getirilmesi)
- Katı atık toplama tesisi yer seçim uygunluğunun haritalanması
- Katı atık toplama tesisi alanının uygunluğunun belirlenmesi ve derecelendirilmesi
- Sonuçlar doğrultusunda önerilerin geliştirilmesi

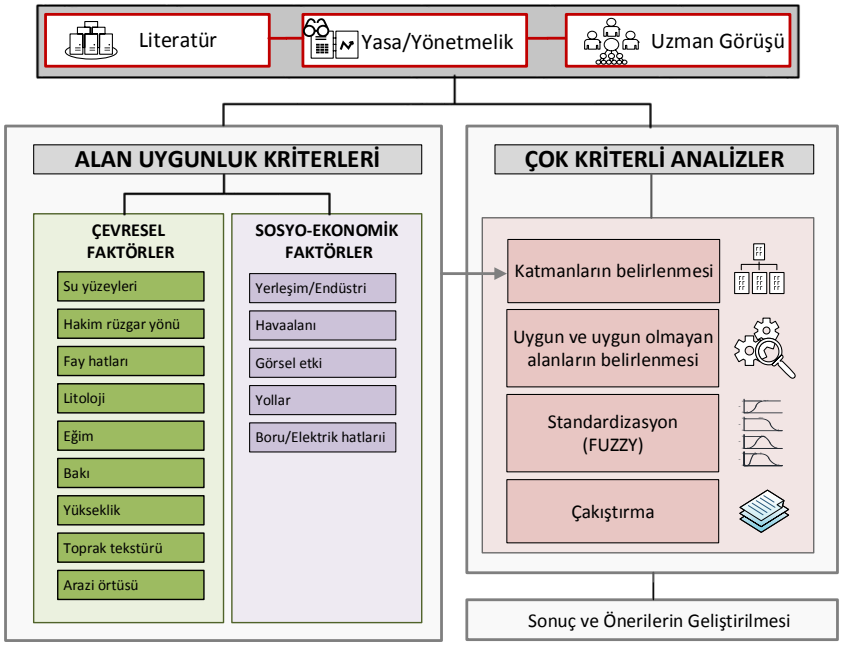

Şekil 2. Çalışmanın akış diyagramı

2.2.1. Verimlilik Kavramı ve Verimliliği Artırmaya Yönelik Uygulamalar

Uygun bir depolama sahasının seçilmesinde, çevresel, ekonomik, sosyolojik, teknik ve politik yönden önemli olan en uygun yeri belirlemek için kapsamlı bir değerlendirme süreci gerekmektedir (Ersoy ve Bulut, 2009; Nas vd., 2010; Yildirim, 2012; Soltani vd., 2015). Çünkü depolama sahası çevre, halk sağlığı ve güvenliği üzerinde olası bir etkiden kaçınmalı, diğer doğal ve insan yapımı sistemlerle herhangi bir etkileşimde bulunması engellenmelidir (Gorsevski vd., 2012; Soltani vd., 2015). Bu yüzden yer seçiminin uygunluğunun değerlendirilmesinde en önemli ilkeler çevre koruma, halk sağlığı ve güvenliğidir (Kontos vd., 2005; Önüt ve Soner, 2008; Sumathi vd., 2008).

Bu belirlemeler doğrultusunda çalışmada kullanılan kriterler ulusal ve uluslararası yayınlanmış yazınlardan faydalanarak belirlenmiştir (Çizelge 1). Pek çok çalışmada değerlendirme kriterleri çevresel, sosyal, ekonomik ve teknik faktörlerden ikisini ya da üçünü içerecek şekilde faktör grupları altında toplanmıştır (Su vd., 2007; Ramjeawon ve Beerachee, 2008; Tuzkaya vd., 2008; Ersoy ve Bulut, 2009; Wang vd., 2009; Aragonés-Beltrán vd., 2010; Şener vd., 2010; Tavares vd., 2011;

Effat ve Hegazy, 2012; Eskandari vd., 2012; Gorsevski vd., 2012; Nazari vd., 2012; Zelenović Vasiljević vd., 2012; Demesouka vd., 2013; Gbanie vd., 2013; Motlagh ve Sayadi, 2015; Torabi-Kaveh vd., 2016).

Bu çalışmada ise kriterler çevresel ve sosyo-ekonomik olmak üzere iki faktör grubu altında toplanmış, 8 ana grup ve 14 kriter depolama alanını değerlendirmek için belirlenmiştir. Çevresel faktörler hidroloji, hava, jeoloji, toprak ve alan kullanımı ana kriterlerinden oluşmakta iken, sosyo-ekonomik faktörler sosyal ve tekno-ekonomik ana kriterlerinden oluşmaktadır. Çevresel faktörler katı atık toplanma alanlarının çevreye vereceği zararların minimuma indirgemesini hedeflemekte iken, sosyo-ekonomik faktörler ise katı atık toplama alanlarının hem yapım hem de işletme aşamasındaki maliyetlerini minimum düzeyde olmasını sağlayacak kriterlerden oluşmaktadır. Çizelge 1 alan kullanım uygunluğunun belirlenmesinde kullanılacak kriterlerin hiyerarşik yapısını göstermektedir.

Çizelge 1. Alan uygunluk kriterlerinin hiyerarşik yapısı

FAKTÖRLER	ANA KRİTERLER	ALT KRİTERLER
ÇEVRESEL FAKTÖRLER	Hidroloji	Yüzey suları (göller, nehir, sulama kanalları vb.)
	Hava	Rüzgar yönü
	Jeoloji	Fay hattına yakınlık
		Litoloji
	Topoğrafya	Eğim
		Bakı
		Yükseklik
	Toprak	Toprak tekstürü
	Alan Kullanımı	Korunan alanlar (milli parklar, yaban hayatı koruma ve geliştirme sahaları, sulak alanlar vb.), orman, tarım, kültürel alanlar (Arkeolojik, tarihi, turistik alanlar vb.)
SOSYO-EKONOMİK FAKTÖRLER	Sosyal	Yerleşim alanlarına yakınlık
		Hava alanına yakınlık
		Görsel etki
	Tekno-ekonomik	Yoldan uzaklık
		Elektrik, gaz ve güç kaynaklarına yakınlık

2.2.2. Çalışmada kullanılan veriler

Depolama sahası seçim sürecini etkileyen her bir kriterin Coğrafi Bilgi Sistemi (CBS) ortamında haritalanabilmesi için bir veri seti oluşturulmuş. Bu veri setleri farklı veri tabanları ve kurumlardan sağlanmıştır. Toprak verileri, Tarım ve Köy İşleri Bakanlığı'ndaki Köy Hizmetleri Genel Müdürlüğü'nden sayısal olarak temin edilmiştir. Verilerdeki bilgiler arasında büyük toprak grupları, mevcut arazi kullanımları, arazi kullanım kabiliyeti ve arazi tipi yer almaktadır. Adana şehri için her bir toprak birimi için geçirgenlik ve toprak tekstürü bilgilerini içeren toprak hidrolojik özellikleri önceki çalışmalar ve bilimsel raporlardan elde edilmiştir. (Cilek, 2017; Cilek ve Berberoglu, 2019). Alan kullanımlarının sınıflandırılmasında CORINE arazi örtüsü sınıflarından faydalanılmış ve Tarım ve Orman Bakanlığı'ndan temin edilen veriler, yüksek çözünürlüklü uydu görüntüleri ve topografik haritalar aracılığıyla farklı alan kullanımları (yerleşim alanı, havaalanları, tarım alanları, su yüzeyleri, vb.) haritalanmıştır. Ayrıca eğim, bakı ve yükseklik haritaları 30 m çözünürlüklü ASTER uydu verisinden elde edilmiştir. Litoloji, fay hattı, akarsu ve yüzey suyu verileri 1/100.000 ölçekli jeolojik haritalardan elde edilmiştir. Yedi farklı litolojik grup farklı kaya türlerine göre sınıflandırılmıştır. Ek olarak, anayollar ve diğer tali yolları içeren yol ağı haritası OpenStreetMap, topografik haritalar ve yüksek çözünürlüklü uydu görüntülerinden elde edilen veriler doğrultusunda sayısallaştırılmıştır. Boru hatları, Petrol Boru Hattı Şirketi tarafından, elektrik hatları ise Türkiye Elektrik İletim Şirketi Bölge Ofisi tarafından dijital olarak sağlanmıştır.

2.2.3. Çok katmanlı analizler

Katı atık depolama arazileri için alan uygunluğunu belirlemek için kullanılan CBS ortamında Fuzzy fonksiyon standardizasyonu ile birleştirilmiş çok kriterli analizler metodolojinin ikinci aşamasıdır. . Karar verme sürecinde günümüzde kullanılan en yaygın yöntemlerden birisi olan çok kriterli analizlerin (MCA) temel amacı, olası çözümlerin karşılaştırılmasında bir belirleyici olarak, karar verme sürecinde çoklu kriterlerin entegrasyonunun sağlanmasıdır. Bu sonuca ulaşabilmek için MCA değerlendirme setlerine, alternatif setlerine ve fikirleri uygulayabilmek için doğru tekniklere ihtiyaç duyulmaktadır.

MCA yapılan uygulamalarda değerlendirme aşamalarını özetlemek gerekirse;

- Gerekli katmanların belirlenmesi,
- Uygun ve uygun olmayan alanları belirtecek şekilde sınıflandırma yapılması,
- Standardizasyon (Haritaların aynı birime getirilmesi)
- Kriterlere ait haritaların çakıştırılarak sonuç haritasının elde edilmesi

Katmanların belirlenmesi: Bu çalışmada, belediye katı atık bertaraf tesisi yer seçiminin uygunluğunun çevresel ve sosyo-ekonomik yönden değerlendirilmesi ve analiz edilmesi amaçlanmıştır. Bu bağlamda, çalışma alanı için çevresel ve sosyo-ekonomik faktörleri içeren geniş bir veri seti üretilmiştir. Elde edilen sonuçların daha kolay ve anlaşılır bir şekilde karar vericiler tarafından anlaşılabilmesi için farklı özellikleri içeren 14 değerlendirme kriteri önceki çalışmalar aracılığıyla belirlenmiştir.

Uygun ve uygun olmayan alanların belirlenmesi: Çok kriterli analizlerde önemli noktalardan biri de çalışma alanına ait faktörlerin ve kısıtlayıcıların (limitlerin) belirlenmesidir. Faktörler ve kısıtlayıcılar; spesifik alternatiflerin uygunluğunu azaltan veya arttıran kriterlerdir. Bu kriterler hedeflenen aktivitelere bağlı olarak belirlenmektedir. Kısıtlayıcılar, düşünülen alternatiflerin sınırlarını göstermektedir ve uygun olan ya da olmayan alanlar olarak kesin sonuçları belirtmektedir. Kısıtlayıcılar, Boolean haritası olarak ifade edilir ve uygun alanlar için 1, uygun olmayan alanlar için 0 değerini almaktadır.

Standardizasyon: Depolama alanının uygunluğunun saptanmasında, belirlenen her bir kriter farklı katmanlarda haritalanmıştır. Fakat bu aşamadaki önemli noktalardan birisi Fuzzy fonksiyonları temel alınarak standardizasyonun sağlanmasıdır (Saaty, 1990; Saaty, 2008; Forman ve Selly, 2002; De Feo ve De Gisi, 2014) . Kriterler belirlendikten sonra, farklı ölçü değerine sahip olan haritalar ortak bir birime getirilmiştir. Faktörler 0-1 arasında yeniden ölçeklendirilmiştir. 0 değeri, uygun olmayan, 1değeri ise en uygun alanları temsil etmektedir. Standardizasyon adı verilen bu işlemde, Fuzzy yaklaşımı kullanılmıştır. Bu yaklaşımda her bir Fuzzy seti fonksiyonu değerlendirilerek bu setlere ait her bir piksel için değerlendirilme yapılır. Sigmoidal, J-shaped ve doğrusal fonksiyonlar değer ölçeğindeki en yüksek ve en düşük değerlerden elde edilen kontrol noktaları ile biçimlendirilirler. İlk nokta fonksiyonun sıfırdan yükselmeye başladığı alanı temsil etmektedir. İkinci nokta fonksiyonun 1'e ulaştığı yerdir. Üçüncü nokta fonksiyonun yeniden 1 den aşağı doğru düşmeye başladığı alan ve 4. nokta ise fonksiyonun 0 değerine geri döndüğü alandır. The Sigmoidal ("s-shaped") biçim Fuzzy seti teorilerinde en çok kullanılan fonksiyondur ve kosinüs fonksiyonu kullanılarak üretilmiştir. Aşağıda Fuzzy fonksiyonun ihtiyaç duyduğu 4 adet kontrol noktasına ait değerler verilmiştir. Bunlar sigmoidal eğri üzerinde a, b, c, d olarak Şekil 3'te gösterilmiştir:

a = fonksiyonun '0' ın üzerine çıktığı nokta
b = fonksiyonun '1'e ulaştığı nokta
c = fonksiyonun '1' den azalmaya başladığı nokta
d = fonksiyonun '0'olduğu nokta

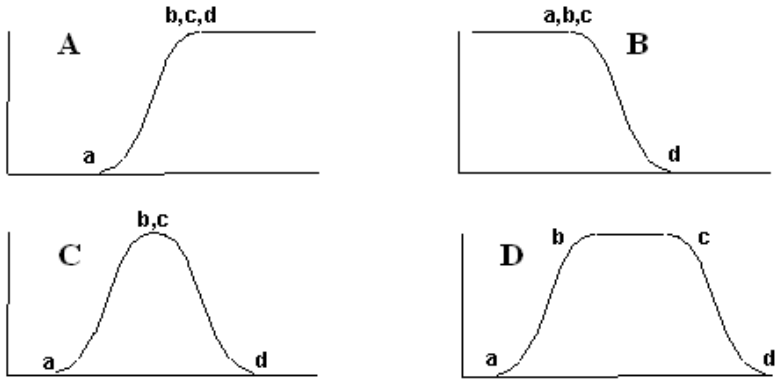

Şekil 3. Sigmoidal Fonksiyonlar (A) Monoton Olarak Artan, (B) Monoton Olarak Azalan, (C) ve (D) Simetrik (Unal vd. 2019)

Sigmoidal fonksiyonuna ait üyeler monoton olarak artan, monoton olarak azalan, simetrik (üst sol, üst sağ, alt sol ve alt sağ) şekilde olabilmektedir. Fonksiyonun monoton olarak arttığı durumlarda b, c, d kontrol noktaları için verilen değerler aynıdır. Aynı şekilde fonksiyonun monoton olarak azaldığı durumlarda ise a, b, c kontrol noktaları aynı değere sahiptir. Fuzzy uygulaması ile aynı zamanda, Boolean yaklaşımı dışında (0-1, uygun değil-uygun), yumuşatılan sınırlar da (uygun olabilir) oluşturulmaktadır.

Çakıştırma: Çok kriterli analizlerin son aşaması ise farklı kaynaklardan elde edilen farklı ölçeklerdeki verilerin standardize edilerek farklı veri formatındaki verilerin (point, line, polygon) çakıştırılmasıdır. Böylece karar verme sürecinde farklı kısıtlayıcıların dahil edildiği en uygun sonuç elde edilebilecektir (Carver, 1991). Çalışmanın bu aşamasında standardize edilen her bir kritere ait ayrı bir uygunluk haritası oluşturulmuş ve bu haritaların çakıştırılması sonucunda sonuç haritası elde edilmiştir. Katı atık tesisi depolama sahasının uygunluk sınıfı 5'li Likert ölçeği aracılığı ile belirlenmiştir (Çizelge 2).

Çizelge 2. Yer seçim uygunluğunun Likert ölçeğine göre sınıflandırılması

Puan Sınıfı	Uygunluk Sınıfı	Renk
% 0–20	Çok düşük	
%20,01-40	Düşük	
%40,01-60	Orta	
%60,01-80	Yüksek	
%80,01-100	Çok yüksek	

3. Bulgular

Katı atık depolama tesisinin yapım ve işletme aşamasında çevre ve halk sağlığına verebileceği zararların en düşük seviyede olmasına özen gösterilmelidir. Bu yüzden çalışmanın yönteminde de bahsedildiği gibi alan seçiminin uygunluğunu değerlendirmede kullanılacak olan kriterlerin belirlenmesi büyük önem taşımaktadır. Çalışmada diğer önemli bir adım ise belirlenen kriterlerinin seçilme sebepleri ve fuzzy yöntemi ile değerlendirme yapılabilmesi için gerekli olan sınır değerlerinin belirlenmesidir. Bu kapsam doğrultusunda son 10 yılı içeren 28 adet çalışma incelenmiş ve çevresel ve sosyo-ekonomik olmak üzere 2 faktör altında toplanan 14 kriter depolama alanının uygunluğunun değerlendirilmesi için seçilmiştir. Kriterlerin belirlenmesinde alanda kullanılabilirliği, veri erişilebilirliği ve farklı bölgelerde de çalışma yönteminin uygulanabilirliği dikkate alınmıştır. Aynı zamanda çalışmalarda en çok kullanılan kriterler

ve kriterlere ait değerler uzman görüşleri tarafından değerlendirilerek seçilmiştir. Bu doğrultuda kriterlerin değerlendirilmesinde dikkat edilen özellikler Çizelge 3'te, değerlendirme aralıkları ise Çizelge 4'te verilmiştir.

Çizelge 3. Alan uygunluk kriterlerinin değerlendirme özellikleri

	Değerlendirme Kriterlerinin Özellikleri
ÇEVRESEL FAKTÖRLER	**1. Yerüstü su kaynakları** Türkiye Su Kirliliği Kontrol Yönetmeliği (2004) ve literatür incelemelerine göre (Dörhöfer ve Siebert, 1998; Kontos vd., 2005; Akbari vd., 2008; Ramjeawon ve Beerachee, 2008; Wang vd., 2009; Moeinaddini vd., 2010; Nas vd., 2010; Şener vd., 2011; Gorsevski vd., 2012; Alavi vd., 2013) depolama alanı su kaynaklarını kirletebileceği için önemli su yüzeyleri (göl, nehir, kanallar, vb.) yakınında konumlandırılmamalıdır. Ayrıca yaban hayatının üremesi ve gelişmesi için önemli sulak alan kenarlarında, evsel ve tarımsal sulama için kullanılan su kaynakları (kuyu, nehir, baraj gölü, vb.) yakınları da çöp depolama alanı için uygun sayılmamaktadır. Aksi takdirde insan ve çevre üzerinde geri dönüşü olmayan etkilere sebep olabilmektedir (Effat ve Hegazy, 2012; Aydi vd., 2013). Bu nedenle depolama alanı olarak seçilen yerin herhangi bir su yüzeyine 500 m' den fazla yakın olmaması gerekmektedir.
	2. Rüzgar yönü Katı atık depolama alanının hakim rüzgar yönünde konumlandırılması ve yerleşime yakın olması tesisten kaynaklı kötü koku ve zararlı gazların yerleşim alanlarına taşınmasına sebep olmaktadır (Ramjeawon ve Beerachee, 2008; Ekmekçioğlu vd., 2010; Şener vd., 2010; Demesouka vd., 2013;). Koku genellikle havada çok düşük konsantrasyonlarda çözünen kimyasal maddelerden kaynaklanmaktadır ve atık alanların yakınlarında yer alan insanlar için çeşitli sağlık sorunlarına neden olabilir (Wu vd., 2018). Bu yüzden kokudan kaynaklı olumsuz etkileri önleyebilmek için bu araştırmada hakim rüzgar yönü dikkate alınmalıdır (Şener vd., 2011; Demesouka vd., 2013; Torabi-Kaveh vd., 2016). Türkiye Ulusal Meteoroloji Ajansı'ndan ölçülen veriler, güneybatı-kuzeydoğu rüzgârlarının çalışma alanında hakim rüzgar yönü olduğunu göstermektedir. Bu nedenle, rüzgârların ortak etkisi altında kalan bölgeler yerleşim yerlerine göre en düşük ağırlık değerlerine sahip olmuştur.
	3. Fay hatlarına yakınlık Fay hatları genellikle yüksek geçirgenlikte ve gözenekli yapıdadır. Bu durum fay hatları üzerinde veya yakınında yer alan depolama tesislerinden kaynaklı yer altı su kaynaklarının herhangi bir deprem sonrasında kirlenmesine neden olabilmektedir. Bu nedenle fay bölgesine yakın alanlarda deprem kaynaklı riskleri önlemek için dikkat edilmesi gereken önemli faktörlerden birisidir (Tuzkaya vd., 2008; De Feo ve De Gisi, 2010; Moeinaddini vd., 2010; Effat ve Hegazy, 2012; Gorsevski vd., 2012; Demesouka vd., 2013).
	4. Litoloji Jeoloji katı atık depolama alanlarına uygunluk kriterini planlamada önemli bir rol oynamaktadır. Bölgeye özgü jeolojik özelliklerin dağılımı farklı kayaç türlerine rocks (Ramjeawon ve Beerachee, 2008; Demesouka vd., 2013;). Seçilecek alanın kayaç tipine göre yüzey geçirgenliği kategorize edilerek belirlenmiş ve en uygun alanlar değerlendirilmiştir (Gorsevski vd., 2012; Demesouka vd., 2013). Çalışmalar incelendiğinde, alüvyon ve kireçtaşı alanlarının silt, kum ve çakıl oranlarından dolayı geçirgenliklerinin yüksek olması ve yeraltı su kaynaklarının kirlenmesine yol açabilecekleri düşüncesi ile uygun olmadığı sonucu elde edilmiştir. Diğer yandan tamamen düşük hidrolik iletkenliği olan kil katmanlarından oluşan karasal çökeltiler en uygun alanlar olarak değerlendirilmiştir (Şener vd., 2011; Aydi vd., 2013).

	Değerlendirme Kriterlerinin Özellikleri
ÇEVRESEL FAKTÖRLER	**5. Eğim** Arazi yüzeyinin eğimi depolama alanının uygunluğunun belirlenmesinde önemli faktörlerden birisidir. Yüksek eğime sahip alanlar inşaat, kazı ve bakım maliyetlerini arttırmakla birlikte erozyon, toprak kayması, infiltrasyonun azalması, toprak ve su içeriğinin kirlenme riski, kara ve yer altı akışının hızı gibi birçok önemli peyzaj süreçlerini etkilemektedir. Ayrıca yüksek eğimler katı atık tesisine ulaşım ve katı atıkların bertaraf edilmesinde maliyetin artmasına sebebiyet vermekte iken düz alanlar veya düşük eğime sahip alanlarda ise fazla suyun tahliye edilmesi yani drenaj problemleri ortaya çıkmaktadır. Bu yüzden çoğu çalışmada %10 eğimden düşük %30 eğimden yüksek alanlar uygunluk açısından değerlendirme dışı tutulmuştur (Gemitzi vd., 2007; Tuzkaya vd., 2008; Wang vd., 2009; Nas vd., 2010; Şener vd., 2010; Tavares vd., 2011; Gorsevski vd., 2012; Aydi vd., 2013; Demesouka vd., 2013).
	6. Bakı Bu aşamada bakının değerlendirilmesinde alanın hakim rüzgar yönü dikkate alınmıştır (Şener vd., 2010; Gbanie vd., 2013;). Depolama alanından kaynaklı koku etkisi ve hava kirliliği rüzgar ile taşınarak yerleşim alanlarını etkileyebilmektedir. Bu yüzden çalışma alanında 30x30 m çözünürlüğünde görüntü ve dijital yükseklik modeli aracılığı ile alanın bakı haritası elde edilmiş. Her bir pikselin hakim rüzgar yönü ve kentle olan ilişkisi kurularak yerleşime göre rüzgar yönünde bulunan bölgeler düşük uygunlukta, bulunmayan bölgeler yüksek uygunlukta olacak şekilde değerlendirilmiştir (Şener vd., 2010; Effat ve Hegazy, 2012; Gbanie vd., 2013).
	7. Yükseklik Yükseklik, atık bertaraf işleminde çok önemli bir faktördür. Yüksek alanlar, yüksek bertaraf maliyeti, alanın görünürlüğünün fazla olması, hakim rüzgardan korunmada yetersizliklerin olmasından dolayı uygunsuz sayılır. Diğer yandan da deniz seviyesine yakın konumlandırılan depolama alanları temiz su kaynaklarının kirlenmesine sebep olabilmekte ve drenaj problemleri ile karşılaşılabilmektedir. (Ekmekçioğlu vd., 2010; Aydi vd., 2013; Demesouka vd., 2013). Bu yüzden uygun alanlar ne yapım ve işletme aşamasında maliyetleri arttıracak kadar yüksekte olmalı, ne de drenaj ve çevre problemlerine yol açabilecek kadar alçakta olmalıdır (Kontos vd., 2005; Akbari vd., 2008; Ekmekçioğlu vd., 2010).
	8. Toprak tekstürü Toprak tekstürü, yeraltı suyunun kirlenme riskini belirlemede önemli bir rol oynamaktadır ve bu nedenle belirli bir alanda bir depolama sahasının uygunluğunun belirlenmesinde anahtar kriterlerdendir (Sumathi vd., 2008; Effat ve Hegazy, 2012;). Alanda bulunan toprak stabil olmalı ve ana toprağın geçirgenliği mümkün olduğunca az olmalıdır (Ramjeawon ve Beerachee, 2008). Bölgedeki toprak geçirgenlik özellikler göz önünde bulundurulduğunda bu kriter 3 grupta değerlendirilmiştir. Yüksek geçirgenliğe sahip kumlu ve kum içeriği yüksek toprakların uygunluğu en düşük düzeyde, orta düzeyde ve nispeten daha az geçirgen olan kumlu-killi topraklar orta düzey, ve neredeyse çok az geçirgenliğe sahip killi ve kil içeriği yüksek toprak türleri ise en yüksek düzeyde uygunluğa sahiptir (Şener vd., 2011; Gorsevski vd., 2012; Aydi vd., 2013; Demesouka vd., 2013). Killi topraklar geçirimsizlik ve gelen suyu filtreleme özelliklerinin yüksek olmasından dolayı en yüksek düzeyde uygun bulunmaktadır.
	9. Arazi örtüsü ve alan kullanımları Katı atık depolama alanının bulunduğu bölgedeki arazi örtüsü ve alan kullanımlarının belirlenmesi özellikle çevresel ve sosyal açıdan etkilenmelerin en düşük düzeyde olmasını sağlamak açısından önemlidir (Tavares vd., 2011). Bu çalışmada, CORINE arazi örtüsü sınıfları dikkate alınarak önceki çalışmalardan elde edilen depolama alanının uygun konumlanabileceği alanlar belirlenmiştir. Sonuç olarak tarıma elverişli alanlar özellikle 1. ve 2. sınıf tarım toprakları, kentsel alanlar, sulak alanlar, korunan alanlar, tarihi ve kültürel alanlar çöp depolama alanlarına uygunluğu değerlendirilirken önceliğe sahip değildirler (Wang vd., 2009; Aragonés-Beltrán vd., 2010; De Feo ve De Gisi, 2010; Ekmekçioğlu vd., 2010; Moeinaddini vd., 2010; Şener vd., 2011; Tavares vd., 2011; Effat ve Hegazy, 2012; Gorsevski vd., 2012; Alavi vd., 2013; Aydi vd., 2013). Fakat maden sahaları, şantiyeler, moloz yığma alanları, bitki örtüsünün seyrek ya da hiç olmadı bölgeler depolama alanları için öncelikli alanlar olarak karşımıza çıkmaktadır (Wang vd., 2009; Moeinaddini vd., 2010; Şener vd., 2011; Gorsevski vd., 2012; Alavi vd., 2013; Demesouka vd., 2013).

Çizelge 3. ün devamı

	Değerlendirme Kriterlerinin Özellikleri
SOSYO-EKONOMİK FAKTÖRLER	**10. Kentsel yerleşim ve endüstriyel alanlardan uzaklık** Çöp alanları koku ve gürültü yayılımı, görsel peyzaj kalitesinin azalması, mülk değerinin azalmasına, tatlı su akiferlerinin kirlenmesinden dolayı sağlık problemlerinin oluşması gibi olumsuz sonuçlara yol açabileceği için kentsel yerleşim alanları ve endüstriyel alanlardan mümkün olduğunca uzakta konumlandırılmalıdır (Wang vd., 2009; Aragonés-Beltrán vd., 2010; Moeinaddini vd., 2010; Nas vd., 2010; Tavares vd., 2011; Effat ve Hegazy, 2012; Gorsevski vd., 2012; Aydi vd., 2013).
	11. Havaalanından uzaklık Çöp depolama alanlarında kuşların beslenmesinden dolayı yüksek sayıda kuşun yer alması ve depolama alanından salınan gaz, toz ve partiküllerin havada bulunmasından dolayı uçakların iniş ve kalkışlarında güvenlik problemi ortaya çıkmaktadır (Wang vd., 2009; Moeinaddini vd., 2010; Demesouka vd., 2013;). Bu yüzden havaalanlarına güvenli bir mesafede konumlandırılması gerekliliği ortaya çıkmaktadır. Önceki çalışmalar temel alındığında havaalanı çevresindeki 3 km yarıçapa sahip alanlarda depolama alanının bulunmasının uygun olmadığı sonucu elde (Kontos vd., 2005; Effat ve Hegazy, 2012; Demesouka vd., 2013). Bu çalışmada da belirlenen mesafe içerisinde kalan alanlar uygun olmayan alanlar olarak belirlenmiştir.
	12. Peyzaj ve görsel etki Depolama sahalarının görüş alanı içerisinde görünmesi estetik açıdan rahatsız eden ve peyzajın görsel kalitesini bozan unsurlardan birisidir (Tavares vd., 2011). Katı atık depolama sahasının karayollarından, demiryollarından ve yerleşim yerlerinden görünmesi peyzajı olumsuz yönde etkileyecektir. Bu yüzden her bir pikselin yoldan görünürlüğü analiz edilmiştir (Moeinaddini vd., 2010).
	13. Yoldan uzaklık Depolama sahası tüm hava şartlarında alternatif yollarla ulaşabilecek bir yerde bulunmalıdır (Çevre ve Orman Bakanlığı, 1991) (Sener vd., 2006; Şener vd., 2010, Şener vd., 2011). Fakat depolama alanları yatırım ve işlerme aşamasındaki maaliyeti çok fazla arttırmaması için mevcut yol ağından çok uzakta olmamalıdır (Ramjeawon ve Beerachee, 2008; Aragonés-Beltrán vd., 2010; De Feo ve De Gisi, 2010; Nas vd., 2010; Gorsevski vd., 2012; Alavi vd., 2013; Aydi vd., 2013).
	14. Elektrik ve boru hatlarına uzaklık Ekonomik düşünce, depolama alanlarının değerlendirilmesinde her zaman önemli rol oynamaktadır. Bu nedenle, enerji hatları ve boru hatları depolama alanına ne kadar yakınsa, yatırım maliyetlerini düşürmeye yardımcı olduğu için o kadar iyidir (Aragonés-Beltrán vd., 2010; Tavares vd., 2011; Effat ve Hegazy, 2012; Gbanie vd., 2013). Öte yandan, elektrik hatları ve boru hatları atık depolama alanından güvenli bir mesafede olmalıdır, çünkü depolama sahası bunlara zarar (Moeinaddini vd., 2010; Demesouka vd., 2013).

Özet olarak, çevresel risklerin önlenmesi ve halk sağlığına kirlilik etkisinin azaltılması için bir depolama sahası kurulmalı ve tasarlanmalıdır. Depolama sahaları için sınırlı alanlar arasında dik yamaçlar, kentsel yerleşimler ve sanayi bölgesi, havaalanları, yüzey su kütleleri, faylar, baskın rüzgar yönü, arazi kullanımı ve son olarak litoloji bulunmaktadır. Depolama sahası bu kriterlere göre yerleştirilmelidir. Öte yandan, atık depolama sahası, karayolu gelişimini korumak, mevcut yollara ulaşım maliyetini azaltmak ve atık üretim merkezi yatırım maliyetlerini azaltmak için elektrik ve boru hatlarına mümkün olduğunca yakın yerleştirilmelidir. Bu çalışma, kısmen ilgili Katı Atık Kontrol Yönetmeliği'ne çoğunlukla ise çevresel ve sosyo-ekonomik faktörleri hesaba katan uluslararası uygulamalara dayandırılmıştır. Böylece çalışma metodolojisi ulusal ve uluslararası çalışmalardan elde edilen değerler doğrultusunda farklı çalışma alanlarında da uygulanabilir hale gelmiştir.

CBS veri tabanında hazırlanan veriler, aynı ölçeğe getirilmesi için Fuzzy yöntemi kullanılmıştır. Yöntem ile veriler yapılan önceki çalışmaların incelenmesi, yönetmelikler ve uzman görüşleri doğrultusunda 0 ile 1 arasında standartlaştırılmıştır. Ölçütlere uygulanan Fuzzy fonksiyon ve kullanılan değerler Çizelge 4'te ve Fuzzy uygulaması sonucunda aynı ölçü birimine getirilmiş haritalar ise Şekil 4'te verilmiştir.

Çizelge 4. Kriterler değerlendirilmesinde kullanılan değer aralıkları ve Fuzzy fonksiyon tipleri (Unal vd. 2019)

Alan Uygunluk Kriterleri	Kontrol noktaları				Fuzzy fonksiyonları
	a	b	c	d	
Yüzey suları	500 m	2000 m	-	-	Increasing - S shaped
Hakim rüzgar yönü	45°	135°	135°	225°	Symmetric sigmodial
	225°	315°	315°	360°	
Fay hattına yakınlık	500 m	1000 m			Increasing - S shaped
Litoloji	Kumullar, Neritik kalkerler	Kırıntılı ve kıtasal kırıntılı kayaçlar, Karbonat kayalar			Increasing - S shaped
Eğim	% 10	% 40			Decreasing - S shaped
Bakı	45°	135°	135°	225°	Symmetric sigmodial
	225°	315°	315°	360°	
Yükseklik	100 m	250 m			Decreasing - S shaped
Toprak tekstürü	Kumlu	Killi			Increasing - S shaped
Alan kullanımı ve arazi örtüsü	CORINE kodu: 120,211,400,500	CORINE kodu: 133			
Yerleşim ve endüstriyel alanlardan uzaklık	1000 m	7500 m	-	14000 m	Symmetric sigmodial
Havaalanından uzaklık	3000 m	8000 m			Increasing - S shaped
Peyzaj ve görsel etki	0 m			10000 m	Decreasing - S shaped
Yoldan uzaklık	500 m			2000 m	Decreasing - S shaped
Elektrik ve boru hatlarına uzaklık	100 m			500 m	Increasing - S shaped
Çizelgedeki sayısal verilerin oluşturulmasında ölçütlerin değerlendirme özelliklerinin açıklandığı Çizelge 3'teki kaynaklardan faydalanmıştır.					

On dört adet standart hale getirilmiş kriterler 0 ile 1 arasında siyah- beyaz renk ölçeğinde her bir kriter için ayrı ayrı haritalanmıştır (Şekil 4). Haritalarda siyah alanlar kriterlerin uygun olduğu bölgeleri gösterir iken, beyaz alanlar ise belirlenen değerler dışında kalan uygun olmayan bölgeleri göstermektedir. Ayrıca çalışma kapsamında değerlendirilen kriterlerin yer seçim uygunluğunu değerlendirmede eşit düzeyde önemli olduğu düşüncesi ile kriter ağırlıklandırması yapılmamıştır. Böylece sonuç haritası üzerinde her bir kriter aynı önem derecesine sahip olacaktır.

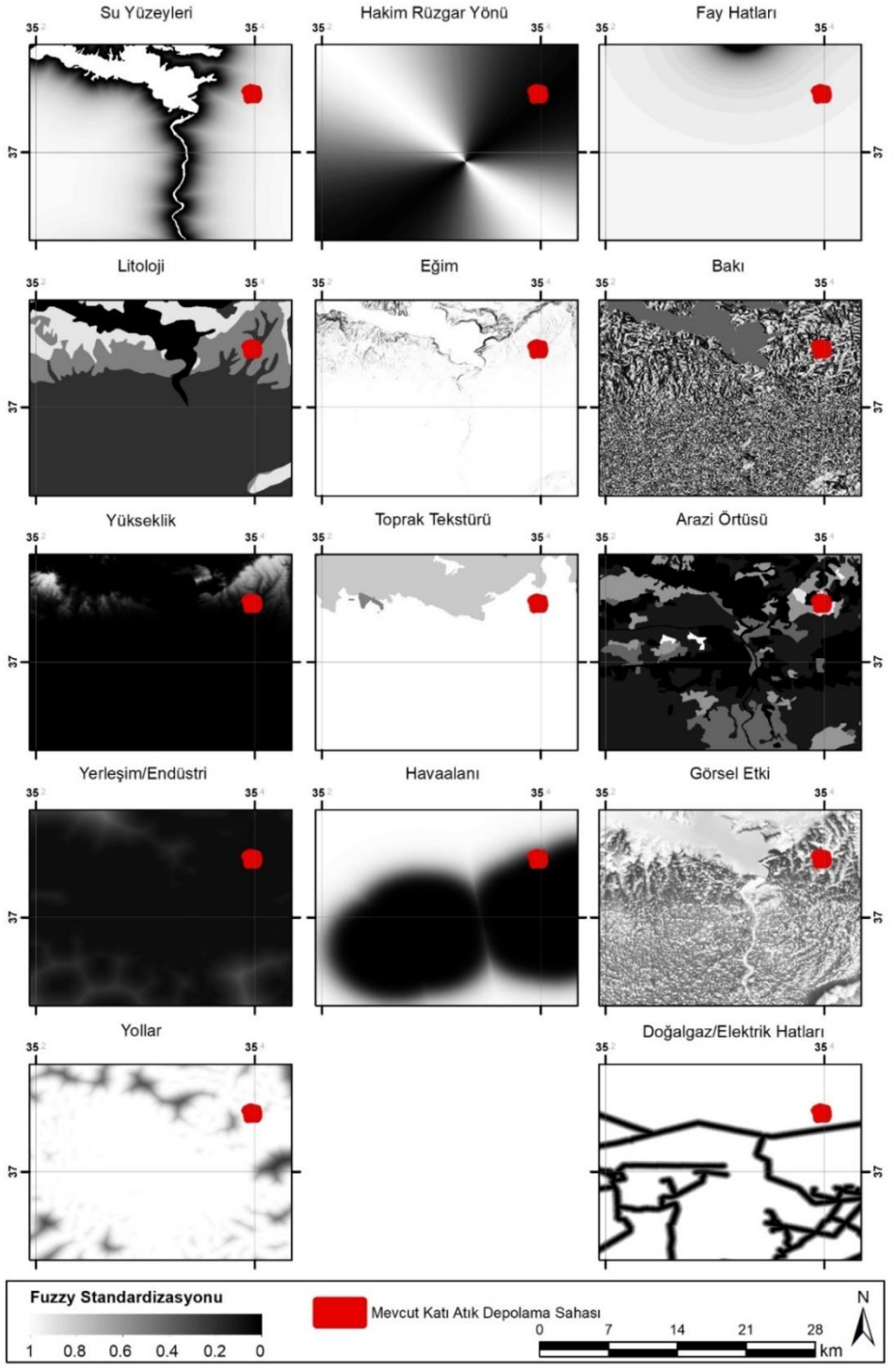

Şekil 4. Standardize edilmiş her bir kriter için uygun alanların haritalanması

Şekil 4 incelendiğinde mevcut katı atık tesisi yerleşim alanına ve İncirlik Askeri Hava Alanına çok yakın konumlanmasından dolayı çok düşük uygunluk değeri almıştır. Ayrıca alanın hakim rüzgar yönünde olması, tesisten kaynaklı zararlı gazların ve kokunun kente taşınmasına sebep olacağı için, bu yönden de uygun bulunamamıştır. Çalışma alanının mevcut yol ağına yakın olması

çöplerin transfer işlemi açısından olumlu değerlendirilirken, kötü görüntülere sebep vermesinden dolayı peyzaj ve görsel kaliteyi olumsuz yönde etkilemektedir. Doğalgaz ve elektrik hatlarına uygun mesafede olması ise ekonomik yönden olumludur. Ekolojik açıdan kriterler değerlendirildiğinde, çalışma alanı filtreleme özelliği yüksek olan killi toprak tekstürüne sahip, aynı zamanda mevcut su yüzeylerine zarar vermeyecek mesafededir. Arazi örtüsünün tarım, mera ve çayır alanı olarak sınıflanması, geçirgenliği ve gözenekliliği yüksek olan karbonatlı kayaç ve traverten gibi litolojik özelliklere sahip olmasından dolayı ise orta derecede uygun bulunmuştur. Alanın eğimi %0-10 arasında değişmekte ve alanı sınırları içerisinde bakı çeşitlilik göstermektedir. Yükseklik açısından ise belirlenen değerler dışında kalmasından dolayı hiç uygun bulunmamıştır. Bütün bu belirlemeler doğrultusunda katmanların çakıştırılması ile elde edilen sonuç haritasında çalışma alanının uygunluğu %56 ile orta derece uygun bulunmuştur (Şekil 5).

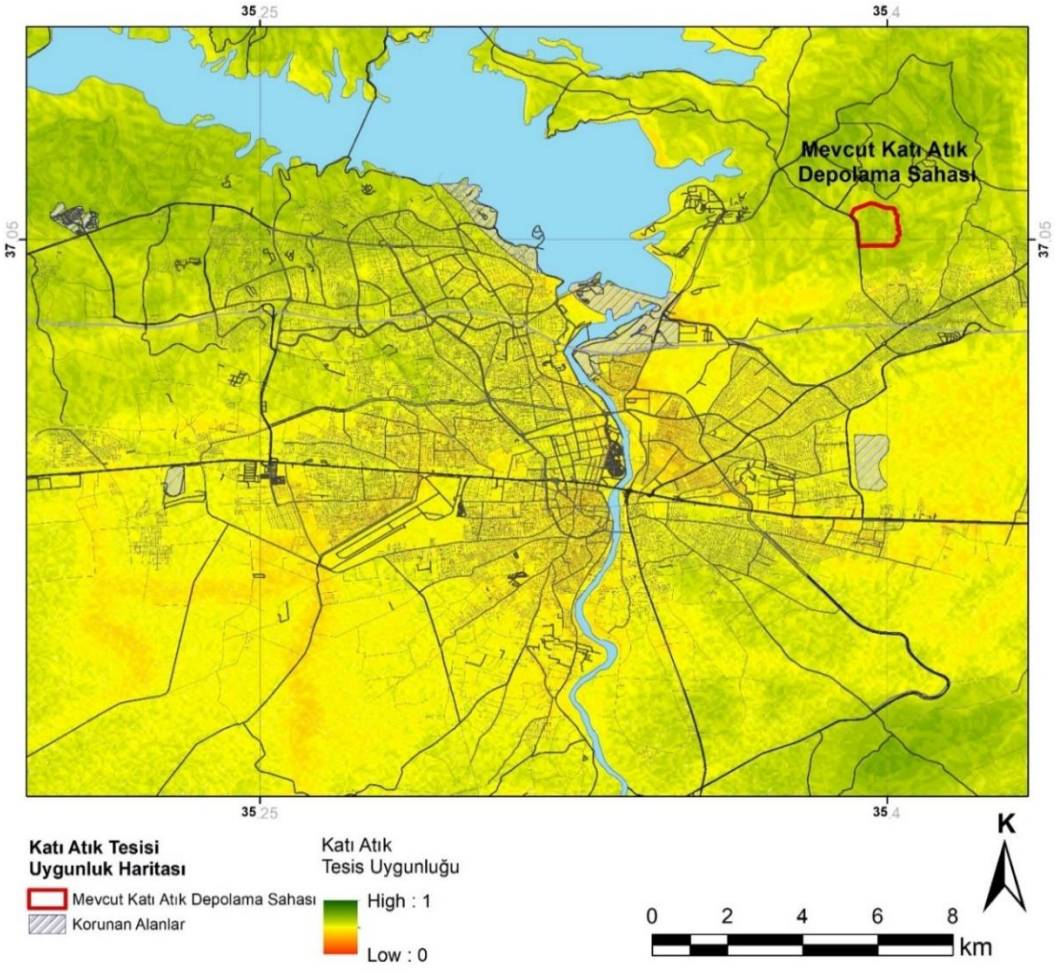

Şekil 5. Katı atık depolama sahası uygunluk haritası

4. Tartışma ve Sonuçlar

Dünyada katı atık depolama alanlarının yapım ve işletme aşamaları pek çok yerel yönetim ve karar vericiler tarafından en önemli konulardan birisi olmuştur. Hızlı nüfus artışı sonucunda yapılaşmaya öncelik tanınması ile birlikte Adana'da yer alan mevcut katı atık entegre tesisi yerleşim alanı içerisinde kalmış, artan katı atık üretimini karşılamakta kapasite olarak yetersiz kalarak gerek çevre gerekse sosyal yaşam üzerinde olumsuz etkilerini hissettirmiştir. Bütün

bu belirlemeler doğrultusunda Adana'da ikinci bir katı atık entegre tesisi inşaatını söz konusu olmuştur. Bu sebepten birinci katı atık sahasının yer seçim uygunluğu incelenmiş ve yeni planlanan alanlarda benzer sorunlardan kaçınmak için pek çok farklı unsurun göz önünde bulundurulduğu çalışma metodolojisi oluşturulmuştur.

Katı atık yönetimi çevresel, teknik, kentsel yaşam kalitesi, halk sağlığı ve sosyal yaşam gibi pek çok farklı faktörlerin anlaşılmasını gerektiren karmaşık bir karar verme sürecidir. Önceki çalışmalar incelendiğinde bu karmaşık karar verme süreci üzerine çeşitli çalışmalar yapılmış ve alan uygunluklarının değerlendirilmesinde çok katmanlı analiz yöntemleri kullanılmıştır. Bu çalışmada da çok katmanlı analizler ve Fuzzy yöntemi alan uygunluğunun değerlendirmesi ve sınıflandırmasında yardımcı olmuştur. Fuzzy yöntemi ile farklı faktörler arasındaki belirsizlikler tanımlanmış ve karar vermedeki karmaşık süreç kolaylaştırılmıştır. Çalışmada politik ve finansal/ekonomik kısıtlamalar (tesisin alan büyüklüğü, yatırım/işletme aşamasındaki maliyetler vb.) plan ve politikalara göre değişebilir ve geliştirilebilir olmalarından dolayı değerlendirme dışında tutulmuşken, değiştirilmesi ve geri dönüşümü zor olan, insan ve yaban hayatı açısından sürdürülebilirliğinin sağlanması gereken önemli çevresel faktörler ve sosyo-ekonomik faktörler altında toplanmış 14 kriter değerlendirmeye dahil edilmiştir. Konu ile ilgili literatür, yasa ve yönetmeliklerin incelenmesi ve uzman görüşlerinin alınması sonucunda bu kriterlere ait değerlendirme aralıkları elde edilmiştir. Bu değerler Fuzzy yönteminde 0 ve 1 olan fonksiyon kontrol noktalarının belirlenmesi ve kriterlerin standardizasyon sürecinde kritik öneme sahip olmuştur. Çünkü farklı değer aralıklarına sahip farklı ölçeklerdeki her değişkenin fiziksel anlamını göz önünde bulundurmak sonuç haritasının doğru yorumlanabilmesi açısından önemlidir. Çalışma da tüm kriterlerin standardizasyonu ile birlikte her bir kriter için ayrı ayrı uygunluk haritaları CBS aracılığı ile oluşturulmuş ve haritaların çakıştırılması sonucunda alan uygunluk haritası elde edilmiştir.

Değerlendirme sonucunda mevcut katı atık depolama alanı orta düzeyde uygun çıkmıştır. Bu durum yeni yapılacak ya da yapılması planlanan katı atık tesislerinde benzer problemlerle karşılaşılmaması için uygun yer seçiminde dikkat edilmesi gereken unsurları ortaya koymaktadır. Kriterlerin değerlendirilmesinde son 10 yılı içeren ulusal ve uluslararası pek çok çalışmadan faydalanılmıştır. Bu yönü ile çalışmanın farklı bölgelerde yer alan benzer çalışmaların değerlendirilmesinde karar vericilere yol gösterici olması beklenmektedir. Ayrıca yeni yapılması planlanan tesislerin yer seçimlerine karar vermede ilgili farklı otoritelerin bir araya gelmesini sağlamaya yardımcı olmakta ve alanın neden seçildiği ile ilgili somut verilere dayalı bir yaklaşım gerçekleştirmeyi sağlaması amaçlanmıştır.

Kaynaklar

Akbari, V., Rajabi, M. A., Chavoshi, S. H., Shams, R. (2008). Landfill Site Selection by Combining GIS and Fuzzy Multi Criteria Decision Analysis, Case Study: Bandar Abbas, Iran. *World Applied Sciences Journal*.

Alavi, N., Goudarzi, G., Babaei, A. A., Jaafarzadeh, N., Hosseinzadeh, M. (2013). Municipal solid waste landfill site selection with geographic information systems and analytical hierarchy process: A case study in Mahshahr County, Iran. *Waste Management and Research*, *31*(1), 98–105. doi:10.1177/0734242X12456092

Alumur, S., Kara, B.Y. (2007). A new model for the hazardous waste location-routing problem. Computers and Operations Research, 34, 1406–1423.

Aragonés-Beltrán, P., Pastor-Ferrando, J. P., García-García, F., Pascual-Agulló, A. (2010). An Analytic Network Process approach for siting a municipal solid waste plant in the Metropolitan Area of Valencia (Spain). *Journal of Environmental Management*, *91*(5), 1071–1086. doi:10.1016/j.jenvman.2009.12.007

Aydi, A., Zairi, M., Dhia, H. Ben. (2013). Minimization of environmental risk of landfill site using fuzzy logic, analytical hierarchy process, and weighted linear combination methodology in a geographic information system environment. *Environmental Earth Sciences*, *68*(5),

1375–1389. doi:10.1007/s12665-012-1836-3

Carver, S. J. (1991). Integrating multi-criteria evaluation with geographical information systems. *International Journal of Geographical Information Systems*. doi:10.1080/02693799108927858

Cilek, A. (2017). Soil organic carbon losses by water erosion in a Mediterranean watershed. *Soil Research*. doi:10.1071/SR16053

Cilek, A., Berberoglu, S. (2019). Biotope conservation in a Mediterranean agricultural land by incorporating crop modelling. *Ecological Modelling*. doi:10.1016/j.ecolmodel.2018.11.008

Chang N Bin, Parvathinathan G and Breeden JB (2008) Combining GIS with fuzzy multicriteria decision-making for landfill siting in a fast-growing urban region. Journal of Environmental Management. DOI: 10.1016/j.jenvman.2007.01.011.

Cheng, S., Chan, C.W., Huang, G.H. (2002). Using multiple criteria decision analysis for supporting decisions of solid waste management. Journal of Environmental Science and Health. Part A, 37 (6), 975–990.

Cheng, S., Chan, C.W., Huang, G.H. (2003). An integrated multi-criteria decision analysis and inexact mixed integer linear programming approach for solid waste management. Engineering Applications of Artificial Intelligence, 16, 543–554

Colebrook, M., Sicilia, J. (2007). Undesirable facility location problems on multicriteria networks. Computers and Operations Research, 34 (5), 1491–1514.

De Feo, G., De Gisi, S. (2010). Using an innovative criteria weighting tool for stakeholders involvement to rank MSW facility sites with the AHP. *Waste Management*, *30*(11), 2370–2382. doi:10.1016/j.wasman.2010.04.010

Demesouka, O.E., Vavatsikos, A. P., Anagnostopoulos, K. P. (2013). Suitability analysis for siting MSW landfills and its multicriteria spatial decision support system: Method, implementation and case study. *Waste Management*, *33*(5), 1190–1206. doi:10.1016/j.wasman.2013.01.030

Demesouka, Olympia E., Anagnostopoulos, K. P., Siskos, E. (2019). Spatial multicriteria decision support for robust land-use suitability: The case of landfill site selection in Northeastern Greece. *European Journal of Operational Research*, *272*(2), 574–586. doi:10.1016/j.ejor.2018.07.005

Dörhöfer, G., Siebert, H. (1998). The search for landfill sites - Requirements and implementation in lower Saxony, Germany. *Environmental Geology*. doi:10.1007/s002540050292

Effat, H. A., Hegazy, M. N. (2012). Mapping potential landfill sites for North Sinai cities using spatial multicriteria evaluation. *Egyptian Journal of Remote Sensing and Space Science*, *15*(2), 125–133. doi:10.1016/j.ejrs.2012.09.002

Ekmekçioğlu, M., Kaya, T., Kahraman, C. (2010). Fuzzy multicriteria disposal method and site selection for municipal solid waste. *Waste Management*, *30*(8–9), 1729–1736. doi:10.1016/j.wasman.2010.02.031

Emek, E., Kara, B.Y. (2007). Hazardous waste management problem: the case for incineration. Computers and Operations Research, 34, 1424–1441.

Erkut, E., Newman, S. (1989). Analytical models for locating undesirable facilities. European Journal of Operational Research, 40, 275–291.

Ersoy, H., Bulut, F. (2009). Spatial and multi-criteria decision analysis-based methodology for landfill site selection in growing urban regions. *Waste Management and Research*, *27*(5), 489–500. doi:10.1177/0734242X08098430

Eskandari, M., Homaee, M., Mahmodi, S. (2012). An integrated multi criteria approach for landfill siting in a conflicting environmental, economical and socio-cultural area. *Waste Management*, *32*(8), 1528–1538. doi:10.1016/j.wasman.2012.03.014

Feo, G. De, De Gisi, S. (2014). Using MCDA and GIS for hazardous waste landfill siting

considering land scarcity for waste disposal. *Waste Management*, *34*(11), 2225–2238. doi:10.1016/j.wasman.2014.05.028

Gbanie, S. P., Tengbe, P. B., Momoh, J. S., Medo, J., Kabba, V. T. S. (2013). Modelling landfill location using Geographic Information Systems (GIS) and Multi-Criteria Decision Analysis (MCDA): Case study Bo, Southern Sierra Leone. *Applied Geography*, *36*, 3–12. doi:10.1016/j.apgeog.2012.06.013

Gemitzi, A., Tsihrintzis, V. A., Voudrias, E., Petalas, C., Stravodimos, G. (2007). Combining geographic information system, multicriteria evaluation techniques and fuzzy logic in siting MSW landfills. *Environmental Geology*, *51*(5), 797–811. doi:10.1007/s00254-006-0359-1

Gorsevski, P. V., Donevska, K. R., Mitrovski, C. D., Frizado, J. P. (2012). Integrating multi-criteria evaluation techniques with geographic information systems for landfill site selection: A case study using ordered weighted average. *Waste Management*, *32*(2), 287–296. doi:10.1016/j.wasman.2011.09.023

H-Forman, E., Selly, M. A. (2002). Introduction: Management Decision-Making Today. *Decision by Objectives: How to Convince Others that You are Right*. doi:10.1142/9789812810694

Khan S and Faisal MN (2008) An analytic network process model for municipal solid waste disposal options. Waste Management 28(9): 1500–1508. DOI: 10.1016/j.wasman.2007.06.015.

Khan, M. M. U. H., Vaezi, M., Kumar, A. (2018). Optimal siting of solid waste-to-value-added facilities through a GIS-based assessment. *Science of the Total Environment*, *610–611*, 1065–1075. doi:10.1016/j.scitotenv.2017.08.169

Kontos, T. D., Komilis, D. P., Halvadakis, C. P. (2005). Siting MSW landfills with a spatial multiple criteria analysis methodology. *Waste Management*. doi:10.1016/j.wasman.2005.04.002

Malczewski, J. (2004). GIS-based land-use suitability analysis: A critical overview. *Progress in Planning*. doi:10.1016/j.progress.2003.09.002

McHarg, I.L. (1992) Design with Nature. *New York: John Wiley and Sons Inc*.

Moeinaddini, M., Khorasani, N., Danehkar, A., Darvishsefat, A. A., Zienalyan, M. (2010). Siting MSW landfill using weighted linear combination and analytical hierarchy process (AHP) methodology in GIS environment (case study: Karaj). *Waste Management*, *30*(5), 912–920. doi:10.1016/j.wasman.2010.01.015

Motlagh, Z. K., Sayadi, M. H. (2015). Siting MSW landfills using MCE methodology in GIS environment (Case study: Birjand plain, Iran). *Waste Management*, *46*, 322–337. doi:10.1016/j.wasman.2015.08.013

Nas, B., Cay, T., Iscan, F., Berktay, A. (2010). Selection of MSW landfill site for Konya, Turkey using GIS and multi-criteria evaluation. *Environmental Monitoring and Assessment*, *160*(1–4), 491–500. doi:10.1007/s10661-008-0713-8

Nazari, A., Salarirad, M. M., Bazzazi, A. A. (2012). Landfill site selection by decision-making tools based on fuzzy multi-attribute decision-making method. *Environmental Earth Sciences*, *65*(6), 1631–1642. doi:10.1007/s12665-011-1137-2

Önüt, S., Soner, S. (2008). Transshipment site selection using the AHP and TOPSIS approaches under fuzzy environment. *Waste Management*, *28*(9), 1552–1559. doi:10.1016/j.wasman.2007.05.019

Queiruga, D., Walther, G., Gonzalez-Benito, J., Spengler, T. (2008). Evaluation of sites for the location of WEEE recycling plants in Spain. Waste Management, 28, 181–190.

Ramjeawon, T., Beerachee, B. (2008). Site selection of sanitary landfills on the small island of Mauritius using the analytical hierarchy process multi-criteria method. *Waste Management and Research*, *26*(5), 439–447. doi:10.1177/0734242X07080758

Saaty, T. L. (1990). How to make a decision: The analytic hierarchy process. *European Journal of Operational Research*. doi:10.1016/0377-2217(90)90057-I

Saaty, T. L. (2008). Decision making with the analytic hierarchy process. *International Journal of Services Sciences*. doi:10.1504/ijssci.2008.017590

Sener, B., Süzen, M. L., Doyuran, V. (2006). Landfill site selection by using geographic information systems. *Environmental Geology*, *49*(3), 376–388. doi:10.1007/s00254-005-0075-2

Şener, Ş., Sener, E., Karagüzel, R. (2011). Solid waste disposal site selection with GIS and AHP methodology: A case study in Senirkent-Uluborlu (Isparta) Basin, Turkey. *Environmental Monitoring and Assessment*, *173*(1–4), 533–554. doi:10.1007/s10661-010-1403-x

Şener, Ş., Şener, E., Nas, B., Karagüzel, R. (2010). Combining AHP with GIS for landfill site selection: A case study in the Lake Beyşehir catchment area (Konya, Turkey). *Waste Management*, *30*(11), 2037–2046. doi:10.1016/j.wasman.2010.05.024

Soltani, A., Hewage, K., Reza, B., Sadiq, R. (2015). Multiple stakeholders in multi-criteria decision-making in the context of municipal solid waste management: A review. *Waste Management*, *35*, 318–328. doi:10.1016/j.wasman.2014.09.010

Su, J. P., Chiueh, P. Te, Hung, M. L., Ma, H. W. (2007). Analyzing policy impact potential for municipal solid waste management decision-making: A case study of Taiwan. *Resources, Conservation and Recycling*, *51*(2), 418–434. doi:10.1016/j.resconrec.2006.10.007

Sumathi, V. R., Natesan, U., Sarkar, C. (2008). GIS-based approach for optimized siting of municipal solid waste landfill. *Waste Management*, *28*(11), 2146–2160. doi:10.1016/j.wasman.2007.09.032

Tavares, G., Zsigraiová, Z., Semiao, V. (2011). Multi-criteria GIS-based siting of an incineration plant for municipal solid waste. *Waste Management*, *31*(9–10), 1960–1972. doi:10.1016/j.wasman.2011.04.013

Torabi-Kaveh, M., Babazadeh, R., Mohammadi, S. D., Zaresefat, M. (2016). Landfill site selection using combination of GIS and fuzzy AHP, a case study: Iranshahr, Iran. *Waste Management and Research*, *34*(5), 438–448. doi:10.1177/0734242X16633777

Tuzkaya, G., Önüt, S., Tuzkaya, U. R., Gülsün, B. (2008). An analytic network process approach for locating undesirable facilities: An example from Istanbul, Turkey. *Journal of Environmental Management*, *88*(4), 970–983. doi:10.1016/j.jenvman.2007.05.004

Unal, M., Cilek, A., Güner, E.D (2019). Implementation of Fuzzy, Simos and SWOT Analysis for Municipal Solid Waste

Landfill Site Selection: Adana City Case Study. Waste Management & Research, in Press.

Wang, G., Qin, L., Li, G., Chen, L. (2009). Landfill site selection using spatial information technologies and AHP: A case study in Beijing, China. *Journal of Environmental Management*, *90*(8), 2414–2421. doi:10.1016/j.jenvman.2008.12.008

Wu, J., Ma, C., Zhang, D. Z., Xu, Y. (2018). Municipal solid waste management and greenhouse gas emission control through an inexact optimization model under interval and random uncertainties. *Engineering Optimization*. doi:10.1080/0305215X.2017.1419347

Vuk, D., Kozelj, B., Mladineo, N. (1991). Application of multicriterional analysis on the selection of the location for disposal of communal waste. European Journal of Operational Research, 55 (2), 211–217.

Yildirim, V. (2012). Application of raster-based GIS techniques in the siting of landfills in Trabzon Province, Turkey: A case study. *Waste Management and Research*, *30*(9), 949–960. doi:10.1177/0734242X12445656

Zelenović Vasiljević, T., Srdjević, Z., Bajčetić, R., Vojinović Miloradov, M. (2012). GIS and the analytic hierarchy process for regional landfill site selection in transitional countries: A case study from Serbia. *Environmental Management*, *49*(2), 445–458. doi:10.1007/s00267-011-9792-3

Bilge International Journal of Science and Technology Research

Web : http://dergipark.gov.tr/bilgesci - **E-mail:** kutbilgescience@gmail.com

Received: 11.12.2019
Accepted: 31.12.2019
DOI: 10.30516/bilgesci.652473

ISSN: 2651-401X
e-ISSN: 2651-4028
3(Special Issue), 106-111, 2019

Effects of Using JP8-Diesel Fuel Mixtures in a Pump Injector Engine on Engine Performance

Hasan AYDOGAN[1]*, Emin Cagatay ALTINOK[2]

Abstract: JP-8 fuel used in the aviation industry, especially in military fields, is used as a common military fuel between NATO countries. As the basic substance of JP-8 fuel, kerosene flares at high temperatures directly increases aircraft safety and freezing point is around -49 ° C, it is advantageous to use easily in fuel systems. In this study, the effects of jp-8 and diesel fuel mixtures on engine performance were investigated experimentally. A 3-cylinder, four-stroke, turbocharged diesel engine with pump injector fuel system was used for this purpose. 5% JP8 was added to diesel fuel. It was used as a fuel in the engine and the obtained values were analyzed according to the diesel fuel..

Keywords: JP8, Diesel fuel, engine emissions, engine performance

1. Introduction

Since the industrial revolution, industrial energy has been suppied by fossil fuels. It leads to an incease in the atmosphere of the Earth and the rate of cabon dioxide and harmful compounds (Sungur, Topaloglu 2018). To reduce the amount of crude oil in the environment and to limit the use of alternative fuels for internal combustion engines. In this frame, it is important that the fuel is a propellant (JP) fuel, JP- 8. In order to improve the efficiency of the fuel distribution system, the US Department of Defense (DoD) introduced a single fuel (JP-8) policy for all its air and ground vehicles. JP-8. Ultra Low Sulfur Diesel. Thus, it is very important, to study the autoignition, combustion, and emissions characteristics of different types of JP-8 fuels used in military diesel engines (Wei, Liu et al. 2019). Unlike conventional diesel fuels, JP-8 has a wide variation, in particular cetane number, volatility and formulation. One of the reasons for the change in JP-8 properties may be refinery and unrefined oil sources. (Uyumaz, Solmaz et al. 2014).

Turbocharged diesel suggestion of high power density, hardness and reasonable reliability. While the Commercial World relies on fuels specifically designed for use in diesel engines, the reduction of army logistics has reduced the total number of fuels. (Fernandes, Fuschetto et al. 2007, Lee and Bae 2011, Asokan, Senthur Prabu et al. 2019). Further, one for both airplane jet engines and vehicle diesels offers a chance for great benefits in weather conditions. (Sundararaj, Kumar et al. 2019).

JP-8 or JP8 (for "Jet Propellant 8") is a jet fuel used in a variety of US military. MIL-DTL-83133 and British Defense Standard 91-87 and similar to Jet A-1 of commercial aviation, but with the addition of corrosion inhibitor and anti-icing additives (Ning, Duan et al. 2019, Sogut, Seçgin et al. 2019).

A kerosene-based fuel, JP-8 is projected to remain in use at least until 2025. It was beginning introduced at NATO bases in 1978. Its NATO code is F-34. The various properties of JP-8 fuel

[1] Selcuk University, Mechanical Engineering Department, Konya, Turkey
[2] Konya Technical University, Mechanical Engineering Department, Konya, Turkey
* Corresponding author (İletişim yazarı): haydogan@selcuk.edu.tr

Citation (Atıf): Kurban, M., Kurban, H., Dalkılıç, M., (2019). Effec of Using JP8-Diesel Fuel Mixtures in a Pump Injector Engine Engine Performance. Bilge International Journal of Science a Technology Research, 3(Special Issue): 106-111.

are shown in Table 1(Lee and Bae 2011, Lee, Oh et al. 2012, Lee, Lee et al. 2015).

2. Material and Method

From fossil diesel fuel and JP-8 fuel. This mixture was prepared by adding 5% by volume JP-8 to the diesel fuel. He opened the chamber of the newly prepared fuels and was allowed to bind within 48 hours and any phase separation and collapse were observed. Before all tests, the fuel system was flushed from the previous fuel. The engine is heated to operating temperature. The tests were repeated 3 times and averaged the measured values.

This level has a tester consisting of diesel engine and hydraulic dynamometer to compare diesel fuel and JP8 diesel fuel. A Volkswagen brand three-cylinder, four-stroke, water-cooled pump injector diesel engine is used in the experiments. 2. The manufacture of a hydraulic dynamometer with a shear power of 100 kW in the experiments.

Table 1. Diesel and JP8 Properties

Property	Diesel	JP-8	Test Method
Density @ 15°C, kg/L	0.8334	0.8001	ASTM D-1298
Distillation, °C 10% Rec. Temperature 50% Rec. Temperature 90% Rec. Temperature	 218 283 348	 151 200 238	ASTM D-86
Sulfur Content, % wt	0.033	0.2532	ASTM D-4294
Copper Strip Corrosion	1A	1A	ASTM D-130
Flash Point	65	44.5 (D-56)	ASTM D-93
Kin. Viscosity @ 40°C, cSt	2.92 (40°C)	4.05 (-20 °C)	ASTM D-445
Cetane Index	57	53	ASTM D-4737
Cetane Number	55	51	FuelTech IQT
CFPP	-7	n/a	IP-309
Freezing Point	n/a	-48	ASTM D-2386
WSD, µm	455	720	CEC F-06-A-96
Conductivity (pS/m)	n/a	420	ASTM D-2624

Table 2. The technical characteristics of the diesel engine used in the study

Type of engine	4 stroke
Engine volume	1422 cc
Number of cylinders	3
Diameter of cylinder	79.50 mm
Stroke length	95.50 mm
Maximum power	52 kW @ 4000 rpm
Maximum Torque	155 Nm @ 1600 rpm
Compression ratio	19.5:1
Fuel system	Pump injector
Fuel Type	Diesel

The characteristics of the engine dynamometer used in the experiments are given in Table 3.

Table 3. The characteristics of engine dynamometers

Model	BT-190 FR
Capacity	100 kW
Maximum rotation	6000 rpm
Maximum torque	750 Nm

The technical information on the exhaust emission device used in the experiments is given in Table 4.

Measurement Ranges	Unit	Value
CO	%	0-9.99
CO_2	%	0.19.99
HC	ppm	0-2500
λ	%	0-1.99
O_2	%	0-20.8
NOx	ppm	0-2000
Operation temperature	°C	5-40
Supply voltages	V	12

The test setup is shown in Figure 1.

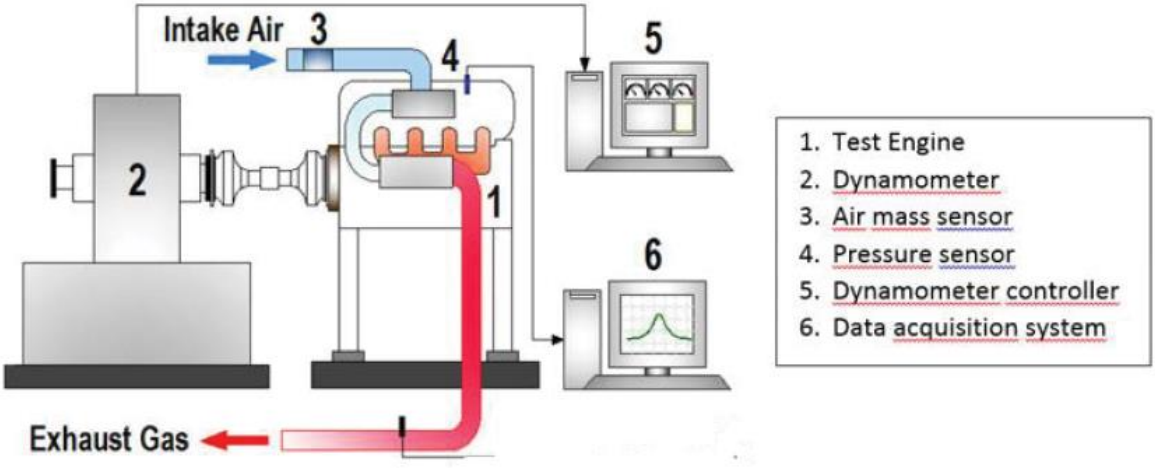

Figure 1. Engine test equipment

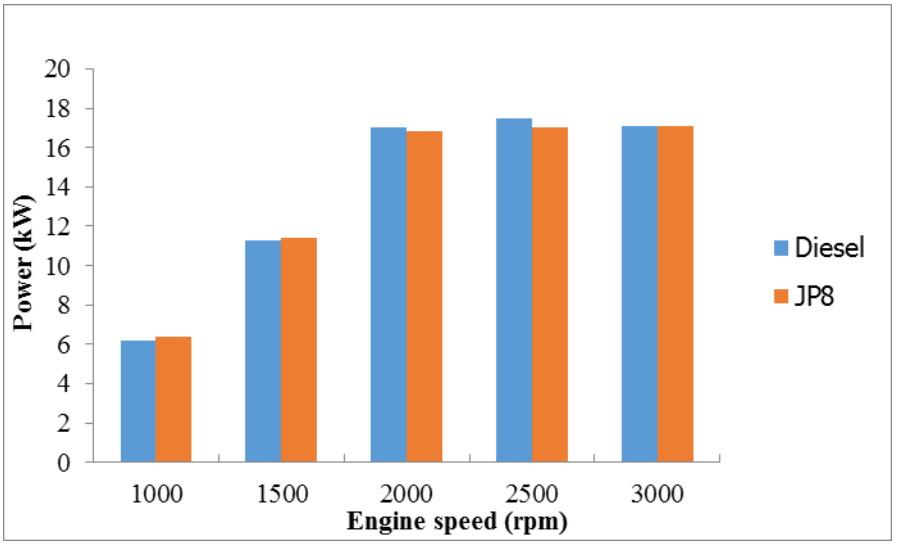

Figure 2. Variation of engine power with engine speed

The changing of the engine torque values is shown in Figure 3. The engine torque numbers showed a reduction with the reduction of the engine brake power. When this shape is analyzed, it can be shown that the max. torque numbers is gain at 2000 rpm. Engine torque at 2000 rpm is measured as 81 Nm with diesel fuel use. The values are very close to each other when using both fuels.

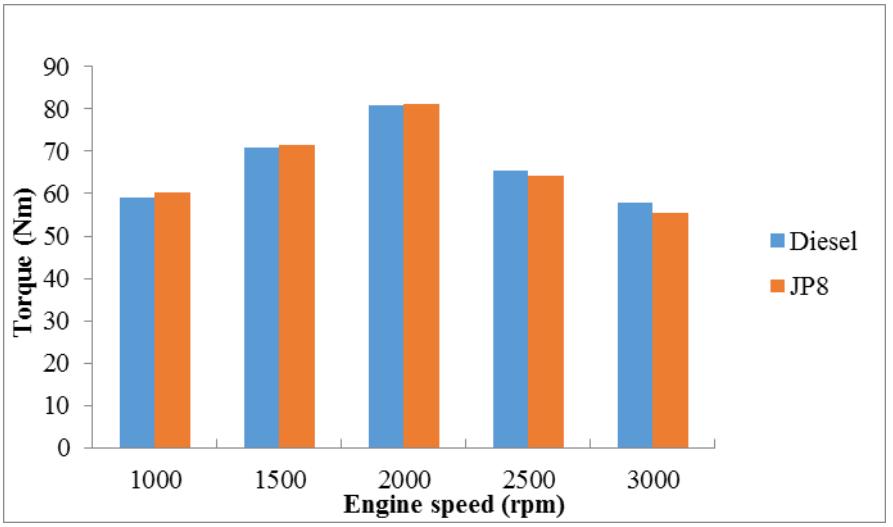

Figure 3. Variation of engine torque with engine speed

The values of specific fuel consumption according to engine speed can be seen in Figure. 4. The lowest specific fuel consumption with all fuels was achieved in the range of 1950-2200 rpm. At this rpm, the use of the JP8 compared to the diesel fuel and the specific fuel consumption values up to 10% increased. Due to the low heating value of the JP8 fuel, the fuel consumption and specific fuel consumption of the pump increases by using diesel fuel, sending more fuel owing to the pump to gain near power.

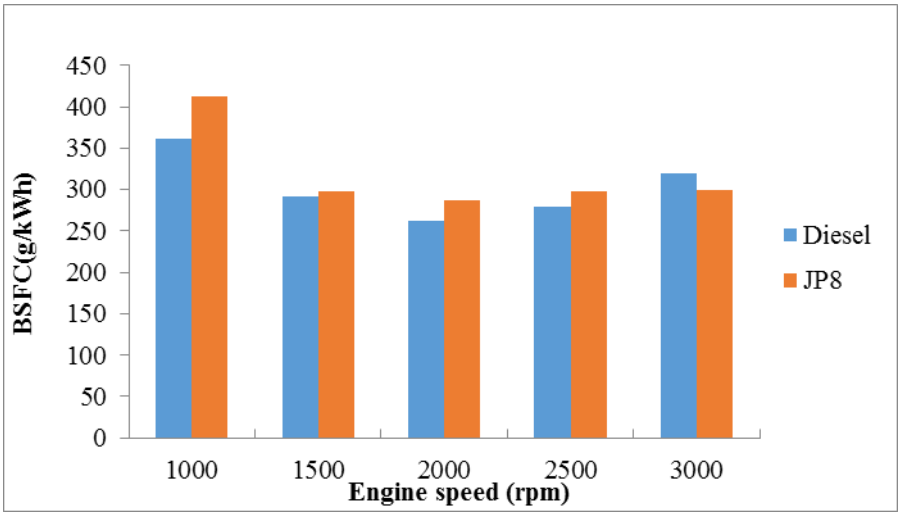

Figure 4. Relationship between specific fuel consumption and engine speed

4. Discussion and Conclusions

In this study, performance tests of fuel mixtures obtained by mixing 5% by volume of aviation fuel JP-8 to reference diesel fuel and diesel fuel were examined comparatively. A 3-cylinder, 4-stroke diesel engine with pump injector was used for these experiments. as a result of experiments although the lower thermal values of the JP-8 and the reference diesel fuel are very close to each other, the lower density of the JP-8 results in less energy being introduced into the unit volume of the cylinder and as a result of this, in blend fuels containing JP-8, a reduction in engine torque was observed due to the amount of JP-8 in the mixture.

Acknowledgements

This study was supported by Selçuk University Scientific Research Projects Center.

References

Asokan, M. A., S. Senthur Prabu, P. K. K. Bade, V. M. Nekkanti and S. S. G. Gutta (2019). "Performance, combustion and emission characteristics of juliflora biodiesel fuelled DI diesel engine." Energy 173: 883-892.

Fernandes, G., J. Fuschetto, Z. Filipi, D. Assanis and H. McKee (2007). "Impact of military JP-8 fuel on heavy-duty diesel engine performance and emissions." Proceedings of the Institution of Mechanical Engineers, Part D: Journal of Automobile Engineering 221(8): 957-970.

Lee, J. and C. Bae (2011). "Application of JP-8 in a heavy duty diesel engine." Fuel 90(5): 1762-1770.

Lee, J., J. Lee, S. Chu, H. Choi and K. Min (2015). "Emission reduction potential in a light-duty diesel engine fueled by JP-8." Energy 89: 92-99.

Lee, J., H. Oh and C. Bae (2012). "Combustion process of JP-8 and fossil Diesel fuel in a heavy duty diesel engine using two-color thermometry." Fuel 102: 264-273.

Ning, L., Q. Duan, Y. Wei, X. Zhang, K. Yu, B. Yang and K. Zeng (2019). "Effects of injection timing and compression ratio on the combustion performance and emissions of a two-stroke DISI engine fuelled with aviation kerosene." Applied Thermal Engineering 161.

Sogut, M. Z., Ö. Seçgin and S. Ozkaynak (2019). "Investigation of thermodynamics performance of alternative jet fuels based on decreasing threat of paraffinic and sulfur." Energy 181: 1114-1120.

Sundararaj, R. H., R. D. Kumar, A. K. Raut, T. C. Sekar, V. Pandey, A. Kushari and S. K.

Puri (2019). "Combustion and emission characteristics from biojet fuel blends in a gas turbine combustor." Energy 182: 689-705.

Sungur, B. and Topaloglu, B. (2018). “Numerical Analyses of the Effects of Fuel Load Variation on Combustion Performance of a Pellet Fuelled Boiler” Bilge International Journal of Science and Technology Research 2(1): 1-8.

Uyumaz, A., H. Solmaz, E. Yılmaz, H. Yamık and S. Polat (2014). "Experimental examination of the effects of military aviation fuel JP-8 and biodiesel fuel blends on the engine performance, exhaust emissions and combustion in a direct injection engine." Fuel Processing Technology 128: 158-165.

Wei, H., W. Liu, X. Chen, Q. Yang, J. Li and H. Chen (2019). "Renewable bio-jet fuel production for aviation: A review." Fuel 254.

Bilge International Journal of Science and Technology Research

Web : http://dergipark.gov.tr/bilgesci - **E-mail:** kutbilgescience@gmail.com

Received: 26.11.2018
Accepted: 07.01.2020
DOI: 10.30516/bilgesci.647669

ISSN: 2651-401X
e-ISSN: 2651-4028
3(Special Issue), 112-116, 2019

Development of Reinforced Composites Containing Tea Tree Oil and Propolis for the Treatment of Horse Hoof Cracks

Kamila Sobkowiak[1*], Tomasz Gozdek[1], Mustafa Karaboyacı[2]

Abstract: The aim of the study was the evaluation of properties of variously composed composite materials based on polyurethane filled with tea tree oil (TTO) and addition of other ingredients. The tea tree oil/cyclodextrin inclusion complex was prepared by using the 'Paste method' described in Shrestha, M and others. (2017) (Shrestha et al. 2017). To analyse the properties of composite materials following testing methods were conducted: density, tensile strength, compression test, impact resistance. In the study, pursued in the Lodz University of Technology in Poland, thirteen materials with different percentile content of additives: TTO/β-CD, propolis, TTO/β-CD/Propolis, TTO were prepared and tested to establish the most favourable characteristics. Properties of sample containing Tea tree oil/ β-cyclodextrin/Propolis were the most satisfying and were assumed to be accurate in fulfilling the role of the hoof crack filler the best in the first study. With the higher amount of the additive the mechanical properties weakened preventing the use of the product in the hoof cracks.

Keywords: Polyurethane, Tea Tree Oil, Cyclodextrin, Propolis, Encapsulation, Hoof Cracks

1. Introduction

Hoof crack is a damage in the wall of the hoof. There are various types of cracks such as grass, sand, heel, bar, toe and quarter cracks. These defects might appear in every hoof of hoofed animal, whereas this study is focused on horses. Hoof-wall defects, especially quarter cracks, are a prevalent cause of decreased athletic performance in competition horses and frequently lead to foot lameness. (O'Grady, 2001).

Unluckily, quarter cracks might be painful. Generally, the reasons are infection or instability, caused by movement of the hoof wall posterior to the crack. This frustrating cause of lameness originating in the foot usually represent a significant therapeutic challenge for both veterinarian and farrier. It is especially problematic for equine practitioners according to the fact that in general horses that develop quarter cracks must continue to perform. To let that happen, it is crucial for the reconstruction to arrange both stability and strength to the hoof wall injury. As the result, the horse will be allowed to perform while the healing will take place so that the crack will grow out.

In most cases, it is unlikely that hale regular horn will split. However, if a line of weakness exists in the hoof wall, resultant domestic stress concentration might result in the formation of a fissure in the hoof wall. (O'Grady, 2001).

Mechanical stabilization is required for the treatment of hoof cracks. Both in this study and in the previous one composite materials were used. In the first study, in the Suleyman Demirel University, the composite consisted of: solid polyurethane, β-cyclodextrin and tea tree oil, whereas in discussed study, executed in the Lodz University of Technology, the same ingredients with the addition of propolis were used. The addition of propolis was intended to make the fragile samples from the previous study more flexible.

[1]Lodz University of Technology, Faculty of Chemistry, Institute of Polymer and Dye Technology, POLAND.
[2]Suleyman Demirel University, Faculty of Engineering, Chemical Engineering Dept. 32260, Isparta, TURKEY
[3]*Corresponding author (İletişim yazarı): kames1901@gmail.com

Citation (Atıf): Sobkowiak, K., Gozdek, T., Karaboyacı, M., (2019). Development of Reinforced Composites Containing Tea Tree Oil and Propolis for the Treatment of Horse Hoof Cracks. Bilge International Journal of Science and Technology Research, 3(Special Issue): 112-116.

Polyurethane is a copolymer formed by conjugation of diol and diisocyanate groups has high strength; extremely good abrasion resistance; good resistance to gas, greases, oils, and hydrocarbons; and excellent resistance to oxygen and ozone. (Ebewele, 2000) Moreover, it is biocompatible. The tea tree oil was used according to its properties: antifungal, antibacterial, antiseptic, anti-inflammatory, anti-cancer, insect repellent and insecticide. (Callander, 2012) However, this essential oil cannot be used without a sufficient and appropriate barrier to increased solubility in water and volatilization. In order to attain the barrier, the TTO is being encapsulated in β-cyclodextrin particles. (Bhandari, 1998).

The propolis is a new ingredient used in this research. It is a natural resinous mixture produced by honeybees from substances collected from parts of plants, buds, and exudates, is a lipophilic in nature, brittle and hard material and it becomes soft, gummy, pliable and very sticky when heated. (Hausen et al. 1987) Generally, raw propolis is composed of about 50% resins, 30% waxes, 10% essential oils, 5% pollen, and 5% of various organic compounds. (Wagh, 2013) The temperature mainly affects the consistency of propolis. It is much harder and more resistant to temperature than wax. At 15 ° C, propolis is hard and brittle, at 34.5-36 ° C (nest temperature) it becomes soft and plastic, and at temperatures above 45 ° C - sticky and sticky. It is liquid at 70-80 ° C, although for some propolis samples the melting point is above 100 ° C. (Kujumgiev et al. 1999) Propolis has various pharmacological activities. It is the most biologically active among bee products. The most important and known properties of propolis are antimicrobial and antiinflammatory, antioxidant, antitumor and immunostimulatory activity (Wagh, 2013). Propolis presence should strengthen the composite and improve its properties. (Wolska et al. 2016)

2. Material and Method

Ingredients: Izopianol 40/30 W/PIR, Purinova Sp. z.o.o being a mixture of polyols and selected auxiliary agents. Purocyn B, Purinowa Sp. z.o.o being a polymeric diisocyanate of diphenylmethane. Propolis: Gospodarstwo Pasieczne Łukasiewicz (Poland). B-cyclodextrin from Pol-Aura (Poland). Tea tree oil from Vivio (Poland). All solvents used in the studies were analytical grade.

2.1. Preparation of tea tree oil/cyclodextrin inclusion complex

The inclusion complex was received by following the 'Paste method' recipe described in Shrestha, M., Ho, T. M., & Bhandari, B. R. (2017). (Shrestha et al. 2017). The preparation method was made in the exact way as the complex in the first study. (Sobkowiak et al. 2018)

2.2. Preparation of the composite material

Thirteen samples were prepared; they varied according to ingredients and its amounts:

- • Pure polyurethane – the reference sample (sample No. 1)
- • 1%, 3% and 5% TTO/β -CD and 99%, 97%, 95% polyurethane (sample No.2, No.3, No. 4)
- • 1%, 3% and 5% propolis and 99%, 97%, 95% polyurethane (sample No.5, No.6, No.7)
- • 1% TTO/β -CD + 1% propolis and 98% polyurethane (sample No.8)
- • 3% TTO/β -CD + 3% propolis and 94% polyurethane (sample No.9)
- • 5% TTO/β -CD + 5% propolis and 90% polyurethane (sample No.10)
- • 1%, 3% and 5% TTO and 99%, 97%, 95% polyurethane (sample No.11, No.12, No.13)

All samples were prepared by mixing an additive and polyol firstly and adding isocyanate afterwards: 65g ingredient A (polyol mixture) and 104g ingredient B (isocyanate). They were formed in plastics buckets.

3. Results

Four quantities were measured: density, tensile strength, compression test and impact resistance.

3.1. Density

Sample size: 25 mm x 25 mm x 25 mm. Five samples were tested. Samples were weighed on the laboratory balance. For the additive TTO/CD the density is decreasing with the increase in the amount of it. The same situation is for composite containing TTO/CD/Propolis. On the other hand, for samples with propolis and TTO tendency differs.

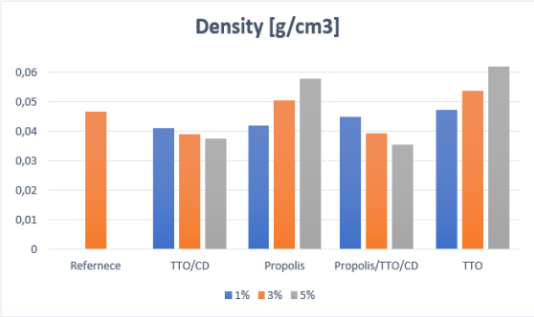

Figure 1. Density of the composites

3.2. Tensile strength

Tensile strength test was performed according to ASTM D3039 standard test method by means of Zwick Roell 1435. Sample size: 100 mm x 25 mm x 10 mm. Five samples were tested. Tensile strength for the reference is the highest. Results are the lowest for TTO/CD. Only for composite comprising propolis the tensile strength is growing with the percentage of a supplement.

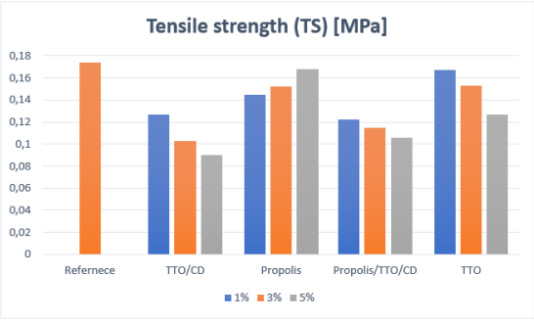

Figure 2. Tensile strength of the composites

3.3. Compression test

Compression test was performed according to ASTM D3574-C standard test method by means of Zwick Roell Retroline. Sample size: 25 mm x 25 mm x 25 mm. Five samples were tested. Addition of both TTO/CD and TTO/CD/Propolis resulted in gradual weakening of the composite. Results are the most satisfying for the sample with propolis. Composite containing TTO seems to be also successful, however, errors in the measurements are significant.

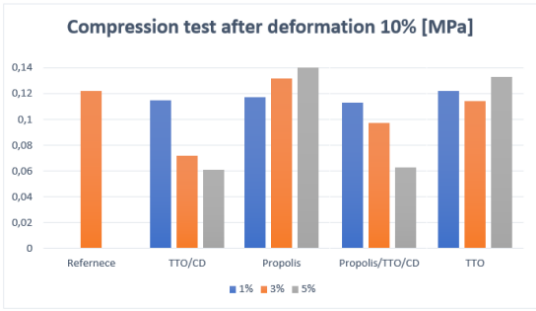

Figure 3. Compressive strength of the composites

3.4. Impact resistance

Impact resistance test was performed according to ASTM D 256 standard test method by means of Cometech QC-639P/Q with charpy's hammer of strength 2J. Tests were carried out on a cross-section not on the width. Sample size: 10 mm x 15 mm x 100 mm. Five samples were tested. Addition of TTO/CD resulted in significant weakening of the composite. Addition of TTO/CD/Propolis partly affected the lowering strength. 1% and 3% of propolis increased the strength while 5% decreased it. Here again the TTO seems to be also successful, however, errors in the measurements are significant.

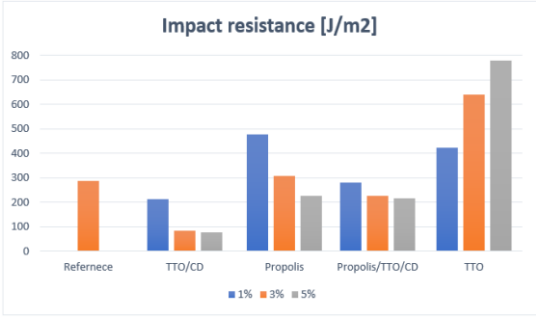

Figure 4. Impact resistance values of the composites

4. Discussion and Conclusions

First of all, in the composite material containing TTO/CD and TTO/CD/Propolis the density is decreasing, which means that pores inside the structure were increasing. According to this the tensile strength is decreasing. Over the compression test we can see lower shears, what is consistent with the theory. What is more, impact resistance test results are compatible. Unfortunately, the addition of the tea tree oil/b cyclodextrin inclusion complex in the composite influences the increase of porosity. The reason is

probably the moisture residues. On the other hand, for samples containing TTO/CD/Propolis for the impact resistance test, there is no big drop in strength as it is for sample containing only TTO/CD. All test results are satisfying, especially for 1% of TTO/CD/Propolis, errors are not significant. In all likelihood, TTO/CD/Propolis is a promising sample and small changes in the system could be enough, such as changing the proportions of ingredients or finer grinding of propolis, heating it and dispersing to achieve better results. (samples No.2,3,4 and No.8,9,10).

The density of the composite material containing propolis, in comparison to the reference sample, is decreasing at the begging and increasing afterwards. Notwithstanding, during the tensile strength test the endurance does not show an upward trend with the increasing amount of propolis. Furthermore, it is not even higher the endurance for the reference sample. There is a possibility that addition of larger particles of propolis in the composite might cause the increase of an error (in the structure it appears as a dispersed wax in the form of slightly larger fragments). Whereas, these errors do not differ between each sample. The propolis affects the increase of compressive strength except for the sample containing 1%. The reason might be an insufficient amount of the ingredient. (samples No.5,6,7).

For samples containing tea tree oil the heterogeneous structure is visible after cutting the prepared composite. Moreover, it is visible in large measurement errors, which results from the dependence: the more homogeneous the structure, the more accurate the measurements. Therefore, despite the fact that the results in the impact resistance test are satisfying, they cannot be taken into account. Same of samples could not be tested according to its incorrect structure (Picture 1):

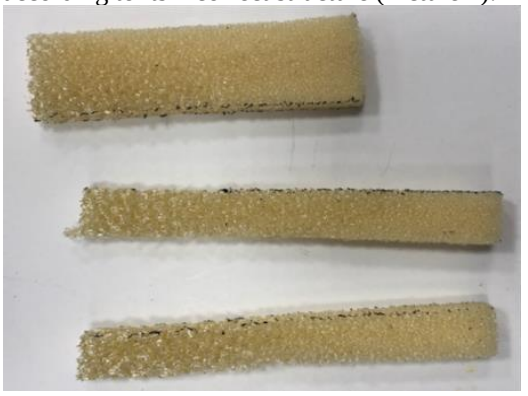

Figure 5. The incorrect structure of samples containing TTO

To summarise, both of studies conducted in Suleyman Demirel University, Isparta, Turkey and Lodz University of Technology, Lodz, Poland were very evolving and gave us the opportunity to get to know with the properties of composite materials with selected compositions. In both studies an addition of TTO/CD lowered the strength of the substance as its content increased. The reason is probably the moisture residues. It cannot be said that samples comprising tea tree oil/cyclodextrin inclusion complex or only propolis were unsuccessful, while they were worse than the another one. The sample containing mixture of propolis and tea tree oil/b-cyclodextrin was the most successful. Errors were not significant, and all results formed a coherent whole. The last composite, which included the tea tree oil could not be compared with the rest of samples according to big errors and heterogeneous structure, on the other hand, its reinforcement of the material is visible and might be inspected in future research.

Acknowledgements

This research is a continuation of the study conducted in the Suleyman Demirel University in Isparta, Turkey described in the article: Sobkowiak, K., Kocabıyık, A., & Karaboyacı, M. (2018). Development of Cyclodextrin Particle Reinforced Composites Containing Tea Tree Oil for The Treatment of Horse Nail Fractures. (Sobkowiak et al. 2018)

References

Bhandari, B. R., D'Arc, B. R., & Thi Bich, L. L. (1998). Lemon oil to β-cyclodextrin ratio effect on the inclusion efficiency of β-cyclodextrin and the retention of oil volatiles in the complex. Journal of Agricultural and Food Chemistry, 46(4), 1494-1499.

Callander, J. T., & James, P. J. (2012). Insecticidal and repellent effects of tea tree (Melaleuca alternifolia) oil against Lucilia cuprina. Veterinary Parasitology, 184(2-4), 271- 278.

Ebewele, R. O. Polymer science and technology. 2000, 458-459.

Hausen, B. M., Wollenweber, E., Senff, H., & Post, B. (1987). Propolis allergy.(II). The sensitizing properties of 1, 1-dimethylallyl

caffeic acid ester. Contact Dermatitis, 17(3), 171- 177.

Kujumgiev, A., Tsvetkova, I., Serkedjieva, Y., Bankova, V., Christov, R., & Popov, S. (1999). Antibacterial, antifungal and antiviral activity of propolis of different geographic origin. Journal of ethnopharmacology, 64(3), 235-240.

O'Grady, S. E. (2001). Quarter crack repair: an overview. Equine Veterinary Education, 13(4), 216-219

Shrestha, M., Ho, T. M., & Bhandari, B. R. (2017). Encapsulation of tea tree oil by amorphous beta-cyclodextrin powder. Food chemistry, 221, 1474-1483.

Sobkowiak, K., Kocabıyık, A., & Karaboyacı, M. (2018). Development of Cyclodextrin Particle Reinforced Composites Containing Tea Tree Oil for The Treatment of Horse Nail Fractures. ICONST 2018, 888-893.

Wagh, V. D. (2013). Propolis: a wonder bees product and its pharmacological potentials. Advances in pharmacological sciences, 2013.

Wolska, K., Górska, A., & Adamiak, A. (2016). Właściwości przeciwbakteryjne propolisu. Postępy Mikrobiologii, 55(4).

Yazar rehberi

Makale A4 sayfa boyutunda, Times New Roman yazı tipinde, 10 punto olarak ve düz metin şeklinde yazılmalıdır. Makaleye sayfa ve satır numarası eklenmelidir.

Kapak sayfası: Kapak sayfasında sırasıyla makale başlığı, yazar adı soyadı, yazar iletişim bilgileri bulunmalıdır.

Başlık ve özet (Türkçe ve İngilizce): Özet 500 kelimeyi geçmeyecek şekilde yazılmalıdır. Araştırmanın gerekçesini, amaçlarını, uygulanan yöntemi, sonuç ve önerileri içermelidir. Özet sonuna 3-6 kelimeden oluşan anahtar kelimeler eklenmelidir.

Ana metin: Makale ana metni tek satır aralıklı olarak yazılmalı, çizelge ve şekillerle birlikte toplam 15 sayfayı geçmemelidir. Konu başlıkları 1., 1.1., 1.1.1., şeklinde numaralandırılmalıdır.

Dipnotlar: Metin içerisinde dipnotlardan olabildiğince kaçınılmalıdır. Çizelge ve şekillerde ise gerekli olması halinde ilgili objenin altında yer almalıdır.

Semboller ve kısaltmalar: Birim sembolleri Uluslararası Birimler Sistemine (The International System of Units; SI) göre olmalıdır.

Kaynaklar: Metin içinde geçen kaynaklar yazarların soyadları ve yayın yılı ile birlikte verilmelidir (Örnek: Özkan vd., 2008; Özdemir, 2015). Metin sonundaki kaynaklar önce alfabetik sonra kronolojik sıraya göre sıralanmalıdır. Bir yazarın aynı yılda birden fazla yayınına atıf yapılmışsa, bu kaynaklar yayın yılından sonra gelecek a, b, c… harfleriyle ayrılmalıdır (Örnek: Kandemir, 1999a; 2000b; 2001).

Çizelgeler ve şekiller: Bütün çizelge ve şekiller metin içerisinde atıf sıralarına göre ardışık olarak numaralandırılmalı ve ilgili yere eklenmelidir. Çizelgelerin üzerinde ve şekillerin altında başlıkları yer almalıdır. Çizelge ve şekiller hem elektronik ortamda hem de kağıt baskıda net olarak görünür ve anlaşılabilir olmalıdır. Şekiller en az 300 dpi çözünürlüğünde hazırlanmalıdır. Şekillerde kullanılan karakterler Times New Roman yazı tipinde olmalıdır.

Makalenin gönderilmesi: Dergimizin bütün hakemlik ve yayıncılık işlemleri elektronik sistem üzerinden gerçekleştirilmektedir. Dergimize yayın göndermek isteyen yazarların ilk olarak dergimizin "web sitesine" girerek "kayıt" ekranından üye olmaları gerekmektedir. Kayıtlı yazarlarımız sisteme "giriş" yaptıktan sonra, makaleleri ile birlikte ve hakem önerilerini de içeren "Telif Hakkı Devri Formunu" sisteme ek belge olarak yüklemelidirler.

Instructions for authors

Manuscript should be written in A4 page size, with Times New Roman font and 10 pt font size, as plain text. Page and line numbers should be included into the manuscript.

Cover page: Cover page should include title of the manuscript, names and contact information of the authors.

Title and abstract (Turkish and English): Abstract should not written exceed 500 words. Explains rationale, goals, methods, results and recommendations of the study. Keywords with 3-6 words should be included at the end of the abstract.

Main text: Main body of the manuscript should be written in single line spacing, and it should not exceed a total of 15 pages including tables and figures. Headings should be numbered as follows: 1., 1.1., 1.1.1.

Footnotes: Use of footnotes within the text should be avoided as much as possible. If necessary, it can be located below tables and figures.

Symbols and abbreviations: Unit symbols should comply with The International System of Units.

References: In the text, literature should be given with the last name of the author and year of the publication (For example: Özkan et al., 2008; Özdemir, 2015). At the end of the paper, references should be ordered first alphabetically and then chronologically. If there is more than one paper from the same author for a given year, these references should be identified by the letters a, b, c…, after the year of publication (For example: Kandemir, 1999a; 2000b; 2001).

Tables and figures: All tables and figures should be numbered in the order of their citation in the text, and they should be located in suitable places. Titles of the tables should be located above, and titles of the figures should be located below the related table or figure. Tables and figures should be easily visible and understandable both in print and electronic versions. Figures should be prepared in at least 300 dpi resolution. Characters within the figures should be in Times New Roman font type.

Submission of a manuscript: In our journal, all review and publishing processes are conducted within an electronic system. Authors who want to submit their manuscript to our journal should first visit our "web page" and "register" as an author. Our registered members can "log in" to the system and then upload their manuscript and "COPYRIGHT RELEASE FORM" as an appendix, containing their suggested referees.

Kaynaklar

Kaynak kullanımları aşağıda örneklerde belirtilen şekillerde olmalıdır.

References

Using of references should be in the form as follows.

Article in periodical journals / Periyodik dergilerde makale

Akyıldırım, O., Gökce, H., Bahçeli, S., Yüksek, H. (2017). Theoretical and Spectroscopic (FT-IR, NMR and UV-Vis.) Characterizations of 3-p-chlorobenzyl-4-(4-carboxybenzylidenamino)-4,5-dihydro-1H-1,2,4-triazol-5-one Molecule. Journal of Molecular Structure, 1127: 114-123.

Tan, S., Williams, C.T. (2013). An In Situ Spectroscopic Study of Prochiral Reactant–Chiral Modifier Interactions on Palladium Catalyst: Case of Alkenoic Acid and Cinchonidine in Various Solvents. J. Phys. Chem. C, 117(35): 18043–18052.

Book / Kitap

Özkan, K. (2016). Biyolojik Çeşitlilik Bileşenleri (α, ß, γ) Nasıl Ölçülür? Süleyman Demirel Üniversitesi, Orman Fakültesi Yayın No: 98, ISBN: 976-9944-452-89-2, Isparta, 142 s.

Whittaker, E. T. (1988). A treatise on the analytical dynamics of particles and rigid bodies. Cambridge University Press.

Reference to a chapter in an edited book / Kitapta bölüm

Westhoff, V., Van Der Maarel, E. (1978). The braun-blanquet approach in classification of plant communities, Reinhold Tüxen (Ed.), Handbook of Vegetation Science, Springer Netherlands, pp. 619-704.

Şencan, A., Sevindir, H.C., Kiliç, M., Karaboyaci, M. (2011). Biosorption of CR+ 6 from Aqueous Solution with Activated Sludge Biosolids (Ref. NO: MT11-OP-475), Gökçekus, H., Türker, U., LaMoreaux, J.W., (Ed, Survival and Sustainability, 973-984.

Thesis and dissertation / Tez

Gülsoy, S. (2011). *Pistacia terebinthus* L. subsp. *palaestina* (Boiss.) Enler (Anacardiaceae)'in Göller Yöresi'ndeki Yetişme Ortamı Özellikleri ve Yetişme Ortamı-Meyve Uçucu Yağ İçeriği Etkileşimleri. SDÜ, Fen Bilimleri Enstitüsü, Orman Mühendisliği Anabilim Dalı, 194 s.

Özdemir, S. (2015). Ovacık Dağı Yöresi'nde Türk Kekiği (*Origanum onites* L.) ve Büyük Çiçekli Adaçayı (*Salvia tomentosa* Miller) Türlerinin Ekolojik Özellikleri. SDÜ, Fen Bilimleri Enstitüsü, Orman Mühendisliği Anabilim Dalı. 74s.

Conference proceedings / Konferans bildirisi

Özkan, K., Kavgacı, A. 2009. Küresel ısınmanın orta dağlık alanlarda tür çeşitliliği üzerine olası etkileri (Acıpayam yöresi örneği). I. Ulusal Kuraklık ve Çölleşme Sempozyumu (Eds: Palta, Ç.,), 16-18 Haziran 2009, Konya, Türkiye, 277-284.

Özkan, K., Negiz, M.G., Şentürk, Ö., Kandemir, H. (2012). Göller Bölgesi'ndeki Bazı Önemli Rekreasyon Alanları ve Onların Ekolojik Özellikleri, I. Rekreasyon Araştırmaları Kongresi 2012, Bildiri Kitabı, 12-15 Nisan, 587-596, Detay Yayıncılık, Kemer-Antalya.

Electronic reference / Elektronik kaynak

FAO, (2016). Sustainable Food and Agriculture. Food and Agriculture Organization of the United Nations, Rome, http://www.fao.org/sustainability/en/, Accessed: 14.06.2016.

Milliparklar, (2017). Doğa Koruma ve Milli Parklar Genel Müdürlüğü. http://www.milliparklar.gov.tr/korunanalanlar/kavramlar.htm, Erişim Tarihi: 18.06.2017.

Bilge International Journal of Science and Technology Research online ve açık erişimli yayınlanan uluslararası hakemli bir dergidir. Dergi dili İngilizce ve Türkçe'dir. Yılda iki sayı yayınlanan dergide Temel bilimler, Doğa bilimleri, Mühendislik ve Teknoloji bilimleri konularında bilimsel makaleler yayınlanmaktadır. Dergimize gönderilen makalelerin daha önce yayınlanmamış orijinal çalışmalar olması gerekmektedir. Dergide yayımlanacak makalenin atıflarından, bilimsel verilerinden, sonuçlarından ve etik kurallara uygun olup olmadığından yazarlar sorumludur (yazar/yazarlar bu durumu telif hakkı sözleşmesinde kabul eder). Orijinal araştırmaya dayalı çalışmalara öncelik verilmekte, sınırlı sayıda derleme makale yayınlanmaktadır. Dergiye gönderilen makale, yayın kurulu tarafından yayına uygunluk açısından incelendikten sonra en az iki hakeme gönderilir. Hakemlerin değerlendirmeleri sonucunda en az iki yayınlanabilir raporu alan makale, dergi yönetimince uygun görülen bir sayıda yayınlanır. Hakem raporlarının birisinin olumlu, diğerinin olumsuz olması durumunda makale üçüncü bir hakeme gönderilir. Bu durumda makalenin yayınlanıp yayınlanmamasına üçüncü hakemin raporuna göre karar verilir. Hakemler tarafından düzeltme istenen makaleler gerekli düzeltmeler için yazara geri gönderilir. Düzeltilen metnin belirtilen sürede dergi sistemine yüklenmesi yazarın sorumluluğundadır. Makalenin yayınlanması konusunda son karar, dergi editörlüğüne aittir.

Bilge International Journal of Science and Technology Research is an online, open access, peer-reviewed, international research journal. Language of the journal is English and Turkish. The journal published two issues a year publishes scientific articles on the subjects of Basic Sciences, Natural Sciences, Engineering and Technology. Authors should only submit original work, which has not been previously published and is not currently considered for publication elsewhere. The authors are responsible for the citations of the article to be published, its scientific data, its results, and whether it is in line with ethical rules (Author / authors accept that in the copyright agreement). Research papers will be given priority for publication while only a limited number of review papers are published in a given issue. The articles are sent to least two reviewer after examined by the editor board in terms of compliance with the publication. As a result of the evaluations of the reviewers, the article which received at least two publishable reports will be published at a suitable number for the management of the journal. If one of the reviewer reports is positive and the other is negative, the article will be sent a third reviewer. In this case, the publication of the article is decided according to the third report. The articles corrected by the referees are returned to the author for necessary corrections. It is the responsibility of the author to upload the revised text to the journal system for the specified period. The final decision on the publication of the article belongs to chef editor.